**University of Bath**

**PHD**

# Bio-Photo-Voltaic Cells (Photosynthetic-Microbial Fuel Cells)

Thorne, Rebecca

*Award date:*
2012

*Awarding institution:*
University of Bath

Link to publication

## Alternative formats
If you require this document in an alternative format, please contact:
openaccess@bath.ac.uk

Copyright of this thesis rests with the author. Access is subject to the above licence, if given. If no licence is specified above, original content in this thesis is licensed under the terms of the Creative Commons Attribution-NonCommercial 4.0 International (CC BY-NC-ND 4.0) Licence (https://creativecommons.org/licenses/by-nc-nd/4.0/). Any third-party copyright material present remains the property of its respective owner(s) and is licensed under its existing terms.

**Take down policy**
If you consider content within Bath's Research Portal to be in breach of UK law, please contact: openaccess@bath.ac.uk with the details. Your claim will be investigated and, where appropriate, the item will be removed from public view as soon as possible.

Download date: 05. May. 2023

# Bio-Photo-Voltaic Cells (Photosynthetic - Microbial Fuel Cells)

**REBECCA THORNE**

A thesis submitted for the degree of Doctor of Philosophy

University of Bath

Department of Chemistry

November 2011

## COPYRIGHT DECLARATION

Attention is drawn to the fact that copyright of this thesis rests with the author. A copy of this thesis has been supplied on condition that anyone who consults it is understood to recognise that its copyright rests with the author and that they must not copy it or use material from it except as permitted by law or with the consent of the author.

This thesis may be made available for consultation within the University Library and may be photocopied or lent to other libraries for the purposes of consultation.

Rebecca Thorne

# x.1 Table of Contents

# x.2 List of Figures

## Chapter 1



## Chapter 2

**Chapter 3**



**Chapter 4**

**Chapter 5**

**Chapter 6**

**Chapter 7**

**Chapter 8**

**Chapter 9**

# x.3 List of Equations

## Chapter 1



## Chapter 2

**Chapter 3**

**Chapter 5**



**Chapter 6**



**Chapter 8**



**Chapter 9**

**Appendix A**

# x.3 List of Tables

**Chapter 2**



**Chapter 4**



**Chapter 5**



**Chapter 6**



**Chapter 7**



**Chapter 8**



**Appendix A**

# x.4 List of Symbols

| | |
|---|---|
| $[O]_0$ | Concentration of O at electrode surface (mol $cm^{-3}$) |
| $[O]_{bulk}$ | Concentration of O in bulk solution (mol $cm^{-3}$) |
| $[R]_0$ | Concentration of R at electrode surface (mol $cm^{-3}$) |
| $[R]_{bulk}$ | Concentration of R in bulk solution (mol $cm^{-3}$) |
| $\Delta E_p$ | Pulse height in square wave voltammetry (mV) |
| $\Delta E_s$ | Staircase step height in square wave voltammetry (mV) |
| $\Delta G^{0\ddagger}$ | Standard Gibbs free energy of activation (kJ $mol^{-1}$) |
| A | Area of electrode ($cm^{-2}$) |
| A | frequency factor (unit depends on order of rate) |
| a | UME tip radius (cm) |
| Å | Angstrom |
| $A_{ox}$ | Frequency factor for oxidation reaction |
| $A_{red}$ | Frequency factor for reduction reaction |
| C | Constant |
| $d_{tip\text{-}sub}$ | UME tip-substrate separation distance (cm) |
| d | Planar distance (cm) |
| $D_O$ | Diffusion coefficient of species O ($cm^2$ $s^{-1}$) |
| E | Potential difference (V) |
| $e^-$ | Electron |
| $E_t$ | Potential at time t (V) |
| $E_A$ | Activation energy (kJ $mol^{-1}$) |
| $E_{cell}$ | Cell voltage (V) |
| $E_{eq}$ | Equilibrium potential (V) |
| $E_F$ | Fermi level of metal electrode (eV) |
| $E_0$ | Maximum amplitude of sine wave (V) |
| $E^O$ | Standard electrode potential of a reaction (V) |
| $E_p$ | Peak potential (V) |
| $E_S$ | Substrate potential (V) |
| $E_T$ | UME tip potential (V) |
| F | Faradays constant (96485 C $mol^{-1}$) |
| f | Rotation speed of working electrode in RDE experiments (rpm) |
| F | Fluorescence (measured in fluorescence units or FU) |

| | |
|---|---|
| G | Gibbs free energy (kJ, kJ $mol^{-1}$) |
| g | A factor relating to UME radius of microdisk and surrounding glass |
| $G^{‡}$ | Gibbs free energy of transition state (kJ $mol^{-1}$) |
| $G_{ox}$ | Gibbs free energy of oxidised species (kJ, kJ $mol^{-1}$) |
| $G_{red}$ | Gibbs free energy of reduced species (kJ, kJ $mol^{-1}$) |
| i | Current (A) |
| i(t) | Current at time t (A) |
| $i_0$ | Exchange current when the net current = 0 (A) |
| $i_A$ | Anodic current (A) |
| $i_C$ | Cathodic current (A) |
| $i_{CT}$ | Current related to charge transfer (A) |
| $i_f$ | Forward cycle in square wave voltammetry (A) |
| $I_f(0)$ | Fluorescence intensity in absence of quencher (measured in fluorescence units or FU) |
| $I_f(0)/I_f(Q$ | Fluorescence ratio |
| $I_fQ$ | Fluorescence intensity in the presence of quencher (measured in fluorescence units or FU) |
| $i_K$ | Kinetic limiting current (A) |
| $i_L$ | Limiting current (A) |
| $i_L/\omega^{1/2}$ | The Levich constant |
| $i_{mt}$ | Mass transport limited current (A) |
| $i_{ox}$ | Oxidation current (positive by convention A) |
| $i_p$ | Peak current (A) |
| $i_r$ | Reverse half cycle in square wave voltammetry (A) |
| $i_{red}$ | Reduction current (negative by convention -A) |
| $i_T$ | UME tip current (A) |
| $i_{T,\infty}$ | UME tip current in bulk solution (A) |
| j | Flux of reactant reaching electrode surface (mol $cm^{-2}$ $s^{-1}$) |
| J | Joule |
| $j_L$ | Mass transport limited flux (mol $cm^{-2}$ $s^{-1}$) |
| k | Rate constant (unit depends on order) |
| $k_f$ | Fluorescence rate constant |
| $k^o_{ox}$ | A rate constant for oxidation independent of overpotential |

| | |
|---|---|
| $k^{o}_{red}$ | A rate constant for reduction independent of overpotential |
| $k_{ox}$ | Heterogeneous rate constant for an oxidation reaction (cm $s^{-1}$) |
| $k_{red}$ | Heterogeneous rate constant for a reduction reaction (cm $s^{-1}$) |
| $K_{SV}$ | Stern-Volmer constant |
| O | A typical oxidised species |
| OCP | Open circuit potential (V) |
| OCV | Open circuit voltage (V) |
| P | Power (W) |
| P | Phosphorescence |
| Q | Charge (C ) |
| Q | Quencher concentration (mol $cm^{-3}$) |
| $q_m$ | Charge on metal electrode (C ) |
| $q_s$ | Charge in solution (C ) |
| R | A typical reduced species |
| R | The Universal gas constant (8.415 J $K^{-1}$ $mol^{-1}$) |
| R | Pure resistor (ohm) |
| $r_c$ | Radius of working electrode cylinder in RDE experiments (cm) |
| $R_e$ | Reynolds number in RDE |
| $R_uC_{dl}$ | Time constant of electrochemical cell |
| T | Temperature (K) |
| $t_p$ | Pulse width in square wave voltammetry (s) |
| V | Volt |
| *v* | Linear potential scanrate (V $s^{-1}$) |
| *v* | Viscosity of solution (used in RDE experiments) ($cm^2$ $s^{-1}$) |
| $v_z$ | The component of velocity in the z direction ($cm^2$ $s^{-1}$) |
| x | Distance from electrode surface, where x=0 at the surface and infinity in bulk (cm) |
| $z_0$ | Charge magnitude on one ion |
| A | Transfer coefficient. A value of one half means the transition state is intermediate between reactants and products |
| H | Overpotential (V) |
| $\eta_{act}$ | Charge transfer derived overpotentials of the anode and cathode (V) |
| $\eta_{conc}$ | Concentration overpotentials of the anode or cathode (V) |

| | |
|---|---|
| $\eta_{ohm}$ | Ohmic overpotential (or losses) of MFC/p-MFCs (V) |
| $\theta$ | Angle of incidence |
| $\Lambda$ | Wavelength (nm) |
| $\tau^0$ | Fluorescence lifetime of a fluorophore (s) |
| $\upsilon$ | Linear velocity of solution flow, as a function of position (cm $s^{-1}$) |
| $\omega$ | Rotation speed of working electrode (in RDE experiments) (Hz) |
| $\delta_o$ | Nernst diffusion layer thickness for species O at an electrode fed by Convective transfer (cm) |
| $\Phi_{m-s}$ | Potential drop across the electrode/solution interface (V) |
| $\Phi_m$ | Metal potential (V) |
| $\Phi_s$ | Solution potential (V) |

## x.5 List of Abbreviations

| | |
|---|---|
| 3N-BBM+V | Three fold nitrogen bold basal medium plus vitamins |
| Ac | Alternating current |
| ADP | Adenosine diphosphate |
| ATP | Adenosine triphosphate |
| basic p-MFC device | A p-MFC device containing Chlorella vulgaris, a potassium ferricyanide mediator and ITO anode |
| BDD | Boron doped diamond electrode |
| BPV | Bio-Photo-Voltaic Device, a less commonly used name for a p-MFC device |
| *C. vulgaris* | *Chlorella vulgaris* |
| cyt C | Cytochrome C |
| Cytb6f | Cytochrome b6f complex |
| DAD | Diaminodurene |
| dc | Direct current |
| DCIP | 2,6-dichloroindolphenol |
| DMBQ | 2,6-dimethyl-1,4-benzoquinone |
| ECM | Extra cellular matrix |
| FAD/FADH2 | Flavin adenine dinucleotide |
| Fd | Ferredoxin |
| ferricyanide | Potassium ferricyanide |
| FNR | Ferredoxin $NADP^+$ oxidoreductase |
| FTO | Fluorine doped tin oxide coated glass |
| HNQ | 2-hydroxy-1,4-naphthoquinone |
| HOMO | Highest occupied molecular orbital |
| ITO | Indium doped tin oxide coated glass |
| LUMO | Lowest unoccupied molecular orbital |
| MFC | Microbial fuel cell |
| NADH | Nicotinamide adenine dinucleotide |
| NADP+/NADPH | Nicotinamide adenine dinucleotide phosphate |
| P | Inorganic phosphate |
| PAM | Pulse amplitude modulation fluorescence |
| PANI | Polyaniline |

| | |
|---|---|
| PC | Plastocyanin |
| PEM | Proton exchange membrane |
| p-MFC | Photosynthetic microbial fuel cell |
| PolyP | Polypyrrole |
| PQ | Plastoquinone |
| PSI | Photosystem I |
| PSII | Photosystem II |
| RDE | Rotating disk electrochemistry |
| RuBP | Ribulose-1,5-bisphosphate |
| SECM | Scanning electrochemical microscopy |
| SEM | Scanning electron microscopy |
| UME | Ultra microelectrode |

## x.6 Acknowledgements

I would like to take this opportunity to thank Dr Petra Cameron, who has been invaluable in support, ideas, inspiration and guidance. I wish her well in her illustrious academic career. Other people imperative to the success of this work include Professor Laurie Peter, Dr Andrew Dent and Dr Guy Denault. Without Dr Andrew Dent and Dr Guy Denault the ceramics work and the SECM experiments would not have been possible. Additionally, I would like to thank the rest of the group (Dr. Huaining Hu, Eleanor Johnson, Kenneth Schneider, Shane McDonald, Kathryn Wills and Thomas Risbridger); I could not have asked for a nicer group of people to work with. Thanks also to my other amazing friends (you know who you are) for making the last three years so much fun and leaving me with so many happy memories of Bath.

Most of all I would like to thank my mum Sue Thorne, my dad Mike Thorne, my sister Jenny Thorne and my super boyfriend Vegar Øygarden. You have all been there to share the good times with me, and put up with me during the stressed out (harder) times - Much love to you all.

## x.7 Declaration of work performed in conjunction with others

A small amount of work was performed in conjunction with others. Where collaboration occurred, all experimental planning, calculations and data analysis shown in this thesis were performed by the author.

1. Chapter 4 – UV-Vis spectroscopy on 1mM potassium ferricyanide (ferricyanide) and 7.69 x $10^7$ cells $ml^{-1}$ *C. vulgaris* cells was performed by William Doble (a Masters student), under close supervision by the author.
2. Chapter 6 – UV-Vis spectroscopy of 1mM ferricyanide and 7 x $10^7$ *Synechocystis* cells $ml^{-1}$, toxicity tests of *Synechocystis* with varying concentrations of ferricyanide and chronoamperometry experiments of *Synechocystis* and ferricyanide was performed by Rupert Cape (a Masters student), under close supervision by the author.
3. Chapter 7 – UV-Vis spectroscopy of cytochrome C solutions and *C. vulgaris* was preformed by William Doble (a Masters student), under close supervision by the author.
4. Chapter 8 – The polarisation curves shown were performed in collaboration with Dr. Huaining Hu.
5. Chapter 9 – SECM work was performed in collaboration with Kenneth Schneider and Guy Denault at the University of Southampton.

## x.8 Abstract

Photosynthetic Microbial Fuel Cell (p-MFC) research aims to develop devices containing photosynthetic micro-organisms to produce electricity. Micro-organisms within the device photosynthesise carbohydrates under illumination, and produce reductive equivalents (excess electrons) from both carbohydrate production and the subsequent carbohydrate break down. Redox mediators are utilised to shuttle electrons between the organism and the electrode. The mediator is reduced by the micro-organism and subsequently re-oxidised at the electrode. However this technology is in its early stages and extensive research is required for p-MFC devices to become economically viable.

A basic p-MFC device containing a potassium ferricyanide mediator and the algae *Chlorella vulgaris* was assembled and tested. From these initial experiments it was realised that much more work was required to characterise cell and redox mediator activities occurring within the device. There is very little p-MFC literature dealing with cellular interaction with redox mediators, but without this knowledge the output of complete p-MFC devices can not be fully understood. This thesis presents research into the reduction of redox mediators by the micro-organisms, including rates of mediator reduction and factors affecting the rate. Both electrochemical and non-electrochemical techniques are used and results compared. Additionally, cellular effects relating to the presence of the mediator are studied; crucial to provide limits within which p-MFCs must be used. After basic characterisation, this thesis presents work into the optimisation of the basic p-MFC. Different redox mediators, photosynthetic species and anodic materials are investigated. Importantly, it is only through fundamental characterization to improve understanding that p-MFCs can be optimised.

# Chapter 1. Introduction

# Chapter 1. Introduction

International consensus has finally been reached that anthropogenic $CO_2$ emissions, in combination with $H_2O$ vapour and other gases, are causing climate change [1]. Additionally, issues surrounding energy security such as fluctuating oil prices, depletion of fossil fuel resources and geopolitical tensions have led to sustainable energy becoming the single most important issue of the 21st century [2]. Many legislative targets have been introduced to initiate the shift from fossil fuels to clean, efficient fuels; in the UK, an EU directive states that 15 % of energy delivered to consumers, and 10 % of energy used in surface transport must come from renewable sources by 2020 [3].

Amongst the sustainable resources available to us, the largest by far and the most convenient source to utilise for several reasons is solar energy. The sun continuously provides the Earth with a huge amount of energy; more solar energy reaches the Earth's surface every hour ($4.3 \times 10^{20}$ J) than is consumed on the planet in a year ($4.1 \times 10^{20}$ J) [4]. Additionally, it is fairly distributed. However, the potential as a clean, abundant and economical energy source cannot be exploited unless it is converted to useful forms of energy. Although many promising artificial devices such as silicon solar cells have been developed, general issues with many such technologies include sustainability, high cost of raw materials and production and limited operational lifetime [5]. These are key issues that prevent wider utilisation of large-scale solar power generation.

One solution to this is to utilise natural photosynthetic organisms. Photosynthetic species are highly adapted to convert solar energy to chemical energy, and their huge abundance on the planet gives great scope as an alternative way to capture energy from renewable sources [6]. According to Ragauskas *et al.,* [7], it is likely that bioenergy in some form will make up a considerable share of sustainable renewable energy in the future. The main strategy for harnessing solar energy with photosynthetic organisms to date has been to use them in the production of biofuels; fuels made from organic matter [3, 8]. In 2009 2.4 % of the UKs surface transport energy was obtained from biofuels derived from 'first generation' landcrops [3]. Whilst biofuels produced using oil crops and waste oils have a similar environmental

impact to the combustion of fossil fuels [9], and compete with water and food production for land useage [3, 8, 9], biofuels produced from microalgae (including algae and cyanobacteria) present a more promising feedstock option. Microalgae have faster growth rates than higher plants, higher photosynthetic efficiencies, higher $CO_2$ fixation, higher $O_2$ production and can be grown on non-arable land [8]. Using microalgae, a variety of fuels could potentially be produced for transport, heating or electricity generation including biodiesel, aviation fuel and biogas [3]. Although still in the development stage and not yet commercially viable, many major companies have invested in microalgae biofuels including Airbus, ExxonMobil and the US Navy [3]. However, a major barrier to implementation is cost. One solution to make algal biofuels more cost effective is by extracting other valuable products from algae or incorporating their production into waste water treatment [3, 8, 9].

Aside from biofuel production, another use of microalgae is to utilise them in a bio-photo-Voltaic Solar Cell (far more commonly known as a photosynthetic-microbial fuel cell or p-MFC, and referred as this throughout the thesis) [10-14] for the production of electrical energy. Traditionally, microbial fuel cells (MFCs) traditionally contain non-photosynthetic microbes (*i.e.* bacteria) and rely on metabolic activity to convert chemical energy in organic and inorganic matter to electrical energy. However, using microalgae in a MFC has become more popular in recent years due to their carbon neutral behaviour. [15]. The discovery that microbes in a MFC can even produce electricity from waste biomass and remediate waste in the process has led to a dramatic increase of interest in the technology in recent years [16].

It is likely that if any type of bioenergy is to succeed, combined function is required. If MFC technology were to be used together with that for waste remediation and the production of biofuels, renewable energy from microalgae would be far more economical.

## 1.1 Microbial and photo-Microbial Fuel Cells

Although configurations vary, MFCs typically contain an anodic chamber separated from a cathodic chamber by a proton exchange membrane (PEM), as shown in figure 1. The anodic chamber is usually anaerobic and contains a high surface area anode on

which a bacterial biofilm grows. The bacteria catabolise (break down) organic molecules which are added to the electrolyte and reductive equivalents (electrons) are produced as a result. These electrons can be transferred from the bacteria to the anode, which can act as the terminal electron acceptor in the redox chain. Protons produced during anaerobic digestion diffuse across the PEM and are reduced to water in the presence of oxygen at the cathode [12, 17, 18]. Although efficiencies are relatively high (over 90 % of electrons from organic compounds can be harvested [12]), a drawback is the net production of carbon dioxide from these devices, due to bacterial respiration.

MFCs containing photosynthetic microbes are less common, but rely on the same principles as MFCs containing bacteria. In a photosynthetic microbial fuel cell (a p-MFC, shown in figure 2), micro-organisms can also donate electrons to the anode through processes thought to include catabolism and photosynthesis [19-22]. Unlike the bacteria in MFCs they do not need to be fed organic substrates, rather they photosynthesise carbohydrates under illumination. This makes the p-MFC device extremely attractive as a self-sustainable way to create energy. In addition, due to photosynthetic carbon sequestration, they also offer the possibility of the production of carbon neutral energy.

Previous work has used tremendously varied photosynthetic material in the anodic chamber. This can be generally classified into four groups; sub-cellular, prokaryotic (cyanobacteria), eukaryotic (algae), and mixed systems. Use of sub-cellular organelles has included thylakoid membranes [23], photosystems (PS1 and PS2) [24, 25][7], bacterial reaction centres [26] and isolated chlorophyll and its derivatives [27]. However, lifetimes of p-MFCs incorporating organelles are short as organelles cannot self-repair. This is a major disadvantage, and makes the use of whole cells highly advantageous [28].

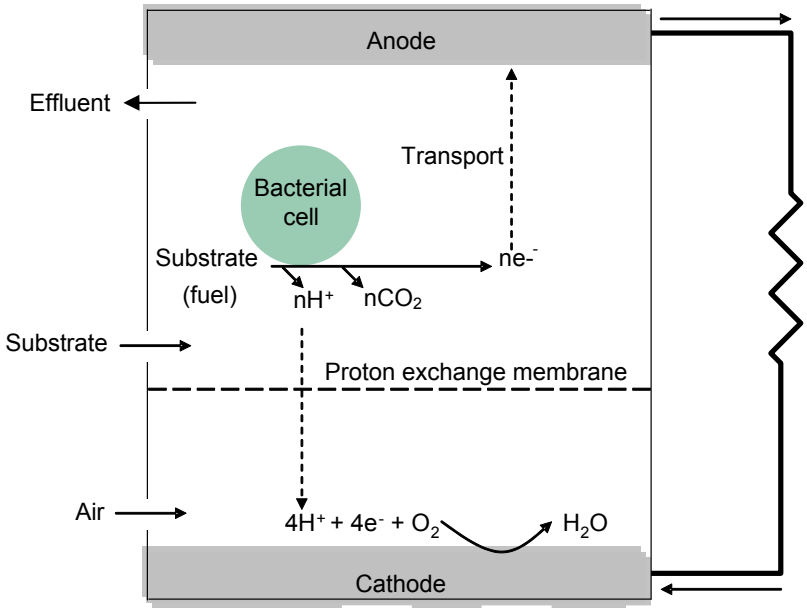


**Figure 1 Typical two chambered MFC: Electron flow from the break down of a substrate to the anode (via a transport step), and consequently to the cathode is shown. A typical substrate reaction occurring at the anode (using acetate as an example) is $CH_3COO^- + 2H_2O \rightarrow 2CO_2 + 7H^- + 8e^-$. Depending on the substrate, different stoichiometries of H, $CO_2$ and $e^-$ can be produced, represented in the figure by 'n'.**

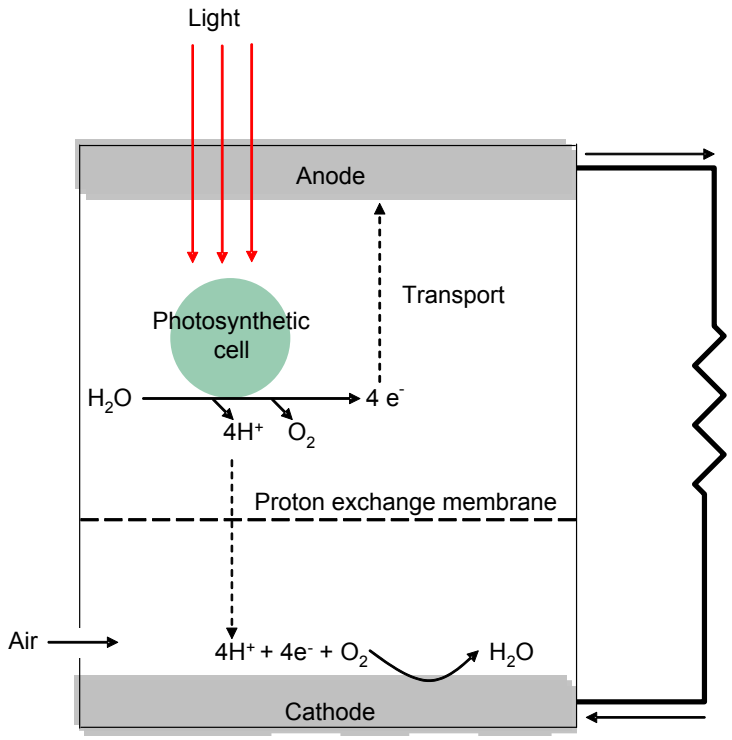


**Figure 2 Typical two chambered p-MFC: Electron flow from the splitting of water to the anode (via a transport step), through an external circuit and to the cathode is shown.**

Evidently, a p-MFC device relies on two main steps to produce energy. The first step involves the production of reductive equivalents (electrons) by the cell. Secondly, these must be passed to the anode in the device. These are now discussed in turn.

## 1.2 First step - Source of Electrons in a p-MFC

Whereas bacteria in a MFC only produce reductive electrons via the catabolism of carbohydrates, an additional process performed by the organisms in a p-MFC (thought to contribute extra electrons for power generation) is photosynthesis [19] [29-31]. However, the literature is unclear about the relative contributions of each process, leaving much to be learned. Due to the underlying reliance on catabolism and photosynthesis to provide the electrons which power a MFC, these processes are first discussed. Two types of catabolism and photosynthesis exist; oxygenic and anoxygenic, with slight variation existing between eukaryotic and prokaryotic organisms. However, oxygenic processes occurring in eukaryotic organisms are focussed upon as only oxygenic systems (and mostly eukaryotic organisms) are studied in this thesis.

*Photosynthesis*

Solar energy capture and conversion into chemical energy and biopolymers by photoautotrophic organisms is the basis for almost all life on Earth. Photosynthesis, (equation 1) occurring within the chloroplasts of a cell, is known to consist of a light dependent reaction, whereby adenosine triphosphate (ATP) is produced from adenosine diphosphate (ADP) and inorganic phosphate (P) and hydrogen harvested, and a light independent reaction whereby carbon dioxide is reduced to carbohydrate [32]. Other related reactions occur in the surrounding cytosol and mictochondria, as depicted by Kruse *et al.* in figure 3 [32].

$$6H_2O + 6CO_2 \rightarrow C_6H_{12}O_6 + 6O_2$$

**Equation 1 A general equation for photosynthesis; in the process water and carbon dioxide are turned into carbohydrate and oxygen**

Light dependent reactions take place in the chloroplast thylakoid membrane, and are driven by light captured by antenna proteins bound to photosystems. The photosystems co-operatively absorb and funnel light energy to a primary pigment

which acts as the reaction center. Two photosystems exist, photosystem I (PSI) and photosystem II (PSII). The reaction centre of PSI is composed of a dimer of chlorophylls (one molecule of chlorophyll a and one molecule of chlorophyll a'), and has an absorption peak at 700 nm. PSII contains a primary pigment of chlorophyll b, and possesses an absorption maximum of 680 nm. In non-cyclic photophosphorylation, when light is absorbed by PSI and PSII, electrons in the chlorophyll molecule are boosted to higher energy levels, before being emitted and passed on to electron carriers. The loss of electrons from PS II causes the splitting of water, with the electrons used to re-reduce PSII. In effect, electrons are passed via redox active species down the potential gradient. The system is also known as a 'Z scheme'. Redox centres along the electron transfer chain include plastoquinone (PQ), the cytochrome b6f (Cytb6f) complex, plastocyanin (PC), photosystem I (PSI) and ferredoxin (Fd) [32]. Finally, ferredoxin $NADP^+$ oxidoreductase (FNR) uses the electrons for the reduction of nicotinamide adenine dinucleotide phosphate from its oxidized form, $NADP^+$, to NADPH (equation 2) [32].

$$NADP + 2H + 2e^- \rightarrow NADPH + H$$

**Equation 2 The reduction of NADP**

As electrons are passed down energy levels, energy is released which can be used to form ATP. A pH gradient is produced by PSII and the $PQ/PQH_2$ cycle through the release of protons from the stroma into the thylakoid lumen [32]. As the hydrogen ions diffuse back down the concentration gradient they flow through proteins. Part of each protein is ATP synthetase, driving ATP production [32].

If large amounts of NADPH exist, cyclic phosphorylation can occur and electrons from the electron transport chain drive cyclic electron transport around PSI. The electron from PSI is passed to the electron carriers used in PSII. ATP is formed and the electrons return to PSI to fill the space, making PSII redundant. Depending on conditions, electrons can also reduce protons to molecular hydrogen or reduce oxygen to water through the Mehler reaction [24].

The light independent reactions occur in the stroma of chloroplasts in light or dark, and require previously generated ATP for energy and NADPH for reducing power. In

the Calvin cycle, carbon dioxide is first combined with the sugar ribulose-1,5-bisphosphate RuBP, as catalysed by rubisco [32]. This is converted to triose phosphates which are used to regenerate RuBP and produce other sugars ( ultimately starch) [32].

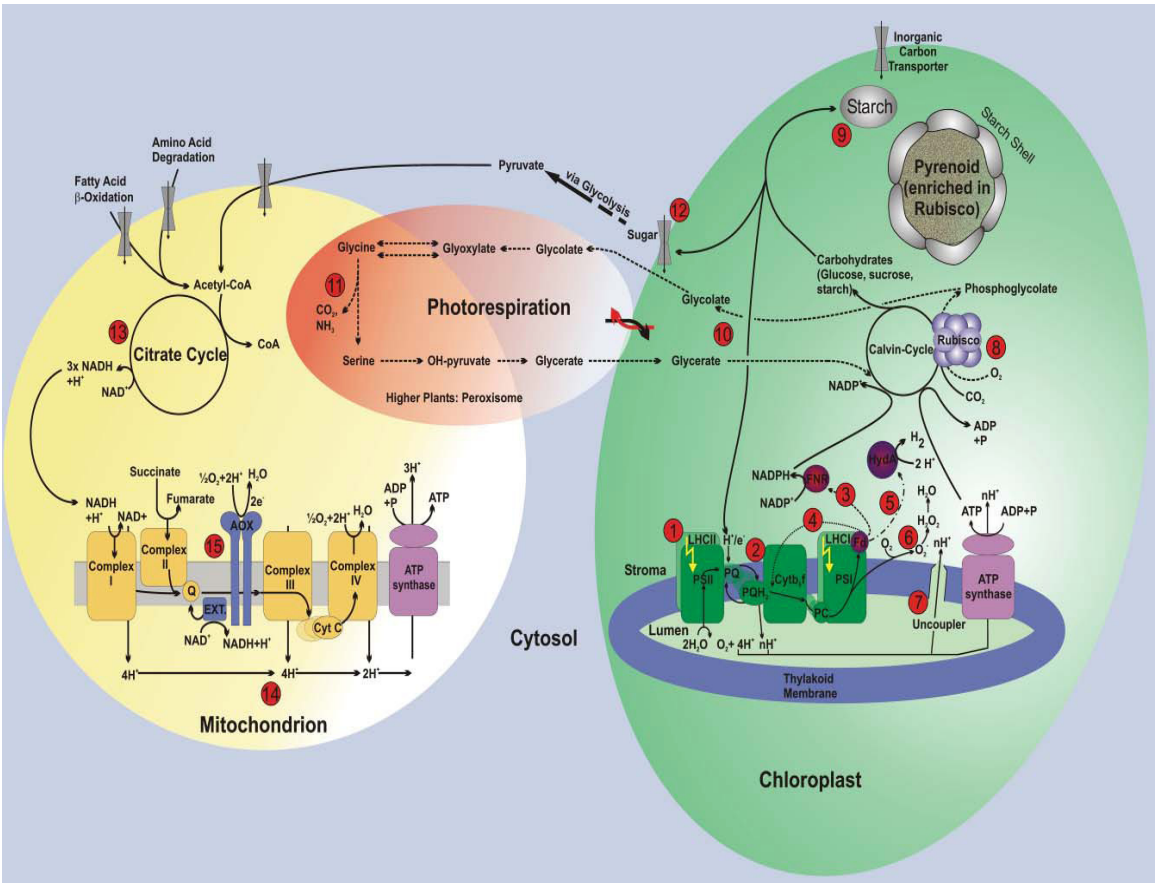


**Figure 3 Reproduced from [32] Biochemical pathways related to photon conversion efficiency in eukaryotic organisms. Prokaryotic pathways are similar, but often utilise other pigments**

*Respiration*

Following photosynthesis whereby solar energy is stored as chemical energy in organic molecules, respiration can occur (equation 3). In this process, molecules are broken down and energy is released in a regulated manner for the production of ATP, the universal currency of biological energy transformations, and reducing power (e.g. Nicotinamide adenine dinucleotide (NADH) and NADPH) [33]. In aerobic respiration, the main processes include glycolysis, the citrate cycle and oxidative phosphorylation.

$$C_6H_{12}O_6 + 6O_2 \rightarrow 6H_2O + 6CO_2$$

**Equation 3 A general equation for respiration; in the process carbohydrate is broken down and water and carbon dioxide are produced**

The first stage of respiration, located in the cell cytoplasm, involves glycolysis, whereby sugars are split to pyruvic acid and reduced NAD (NADH) is formed. If oxygen is available, pyruvic acid enters the mitochondrion where a link reaction occurs and acetyl CoA is formed along with further reduced NAD (NADH). Subsequently, during the citrate pathway, reduced NAD (NADH) and reduced flavin adenine dinucleotide FAD ($FADH_2$) are produced along with ATP. Finally, ATP is produced from the reduced species NADH and $FADH_2$ according to chemiosmotic theory. Similar to photosynthesis, electrons flow down an electron transport chain from low to high redox potential during oxidative phosphorylation and ATP is produced from proton gradients. The flow of electrons is used to create a proton gradient (protonmotive force) across the cell membrane as described by Mitchell [34]. By creating this proton gradient, the potential difference between the electron donor and the electron acceptor is turned into a process for the generation of energy. Energy is released by the inward flux of the protons through the membrane complex ATP synthase and used to regenerate energy carrier molecules such as ATP. Microbes use a large variety of different electron acceptors, including oxygen and iron, but using the acceptor with the highest redox potential increases energy for growth [35].

If no oxygen is present, the citrate cycle and electron transport chain do not function. Other pathways are utilised; for example, in plants, pyruvic acid is converted to ethanol. However, these conditions are outside the scope of this thesis.

## 1.3 Second step - Electron Transfer from Cell to Anode

Once produced, electrons are required to be siphoned from their normal activities and deposited at the anode for power to be produced. Importantly, relatively little is known about specific details of these processes. From the description given in section 1.1 of the biological processes involved, it is apparent that large amounts of reduced material is produced, any of which could potentially contribute reducing power in a MFC. However, from studies performed by Yagishita *et al.,* it has been speculated that electrons are collected from their normal photosynthetic duties either from NADPH or the electron transport chain [19]. Despite the large amount of uncertainty associated with it, the anodic electron transfer mechanism is, according to Du *et al.*,

the key issue for optimising a MFC or p-MFC, with efficiencies vastly affected as a result [12, 15].

To summarise, two principle transfer methods exist. The first type involves microbes (such as *Shewanella* [36-39]) that can directly transfer electrons to the anode via a conductive extracellular matrix involving pili and cytochrome c (cyt C) proteins, as shown in figure 4. In these systems, the key difference with natural biogeochemical processes is that electrons are transferred to an electrode rather than a natural electron acceptor. This requires cells to be grown directly on the anodic surface in biofilms. The huge complexity of biofilm structures (involving, for example, quorum sensing) is outside the scope of this thesis, but should be noted. Direct electron transfer is thought to be protein mediated, possibly via cytochromes in the extracellular matrix (ECM) or bacterial conductive nanowires [21, 22]. However, this research is still in early stages and few additional specifics are known. In one study, some cyanobacteria were been observed to perform direct electron transfer [40], although few other studies could be identified to corroborate this finding.

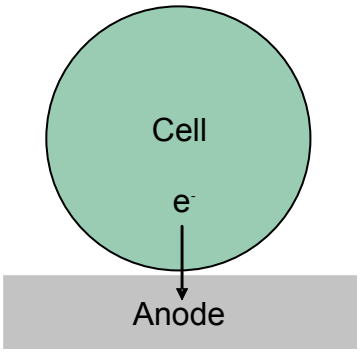


**Figure 4 Schematic of direct transfer of electrons from cells grown in a biofilm to the anode**

Most microbial species have outer layers composed of a non-conductive lipid membrane (consisting of peptidoglycans and lipopolysaccharides) and so cannot perform direct electron transfer (long-range charge transfer) when grown on an electrode surface. Consequently, redox mediators (natural or synthetic) are required, to shuttle electrons from the biological material to the anode [41]. This accelerates the transfer of electrons, makes the use of certain microbial species possible and if the redox mediator is dissolved in solution, cells can be planktonic (whilst still allowing anodic electron transfer to occur) [12]. In these systems, cellular constituents act as

the source of electrons. For example, the reduced form of NAD is NADH, which can serve as a source of electrons to generate power in an MFC [29-31][8]. The majority of p-MFCs use non-natural redox mediators to shuttle electrons between the organism and the electrode [19, 20, 42, 43]. The addition of redox mediators is not ideal, but can be justified if the p-MFC is a closed system and constant addition of fresh mediator is not required [20]. Alternatively a surface immobilised redox system can be employed, again on the condition that it is stable for the life time of the device. However, in efficient MFCs no non-natural redox mediators are added. Bacterial colonies that secrete naturally occurring redox mediators are used [44].

Mediators are thought to interact with cells in a variety of ways as shown in figure 5. Most mediators are hypothesised to cross the cell membrane and accept electrons from one or more electron carriers within the cell, before exiting the cell in a reduced form and transferring electrons to the electrode surface [12] For example, the main coupling sites of a 2-hydroxy-1,4-naphthoquinone (HNQ) mediator with the electron transport chain was found to be the ferredoxin-$NADP^+$ reductase in the dark, and NAD(P)H dehydrogenase in the dark [29]. Others interact with the cell and its electrons externally. However, in many cases it is not known exactly how the mediator interacts with the cell.

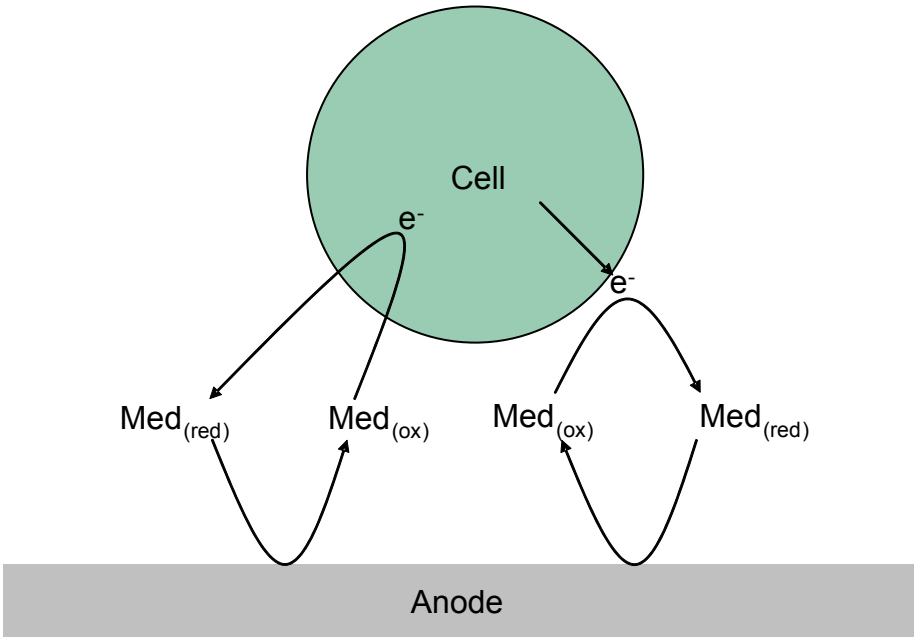


**Figure 5 Schematic illustration of mediated electron transfer via added or self-produced redox mediators**

Currently MFCs can only produce low power outputs (6 W $m^{-2}$ to 500 W $m^{-3}$) [45], and p-MFCs even lower. Many factors limit power output, including the internal electrolyte resistance, the ion-exchange membrane, fuel cell configuration, operation conditions and electrode reaction mechanisms and processes [46]. However major recurrent issues in the literature include the mechanism of electron transfer from microbial cell to anode and the optimisation of electrode materials. It is clear these require development.

## 1.4 Aims and Objectives

The project is based on previous p-MFC device development performed by collaborators at Cambridge University (referred to as the 'basic p-MFC device' throughout this thesis). The system developed by them was a thin cell, utilising live cells of the algae *Chlorella vulgaris* and a potassium ferricyanide (ferricyanide) redox mediator; both in solution. An indium tin oxide (ITO) coated piece of glass acted as working electrode. The initial aim of the project at Bath was to optimise the basic device for power output, longevity and self sufficiency, using the basic design as a starting point. However, preliminary testing of the basic p-MFC device showed that the system was in no state to be optimised (chapter 3). Due to various factors such as device instability, before the system could be advanced, an improvement in basic understanding was required. Consequently, two aims exist for this thesis; improved p-MFC understanding followed by optimisation of the basic p-MFC.

p-MFC literature has vastly neglected how mediators interact with cells, including how and why electrons are extracted from cells. Aside from cell toxicity, any cellular consequences resulting from mediator interactions are generally unstudied. Consequently, a better understanding of electron transfer is required within the basic p-MFC system containing living *C. vulgaris* cells and the ferricyanide redox mediator. To improve understanding, various methods are used in this thesis, both non-electrochemical and electrochemical. In particular, questions include:

1) What processes (photosynthetic or respiratory) specifically contribute electrons for power production in the p-MFC system? (Chapter 4/5)
2) What is the reduction rate of the redox mediator by the algae? (Chapter 4/5)

3) What factors limit reduction of the redox mediator by the algae? (Chapter 5)
4) Do any techniques exist for the in-situ study of algal biofilms? (Chapter 9)

Secondly, the main factor identified in much literature as limiting p-MFC efficiency is the anodic transfer mechanism (anode material, mediator and the photosynthetic cell population) [15]. In this thesis, experiments are performed with different redox mediators and photosynthetic material. Additionally, although many materials had been successfully utilised as the working electrode in a MFC, none have been specifically designed for use with algae in a p-MFC. These have very different requirements. As such, parts of this thesis focus upon the development of porous electrode materials in which to culture biofilms. In this section, questions include:

1) Are there any major differences between the reduction of ferricyanide by the algal species *C. vulgaris* and a cyanobacterial species? (Chapter 6)
2) Can redox mediators other than ferricyanide be found? (Chapter 7)
3) What are the characteristics of the porous electrodes produced? (Chapter 8)
4) Are the produced electrodes biocompatible? (Chapter 8)
5) How do device outputs change as a result of the usage of different electrode materials (FTO on glass, FTO on ceramic, carbon felt, or polyaniline)? (Chapter 8)

In this way, the main areas where previous p-MFC literature is insufficient are addressed, and improvements are made to the original device.

## 1.5 References

1. Doherty, S.J., Bojinski, S., Henderson-Sellers, A., Noone, K., Goodrich, D., Bindoff, N.L., Church, J.A., Hibbard, K.A., Karl, T.R., Kajefez-Bogataj, L., Lynch, A.H., Parker, D.E., Prentice, I.C., Ramaswamy, V., Saunders, R.W., Smith, M.S., Steffen, K., Stocker, T.F., Thorne, P.W., Trenberth, K.E., Verstraete, M.M., and Zwiers, F.W., *Lessons learned from IPCC AR4: Scientific Developments Needed To Understand, Predict, And Respond To Climate Change.* Bulletin of the American Meteorological Society, 2009. **90**(4): p. 497-+.

2. Balzani, V., Credi, A., and Venturi, M., *Photochemical conversion of solar energy.* Chemsuschem, 2008. **1**(1-2): p. 26-58.
3. Dyer-Smith, C., *Biofuels from Algae*, P.O.o.S.a. Technology, Editor. 2011.
4. Zhu, X.G., Long, S.P., and Ort, D.R., *What is the maximum efficiency with which photosynthesis can convert solar energy into biomass?* Current opinion in Biotechnology, 2008. **19**: p. 153-159.
5. Leong, C.S., Amin, N., Sulaiman, M.Y., Zaharim, A., Sopian, K., and Zaidi, S.H. *Some Key Issues In the Processing and Fabrication of Higher Efficiencies Silicon Solar Cells*. in *3rd WSEAS International Conference on Energy Planning, Energy Saving, Environmental Education*. 2009. Tenerife, Spain: World Scientific and Engineering Acad and Soc.
6. Cho, Y.K., Donohue, T.J., Tejedor, I., Anderson, M.A., McMahon, K.D., and Noguera, D.R., *Development of a solar-powered microbial fuel cell.* Journal of Applied Microbiology, 2008. **104**(3): p. 640-650.
7. Ragauskas, A.J., Williams, C.K., Davison, B.H., Britovsek, G., Cairney, J., Eckert, C.A., Frederick, W.J., Hallett, J.P., Leak, D.J., Liotta, C.L., Mielenz, J.R., Murphy, R., Templer, R., and Tschaplinski, T., *The path forward for biofuels and biomaterials.* Science, 2006. **311**(5760): p. 484-489.
8. Gouveia, L. and Oliveira, A.C., *Microalgae as a raw material for biofuels production.* Journal of Industrial Microbiology & Biotechnology, 2009. **36**(2): p. 269-274.
9. Li, Y., Horsman, M., Wu, N., Lan, C.Q., and Dubois-Calero, N., *Biofuels from microalgae.* Biotechnology Progress, 2008. **24**(4): p. 815-820.
10. Angenent, L.T., Karim, K., Al-Dahhan, M.H., and Domiguez-Espinosa, R., *Production of bioenergy and biochemicals from industrial and agricultural wastewater.* Trends in Biotechnology, 2004. **22**(9): p. 477-485.
11. Lewis, N.S. and Nocera, D.G., *Powering the planet: Chemical challenges in solar energy utilization.* Proceedings of the National Academy of Sciences of the United States of America, 2006. **103**(43): p. 15729-15735.
12. Lovley, D.R., *Bug juice: harvesting electricity with microorganisms.* Nature Reviews Microbiology, 2006. **4**(7): p. 497-508.
13. de Schamphelaire, L., van den Bossche, L., Dang, H.S., Hofte, M., Boon, N., Rabaey, K., and Verstraete, W., *Microbial fuel cells generating electricity*

*from rhizodeposits of rice plants.* Environmental Science & Technology, 2008. **42**(8): p. 3053-3058.

14. Strik, D., Terlouw, H., Hamelers, H.V.M., and Buisman, C.J.N., *Renewable sustainable biocatalyzed electricity production in a photosynthetic algal microbial fuel cell (PAMFC).* Applied microbiology and biotechnology., 2008. **81**(4): p. 659-668.
15. Du, Z.W., Li, H.R., and Gu, T.Y., *A state of the art review on microbial fuel cells: A promising technology for wastewater treatment and bioenergy.* Biotechnology Advances, 2007. **25**: p. 464-482.
16. Bond, D.R., Holmes, D.E., Tender, L.M., and Lovley, D.R., *Electrode-reducing microorganisms that harvest energy from marine sediments.* Science, 2002. **295**(5554): p. 483-485.
17. Park, D.H. and Zeikus, J.G., *Electricity generation in microbial fuel cells using neutral red as an electronophore.* Applied and Environmental Microbiology, 2000. **66**(4): p. 1292-1297.
18. Strik, D., Terlouw, H., Hamelers, H.V.M., and Buisman, C.J.N., *Renewable sustainable biocatalyzed electricity production in a photosynthetic algal microbial fuel cell (PAMFC).* Applied Microbiology and Biotechnology, 2008. **81**(4): p. 659-668.
19. Chiao, M., Lam, K.B., and Lin, L.W., *Micromachined microbial and photosynthetic fuel cells.* Journal of Micromechanics and Microengineering, 2006. **16**(12): p. 2547-2553.
20. Rosenbaum, M. and Schröder, U., *Photomicrobial Solar and Fuel Cells.* Electroanalysis, 2010. **22**(7-8): p. 844-855.
21. Tsujimura, S., Wadano, A., Kano, K., and Ikeda, T., *Photosynthetic bioelectrochemical cell utilizing cyanobacteria and water-generating oxidase.* Enzyme and Microbial Technology, 2001. **29**(4-5): p. 225-231.
22. Ryu, W., Bai, S.J., Park, J.S., Huang, Z.B., Moseley, J., Fabian, T., Fasching, R.J., Grossman, A.R., and Prinz, F.B., *Direct Extraction of Photosynthetic Electrons from Single Algal Cells by Nanoprobing System.* Nano Letters, 2010. **10**(4): p. 1137-1143.
23. Lam, K.B., Johnson, E.A., Chiao, M., and Lin, L.W., *A MEMS photosynthetic electrochemical cell powered by subcellular plant photosystems.* Journal of Microelectromechanical Systems, 2006. **15**(5): p. 1243-1250.

24. Maly, J., Masojidek, J., Masci, A., Ilie, M., Cianci, E., Foglietti, V., Vastarella, W., and Pilloton, R., *Direct mediatorless electron transport between the monolayer of photosystem II and poly (mercapto-p-benzoquinone) modified gold electrode-new design of biosensor for herbicide detection.* Biosensors & Bioelectronics, 2005. **21**(6): p. 923-932.

25. Badura, A., Esper, B., Ataka, K., Grunwald, C., Woll, C., Kuhlmann, J., Heberle, J., and Rogner, M., *Light-driven water splitting for (bio-)hydrogen production: photosystern 2 as the central part of a bioelectrochemical device.* Photochemistry and Photobiology, 2006. **82**(5): p. 1385-1390.

26. Janzen, A.F. and Seibert, M., *Photoelectrochemical conversion using reaction-center electrodes.* Nature, 1980. **286**(5773): p. 584-585.

27. Amao, Y. and Komori, T., *Bio-photovoltaic conversion device using chlorine-e(6) derived from chlorophyll from Spirulina adsorbed on a nanocrystalline TiO2 film electrode.* Biosensors & Bioelectronics, 2004. **19**(8): p. 843-847.

28. Malik, S., Drott, E., Grisdela, P., Lee, J., Lee, C., Lowy, D.A., Gray, S., and Tender, L.M., *A self-assembling self-repairing microbial photoelectrochemical solar cell.* Energy & Environmental Science, 2009. **2**(3): p. 292-298.

29. Yagishita, T., Sawayama, S., Tsukahara, K.I., and Ogi, T., *Effects of intensity of incident light and concentrations of Synechococcus sp. and 2-hydroxy-1,4-naphthoquinone on the current output of photosynthetic electrochemical cell.* Solar Energy, 1997. **61**(5): p. 347-353.

30. Yagishita, T., Sawayama, S., Tsukahara, K., and Ogi, T., *Effects of glucose addition and light on current outputs in photosynthetic electrochemical cells using Synechocystis sp PCC6714.* Journal of Bioscience and Bioengineering, 1999. **88**(2): p. 210-214.

31. Yagishita, T., Horigome, T., and Tanaka, K., *Effects of light, $CO_2$ and inhibitors on the current output of biofuel cells containing organism Synechococcus Sp.* Journal of Chemical Technology and Biotechnology, 1993. **56**(4): p. 393-399.

32. Kruse, O., Rupprecht, J., Mussgnug, J.H., Dismukes, G.C., and Hankamer, B., *Photosynthesis: a blueprint for solar energy capture and biohydrogen production technologies.* Photochemical & Photobiological Sciences, 2005. **4**(12): p. 957-970.

33. Gonzelez-Meller, M.A., Taneva, L., and Trueman, R.J., *Plant respiration and elevated atmospheric CO(2) concentration: Cellular responses and global significance.* Annals of Botany, 2004. **94**(5): p. 647-656.

34. Mitchell, P., *Coupling of phosphorylation to electron and hydrogen transfer by a chemi-osmotic type of mechanism.* Nature, 1961. **191**(478): p. 144-&.

35. Madigan, M.T., *Extremophilic bacteria and microbial diversity.* Annals of the Missouri Botanical Garden, 2000. **87**(1): p. 3-12.

36. Gorby, Y.A., Yanina, S., McLean, J.S., Rosso, K.M., Moyles, D., Dohnalkova, A., Beveridge, T.J., Chang, I.S., Kim, B.H., Kim, K.S., Culley, D.E., Reed, S.B., Romine, M.F., Saffarini, D.A., Hill, E.A., Shi, L., Elias, D.A., Kennedy, D.W., Pinchuk, G., Watanabe, K., Ishii, S., Logan, B., Nealson, K.H., and Fredrickson, J.K., *Electrically conductive bacterial nanowires produced by Shewanella oneidensis strain MR-1 and other microorganisms (vol 103, pg 11358, 2006).* Proceedings of the National Academy of Sciences of the United States of America, 2009. **106**(23): p. 9535-9535.

37. Lovley, D.R., *Extracellular electron transfer: wires, capacitors, iron lungs, and more.* Geobiology, 2008. **6**(3): p. 225-231.

38. Bond, D.R. and Lovley, D.R., *Electricity production by Geobacter sulfurreducens attached to electrodes.* Applied and Environmental Microbiology, 2003. **69**(3): p. 1548-1555.

39. Reguera, G., McCarthy, K.D., Mehta, T., Nicoll, J.S., Tuominen, M.T., and Lovley, D.R., *Extracellular electron transfer via microbial nanowires.* Nature, 2005. **435**(7045): p. 1098-1101.

40. Pisciotta, J.M., Zou, Y., and Baskakov, I.V., *Light-Dependent Electrogenic Activity of Cyanobacteria.* Plos One, 2010. **5**(5).

41. Davis, F. and Higson, S.P.J., *Biofuel cells - Recent advances and applications.* Biosensors & Bioelectronics, 2007. **22**(7): p. 1224-1235.

42. Fu, C.-C., Su, C.-H., Hung, T.-C., Hsieh, C.-H., Suryani, D., and Wu, W.-T., *Effects of biomass weight and light intensity on the performance of photosynthetic microbial fuel cells with Spirulina platensis.* Bioresource Technology, 2009. **100**(18): p. 4183-4186.

43. Rosenbaum, M., Schröder, U., and Scholz, F., *Utilizing the green alga Chlamydomonas reinhardtii for microbial electricity generation: a living solar cell.* Applied Microbiology and Biotechnology, 2005. **68**(6): p. 753-756.

44. Bond, D.R. and Lovley, D.R., *Evidence for involvement of an electron shuttle in electricity generation by Geothrix fermentans.* Applied and Environmental Microbiology, 2005. **71**(4): p. 2186-2189.

45. Zhao, F., Slade, R.C.T., and Varcoe, J.R., *Techniques for the study and development of microbial fuel cells: an electrochemical perspective.* Chemical Society Reviews, 2009. **38**(7): p. 1926-1939.

46. Rismani-Yazdi, H., Carver, M., Christy, A.D., and Tuovinen, O.H., J Power Sources, 2008. **180**: p. 683-694.

# Chapter 2. Theory

# Chapter 2 - Theory

Analytical techniques used to study p-MFCs can be both electrochemical and non-electrochemical. In this chapter, the theory behind these techniques is discussed.

## 2.1 Electrochemical Theory

Electrochemical techniques have an essential role in understanding mechanisms (microbial, physiological, chemical and electron transport) involved in p-MFCs, and in identifying limitations with each component. This section begins by fully exploring the fundamentals of electrochemistry, before main techniques are discussed with specific reference to p-MFC study.

### 2.11 Electrode reaction mechanisms and processes

Typically, electrochemistry is the study of electron transfer reactions between electrodes and a reactant, an example of which is given in equation 1 (referred back to throughout the section). This can only proceed once an electrode has been inserted into the solution to provide a supply or sink of electrons.

$$O_{(aq)} + ne_{(m)}^{-} \leftrightarrow R_{(aq)}$$

**Equation 1 An example of a typical redox reaction, where O is the oxidised form and R is the corresponding reduced form of a redox couple. Oxidation involves the loss of electrons, and reduction the gain of electrons**

As electrode processes involve the transfer of charge across the interface between two phases, as the electron transfer reaction moves towards equilibrium, a net charge separation develops. This creates a potential difference at the electrode/solution interface, given by equation 2

$$\Delta\phi_{m/s} = \phi_m - \phi_s$$

**Equation 2 The potential drop across the electrode/solution interface ($\phi_{m/s}$), where $\phi_m$ is the metal potential and $\phi_s$ is the solution potential (both in V)**

To measure this, a complete conducting circuit is required. In addition to the primary (working) electrode, a second, reference electrode is introduced which maintains a

constant potential drop across its interface with the solution (under normal conditions). Equation 3 illustrates the potential difference between the reference electrode and the working electrode. In practice, the potential difference between the electrodes is measured within an electrochemical cell composed of two half cells, separated by a porous membrane/salt bridge. The redox species of interest, O/R, is contained in one half cell with the working electrode, with the reference electrode positioned in the other half cell. Providing no net current flows equilibrium is reached and the working electrode holds its equilibrium potential for the half cell ($E_{eq}$).

$$E = (\phi_m - \phi_s) + c$$

**Equation 3 Potential difference (V) between two electrodes, where the bracketed term relates to the working electrode and c (constant) refers to the reference electrode**

The Nernst equation describes the potential established at the working electrode under equilibrium conditions for the half cell (with respect to a reference electrode), and is shown in equation 4. Here, $E_{eq}=E^o$ when [O]=[R], thus when no external potential is applied these conditions exist and forward and reverse rates are equal. Figure 1 shows a schematic of the Standard hydrogen electrode (SHE), and applies the Nernst equation to calculate its equilibrium half cell reduction potential.

$$E_{eq} = E^O + \frac{RT}{nF}\ln\frac{[O]}{[R]}$$

**Equation 4 The Nernst equation, where $E_{eq}$ (V) results from the standard electrode potential $E^O$ (V) of the reaction, and the concentrations of O and R at the electrode surface are the same as their values in bulk solution (under equilibrium conditions), and relate to reactants/products. Strictly, concentrations should be replaced by activities $a_R$ and $a_O$, where $a_X = \gamma_X c_X$ ($\gamma_X$ is the activity coefficient of species X). However, since activity coefficients tend to unity at low concentrations, activities in the Nernst equation are frequently replaced by simple concentrations. In the example it has been assumed that the activity coefficients of O and R are unity (1). The standard electrode potential is that for the case where the half cell of interest has unit activity of all potential determining ions and potential is measured relative to SHE. R = the Universal gas constant (8.415 J $K^{-1}$ $mol^{-1}$), T = temperature (K), n = the number of electrons transferred in one redox step and F = Faraday's constant (96485 C $mol^{-1}$)**

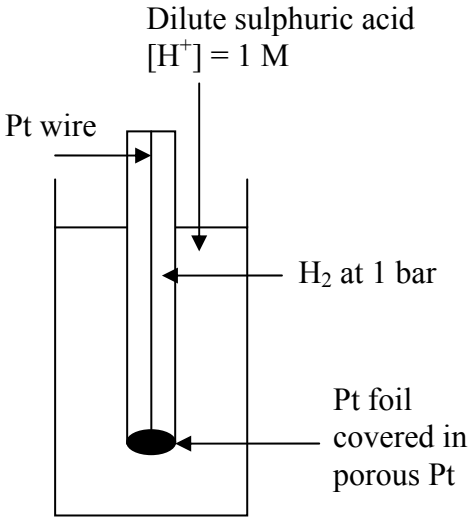


**a)** $H^+ + e^- \leftrightarrow 1/2H_2$

**b)** $p(H_2) = 1bar; a(H_2) = 1$

**c)** $pH(H^+) = 0; a(H^+) = 1$

**d)** $E_{H^+/H_2} = E^o{}_{H^+/H_2} + \frac{RT}{nF}\ln\frac{a_{H^+}}{a_{H_2}}$

$E_{H^+/H_2} = E^o{}_{H^+/H_2} = 0$

**Figure 1 A schematic of the standard hydrogen electrode, with the half cell reaction given in equation a), activities of products and reactants given in equations b) and c) respectively (note, activity of metal is taken to be unity), and equilibrium half cell reduction potential calculated by the Nernst equation in equation d).**

The Nernst equation can also be used to calculate the total voltage (electromotive force or $E_{cell}$), for a full electrochemical cell. An example of a typical electrochemical cell is given in equation 5.

**a)** $Zn + Cu(II) \leftrightarrow Zn(II) + Cu$

**b)** $Zn\,|\,Zn(II)_{(aq)}\,\vdots\,Cu(II)_{(aq)}\,|\,Cu$

**c)** $Zn + 2e^- \rightarrow Zn(II)$

**d)** $Cu(II) + 2e^- \rightarrow Cu$

**Equation 5 a) An example of a full electrochemical cell equation b) electrochemical notation, whereby | represents a phase transition from metal to liquid, and ⋮ represents a salt bridge. c) and d) give half reactions for oxidative (anodic) and reductive (cathodic) reactions, of which $E^o$ are -076 V and 0.34 V respectively. Note, it is convention to write all half reactions as reductions.**

The standard cell potential across an electrochemical cell ($E^o_{cell}$) is given by $E^o_{red}$-$E^o_{ox}$. $E^o_{cell}$ of equation 5 is therefore equal to 0.34 V - (-0.76 V) = 1.1 V. As $E^o_{cell}$ is positive, $\Delta G$ (kJ $mol^{-1}$) is negative as $\Delta G = -nFE^o_{cell}$, and the reduction of copper by zinc is spontaneous. When electrodes are added to the Zn and Cu system, there is an immediate potential difference of 1.1 V, before current flows until the potential difference between the electrodes is equalised. Modified values of $E^o_{cell}$ ($E_{cell}$) can be calculated from the Nernst equation, as outlined in equation 6. As the reaction progresses, the concentration of Zn(II) increases and Cu(II) decreases. This makes the

ratio of [Cu(II)] / [Zn(II)] small. Eventually $E_{cell}$ becomes negative and the reaction is not spontaneous any more (each half reaction essentially becomes one way). It is impossible to control the potential difference of the system; no reference is employed, and the flow of current shifts the electrode potentials.

$$E_{cell} = E^{o}{}_{cell} + \frac{RT}{nF}\ln\frac{a_{ox}}{a_{red}}$$

$$E_{cell} = E^{o}{}_{cell} + \frac{RT}{nF}\ln\frac{a_{(Cu(II)}a_{Zn}}{a_{Zn(II)}a_{Cu}}$$

$$E_{cell} \approx E^{o}{}_{cell} + \frac{RT}{nF}\ln\frac{[Cu(II)]}{[Zn(II)]}$$

**Equation 6 Calculation of $E_{cell}$, where it is assumed that the activity of metals is unity.**

The potential of an electrode where a half cell reaction occurs can be controlled by a potentiostat, and monitored against a reference electrode. When a potential difference (E=J/C) is applied to the working electrode of an electrochemical cell, if the potential is different to $E_{eq}$ a net current flows and electrolysis occurs. The exchange of electrons between electrode and solution can be in either direction, forcing a reaction to go to completion or in reverse. In practice, a third, or counter electrode is required, as a reference electrode can only maintain its fixed interfacial potential if the currents flowing through it are small. Subsequently, all current flows mainly between the counter and working electrode, the magnitude of which is given by equation 7.

$$i = nAFj$$

**Equation 7 The magnitude of the current (i in A, 1A=1Cs$^{-1}$) flowing during electrolysis, where A is the electrode area (cm$^2$), and j is the flux of reactant reaching the electrode surface (mol cm$^{-2}$ s$^{-1}$). J is known as the 'rate' of the electrochemical reaction as $j = k_0[O]_0$, where $k_0$ is the heterogeneous rate constant and $[O]_0$ is the concentration of O at the electrode surface. It has been assumed the reaction is first order; this is frequently, but not always, the case.**

The direction of the current flow is governed by the respective energy levels of working electrode and molecules in solution. Electrodes are usually metal, which consist of a lattice of close packed atoms. Electrons within are able to move freely; due to atomic orbital overlap within the lattice; to occupy all energy states up to the Fermi level (the energy level at which the Fermi-Dirac distribution function of an

assembly of fermions is equal to one-half). When an electrode is placed in a solution containing redox ions, electrons flow to equalise the Fermi-levels. The application of a potential to the working electrode serves to increase or decrease the Fermi level in the electrode (figure 2). If the Fermi level ($E_F$) of the working electrode is raised, by applying a negative potential, higher than the lowest unoccupied molecular orbital (LUMO) of reactant O, electron transfer becomes thermodynamically favourable and O is reduced. That is, if the potential applied to the working electrode is negative with respect to $E_{eq}$, electrons from the working electrode will flow to the redox ions in solution. Conversely, if the potential is positive with respect to $E_{eq}$, electrons will flow from solution to the working electrode.

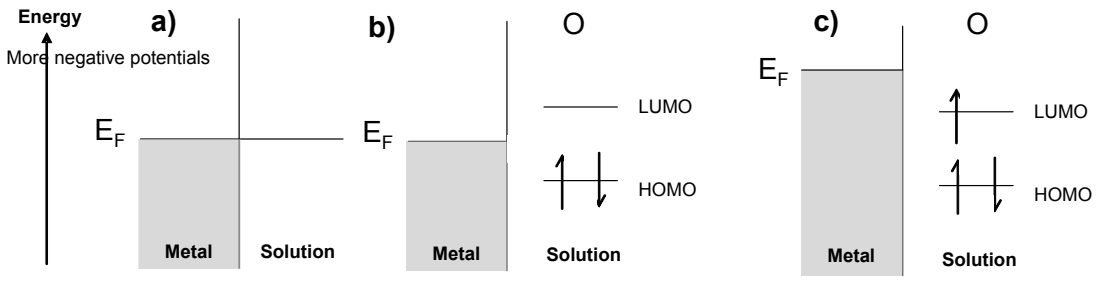


**Figure 2 Adapted from [1] a) $E_F$ of metal in solution, no applied potential, b) $E_F$ of metal is insufficient to drive reduction of O, c) $E_F$ is sufficient to drive reduction of O**

Passing net current moves the system away from equilibrium, and reactants are depleted at the electrode surface compared to that in the bulk. The electrochemical reaction may be controlled by the reactivity of O or R species, temperature, applied potential difference, transport of materials or the nature of the electrode surface. Fundamentally, the observed current may be dependent on either the transport of reactants to, or products away from the electrode (rate determining mass transport), or the rate of the heterogeneous electron transfer (rate determining electrode kinetics). One of these processes will be the rate-limiting step and define maximum reaction limits and the magnitude of the current flowing at the working electrode.

### 2.12 Electron transfer rates

First the case where the reaction at the electrode surface is rate limiting is examined. Transition state theory can be used to describe reaction rates. The rate of electron

transfer in which two chemical species are inter-converted by a single electron transfer at the electrode can be predicted using equation 8

$$O_{(aq)} + e^{-}{}_{(m)} \xrightarrow{k_{red}} R_{(aq)}$$

$$R_{(aq)} - e^{-}{}_{(m)} \xrightarrow{k_{ox}} O_{(aq)} + e_{(m)}$$

**Equation 8. The rate of electron transfer accompanying a simple one electron transfer reaction. $k_{red}$ and $k_{ox}$ describe the first order heterogeneous rate constants for the forward (reductive) and back (oxidative) reactions (occurring at cathode and anode respectively).**

Convention dictates that oxidation currents are taken as positive and reduction currents taken to be negative. If the metal electron concentration is assumed to be a constant, the rate of oxidation and reduction is given by the pseudo first order rate constant $k_{redox}$ (= [O or R]k) (units of cm $s^{-1}$). At equilibrium, the rates are balanced, where $k^0{}_{red}[O]_o = k^0{}_{ox}[R]_o$, $i_a = i_c$ and [O]=[R] ($k^0 = k^0{}_{red} = k^0{}_{ox}$). The exchange current is thus equal to equation 9.

$$i^0 = nFAk^0[OorR]_o$$

**Equation 9 The exchange current ($i^0$) at equilibrium, where $k^0$ is the standard rate constant in the absence of applied potential (cm $s^{-1}$)**

The net current (not at equilibrium) can be written as equation 10.

a) $i = i_a + i_c$

b) $i_c = -nFAk_{red}[O]_o$

c) $i_a = nFAk_{ox}[R]_o$

*or*

d) $i = nFA(k_{ox}[R]_o - k_{red}[O]_o)$

**Equation 10 a) Net current (A) flowing at an electrode, where $i_a$ and $i_c$ are anodic (oxidative) and cathodic (reductive) currents respectively, b) and c) Current predictions for $i_a$ and $i_c$ respectively d) Net current flowing at the electrode using equations 10b) and 10c) Note that at equilibrium, equation 10b) = equation 10c)**

The reaction can be viewed as occurring via a path whereby reactants [$O_{(aq)}$ + $e^{-}{}_{(aq)}$] overcome an energy barrier, or transition state, greater in energy that reactants or products. The energy required to get over the barrier is often termed the activation

energy ($E_A$) or in the condensed phase the standard free energy of activation ($\Delta G^{\ddagger}$). Figure 3 shows transition state theory for the reaction at equilibrium.

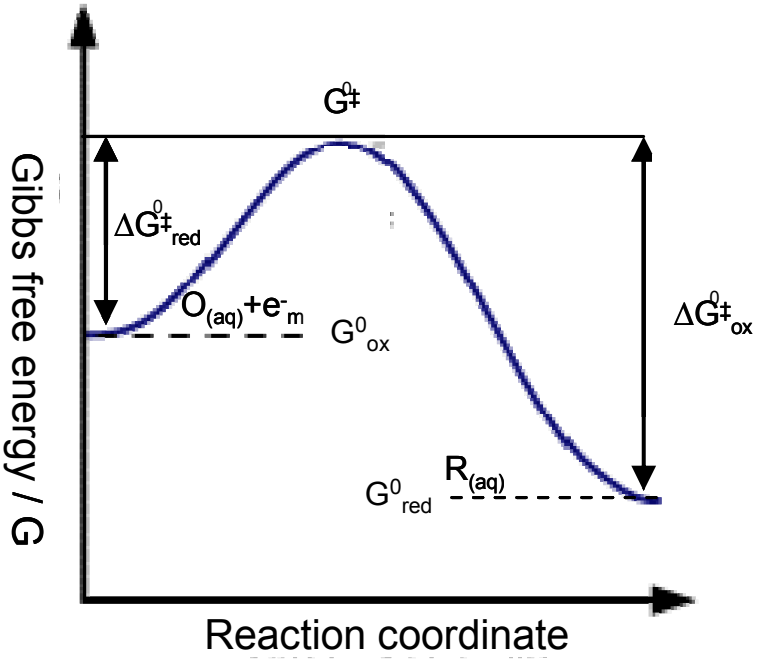


**Figure 3 Free energy plot for a reduction reaction, where $\Delta G^{0\ddagger}$ = the standard free energy of activation for a reduction or oxidation process (often kJ mol), and $G^0_{ox}$, $G^0_{red}$ and $G^{0\ddagger}$ are the Gibbs energy of oxidised, reduced and transition state respectively (often kJ $mol^{-1}$) all in absence of applied potential, at equilibrium.**

The activation free energy at equilibrium for the reduction and oxidation reactions are given in equation 11. $k^0_{red}$ and $k^0_{ox}$ are then thought to relate to $\Delta G^{0\ddagger}$ by the Arrhenius equation, as given in equation 12.

a) $\Delta G^{0\ddagger}_{red} = G^{0\ddagger} - G^0_{ox}$

*and*

b) $\Delta G^{0\ddagger}_{ox} = G^{0\ddagger} - G^0_{red}$

**Equation 11 a) and b) $E_A$ for the reduction and oxidation reactions respectively. For example, for a fixed temperature or pressure, $\Delta G^{0\ddagger}_{red}$ is the free energy change between the reductant and transition state in absence of applied potential.**

$$\text{a)}\quad k^{0}{}_{red} = A\exp\left(\frac{-\Delta G^{0\ddagger}_{red}}{RT}\right)$$

*and*

$$\text{b)}\quad k^{0}{}_{ox} = A\exp\left(\frac{-\Delta G^{0\ddagger}_{ox}}{RT}\right)$$

**Equation 12 a) and b) Transition state theory prediction of $k^{0}_{red}$ and $k^{0}_{ox}$ respectively (in cm $s^{-1}$), where A is a frequency factor (rate of collision of the electroactive molecule with the electrode surface, whose unit depends on order of rate). The term in the exponential is the ratio of activation energy compared with thermal energy in the system**

By applying a potential difference, the potential energy curve can be shifted to make the reaction more or less favourable. If a series of free energy profiles as a function of potential are plotted (figure 4), the plots alter with the change in potential. The reactant energies are invariant with potential, whereas the free energy of the products is largely affected by applied potential.

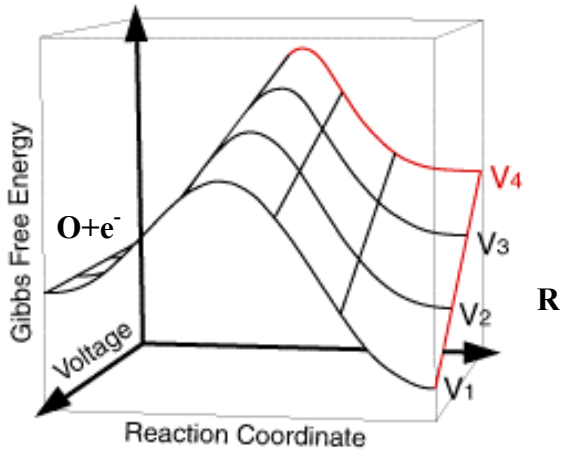


**Figure 4 Adapted from [2] Free energy plots at various potentials for a reduction reaction whereby O is reduced to R**

At potential $V_1$ in figure 3 the formation of R is favoured. However as the potential is changed to $V_4$ the formation of $O+e^-$ becomes the thermodynamically favoured product. As the potential is altered $E_F$ is changed, changing the energy state of the electrons. Additionally, $E_A$ alters as a function of the applied voltage (equation 13).

$$\Delta G^{\ddagger} = -nF\Delta E$$

**Equation 13 Change in $\Delta G^{\ddagger}$ with applied E (V)**

If it is assumed the effect of potential on the free energy change is linear, $\Delta G^{\ddagger}$ for reduction and oxidation when moving away from $E^0$ to a new potential E (over-potential ($\eta$) = E- $E^O$) varies by a fraction of the total change in free energy -nF(E- $E^O$). The free energies of the forward and backward reaction respectively are given in equation 14. The free energy on the right hand side of equations 14a and 14b is akin to the chemical component of the activation free energy change as it is not dependent on the applied voltage.

$$\text{a)}\ \Delta G_{red}^{\ddagger} = \Delta G_{red}^{0\ddagger} - \alpha nF(E - E^0)$$

*and*

$$\text{b)}\ \Delta G_{ox}^{\ddagger} = \Delta G_{ox}^{0\ddagger} - (1-\alpha)nF(E - E^0)$$

**Equation 14 the variation in $\Delta G^{\ddagger}$ of a) reduction and b) oxidation as a function of the applied potential, where $\Delta G_{red}^{0\ddagger}$ and $\Delta G_{ox}^{0\ddagger}$ have no voltage applied. The fractional change is denoted by α, the transfer coefficient, where $0 \geq \alpha \geq 1$, reflecting the sensitivity of the transition state to the drop in electrical potential between metal and solution. A value of 0.5 means the transition state lies intermediate between reactants and products to applied potential. $\alpha_{red} + \alpha_{ox} = 1$, therefore $\alpha_{ox} = 1 - \alpha_{red}$**

The terms for activation free energy can be substituted into the Arrhenius equation giving expressions for $k_{red}$ and $k_{ox}$ (equation 15).

$$\text{a)}\ k_{red} = A_{red}\exp\left(\frac{-\Delta G_{red}^{0\ddagger} - \alpha nF(E - E^0)}{RT}\right)$$

$$= A_{red}\exp\left(\frac{-\Delta G^{0\ddagger}_{red}}{RT}\right)\exp\left(\frac{-\alpha nF(E - E^0)}{RT}\right)$$

*and*

$$\text{b)}\ k_{ox} = A_{ox}\exp\left(\frac{-\Delta G^{0\ddagger}_{ox} + (1-\alpha)nF(E - E^0)}{RT}\right)$$

$$= A_{ox}\exp\left(\frac{-\Delta G^{0\ddagger}_{ox}}{RT}\right)\exp\left(\frac{(1-\alpha)nF(E - E^0)}{RT}\right)$$

**Equation 15 Expressions for a) $k_{red}$ and b) $k_{ox}$, where $A_{red}$ and $A_{red}$ are the frequency factors for oxidation and reduction reactions respectively**

Equations 15a and b demonstrate that as $k_{red}$ and $k_{ox}$ are proportional to the exponential of applied potential, the rate of electron transfer can be varied by varying the applied potential. In a solution containing equal quantities of species O and R, $k_{ox} = k_{red}$ when $E = E^0$. By introducing $k^o$ to represent the situation at equilibrium with no potential applied, equation 15 can be simplified to give equation 16a and b.

$$\text{a)}\quad k_{red} = k^o{}_{red} \exp\left(\frac{-\alpha nF\eta}{RT}\right)$$

*and*

$$\text{b)}\quad k_{ox} = k^o{}_{ox} \exp\left(\frac{(1-\alpha)nF\eta}{RT}\right)$$

**Equation 16 a) $k_{red}$ and b) $k_{ox}$ as a function of the constants $k^o_{red}$ and $k^o_{ox}$**

Equations 16a and b can be substituted into equation 10d to give the Butler-Volmer equation for the net current flowing at the working electrode (equation 17). This describes how the current depends on the electrode potential and transfer coefficient, considering that both a cathodic and an anodic reaction occur on the same electrode. $i_0$ is the exchange current density when the net current flow is zero ($i_0 = A/m^2$).

$$i = i_0\left(\frac{[R]_0}{[R]_{bulk}} \exp\left\{\frac{(1-\alpha)nF\ \eta}{RT}\right\} - \frac{[O]_0}{[O]_{bulk}} \exp\left\{\frac{-\alpha nF\ \eta}{RT}\right\}\right)$$

**Equation 17 Butler Volmer equation for calculation of i where $i_0$ is defined as the exchange current when the net current is zero. $[R]_0$ and $[O]_0$ are concentrations of R and O close to the electrode, and $[R]_{bulk}$ and $[O]_{bulk}$ are concentrations of R and O in bulk solution.**

If the solution is well stirred, the concentration of reactants will be equal at the electrode surface to that in the bulk. The Butler-Volmer equation then simplifies to equation 18.

$$i = i_0\left(\exp\left\{\frac{(1-\alpha)nF\eta}{RT}\right\} - \exp\left\{\frac{-\alpha nF\eta}{RT}\right\}\right)$$

**Equation 18 Butler Volmer equation (for calculation of i) for situations where the surface concentration of reactants is equal to the bulk values**

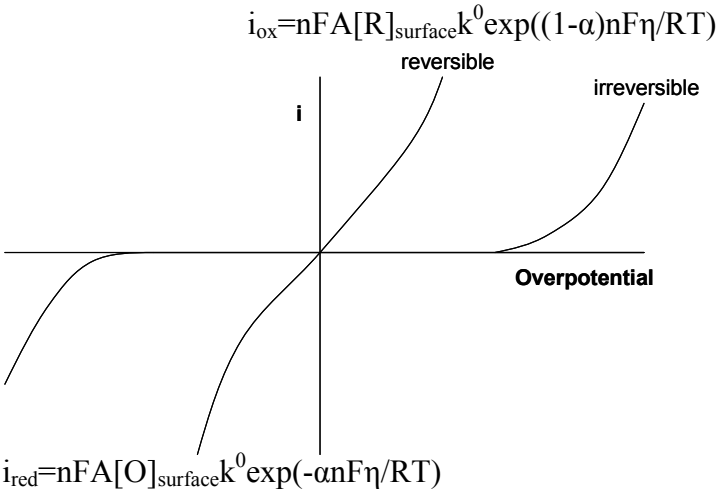


**Figure 5 The variation of i as a function of the η for a reversible and irreversible reaction**

The variation of current with overpotential in a reversible (large $i_0$) or irreversible reaction (small $i_0$) is shown in figure 5. In both, when no overpotential is applied, no current flows; however, they differ in their response to small overpotentials. In the reversible reaction a low overpotential is required to drive the reaction, and current flows in anodic and cathodic directions (depending on the overpotential sign). This is aside from at very high overpotential when the opposite process becomes negligible. Conversely in the irreversible reaction, a high overpotential is required to induce current. If overpotential is increased to a value where a reaction (for example, reduction) can occur, then the corresponding (for example oxidative) process is negligible.

A reaction is reversible or irreversible, depending on whether fast or slow electrode kinetics occurs. This can be discussed at the molecular level using Marcus theory. The electron transfer reduction of O to R occurs within $10^{-15}$-$10^{-16}$ seconds via quantum mechanical tunnelling, faster than the vibrations within O ($10^{-13}$ seconds). When the reaction occurs, molecular geometry (solvation structure, bond length and angles comprising the molecular shape) of the product R must be the same as reactant O. R must be formed with an energy that exactly matches the sum of the electron in the metal Fermi level, and the energy of O. This implies that for an electron transfer, O and R (formed) are energetically excited, with the activated state of O forming the transition state (where O and R have the same geometry and satisfy the energy rules above). The energy required for the transition is greater the more different reactants and products are in molecular shape and solvation, making activation energies larger

and $k_{red}$ smaller. Fast electrode processes are therefore observed when reactants and products have comparable shapes and solvation.

### 2.13 The Electrical Double Layer

The electrode possesses a charge which can be controlled by the potential applied to it, inducing electrostatic interactions between the electrode and electrolyte ions, as well as with dipole moments of the solvent. The phase boundary between the solid electrode and the electrolyte solution will therefore interrupt the nature of the electrolyte solution.

The basic concept of a double layer arises from the idea that for an interface to maintain electrical neutrality, charge on the electrode must be matched by an opposite charge (in solution). Equation 19 demonstrates this.

$$q^m = -q^s$$

**Equation 19 charge matching in a double layer, where $q^m$ (C) on a metal electrode is equal and opposite to $q^s$ (C), the charge in solution**

Many models for the double layer exist; figure 6 summarises the main ones. Three main layers exist at the electrode-solution interface; the Helmholtz double layer (inner and outer), the Gouy Chapman region, and the bulk (where charges are equal and electrode forces are screened). In the Helmholtz layer, attracted ions approach the electrode to a distance limited by the solvation shell of the ion, forming a monolayer of solvation between the ion and electrode. Also known as the 'electrical double layer', it is equivalent to an electrical capacitor, and exists as a linear potential drop.

The Gouy-Chapman Region exists as excess charge density in solution (not exclusively situated at the Helmholz plane). Electrostatic forces attracting or repelling ions from the electrode are counteracted by Brownian motion, dispersing the excess ions. The potential drop across this layer is not linear.

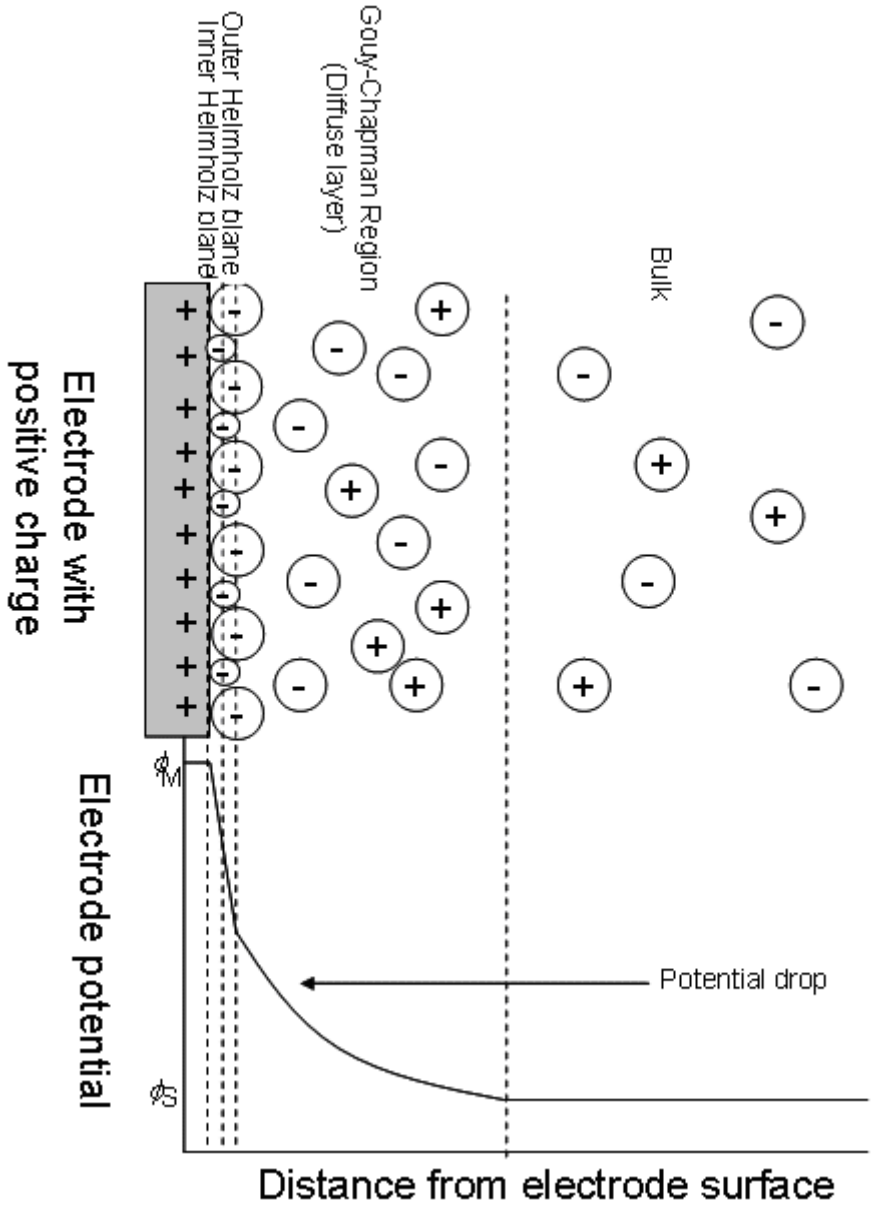


**Figure 6 Electrode-solution interface (based on the Gouy Chapman model, the Stern model and the Grahame model)**

## 2.14 Mass transport

Section 2.12 showed the rate of electron transfer in a reaction is affected by the cell potential difference, with an exponential relationship existing between the two. In practice, the rate of an overall reaction is affected not only by the reaction processes at the electrode, but also by the mass transport of species between the bulk solution and electrode interface. Figure 7 outlines these processes in full.

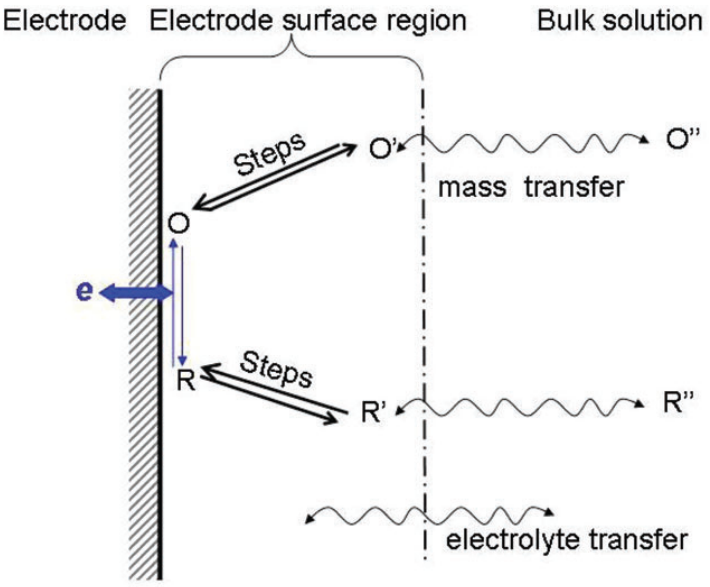


**Figure 7 Reproduced from [3] Schematic of pathways involved in electrochemical reactions in solution; 1. Mass transport of O to the electrode where reaction occurs, 2) Chemical reaction (adsorption, desorption, protonation and decomposition steps that might not involve redox reactions but may precede or follow electron transfer steps, 3) Electron transfer, 4) Transport of R from electrode to the bulk and 5) Transport of electrolyte**

As mass transport is particularly important in relation to the electrical currents produced in a p-MFC, diffusion, convection and migrational effects will be discussed in further detail. In the electrochemical reaction above, if mass transport of species O is considered the rate limiting step, the mass transport limited current ($i_{mt}$) is given by equation 20.

$$\frac{i_{mt}(x)}{nFA} = -D_0 \frac{\partial [O](x)}{\partial x} - \frac{z_0 F}{RT} D_0 C_0 \frac{\partial \phi(x)}{\partial x} + [O]v(x)$$

**Equation 20 The mass transport limited current ($i_{mt}$ in A), where $D_O$ is the diffusion coefficient of species O ($cm^2\ s^{-1}$), x is the distance normal from the electrode surface (cm) with x =0 at the surface and x = ∞ in the bulk, $\phi$ = an electric field (V), $v$ = linear velocity of solution flow as a function of position ($cms^{-1}$) and $z_0$ = charge magnitude on one ion. In the equation, the first term describes diffusion along a diffusion gradient, the second migration along an electric field gradient, and thirdly, the convection contribution.**

In electrochemical systems, it is usual to design experiments where mass transport effects other than diffusion are minimised. Migration effects are minimised through the use of a chemically and electrochemically inert background electrolyte (>0.1 M).

This screens the external electric field at the electrode/solution interface due to the drop in electrical potential between the two phases. Without a supporting electrolyte, the distance over which the electrode exerts an electrostatic force on charged species present in the solution is larger, and can alter the rate of migratory fluxes and the rate of mass transport of electroactive material to and from the electrode. Additionally, effects resulting from natural convection arising from thermal or density gradients can be overcome by introducing forced convection (through external forces).

Under these circumstances the current is therefore limited by diffusion of the reactant species from the bulk to the surface. Diffusion arises from uneven concentration gradients and acts to maximise entropy by minimising composition differences in a system. Rates are therefore dependent, at any point in solution, on the concentration gradient at that location. Fick's first law (equation 21) allows the diffusion limited current to be calculated. Here the diffusional flux j of a species is related to the concentration gradient and the diffusion coefficient with the negative sign signifying that material moves down a concentration gradient from high to low. The second law (equation 22) allows local changes in the concentration of the electroactive species normal to an electrode surface as a function of time to be predicted. The steeper the change in concentration the greater the rate of diffusion.

$$j_O(x,t) = -D_O \frac{\partial C_O(x,t)}{\partial x}$$

*or*

$$\frac{i_{mt}(x,t)}{nFA} = D_0 \frac{\partial C_0(x,t)}{\partial x}$$

**Equation 21 Fick's first law, whereby flux of a substance O at location x and time t is related to the $D_O$ of species O, $C_O$ and x**

$$\frac{\partial C_0(x,t)}{\partial t} = D_0 \left( \frac{\partial^2 C_0(x,t)}{\partial x^2} \right)$$

**Equation 22 Fick's second law, where local changes in the concentration of the electroactive species as a function of time can be predicted from $C_O$, $D_O$, x and t**

During electrolysis, reactants are transported to within 10-20Å of the electrode surface (by diffusion and convection – as negligible gradients of electric potential

exist for migration), where electron transfer occurs. When a planar electrode is placed in a solution of reactant, O, the composition of solution is constant. When the electrode is connected to a potential source, and O is used as a reactant, if diffusional transport dominates, a concentration gradient is induced perpendicular from between electrode (outside the 10-20 Å 'double layer') and the bulk solution (shown in figure 8). As electrolysis proceeds, the thickness of the diffusion layer becomes larger, in a linear manner close to the electrode surface, before approaching the bulk value asymptotically. This evolves to a steady-state diffusion layer thickness, controlled by the extent of natural convection in the bulk. Therefore diffusion control occurs within the diffusion layer, whilst the bulk concentration is maintained by convection.

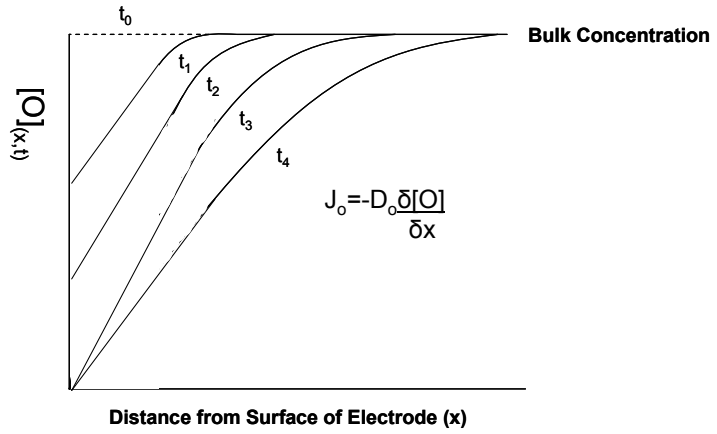


**Figure 8 The growth of diffusion layer thickness with time**

The diffusion layer thickness ($\delta_O$) can be estimated by equation 23, whereby the linear region of the diffusion layer is extrapolated to the bulk value, also enabling the flux of material to the electrode to be estimated by the current.

$$\frac{i}{FA} = j_O = D_O \frac{[O]_{bulk} - [O]_0}{\delta_O}$$

**Equation 23 The relationship of $\delta_O$ to $j_O$ and $D_O$**

Where convection in addition to diffusion effects are main contributors to mass transport, extra material is brought to the electrode surface and observed currents are larger than with diffusion alone, with a smaller diffusion layer existing. The maximum observable current is limited by the rate at which reactant reaches the electrode/solution interface. A limiting current, $i_L$ is eventually reached, as given in equation 24.

$$i_L = \frac{nD_o FA[O]_{bulk}}{\delta_O}$$

**Equation 24 $i_L$ (A) as a function of $D_O$, F, A, $[O]_{bulk}$ and $\delta_O$**

## 2.15 Electrochemical Techniques for p-MFC study

The power generated by a p-MFC is typically quantified in terms of power output, as given by equation 25.

$$P = E_{cell} i$$

**Equation 25 Power (W) as a product of $E_{cell}$ and current**

Other general parameters are often given in p-MFC studies. The open circuit voltage (OCV) is the voltage of a p-MFC under a no-load condition (no current generation), and can be measured with a high impedance voltmeter or potentiometer. The open circuit potential (OCP) is the potential of an electrode (cathode or anode) measured against a suitable reference electrode. The cell voltage of a p-MFC can be expressed in terms of the overpotential associated with different factors, as given in equation 26.

$$E_{cell} = E_c - \eta_{act,c} - \eta_{conc,c} - E_a - \eta_a - \eta_{conc,a} - \eta_{ohm}$$

**Equation 26 [3] $E_{cell}$ of a p-MFC, where $\eta_{act}$ are the charge transfer derived overpotentials of the anode and cathode (charge transfer or activation losses), $\eta_{conc}$ are the concentration overpotentials of the anode or cathode (mass transport losses), $\eta_{ohm}$ are the ohmic overpotential (or losses) of MFC/p-MFCs. Note that each step can also be represented by an associated resistance.**

Other electrochemical techniques are often used, which include polarisation curves (2.151), cyclic voltammetry (2.152), square wave voltammetry (2.153), potential step chronoamperometry (2.154), rotating disk electrochemistry (2.155), scanning electrochemical microscopy (2.156) and electrical impedance spectroscopy (2.157).

### 2.151 Polarisation Curves

Polarisation curves are plots of electrode potential (or p-MFC voltage) as a function of current or current density. These can be measured by constant resistance discharge,

measuring current and voltage whilst different resistances are applied, by linear sweep voltammetry, by galvanostatic discharge (where current is controlled and voltages measured) or by potentiostatic discharge (where voltage is controlled and currents measured). Zhou *et al.* [3] suggest that potentiostatic discharge measurements may be the most suitable for biofuel cell measurements, especially when the electrochemistry of enzymes is involved (whose behaviour is potential sensitive) [3]. With chemical fuel cell studies galvanostatic discharges are favoured as constant reaction rates occur at the electrode. In comparison, for constant resistance discharge techniques, both current and cell voltages will be varying.

The time required for the p-MFC device to reach equilibrium before taking measurements is disputed, varying between seconds to hours [3]. Unlike with chemical fuel cells, p-MFCs do not usually reach steady state (thought to be due to the constant changing of microbes) [3]. Different sampling rates may also be required for individual devices, as biofilms vary leading to different electrode mechanisms.

A typical polarisation curve for a MFC (p-MFC would be similar) is shown in figure 9. Three characteristic regions are exhibited, which although well separated in a chemical fuel cell, often overlap in MFCs. The first region is due to charge transfer overpotentials ($\eta_{act,a}$ and $\eta_{act,c}$) located at low currents, derived from the slow (irreversible) reactions taking place at electrode surfaces. This is dependent on operating conditions, electrode materials and catalysts (including microstructure), electrolyte, mediators and the type of microbial population present [3]. Secondly, ohmic overpotentals are present at intermediate currents and are caused by ionic resistances in the electrolyte, membrane and biofilm and electronic resistance in the electrodes and electrical connections [3]. Finally, mass transport overpotentials are present at high currents. This overpotential is common at high current densities if the supply of reactants limit the current, or if products build up to affect reactant flux [3]. Factors which contribute to mass transport overpotentials include structure and geometry of electrodes, electrolyte nature, and products and metabolites produced [3].

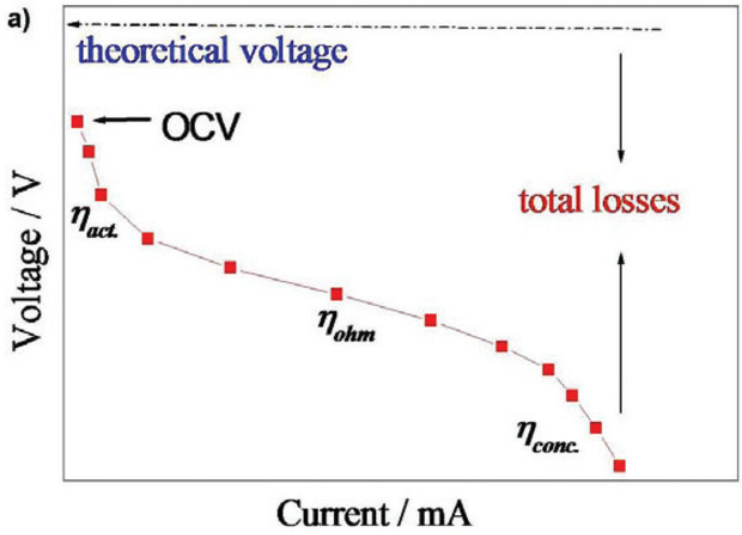


**Figure 9 Reproduced from [3] The ideal current-voltage polarisation curve of a biological fuel cell. The characteristic regions of a polarisation curve are labelled. Note that the OCV does not equal the theoretical voltage as the system is not under standard conditions**

### 2.152 Cyclic voltammetry

Cyclic voltammetry, whereby the voltage of the working electrode is ramped linearly versus time in a triangular waveform with respect to a reference electrode, is one of the simplest ways to determine mechanisms of the underlying oxidation and reduction reactions which take place in electrode reactions.

Experiments are conducted in stationary solution, relying on diffusion (governed by Fick's laws) for reactant transport. The potential of the working electrode is swept from a value $E_1$ at which a redox species cannot undergo reaction, to a potential $E_2$ whereby an electron transfer is favoured. The applied potential is a function of the scan rate ($v$ in v $s^{-1}$, typically between 5 mV $s^{-1}$ and 100 V $s^{-1}$) and the time of the sweep (t) (equation 27)

$$E_{(t)} = E_1 - vt$$

**Equation 27 Applied potential (V) as a function of the initial potential sweep value ($E_1$), t and $v$**

A cyclic voltammogram is shown in figure 10. In a typical cyclic voltammograms, initially, at potential $E_1$, no electron transfer occurs as applied potentials are not in the range to induce transfer. When more negative, reducing values are reached, the reduction of O to R occurs and current flows. In irreversible cases, as E (and E = $(\Phi_m-\Phi_s)$) becomes more negative, the current rises exponentially with potential, as

suggested by the rate constant equation (equation 15); this part of the curve is said to be under kinetic control. A trade-off peak of current ($i_p$) is then reached, which reflects the depletion of O as a result of mass transport limitation (according to Fick's second law), despite the increasing heterogeneous rate constant. As depletion of O becomes greater, and the diffusion layer becomes thicker, new O diffusing in has further to diffuse to the electrode. This current therefore reflects the rate at which O can diffuse. In contrast, reversible cases are totally under mass transport control.

The sweep is then reversed, and if fully reversible, when the potential is scanned back to $E_1$, R is oxidised to O. The area under the voltammogram of the reverse peak current is equal but opposite to that of the forward scan.

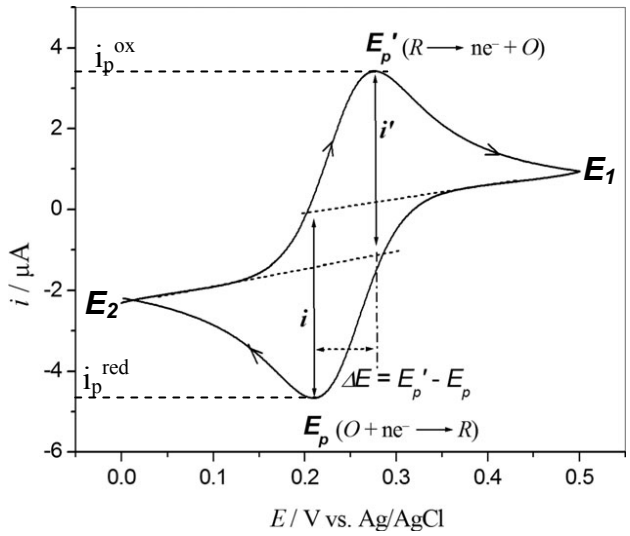


**Figure 10 Reproduced from [3] Reversible cyclic voltammogram showing peak potentials ($E_p$), peak currents ($i_p$) and the potential difference between oxidation and reduction peaks. Note that this is a multi-scan cyclic voltammogram, thus the current at terminal potentials is not zero.**

Regardless of whether systems are reversible or irreversible, peak currents are directly proportional to the concentration of reactants and scan rate. This latter factor can be explained by Fick's first law, which dictates that peak current reflects the concentration gradient of O near the electrode, as determined by the diffusion layer thickness. When the scan rate is fast, less time exists for O to be depleted and for electrolysis to occur, resulting in thinner diffusion layers. A larger peak is then achieved as a larger flux can be obtained

The shape of the voltammograms depends on the reversibility of the electrode kinetics (figure 11). Here, the terms reversible or irreversible refer to limiting cases whereby the kinetics are fast (reversible) or slow (irreversible) with respect to mass transport conditions. Quasi-reversible reactions have different values of rate constants between reduction and oxidation reactions. By analysing the variation of peak position as a function of scan rate it is possible to gain an estimate for the electron transfer rate constants.

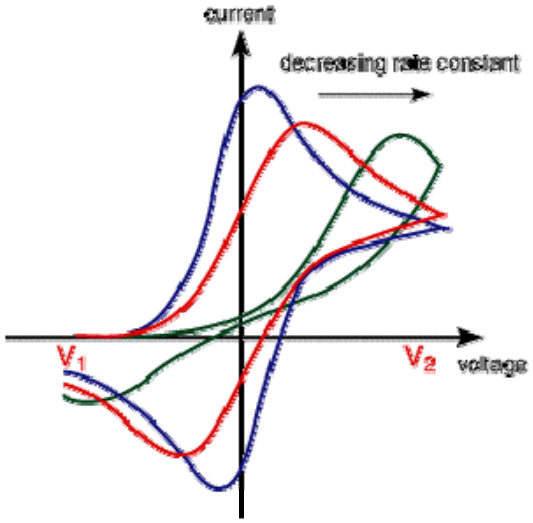


**Figure 11 Reproduced from [2] Cyclic voltammograms for reversible (blue), quasi reversible (red) and irreversible (green) reactions**

In reversible cases, as soon as reactions become thermodynamically favourable, they occur as a result of rapid electrode kinetics, with a separation of 59 mV/ n at standard room temperature and pressure (298 K and 1 atm) between peaks (independent of scan rate, see equation 30). In contrast, no currents flow in the irreversible case until E is considerably past $E_{eq.}$ That is, irreversible reactions require higher overpotential for reactions to occur, and peak separation is greater than 59 mV. Peak potentials also depend on reversibility. For irreversible reactions, peak $E_p$ shifts to more negative potentials at faster scan rates (equation 29), whilst $E_p$ of reversible reactions are constant and independent of scan rate (equation 28).

$$\left| E_p - E_{\frac{p}{2}} \right| = 2.20 \frac{RT}{F}$$

**Equation 28 $E_p$ of reversible reactions**

$$\left| E_p - E_{\frac{p}{2}} \right| = 1.86 \frac{RT}{\alpha F}$$

**Equation 29 $E_p$ of irreversible reactions**

$$E_p^{ox} - E_p^{red} = 2.218 \frac{RT}{nF}$$

**Equation 30 $E_p$ separation of a reversible reaction with n transfer of electrons**

Peak current is also larger for a reversible couple than for an irreversible couple at the same scan rate (equations 31 and 32 respectively). This is due to the contrasting electrode kinetics of the different systems. In a reversible system, kinetics are such that $k_{red}$ and $k_{ox}$ are large in comparison to the scan rate, meaning [O] and [R] are near the equilibrium values predicted by the Nernst equation (at the electrode surface). When rate constants are lowered, the curves shift, as the equilibrium at the surface is not establishing so rapidly. In an irreversible system, back reactions are negligible.

$$\left| i_p \right| = 0.4663 n^{\frac{3}{2}} A F D_O^{\frac{1}{2}} v_s^{\frac{1}{2}} [O]_{bulk} \left( \frac{F}{RT} \right)^{\frac{1}{2}}$$

**Equation 31 $i_p$ for a reversible couple**

$$\left| i_p \right| = 2.99 x 10^{-5} (\alpha)^{\frac{3}{2}} A D_O^{\frac{1}{2}} v_s^{\frac{1}{2}} [O]_{bulk}$$

**Equation 32 $i_p$ for an irreversible couple at 298 K**

Equation 31 can be rewritten as the Randles Sevcik equation (equation 33), from which diffusion coefficients of the electroactive species can be determined. To calculate the diffusion coefficient, $i_p$ is plotted versus the square root of the scan-rate. This is linear with a slope $\alpha D^{1/2}$. Linear plots of $i_p$ vs. $v^{1/2}$ provide evidence for a chemically reversible redox process in solution (if $i_p$ vs $v$ is linear then this is evidence for redox species adsorbed on a surface). For species where the diffusion coefficient is known (or can be estimated), the slope of the plot of $i_p$ vs. $v^{1/2}$ provides information about the stoichiometry of the redox process

$$i_p = (269{,}000)n^{\frac{3}{2}} F A D_O^{\frac{1}{2}} [O]_{bulk} v^{\frac{1}{2}}$$

**Equation 33 The Randles Sevcik equation, for a solution at 298 K**

In summary, when applying cyclic voltammetry to p-MFC study, several parameters can be investigated. First and foremost it can be established whether a chemical system under investigation is reversible or irreversible. For a fully electrochemically reversible couple such as ferricyanide/ferrocyanide (Fe(III)/Fe(II)), the ratio of anodic to cathodic peak currents = 1, and peak potential separations = 59.2 mV/ *n* at 298 K. Quasi or irreversible systems exhibit larger peak separations, and one or more peaks that are reduced in size. Redox potentials of the chemical and biological species involved at the anode and cathode can be determined, and mechanisms of electron transfer between biofilms and planktonic cells studied. Finally, catalyst performance can be studied. However, characteristics of a cyclic voltammogram also depend on factors such as the electrode surface pre-treatment, with many electrode materials used in p-MFCs unable to produce reversible electrochemical reactions even the redox couple ferricyanide/ferrocyanide [3]. This is because electrode reactions can be significantly affected by the microstructure, roughness and functional groups present on the electrode surface [3].

### 2.153 Square wave voltammetry

An important limitation of cyclic voltammetry methods is the substantial background current levels from capacitative, non-Faradaic currents. Enhanced discrimination of Faradaic currents ($i_{CT}$) can be obtained from pulse voltammetry techniques such as square wave voltammetry, making this technique ideal to identify small quantities of any redox products produced by microbial species.

All pulse techniques rely on the difference in decay rates following a potential step between charging and Faradaic currents. The charging current decays exponentially, whereas the diffusion controlled Faradaic current decays slower as a function of $1/(\text{time})^{½}$. The charging current becomes negligible at a time as given in equation 34, meaning that after this time, measured current is Faradaic. Thus, measuring current at the end of a potential pulse allows discrimination between Faradaic and charging currents.

$$Time = 5R_uC_{dl}$$

**Equation 34 Time (s) taken for the charging current to become negligible after a potential step, where $R_uC_{dl}$ is the time constant (from µs to ms) of the electrochemical cell.**

Various pulse techniques exist, differing on the type of electrode, the pulsed potential wave forms and the number of sampling points. Square wave voltammetry is a form of pulse voltammetry which combines the background suppression and sensitivity of differential pulse voltammetry, the diagnostic value of normal pulse voltammetry and the ability to differentiate products directly similar to reverse pulse voltammetry, with an option to use longer time scales than any of the pulse polarographic techniques. The wave form applied consists of a square wave of constant amplitude superimposed on a staircase wave form, with current measured at the end of each plateau half cycle (figure 12). Current measured on the reverse half-cycle ($i_R$) is subtracted from current measured on the forward half-cycle ($i_F$), and the difference ($i_F - i_R$) as a function of potential is presented.

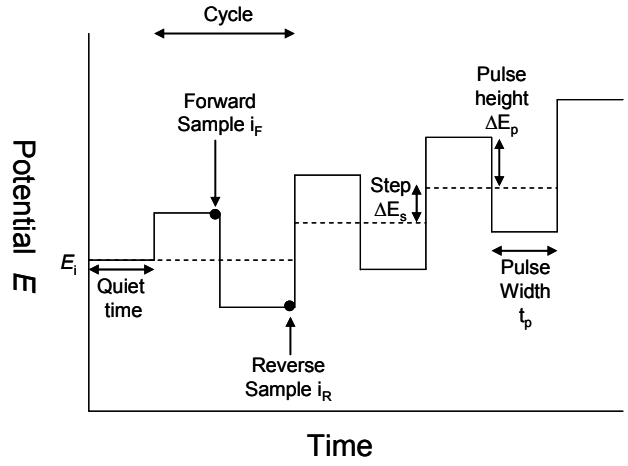


**Figure 12 Waveform and measurement scheme for square wave voltammetry with important parameters defined. Pulse height ($\Delta E_p$) is the height of the potential pulse, pulse width ($t_p$) is the duration of the pulse, sample period is the time at the end of the pulse when current is measured. In general $t_p$ defines the experimental time scale, step size ($\Delta E_s$) fixes the spacing of the data points along the potential axis, and these parameters define the time time taken for a scan. In normal practice $\Delta E_s$ is significantly less than $\Delta E_p$, which defines the span of interrogation of each cycle and hence the voltammograms resolution. $t_p$ is then varied over a wide range (1-500 ms or 1-500 Hz)**

A symmetric peak is gained, rather than the sigmoid curve gained with normal pulse voltammetry (figure 13). The shape can be explained as follows; for a reduction of

species O, at potentials positive of the redox potential, $i_F$ and $i_R$ equal zero (and $i_F$-$i_R$ is zero). At negative potentials of the redox potential, the current is diffusion-controlled and $i_F$ and $i_R$ are equal. Consequently $i_F$ and $i_R$ is largest (and hence the largest current response) is gained at the redox potential.

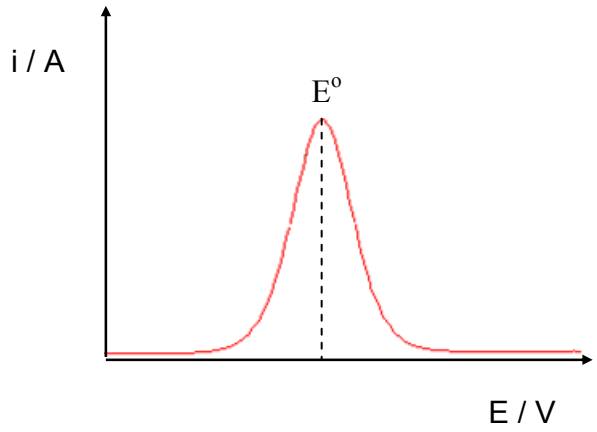


**Figure 13 Typical square wave voltammograms. $E^o$ is labelled**

### 2.154 Potential step chronoamperometry

Chronoamperometry is a technique whereby the potential of anode or cathode is controlled or stepped between two constant values and held constant, with the resulting currents measured (figure 14). When applied to p-MFC studies, it is important to note that the anode potentials also influence and regulate biofilm growth and activity.

Immediately following a potential step, between values of $E_1$ (no electrolysis) and $E_2$ (electrolysis), a large current is detected which falls with time. Current magnitudes are diffusion controlled; initially, little reactant (O) is depleted so currents are large. As depletion occurs, $\delta_d$ increases and currents fall to $i_L$, governed by the mass transport levels existing in the bulk. The Cottrell equation (equation 35) arises from integrating Fick's second law (for planar boundary conditions), and describes current magnitude as a function of time. The equation suggests that diffusion coefficients can be measured, by linearising the Cottrell equation and plotting 1/i vs t (gradient = $\pi/n^2F^2A^2[O]^2D$). However, no information about electrode kinetics can be gained, providing $E_2$ is negative of the reduction peak from cyclic voltammetry (for a reduction).

$$|i| = \frac{nFAD_O^{1/2}[O]_{bulk}}{\pi^{1/2}t^{1/2}}$$

**Equation 35 The Cottrell Equation**

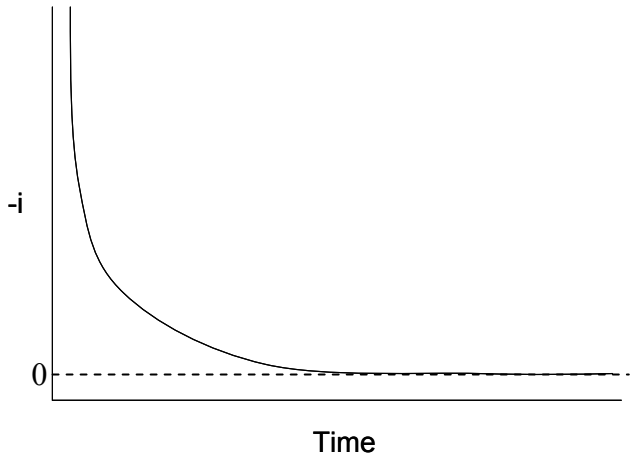


**Figure 14 Typical current response observed during a potential step experiment**

## 2.155 Rotating Disk Electrochemistry

This technique uses a hydrodynamic electrode, inducing forced convection in solution (which dominates mass transport) by rotating the electrode. A small metallic disk acts as the working electrode, embedded centrally in a large insulating cylinder; once placed within a solution of interest, it is rotated. The electrode rotation pulls material upwards, and spins the solution out from the cylinder surface in a radial direction, creating a vortex and drawing fresh reactant towards the electrode.

Laminar flow, as opposed to turbulent flow, is required, where the solution moves smoothly in layers (laminae) along streamlines, and this can be predicted by a Reynolds number (Re) of less than $1x10^{-5}$ (using equation 36).

$$\mathrm{Re} = \frac{\omega r^2_c}{v}$$

**Equation 36 Re for an RDE experiment, where $r_c$ is the radius of the cylinder (cm), ω the rotating speed (Hz), and *v* the viscosity of the solution ($cm^2\ s^{-1}$)**

By rotating the electrode, solution is kept homogeneous due to convection. However, a stagnant layer called the Levich layer clings to the electrode, rotating with it. Inside this layer, diffusion is the primary mode of mass transport. When ω (Hz) (ω=2πf

where f = rotation speed in rpm) is fixed and rotation is constant, a potential step in the limiting current region causes the appearance of a current transient to that observed in the absent of forced convection. However, unlike with a stationary electrode, the concentration gradient at the electrode rapidly reaches steady state. To predict the flux of electroactive material, O, to the electrode surface, diffusion (the first term in equation 37) and convection (the second) are taken into account. Sufficient background electrolyte is assumed present to minimise migration.

$$\frac{\partial[O]}{\partial t} = D_O \frac{\partial^2[O]}{\partial x^2} - v_x \frac{\partial[O]}{\partial x} = 0$$

**Equation 37 Flux of electroactive reactant species O to the electrode surface, under steady state mass transport conditions, where $v_x$ is the component of velocity in the x direction ($cm^2s^{-1}$)**

By assuming [O] is found as a function of distance (x) and is zero at the electrode surface (at the mass transport limited steady state current $i=i_L$), equation 37 can be solved to result in the Levich equation (equation 38). This predicts the $i_L$ is proportional to $\sqrt{\omega}$ and $[O]_{bulk}$. Therefore a plot of transport limited current against the square root of rotation speed should yield a straight line passing through the origin. However, $i/\omega^{1/2}C$ is a constant only when the kinetic limited current ($i_k$) [or $k_f(E)$] is very large. If $i_K$ is small, a plot of i vs $\omega^{1/2}$ will be curved and tend toward the limit $i=i_k$ as $\omega \rightarrow$ infinity.

$$i_L = 0.62nFA[O]_{bulk} D_O^{1/2} v^{-1/6} \omega^{1/2}$$

**Equation 38 Levich equation, which applies to the totally mass transfer limited condition at the RDE – from this the Levich constant can be defined as $i_L/\omega^{1/2}$**

Limiting currents increase with rotation speed due to the increased velocity of the solution leading to enhanced convective transport of reactants, and the shrinking of diffusion layers. The Levich (or diffusion) layer thickness varies inversely to the square root of the rotation speed (equation 39); as this shrinks, the concentration gradient of O becomes steeper, flux increases, and consequently currents increase.

$$\partial_O = 1.61 D_O^{1/3} \nu^{1/6} \omega^{-1/2}$$

*and*

$$j_L = \frac{D_O [O]_{bulk}}{\partial_O}$$

**Equation 39 The relationship between $\delta_O$ and the mass transport limited flux ($j_L$)**

Koutecky-Levich rotating disk electrochemistry is used to extract heterogeneous rate constants for the species of interest. This is accomplished by extrapolating what the limiting current would be at infinitely high rotation speeds. The Koutecky-Levich equation is given in equation 40. Plotting $1/i_L$ vs. $1/\omega^{1/2}$ will give a linear plot such as that shown in figure 15, whose y-intercept (at $\omega^{-1/2} = 0$) is $1/i_K$. Determination of $i_K$ at different values of E then allows determination of the kinetic parameters of $k^0$ and $\alpha$, and the heterogeneous rate constant can be calculated by equation 41.

$$\frac{1}{i} = \frac{1}{i_K} + \frac{1}{i_L} = \frac{1}{i_k} + \frac{1}{0.62 n F A D_O^{2/3} \omega^{1/2} \nu^{-1/6} C_O}$$

**Equation 40 The Koutecky-Levich equation, where $i_k$ (the heterogeneous rate constant limiting current) represents the current flowing in a absence of mass transfer effects, under kinetic limitation (if mass transport was efficient enough to keep surface concentrations equal to the bulk**

$$i_K = nFAk^0 C_0$$

**Equation 41 Calculation of the heterogeneous rate constant (unit depends on order but is often cm $s^{-1}$)**

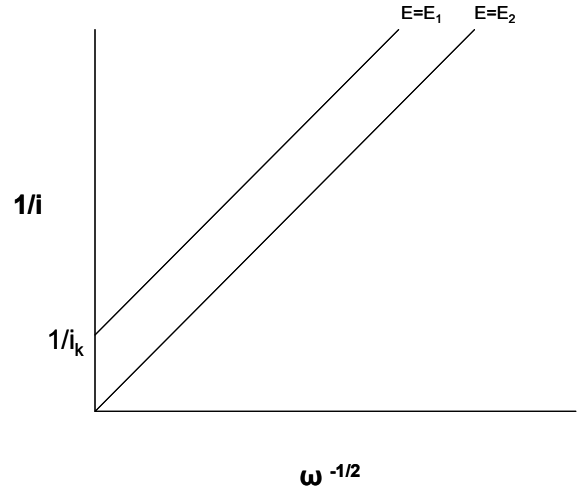


**Figure 15 Koutecky-Levich plots at potential $E_1$ where the rate of electron transfer is sufficiently slow to act as a limiting factor, and at $E_2$ where electron transfer is rapid**

**2.156 Scanning Electrochemical Microscopy**

Scanning electrochemical microscopy (SECM) is an electrochemical scanning probe technique whereby the measured current is caused by an electrochemical reaction at the tip of an ultra microelectrode (UME). The fact that measurements can be taken whilst the UME is moved relative to a conductive, semi conductive or insulating substrate makes it ideal to characterise chemical processes occurring at the solution-substrate interface and obtain topographic profiles. Importantly, this is an extremely useful technique to use in the study of biofilms and biofilm processes.

UMEs are electrodes with at least one dimension in the range of 0.1 to 20 μm. Their size means they can be employed in analytical, *in vivo* measurements, but they also have unique properties of increased rate of mass transport processes, faster response times and decreased reliance on the presence of a conducting medium. Due to the minute currents passed (due to small areas), only small amounts of electrolysis are induced, with a hemispherical diffusion layer (with a size similar to the micro-disk radius) rapidly developed over time. This makes diffusion layers extremely thin (μm range), with correspondingly large concentration gradients across them, and hence very fast rates of mass transport.

Due to their small area, the interfacial capacitance in UMEs is much smaller than conventional electrodes. Charging currents are lower and decay more rapidly, meaning the electrodes have faster response times. UMEs also generally have a lower ohmic drop in solution than conventional electrodes. Passing current through a resistive solution generates a potential difference between the working and reference electrodes due to Ohms law, distorting the current/voltage responses expected. However, due to the small currents passed at microelectrodes, this is minimised, and background electrolyte is not required.

The apparatus used in SECM is shown schematically in Figure 16. SECM experimental setup consists of a UME mounted in a micro-positioning system (piezoelectric or electric stepping motors), allowing it to move along a Cartesian axis in x, y and z. The UME is immersed in a cell containing electrolyte and a redox species such as O, and along with reference and counter electrodes (and substrate - WE2 if required), it is connected to a bipotentiostat.

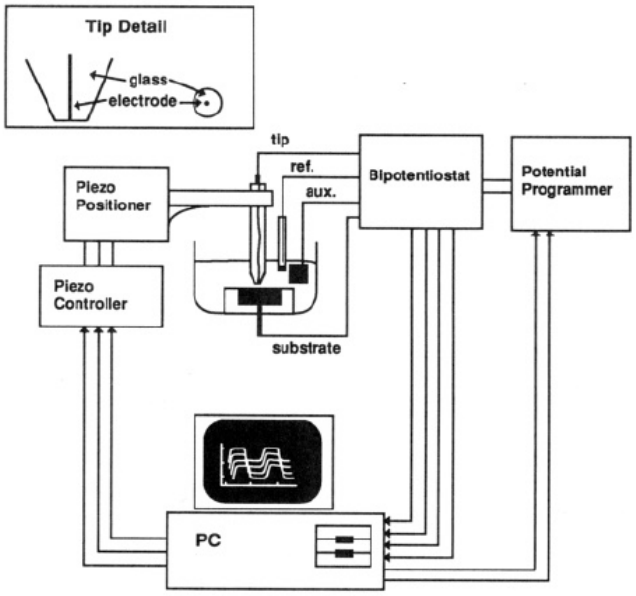


**Figure 16 Reproduced from [4] A Schematic of SECM Instrumentation.**

The current measured at the UME tip is related to the potential at the tip ($E_T$) and substrate ($E_S$) by conventional behaviour. In the bulk solution, at an 'infinite' distance from a substrate (in practice ~1 mm), the steady state current governed by hemispherical diffusion for $i_{T,\infty}$ of a reaction involving reactant O is given by equation 42.

$$i_T = gnF[O]_{bulk} D_O a$$

**Equation 42 $i_T$ (where reactant = O), where g is a factor which depends on the shape of the microdisk and surrounding glass (for disc-shaped electrodes embedded within a UME with an infinitely large glass insulating diameter, rg,∞, g=4) and a is the UME tip radius (cm)**

Modes of operation can be defined according to the movement of the UME relative to the substrate surface. In approach mode the UME approaches the substrate surface along the *z*-axis, probing the diffusion layer of the substrate, and $i_T$ is plotted as a function of tip-substrate separation ($d_{tip\text{-}sub}$). In scanning mode the UME is positioned a few microns away to the substrate surface and scanned parallel to the substrate along the *x* and *y* axes; $i_T$ is plotted relative to its x-y position. Several modes of operation can also be used to study homogeneous reactions of products generated at either the tip or the substrate, these are feedback, generation-collection and direct modes. The latter method is often used to modify surfaces, whilst the others are used to characterise substrates.

In feedback experiments, the effect of any surface coupled reactions on $i_T$ is studied (figure 17). When the tip is brought from the bulk at a constant $i_{T,\infty}$ to a substrate surface (within a few radii), $i_T$ is affected by two factors. Firstly, the surface blocks diffusion of O, decreasing the current. However, if the surface can regenerate O, the result is an increase of flux of O to the tip, and a higher current. In practice, conductive substrates regenerate a redox species, meaning $i_T > i_{T,\infty}$ whereas insulating surfaces hinder diffusion and $i_T < i_{T,\infty}$. These effects are exacerbated the closer the tip is to the substrate, allowing substrate characteristics to be characterised.

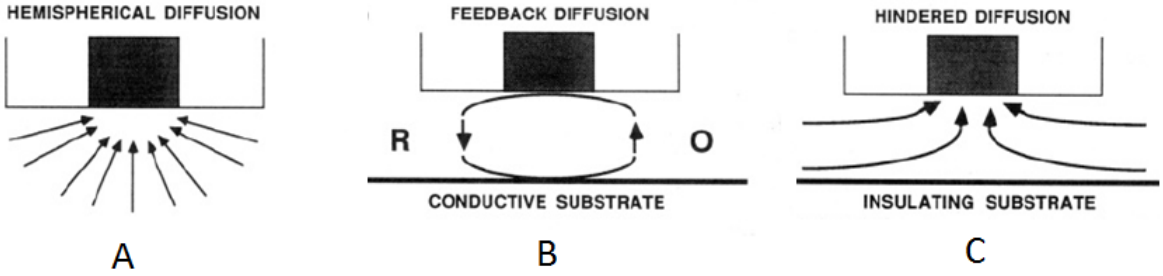


**Figure 17 Reproduced from [4] Scheme showing the diffusion properties surrounding a UME tip in different surroundings**

Generation collection experiments involve one electrode (tip or substrate), behaving as a generator for the species of interest, whilst the other electrode acts as a collector in chronoamperometry mode, at a potential optimised for the reaction. In tip generation substrate collection mode, tip generated redox species are collected by the substrate. Conversely, in substrate generation tip collection mode, an electrolyte containing no redox species is used, and any concentration profile of redox active species produced by the substrate itself is detected by the UME.

Direct mode typically involves using the UME as a working electrode and the substrate as a counter electrode. In this way, by assigning an equal but opposite current at the substrate versus the UME working electrode, modification of the substrate surface can occur via deposition or dissolution of ions. Some difficulties arise whilst using this latter mode, due to UME generated convection currents and overlap of the substrate and UME diffusion layers.

### 2.157 Electrochemical Impedance Spectroscopy (EIS)

EIS is a powerful tool for examining chemical and physical processes in solutions, at solid/liquid interfaces, and at solid-solid interfaces, as it allows the separation of the different voltage loss phenomena. Impedance is a generalised form of resistance, which takes into account the contributions of resistors, capacitors and inductors. Ohm's law states R = E/I and analogously, impedance $Z = E_o / i_o$ where $E_o$ and $i_o$ are the peak amplitude of an alternating voltage and resultant alternating current respectively. Impedance is a vector quantity, containing both a magnitude ($E_o/i_o$) and a direction, in this case a phase separation between the potential and current. Experiments are performed by applying a sinusoidal ac potential *E(t)* to the system or MFC being tested and measuring the current response; small perturbations are used to ensure responses are linear at steady or pseudo-steady state (figure 18), within the range of test equipment, and also to prevent damage to any biofilms present.

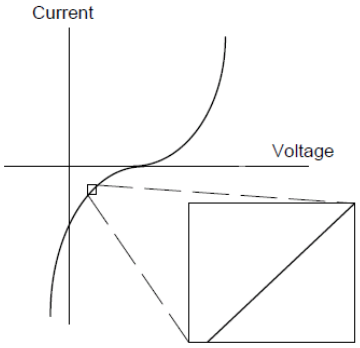


**Figure 18 Reproduced from [5] Pseudo-linearity on a current-voltage curve**

The ac potential (typically 10 mV applied) is given by equation 43.

$$E(t) = E_0 \sin(\omega t)$$

**Equation 43 A purely sinusoidal (ac) potential at time t (E(t)), where $E_0$ is maximum amplitude and $\omega=2\pi f$ (where f is frequency in Hertz ($s^{-1}$))**

It is convenient to think of this voltage as a rotating vector, where the length (projection on x-axis) is amplitude $E_0$ and its frequency of rotation is ω. If the system is linear, the current response is a sine wave often shifted in amplitude and phase angle (Φ), as given by equation 44. To compare the relationship between the voltage and current response, each can be represented by a separate phasor rotating at the same frequency, where one phasor (usually voltage) is taken as a reference signal

(figure 19). Since the phase angle is constant, the rotation notation is usually dropped, and the relationship between phasors can be plotted as vectors.

$$i(t) = i_0 \sin(\omega t + \phi)$$

**Equation 44 Current response at time t (i(t)) from an applied AC potential where $i_0$ is the maximum current amplitude, and Φ is any phase difference between applied voltage and current output**

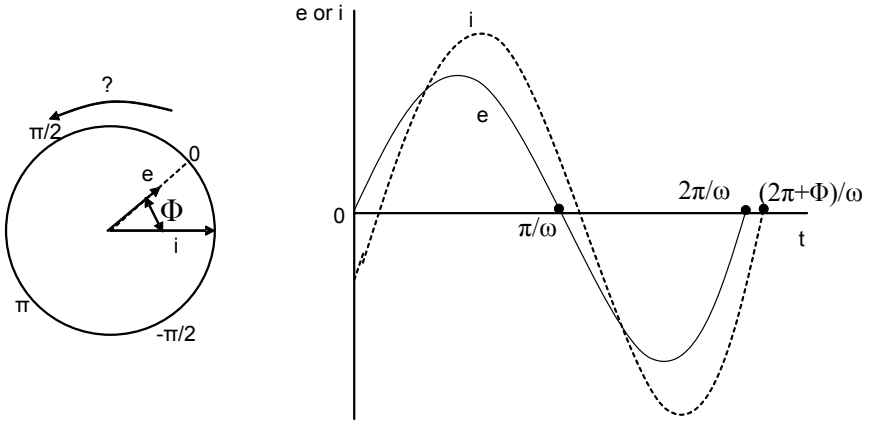


**Figure 19 Adapted from [4] Phasor diagram showing a typical relationship between alternating current and voltage signals at frequency ω. Input voltage and output current are not in phase.**

An expression analogous to Ohm's law allows the derivation of the impedance of the system, shown in equation 45. This shows impedance to be expressed in terms of a phase shift Φ and a magnitude $Z_0$.

$$Z = \frac{E_t}{I_t} = \frac{E_0 \sin(\omega t)}{I_0 \sin(\omega t + \phi)} = \frac{Z_0 \sin(\omega t)}{\sin(\omega t + \phi)}$$

**Equation 45 The impedance (Z) of a system, using Ohm's law**

With Euler's relationship (equation 46) it is possible to express the impedance as a complex function (z = x + jy, where j = √-1). The potential is now described as equation 47, and the current expressed as equation 48. Using these equations, the impedance is expressed as equation 49. The expression for Z(ω) is composed of a real and an imaginary part.

$$\exp(j\phi) = \cos\phi + j\sin\phi$$

**Equation 46 Euler's relationship, whereby cosΦ and jsinΦ correspond to real and imaginary parts respectively**

$$E_t = E_0 \exp(j\omega t)$$

**Equation 47 The potential described as a complex function**

$$I_t = I_0 \exp j(\omega t + \phi) = I_0 \exp(j\omega t)\exp(j\phi)$$

**Equation 48 The current described as a complex function. The first term contains magnitude information, the second term phase information and the third term is the rotating vector.**

$$Z(\omega) = \frac{E}{I} = (E_0 / I_0)\exp(-j\phi) = Z_0(\cos\phi + j\sin\phi)$$

**Equation 49 The impedance as a complex function, showing it to consist of a magnitude ($E_o/I_o$) and a phase (-Φ) (if in phase, this latter term cancels out)**

When a sinusoidal voltage is applied across a pure resistor (R), Ohms law applies and E=IR. Consequently, in response to equation 43, resulting current = (E/R)sinωt and the phase angle is zero. The impedance of the system (Z) is therefore the resistance, (R), independent of frequency (equation 50). Conversely, when a pure capacitor has a sinusoidal voltage applied to it, differential capacitance can be related to the current (I = dQ/dt) through Q = CE, or i(t) = C(dE(t)/dt) (equation 51). The phase angle in this case is π/2 (no 'real' component exists) and the impedance is inversely proportional to AC frequency. If a sine wave is applied to a capacitor, dipoles orientate. These respond to high frequency by moving (and transferring charge); this means at high frequency a capacitor acts like a wire with low impedance. However, at low frequency, no charge transfer occurs and impedance is high.

$$i(t) = \frac{E(t)}{R} = \frac{E_0}{R}\exp j\omega t$$
$$Z = \frac{E_0 \exp j\omega t}{i_0 \exp j\omega t} = R$$

**Equation 50 Impedance of a pure resistor**

$$i(t) = \frac{CdE(t)}{dt} = j\omega C E_0 \exp j\omega t$$
$$E(t) = E_0.\exp(j\omega t)$$
$$dE(t)/dt = E_0.j\omega.\exp(j\omega t)$$
$$i(t) = C.E_o.j\omega.\exp(j\omega t)$$
$$Z_C = E/I = \frac{E_0 \exp j\omega t}{j\omega C E_0 \exp j\omega t} = \frac{1}{j\omega C} = \frac{-j}{\omega C}$$

**Equation 51 Impedance of a pure capacitor**

Table 1 summarises different elements. Real systems can be represented by combining elements (pure resistors and capacitors) in series and parallel, to form 'equivalent circuits'. The most common equivalent circuit used in electrochemistry is the Randles circuit, shown in figure 20.

| Component | Current Vs.Voltage | Impedance |
|---|---|---|
| resistor | E= IR | Z = R |
| inductor | E = L di/dt | Z = jωL |
| capacitor | I = C dE/dt | Z = 1/jωC |

**Table 1 Adapted from [5]Summary of elements used in impedance**

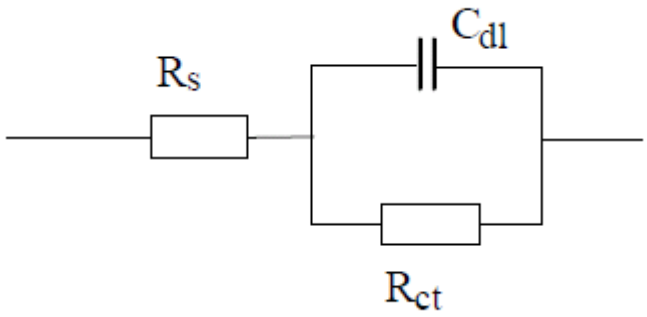


**Figure 20 The Randles circuit representing a typical electrochemical system. $R_s$ represents a series resistance (for example, resulting from the resistance of connections), $R_{ct}$ represents the resistance from charge transfer and $C_{dl}$ relates to the capacitance of the electrical double layer.**

Impedance can be plotted in various ways. On a Nyquist plot (figure 21), the real component is plotted on the X-axis, and the imaginary part on the Y-axis (negative). Each point is the impedance at one frequency, and the impedance is represented by a vector of length Z (the angle from the x axis = Φ). Another way to represent data is a Bode plot (figure 22), which has the advantage of showing frequency. Impedance is plotted with log frequency on the x-axis and both the phase shift and the absolute values of impedance ($|Z|=Z_0$) on the y-axis. Values of resistance and capacitance can be obtained by fitting plots to equivalent circuits, such as that shown in figure 20.

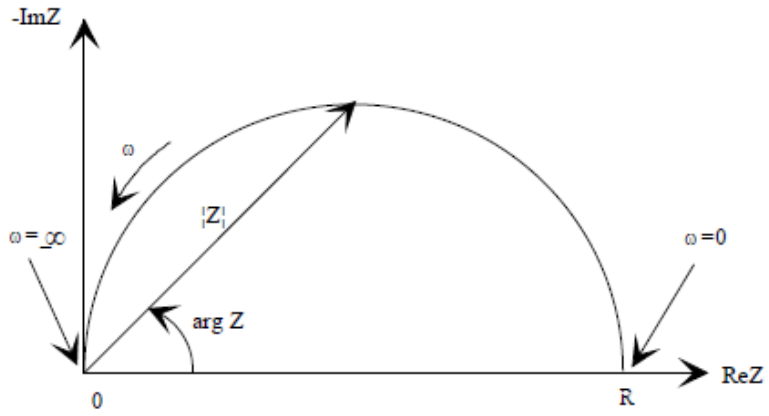


**Figure 21 Reproduced from [5] A Nyquist plot for an (RC) circuit, showing a semicircle characteristic of electrical circuits with one time constant**

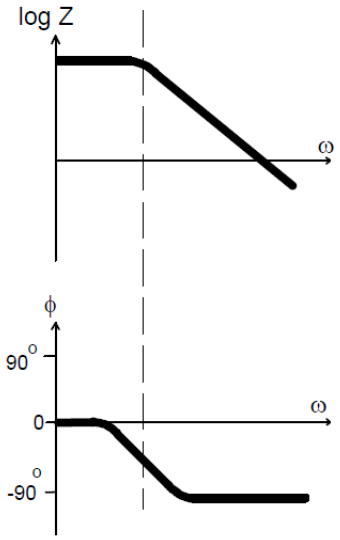


**Figure 22 Reproduced from [5] A Bode plot for an (RC) circuit (with one time constant)**

When applied to p-MFC fuel cell study, detailed information of internal ohmic resistances, and charge and mass transfer impedances, can be obtained from Nyquist and Bode plots through fitting with equivalent circuits. The internal ohmic resistance of a device can be determined by the high frequency intercept of the curve with the real impedance x-axis ($Z_{re}$). However, EIS measurements can overestimate internal ohmic resistances, especially at high dc discharge current densities (although this usually occurs at current densities of >0.5 A $cm^{-2}$ unlikely to be achieved with a p-MFC). The conductivity of electrode and membrane materials can also be easily measured using impedance. Charge transfer processes occur with different time constants ($R_{act}C_{dl}$ if modelled by parallel RC circuits, where $R_{act}$ is the charge transfer

impedance and $C_{dl}$ is the capacitance of the electrodes double layer) when compared to mass transport processes. This means that charge transfer parallel RC impedance (kinetic control semicircle at medium high frequencies) can be distinguished from mass transfer derived impedances (sloped line at low frequencies). Overall impedance is an extremely useful technique, but care must be taken with interpretation of data.

## 2.2 Non-electrochemical techniques

Non-electrochemical techniques have an essential role in materials characterisation, and in studying cellular responses. In this thesis, X-ray diffraction (XRD) and scanning electron microscopy (SEM) were used for materials characterisation (2.21 and 2.24 respectively), and Ultra-violet visible (UV-Vis) spectrophotometry and fluorescence were used to study cell and mediator interactions (2.22 and 2.23 respectively). SEM was additionally used to study cellular biofilms.

### 2.21 X-Ray diffraction (XRD)

When X-rays interact with a crystalline substance (phase), a diffraction pattern results which is characteristic of that particular substance. Furthermore, the areas under peaks are related to the amount of each phase present in a sample. Powder diffraction is thus ideally suited to characterisation and identification of polycrystalline phases.

An electron in an alternating electromagnetic field will oscillate at the same frequency as the field. When an X-ray beam hits an atom, the electrons around the atom start to oscillate at the same frequency as the beam, with destructive interference in almost all directions. However, atoms around a crystal are arranged in a regular pattern, and in a few directions constructive interference will occur whereby the waves will be in phase, and there will be well defined X rays leaving the sample at various directions. X-ray diffraction is based on constructive interference of monochromatic X-rays and a crystalline sample.

X-rays are generated by a cathode ray tube, filtered to produce monochromatic radiation, collimated to concentrate, and directed toward the sample. The interaction of the incident rays with the sample produces constructive interference (and a

diffracted ray) when conditions satisfy Bragg's Law ($n\lambda=2d \sin\theta$) (Figure 23). This law relates the wavelength of electromagnetic radiation to the diffraction angle and the lattice spacing in a crystalline sample. Each rational plane of atoms in a crystal will undergo refraction at a single, unique angle (for x-rays of a fixed wavelength). Diffracted X-rays are then detected, processed and counted. By scanning the sample through a range of 2θ angles, all possible diffraction directions of the lattice should be attained due to the random orientation of the powdered material.

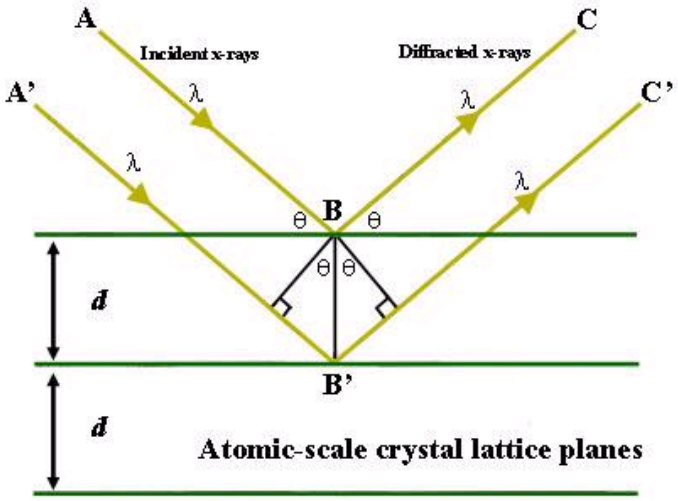


**Figure 23 Constructive interaction of X rays with a crystalline sample. For example, in a crystal with crystal lattice planar distances d, where the travel path length difference between the ray paths ABC and A'B'C' is an integer multiple of the wavelength, constructive interference will occur for a combination of that specific wavelength, crystal lattice planar spacing and angle of incidence (θ).**

## 2.22 Ultra-violet visible Spectrophotometry

UV-Vis spectrophotometry is a method where the absorbance of a solution over a range of wavelengths can be measured. The method presents a quantitative way to determine the concentration of an absorbing species within a solution; the Beer-Lambert law (equation 52) can be used to relate the absorption of light to the concentration of the species present in solution.

$$A = \log_{10}\frac{I_o}{I} = \varepsilon l c$$

**Equation 52 The Beer-Lambert Law: here A refers to the Absorbance, ε is the extinction coefficient, l is the pathway length and c is the concentration. This law assumes that an absorbing species has a uniform concentration distribution in solution**

To calculate the concentration of a species from the measured absorbance a calibration curve is used. This graph plots absorbance (at some wavelength) against known concentration. The gradient from the calibration curve gives the extinction coefficient of the absorbing solution. This can be applied to the Beer-Lambert law in order to find the concentration of an unknown solution.

## 2.23 Fluorescence

In this thesis, fluorescence is specifically used to study chlorophyll. When light is absorbed by chlorophyll pigments, it can undergo three fates which operate in competition; used for photosynthesis, dissipated as heat, or re-emitted as light (chlorophyll fluorescence). An increase in one results in a decrease of the others. Hence by measuring the yield of chlorophyll fluorescence, information about photochemistry and heat dissipation can be obtained [6]. The fluorescence of a molecule is the light emitted spontaneously due to the transitions from excited singlet sates (usually $S_1$) to various vibrational levels of the electronic ground state [26]. A schematic representation of the spontaneous molecular relaxation processes that follow any excitation of a molecule to a higher electronic excited state i.e. by the absorption of a photon is given by a Jablonski diagram, shown in figure 24.

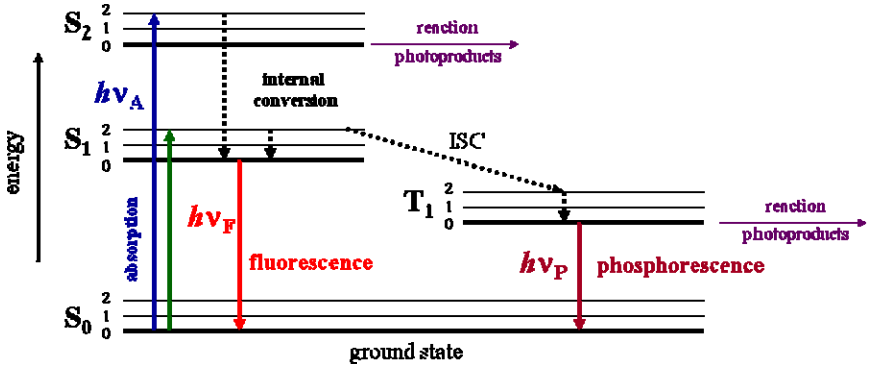


**Figure 24 Reproduced from [7] Jablonski diagram with fluorescence (F) highlighted in red. After absorption of a photon, a fluorophore is excited to some higher vibrational level of either $S_1$ or $S_2$, before relaxing to the lowest vibrational level of $S_1$ by internal conversion (a non-radiative process). Such transitions are quantum mechanically allowed, and the lifetimes of the excited states are short (typically $10^{-8}$ s). Phosphorescence (P) is quantum mechanically forbidden and lifetimes are long, ranging from $10^{-3}$- 1 s.**

Electronic energy transfer to a quencher molecule can also occur. Here a bimolecular collision typically occurs between the excited fluorophore and the quencher species,

resulting in the quenching of the excited state, $S_1$. The excited state fluorophore is then returned to ground state with no emission of a photon. The Stern-Volmer constant ($K_{SV}$) can be found from the gradient of a plot of the fluorescence ratio $I_f(0)/I_f(Q$ (where $I_f(0)$ is the fluorescence intensity in absence of quencher and $I_fQ$ is the fluorescence intensity in the presence of quencher) against the quencher concentration (Q), by equation 53, where $K_{SV}$ is equal to equation 54. This gives a measure of the quenching ability of a molecule.

$$\frac{If(0)}{If(Q)} = 1 + \frac{k_Q}{k_f}[Q]$$

**Equation 53 A plot of the fluorescence ratio ($I_f(0)/I_f(Q)$, against the quencher concentration [Q] is linear with a gradient equal; to the Stern-Volmer constant $K_{SV}$**

$$K_{SV} = \frac{k_Q}{k_f}$$

**Equation 54 The relationship of $K_{SV}$ to the quenching and fluorescence rate constant ($k_Q/k_f$ respectively). Intensity (steady-state) measurements only determine the ratio of $k_Q/k_f$**

Pulse amplitude modulation (PAM) fluorescence is the standard way of measuring photosynthetic activity and related physiological activities *in-vivo* in photosynthetic organisms. It employs a combination of four radiation sources; modulated, actinic, saturating and far red – that produce quantitatively and qualitatively different radiation incident on a photosynthetic object [6]. Alternatively, for the measurement of chlorophyll a fluorescence, the F684 to F735 ratio can be measured with a conventional fluorimeter [6]. These two maxima are apparent in the chlorophyll fluorescence spectra; one in the red region, near 690nm and one in the far-red region, near 735 nm. The ratio, F684:735 reflects the relative PSII and PSI activities, and therefore can be used as a tool to assess performance of the photosynthetic apparatus [6]. This approach does not require dark adaptation of the photosynthetic organism, and uses a conventional fluorimeter.

## 2.24 Scanning electron microscopy

Scanning Electron Microscopy (SEM) is a technique used for imaging samples with an electron beam. Samples are placed within a vacuum in the microscope, before

being scanned with a beam of electrons which can interact with the sample surface (figure 24 compares image formation in SEM to that in other microscopy). Since an electron is a charged particle, the beam has a strong interaction with the sample (due to a Coulomb interaction) and electrons scattered by atomic layers near the sample surface when collisions occur. As a result, the direction of electron motion changes and its energy is partially lost. Once an incident (primary) electron enters a substance, its direction of motion is changed by various obstructions, resulting in multiple complex scattering. Electrons can also be reflected back in the direction of the incident beam (back scattered) or if the specimen is sufficiently thin, the electrons can pass through the sample (figure 25).

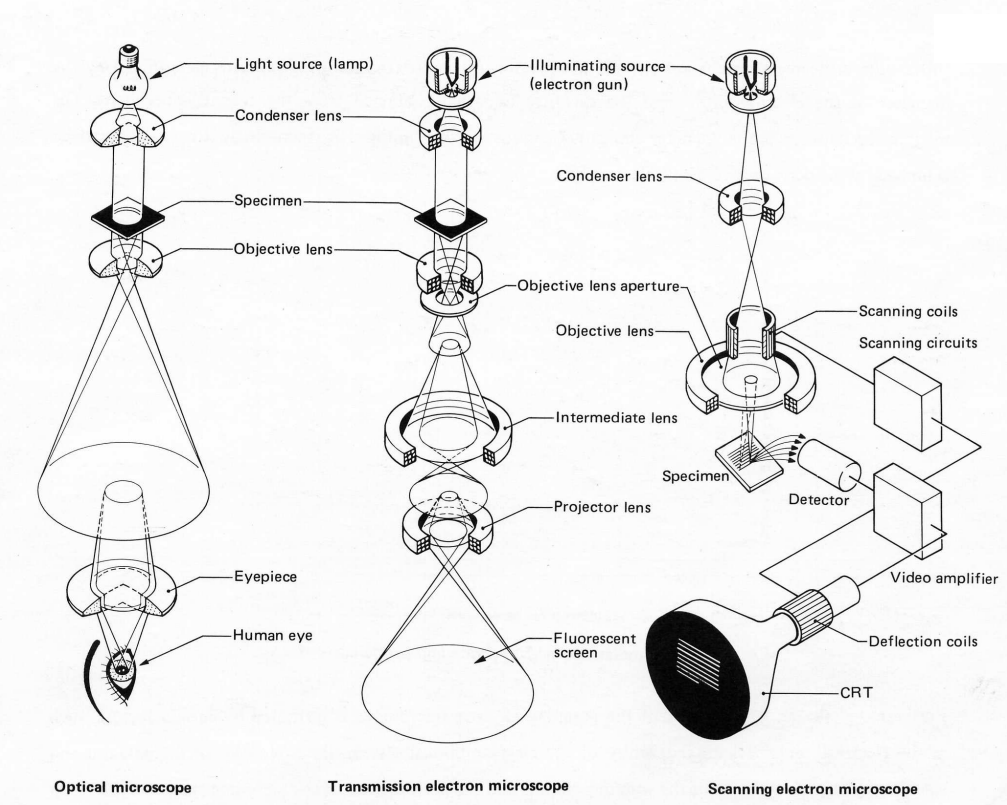


**Figure 25 Adapted from [8] Schematic of optical microscope, transmission electron microscope and scanning electron microscope (SEM), showing the steps towards image formation**

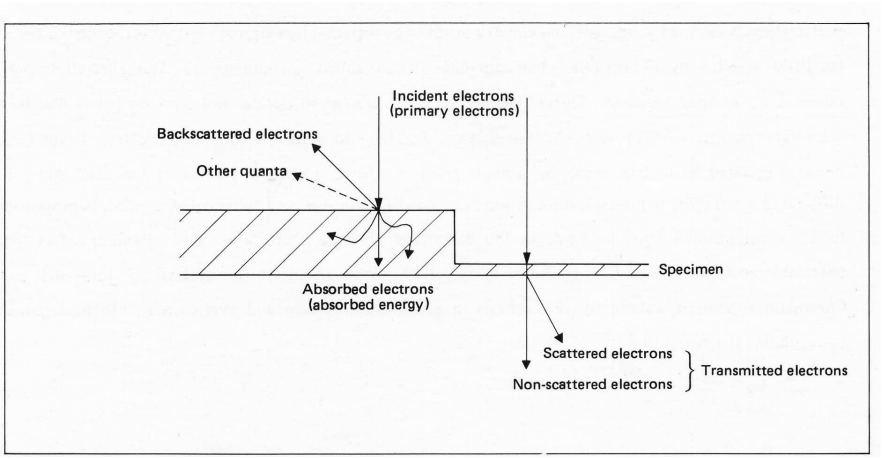


**Figure 26 Adapted from [8] The interaction between an incident beam of electrons and the sample**

After interaction, quanta (for example, secondary electrons) hold information which describes the nature of the sample (for example its atomic number, elemental distribution, topography, surface potential distribution, magnetic domain, chemical and crystallographic characteristics). This information is converted into a video signal and displayed as a scanning image. Table 2 lists the relation between the types of scanning image and obtainable information.

| Types of scanning image | Major information | Detectors and instruments |
|---|---|---|
| Secondary electron image | Surface structure, potential distribution, magnetic domain | Scintillator-PMT detector |
| Backscattered electron image | Composition, topography, magnetic domain, crystalline state | Paired semiconductor detector |
| Transmitted electron image | Composition, crystalline state | Scintillator-PMT detector |
| Absorbed electron image | Composition, topography | Absorbed current amplifier |
| Auger electron image | Elemental distribution of surface | Auger scanning electron microscope |
| Cathodoluminescence image | Visible or infrared luminescence | PMT detector |
| X-ray image | Elemental distribution | X-ray spectrometer |
| Electromotive force image | Electromotive force distribution in semiconductor devices | Electromotive force amplifier |

**Table 2 Adapted from [8] Types of quanta and obtainable information**

The advantage of SEM over other microscopy analysis methods is the scale of magnification – samples can be studied on the millimetre to the nanometre scale.

## 2.3 References


1. Fisher, A.C., *Electrode Dynamics*. Oxford Chemistry Primers, ed. R.G. Compton. 1998, Oxford: Oxford University Press.
2. Fisher, A.C. *Linear Sweep & Cyclic Voltammetry - The Principles*. [cited 2011 11/11]; Available from: http://www.cheng.cam.ac.uk/research/groups/electrochem/JAVA/electrochemistry/ELEC/l4html/cv.html.
3. Zhao, F., Slade, R.C.T., and Varcoe, J.R., *Techniques for the study and development of microbial fuel cells: an electrochemical perspective.* Chemical Society Reviews, 2009. **38**(7): p. 1926-1939.
4. Bard, A.J. and Faulkner, L.R., *Electrochemical methods. Fundamentals and Applications. 2nd ed*. 2001, John Wiley & Sons.
5. Gamry-Instruments. *Basics of Electrochemical Impedance Spectroscopy-Application Notes*. 2011 [cited 2011 11/11]; Available from: http://www.gamry.com/application-notes.
6. Fai, P.B., Grant, A., and Reid, B., *Chlorophyll a fluorescence as a biomarker for rapid toxicity assessment.* Environmental Toxicology and Chemistry, 2007. **26**(7): p. 1520-1531.
7. Ana Luiza, P., Nery, R., Liegel, M., and Fernandez, C., *Fluorescence and Chemiluminescence:Teaching Basic Principles by Simple Demonstration Experiments* Chemical Education Journal 2009. **13**(2): p. 13-22.
8. JEOL-European-Institute. *Scanning electron microscopy A-Z - Basic knowledge for using the SEM*. 2009 [cited 2011 11/11]; User manual]. Available from: http://www.jeolusa.com/DesktopModules/Bring2mind/DMX/Download.aspx?Command=Core_Download&EntryId=598&PortalId=2&TabId=320.

# Chapter 3. Testing of Basic p-MFC Device

# Chapter 3 – Testing of Original p-MFC Device

## 3.1 Introduction

The basic photo-microbial fuel cell (basic p-MFC) device, as developed by colleagues in Cambridge, consists of a thin cell utilising an indium tin oxide (ITO) coated glass working electrode with the algae *Chlorella vulgaris* held in a filter paper matrix in the anode along with a potassium ferricyanide (ferricyanide) redox mediator. Despite the carbon neutral benefits that algae could bring to a p-MFC, few p-MFC systems have utilised single cultures of algae as the main anodic photosynthetic material. Instead most studies have used cyanobacteria (see chapter 6). This chapter reviews the various strategies taken previously to incorporate whole algal cells into p-MFCs in the literature, before studying the basic p-MFC device in more detail.

Unlike with various bacteria, long range electron transport from eukaryotic organisms (such as algae) to an electrode without a mediator has so far not proved possible. This is thought due to the lack of conductive extracellular matrices. Using *Chlamydomonas reinhardtii*, Ryu *et al.* [1] overcame this issue by inserting a nanoelectrode into the algal chloroplast proximal to thylakoid membranes and collecting high energy photosynthetic electrons from either the plastoquinone pool or reduced ferredoxin sites. Subsequently, electrons travelled out of the cell via the nanowire [1]. When an overvoltage was applied, current densities of 20 A $m^{-2}$ were produced. Although this approach minimised energy losses associated with the transformation of solar energy into reductant products, the nanoelectrode could only collect electrons from the immediate thylakoid stromal vicinity in which it was embedded. This approach would also lead to large scale-up issues.

Another way to overcome the issue of electron transport to the electrode is to use mediators in solution. Few examples in the literature use this approach with algal cells and mediator in the anodic chamber. This is most often due to the fact that problems were experienced with short circuit reactions occurring between the reduced form of mediator and photosynthetically evolved oxygen, reducing p-MFC efficiency [2-4]. Instead, eukaryotic organisms are popularly used with a mediator in the cathodic chamber. In the cathodic chamber, oxygen is beneficial for reacting with

electrons at the cathode. A p-MFC was created using the oxidation of ferrocyanide to ferricyanide at the anode, and a solution of *C. vulgaris* and methylene blue mediator at the cathode which acted as an electron acceptor, whilst simultaneously reducing $CO_2$ to biomass [5]. A net potential difference of 70 mV was achieved between the two half cells and power densities of 2.7 mW $m^{-2}$ of cathode surface area were recorded [5] However, in this paper no further detail was given as to how methylene blue could diffuse through *C. vulgaris* cell outer membranes and how exactly it interacted with cellular machinery. This lack of understanding of the mode of mediator reduction by cells is generally a very commonly encountered issue with all p-MFC literature.

Where algae are present in the anodic chamber of a p-MFC device, most studies rely on photosynthetically produced hydrogen and its *in situ* oxidation at the anode for power production. However, complex strategies are required due to the sensitivity of expression and stability of the hydrogenase enzyme towards molecular oxygen [6]. Genetic mutants tolerant to $O_2$ can be produced, or the PSII oxygen evolving reactions from the hydrogen production process can be suppressed temporarily, by transferring cells into sulphur deprived conditions [6, 7]. This latter method was used to directly produce electricity through *in situ* oxidation of hydrogen at polymer coated electrocatalytic electrodes, using *C. reinhardtii* [6].

Algal cells have been more popularly incorporated into mixed species p-MFC devices in the literature, which in the simplest case involves two electrochemical half cells containing different organisms. This simple approach was employed in a BPV containing two half cells (anodic and cathodic) with platinum electrodes, composed of *Rhodospirillum rubrum* in solution and a marine algal biofilm respectively [8]. With no mediators in solution, this produced an open circuit voltage of 0.96 V after 21 hours, and a SC current density of 750 mA $m^{-2}$ (75 μA $cm^{-2}$) [8]. No detail was given as to pathways of electron transport out of the cells, although this study was very early.

However, much evidence exists to suggest that mixed systems can have greater success than single cultures alone. In nature, photosynthetic organisms are often found together in symbiotic communities, containing heterotrophs that utilise products produced by photosynthetic partners [9], or even photosynthetic species which utilise

products produced by bacteria [10]. For example, a p-MFC equipped with a graphite felt anode and air cathode, and inoculated with a green-hot spring microbial mat produced photo-induced maximum power densities of 3.7 mW $m^{-2}$ six days after assembly, although this increased upon purging with nitrogen gas (thought to be due to the depletion of oxygen) [11]. Here, it was proposed that green algae produced organics that served as substrates for electricity generation by heterotrophic bacteria [11]. Many other natural photosynthetic biofilms studies and sediment type p-MFCs used photo-biocathodes and/or photo-bioanodes composed of uncharacterised photosynthetic natural biofilms, most likely containing algae [9, 12-15]. Although high current densities were obtained with some systems (for example, a p-MFC containing natural a pond biofilm and polyaniline coated anodes produced 5.9 mW $m^{-2}$ [15]), as the photosynthetic material was uncharacterised, the studies are irreproducible by other groups. Additionally, as cell types were unknown, mechanisms of electron transfer could not definitively be specified. Consequently, mixed systems often present interesting stand-alone studies, but single cell activities can not be quantified.

Overall, it can be seen that a large issue with the p-MFC literature is that much is still to be learned about electron transfer mechanisms and cellular behaviour. Although an overview of what occurs is generally known, specifics are often, as of yet, undetermined. In contrast, the fact that the basic p-MFC consists of a pure culture of *C. vulgaris* in a simple set-up means it can be characterised extensively.

### 3.11 Theoretical calculations of cell potential in p-MFC device

The expected potential for a p-MFC device can be calculated according to a general equation (given in equation 26 of chapter 2). For this calculation, individual components including redox potentials at the cathode and anode, charge transfer derived overpotentials at the anode and cathode, concentration potentials at anode and cathode and Ohmic losses need to be considered.

In the basic p-MFC device the redox reaction occurring at the cathode is given in equation 1. The standard potential ($E^o$) for this reaction is 1.229 V w.r.t standard hydrogen electrode (SHE in 1.18 M $H^+$ (pH = 0), T = 298 K, $P(O_2)$ = 1 bar) [16]. However, as the pH at the cathode is pH 3.5, $E^o$ must be adjusted. Using equation 1,

the change in V for each pH decade can be calculated (shown in equation 2). After adjusting for each change in decade (pH unit), $E^o$ = 1.229 V -(3.5 x 59 mV) = 1.052 V

$$O_2 + 4H^+ + 4e^- \leftrightarrow 2H_2O$$

**Equation 1 Water formation at the cathode**

$$E = E^0 - \frac{RT}{nF}\ln K$$
$$E = E^0 - \frac{RT}{nF}\ln\frac{(a^{H_2O})^2}{(a^{O_2})(a^{H^+})^4}$$
$$E = E^0 + \frac{RT}{4F}\ln(a^{H^+})^4$$
$$E = E^0 + \frac{RT2.303}{F}\log(a^{H^+}) = E^0 - 59mVpH$$

**Equation 2 Calculation of change in V at the cathode for each pH decade**

The redox reaction occurring at the anode in the basic p-MFC is given in equation 3, in which ferrocyanide (Fe(II)) is oxidised to ferricyanide (Fe(III)). $E^o$ for this reaction is 0.358 V w.r.t normal hydrogen electrode (NHE) [16]. However, $E^o$ assumes equilibrium conditions where a 50:50 mix of ferricyanide/ ferrocyanide exist at the anode. To calculate theoretical half cell reduction potentials where 100% (9 mM) solutions of ferricyanide or ferrocyanide are present, the Nernst equation must be used (although this also assumes equilibrium). Where 9 mM ferricyanide is present at the anode, equation 4 applies. Conversely, when 9 mM ferrocyanide is present at the anode, equation 5 applies (all w.r.t NHE).

$$[Fe(CN)_6]^{4-} \leftrightarrow [Fe(CN)_6]^{3-} + e^-$$

**Equation 3 Ferrocyanide oxidation at the anode**

$$E_{anode} = E^{\phi} - \frac{RT}{nF}\ln\frac{[\mathrm{Re}d]}{[Ox]}$$
$$E_{anode} = 0.358 - \frac{8.314x298}{1x96485}\ln\frac{1x10^{-9}}{9x10^{-3}}$$
$$E_{anode} = 0.358V - (-0.412V)$$
$$E_{anode} = 0.77V$$

**Equation 4 Using the Nernst equation to calculate the potential at the anode where 100% ferricyanide is present. Although 1 nm was used in the calculations as the low background concentration of ferrocyanide present in solution, this is only approximate.**

$$E_{anode} = E^{\phi} - \frac{RT}{nF}\ln\frac{[Ox]}{[\mathrm{Re}\,d]}$$
$$E_{anode} = 0.358 - \frac{8.314x298}{1x96485}\ln\frac{9x10^{-3}}{1x10^{-9}}$$
$$E_{anode} = 0.358V - 0.412V$$
$$E_{anode} = -0.054V$$

**Equation 5 Using the Nernst equation to calculate the anodic potential with 100% ferrocyanide**

Other factors are required for calculation of $E_{cell}$, such as voltage drop over the membrane and charge transfer and mass transfer overpotentials at anode and cathode (detailed in equation 26 of chapter 2). These factors require study of the p-MFC system for their calculation. For example, to calculate the anode and cathode overpotentials, reference electrodes could be inserted in both anodic and cathodic chambers. However, a generalised equation for the calculation of $E_{cell}$ can be made according to equation 6. This idealised system would only be applicable when the device was under equilibrium conditions, for example at open circuit where no current is flowing, and where no voltage losses occurred (such as from resistance in the membrane and electrolyte). Using equation 6, with a 50:50 mix of ferrocyanide/ ferricyanide, $E_{cell}$ = 0.694 V; with 100% ferricyanide (9 mM), $E_{cell}$ = 0.282 V; and with 100% ferrocyanide (9 mM), $E_{cell}$ = 1.106 V. Figure 1 illustrates the basic calculation of $E_{cell}$, showing a situation where a 50:50 mix of ferricyanide/ ferrocyanide is assumed present at the anode.

$$E_{cell} = E_{cathode} - E_{anode}$$

**Equation 6 Rough estimate of theoretical p-MFC cell voltage**

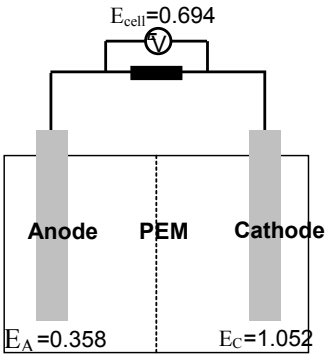


**Figure 1 Theoretical cell potential w.r.t NHE, where a 50:50 mix of ferricyanide/ ferrocyanide exists at the anode, $E_A$ is anodic potential, $E_C$ is cathodic potential (both w.r.t NHE)**

### 3.12 Chapter Aims

In this chapter the basic p-MFC device is assembled and tested for basic characteristics, with results compared to those expected from accepted p-MFC theory. First current outputs are characterised through chronoamperometry in both dark and light with varying amounts of *C. vulgaris* cells and a ferricyanide mediator present in the anodic chamber. Photocurrents are additionally measured with varying light intensity. In the literature, p-MFC outputs are most commonly characterised in light conditions, with all currents thought due to cellular activity. Although both respiration and photosynthesis are thought to contribute reductive equivalents (electrons) which can reduce a redox mediator, the specific contributions of each process to current (and power) output has not been well determined. Secondly, general p-MFC theory is further tested in this chapter by performing chronoamperometry with the anode held at differing potentials and with the redox mediator present in different oxidation states. According to p-MFC theory (given in detail in chapter 1), currents (and photocurrents) should only be produced where cells and an oxidised redox mediator exist in solution in the anodic chamber (as no interaction with ferrocyanide is known to occur). The redox mediator can then be reduced by reductive equivalents produced by cells, before diffusing to the anode. If the anode is at an optimum potential for the reoxidation of the redox mediator, an electron can be transferred, and currents are produced. If these conditions are not satisfied, no power output should be seen (over background levels).

## 3.2 Experimental

### 3.21 Device set up

The basic p-MFC device was assembled as outlined in figure 2 (with a more detailed schematic shown in figure 3). The cathode consisted of a piece of glass, upon which Au, then Pt had been evaporated. The cathodic chamber consisted of a 2 $cm^2$ piece of filter paper inoculated with 100 μL KCl pH3.5. Nafion acted as the proton exchange membrane (PEM), on top of which another piece of filter paper with 100 μL concentrated algal solution and 9 mM Fe (either ferricyanide, ferrocyanide or a 50:50 mix of 4.5 mM ferrocyanide/ 4.5 mM ferricyanide) was placed. The cells were prepared at desired concentrations as outlined in the appendix. An ITO glass anode completed the sandwich. An Ag wire reference electrode was constructed in the

anodic chamber by first Zn etching a strip of the ITO anode and then attaching a Ag wire. Perspex clamps screwed together held the device together tightly.

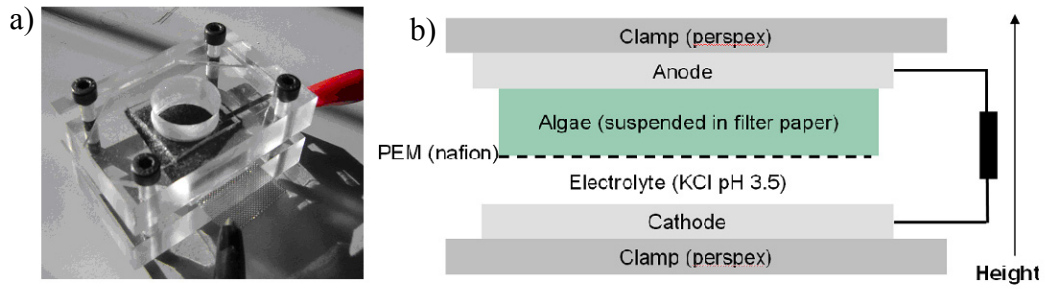


**Figure 2 a) Image of p-MFC device and b) General schematic of p-MFC device**

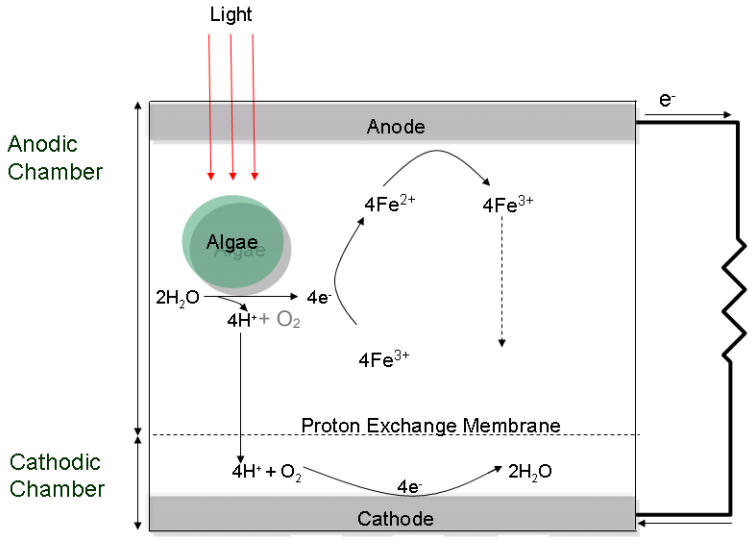


**Figure 3 Schematic of device showing anodic and cathodic reactions**

### 3.22 Device testing

Electrochemistry was carried out on an Autolab PGSTAT with an inbuilt frequency response analyser. Basic testing involved chronoamperometry experiments.

First, it was investigated how the *C. vulgaris* cell concentration in the anodic chamber affected p-MFC current output. The p-MFC device was set up with 9 mM ferricyanide and varying concentrations of *C. vulgaris* cells suspended in the filter paper anodic matrix (between 6 x $10^7$ cells 100 $\mu L^{-1}$ and 4x$10^8$ cells 100 $\mu L^{-1}$ in the anodic chamber). For each cellular concentration, chronoamperometry was performed at the half wave potential as identified from cyclic voltammetry measurements. This potential was chosen for further testing as this was thought the

most sensitive for measuring changes in current (therefore potentially giving largest device outputs). Currents were measured in the dark and, once stable, p-MFC devices were illuminated with an optical fibre light (620 nm) at an intensity of $5x10^{-3}$ W $cm^{-2}$. Photocurrents were calculated by subtracting the (dark) background from the current in the light after 1000 seconds illumination.

The effect of light intensity on p-MFC current output was investigated. Chronoamperometry (at the half wave potential) was performed with $3x10^{8}$ cells 100 $\mu L^{-1}$ in the anodic chamber. Once stable, the p-MFC device was illuminated with an optical fibre light (620 nm) at varying intensity between $5x10^{-4}$ and $5x10^{-3}$ W $cm^{-2}$ and photocurrents calculated.

Finally, the effect of operating potential on p-MFC current output was studied. Cyclic voltammetry (between 0.3 and 0.5 V at 5 mV $s^{-1}$) was carried out on the constructed p-MFC device (containing $3x10^{8}$ cells 100 $\mu L^{-1}$ in the anodic chamber) to identify the reduction potential of ferricyanide, the oxidation potential of ferrocyanide, and the half-wave potential of the ferricyanide/ ferrocyanide couple. Experiments first involved performing chronoamperometry at these potentials with either 9 mM ferricyanide, 9 mM ferrocyanide or a 50:50 mix of 4.5 mM ferrocyanide/ 4.5 mM ferricyanide. Currents were allowed to stabilise in the dark, before illuminating with an optical fibre light (620 nm) at an intensity of $5x10^{-3}$ W $cm^{-2}$. Photocurrents were calculated by subtracting the (dark) background from the current in the light. Note that in all results, currents from a p-MFC control where no cells were present were subtracted before calculations.

## 3.3 Results and Discussion

### 3.31 Device testing

The device was first set up with 9 mM ferricyanide, and chronoamperometry was performed at the half wave potential for the ferricyanide/ ferrocyanide redox couple (w.r.t Ag wire reference), as determined by cyclic voltammetry (results not shown). The *C. vulgaris* cell concentration suspended in the filter paper matrix in the anodic chamber was varied, and background (dark) currents and photocurrent (additional

currents in light) were measured. Background (dark) currents are shown in figure 4, and calculated photocurrents are shown in figure 5.

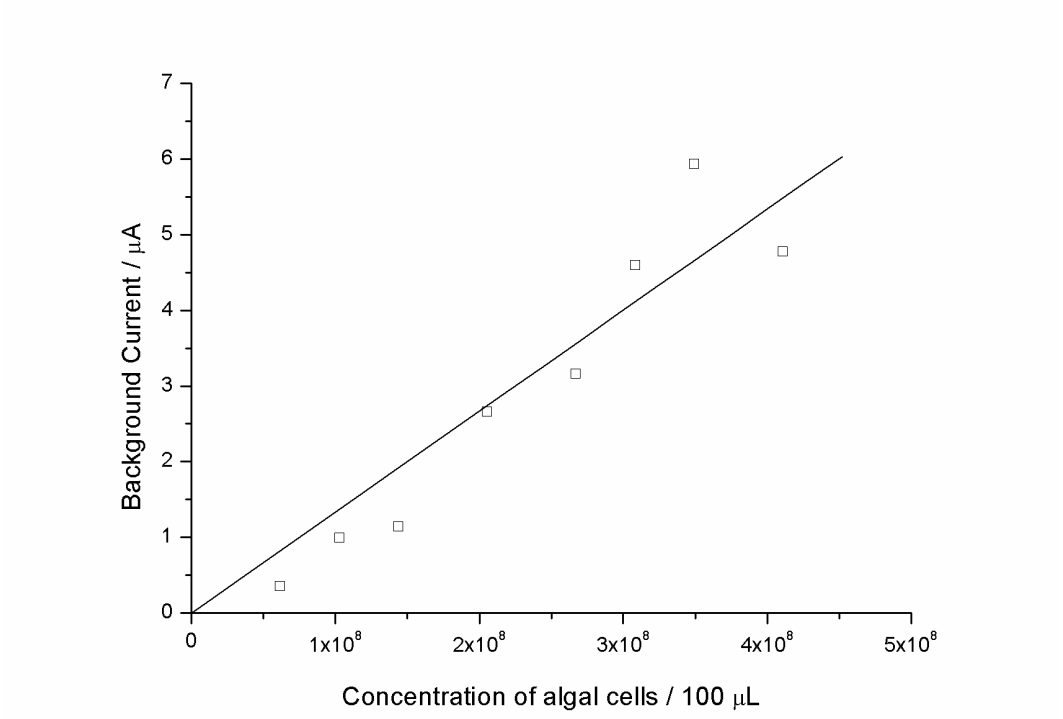


**Figure 4 The relationship between background dark current and algal cells**

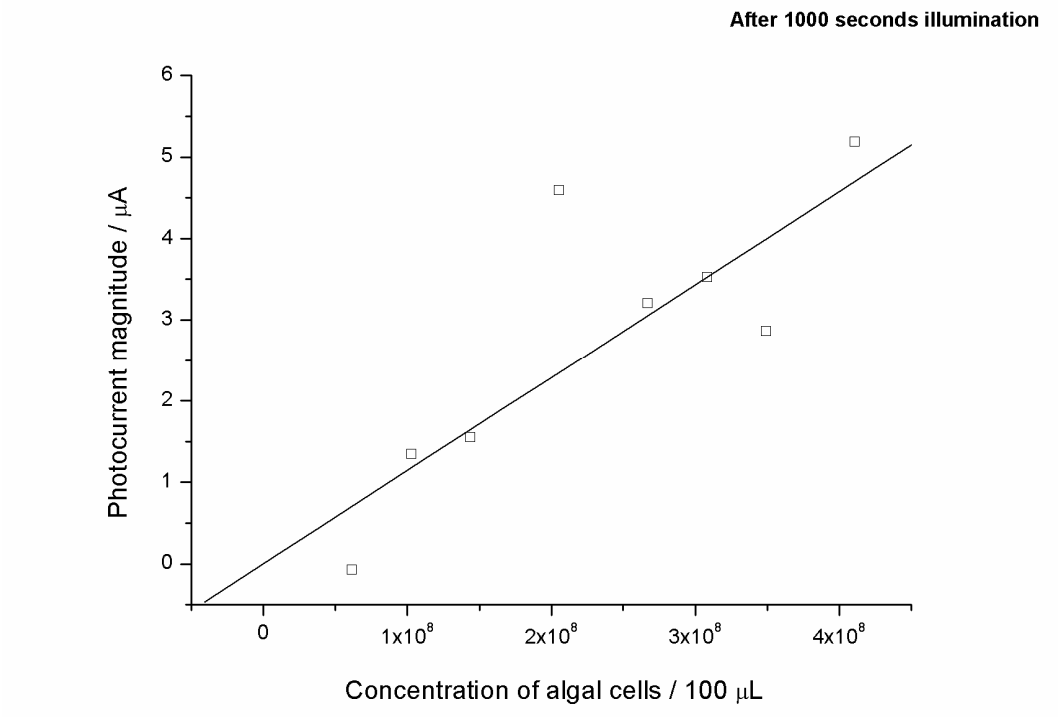


**Figure 5 The relationship between photocurrent and the number of algal cells (after 1000 seconds illumination)**

Measured open circuit potential ($E_{cell}$) of the p-MFC device varied greatly, between 50-200 mV. Although inconsistent, this fit reasonably well with the theoretical value for $E_{cell}$ with 9 mM ferricyanide present in the anodic chamber (calculated as 0.282 V). The low measured $E_{cell}$ (when compared to theoretical values) could be explained as the theoretical $E_{cell}$ did not take into account voltage losses from such factors as cell resistance, and approximated some concentrations in the calculations.

In the literature it is assumed that all currents observed in the p-MFC device are directly as a result of cellular activity. It is widely accepted that reductive equivalents produced in a p-MFC, and used to reduce a mediator, come from both respiration (occurring in dark and light) and photosynthesis occurring in light (see chapter 1 for more detail and references). However, some papers in the literature only test p-MFC devices in light, only citing photosynthesis as the responsible process for device activity. Figure 4 shows that as the number of *C. vulgaris* cells in the anodic chamber of the p-MFC increased, the background (dark) currents also increased. This could be explained as reductive equivalents from respiration are thought able to reduce a mediator (in this case ferricyanide) in solution. The more algal cells in solution, the more reductive equivalents generated and the greater the reduction of the ferricyanide mediator. As more reduced ferricyanide existed to be reoxidised at the anode, current output of the p-MFC was higher. It has been postulated that the ferricyanide mediator can react with cell-derived reductive equivalents at ferri-reductase membranes on the cell outer membrane [17, 18], but this is discussed further in chapter 4.

Figure 5 illustrates that the magnitude of photocurrents produced in light also increased with *C. vulgaris* cell concentration. This inferred that extra reductive equivalents generated in photosynthesis were used to reduce the ferricyanide mediator. If this was the case, it followed that the more cells present, the more extra reductive equivalents were produced. However, interestingly, when photocurrent magnitude was measured with changing light intensity, no correlation was observed (data not shown). This could be due to all light concentrations tested being higher than the intensity needed for maximum photosynthetic action. However, this could also infer that the photocurrents were not directly as a result of algal photosynthesis.

According to p-MFC theory, currents are produced when photosynthetic cells produce reductive equivalents which are used to reduce an oxidised mediator. Once reduced, the mediator diffuses to the anode, becoming reoxidised. The resulting electron at the anode subsequently travels round an external circuit to the cathode, where it reduces oxygen to form water. Consequently, p-MFC current output would only be expected where two criteria are satisfied. Firstly, an oxidised mediator is required in the anodic chamber. Without this, the reduced equivalents produced by cells would have no way to reach the anode, and electrons would not be deposited. Second, p-MFC currents outputs would only be expected where the potential of the anode is set at the oxidation potential for ferrocyanide. If the potential of the anode is not optimum for ferrocyanide to become oxidised, electrons from the reduced equivalents produced by cells would not be transferred. It is, however important to note that small currents would still be expected at conditions not matching the above criteria due to background levels of reactions occurring. To test whether currents (and photocurrents were directly due to cellular activity (both respiration and photosynthesis), chronoamperometry was performed whilst holding the anode at different potentials identified from cyclic voltammetry (either at the reduction potential for ferricyanide or the oxidation potential for ferrocyanide). Additionally, the anodic chamber contained either 9 mM ferricyanide, 9 mM ferrocyanide or a 50:50 mix of 4.5 mM ferricyanide/ 4.5 mM ferrocyanide in solution. Initially the current was measured in the dark; when stable, the p-MFC device was periodically illuminated. Typical results (obtained with 9 mM ferricyanide) are shown in figure 6.

As shown in figure 6, when the basic p-MFC anode was held at the reduction potential, a negative background current was measured. Conversely, when the anode was held at the oxidation potential, a positive background current was measured. This made sense as by convention oxidation currents are positive and reduction currents negative. Summary graphs of both background (dark) currents and photocurrents are shown in figures 7 and 8 over the full range of potentials and range of ferricyanide/ferrocyanide tested.

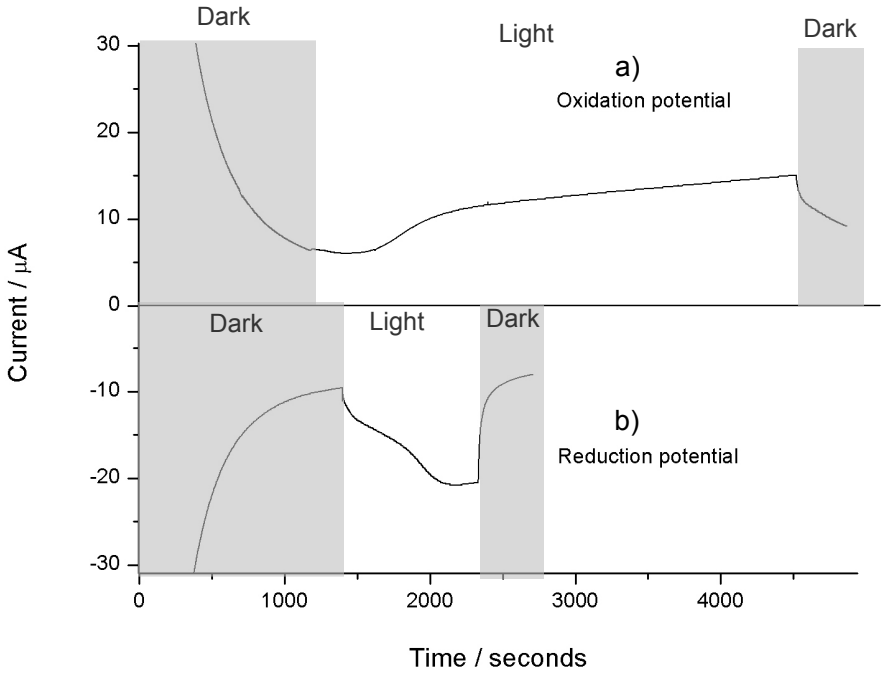


**Figure 6 Photocurrents at either the reduction potential for ferricyanide (b) or the oxidation potential for ferrocyanide (a), with 9 mM ferricyanide and $3x10^8$ cells 100 $\mu L^{-1}$ *C. vulgaris* in the anodic chamber. The shaded areas represent periods in the dark, whilst unshaded areas represent illumination at 625 nm from an optical fibre at intensity $5x10^{-3}$ W $cm^{-2}$**

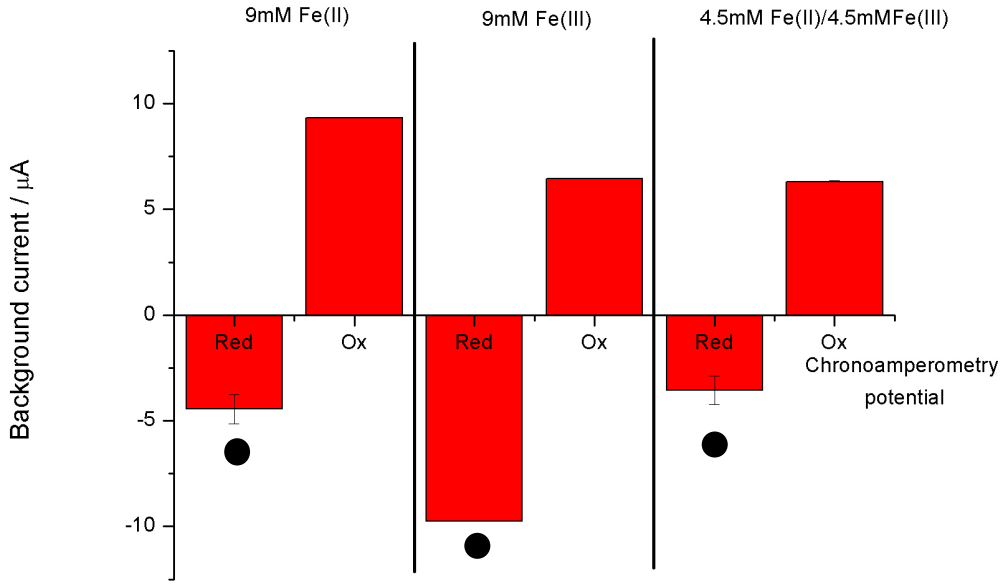


**Figure 7 Background currents gained at reduction and oxidation potentials with either 9 mM ferricyanide, 9 mM ferricyanide or a 50:50 mix of 4.5 mM ferrocyanide/ 4.5 mM ferricyanide and $3x10^8$ cells 100 $\mu L^{-1}$ *C. vulgaris* in the anodic chamber. A black circle indicates a result not explainable by traditional p-MFC theory. NB controls with 0 cells 100 $\mu L^{-1}$ and Fe subtracted**

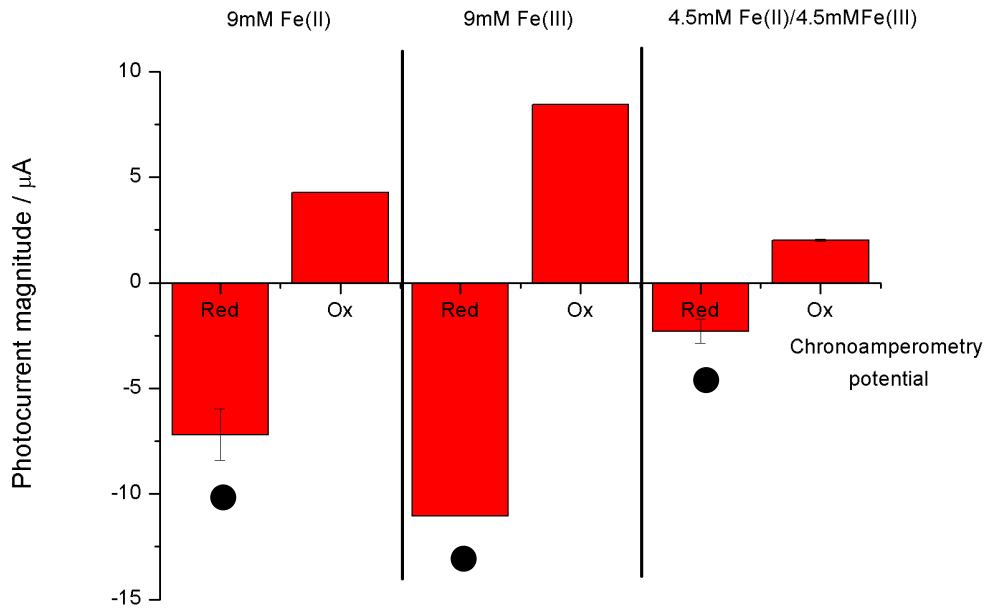


**Figure 8 Photocurrents gained at reduction and oxidation potentials with either 9 mM ferricyanide, 9 mM ferricyanide or a 50:50 mix of 4.5 mM ferrocyanide/ 4.5 mM ferricyanide and 3x10$^{8}$ cells 100 µL$^{-1}$ *C. vulgaris* in the anodic chamber. A black circle indicates a result not explainable by traditional p-MFC theory. NB controls with 0 cells 100 µL$^{-1}$ and Fe subtracted**

Figure 7 shows background currents of the basic p-MFC device. According to the accepted theory, reductive equivalents (such as NADPH) produced during respiration in the dark can be used to reduce an oxidised mediator, which can diffuse to the anode to become reoxidised. Consequently, it was expected that background (dark) currents would be largest with 9 mM ferricyanide in the anodic chamber and the anode set to the oxidation potential for ferrocyanide. However, these were not the conditions where largest currents were seen. With 9 mM ferricyanide present, background currents were highest at the reduction potential. As these currents were after subtraction of controls with no algal cells present, they cannot be simply explained by the Cottrell equation. Therefore, this inferred that as the reduction of ferricyanide increased with algal cells present, the cells were able to oxidise ferrocyanide. This was not thought possible. Other conditions that did not make sense according to p-MFC theory are highlighted on figure 7 with a black circle. Another example is where 9mM ferrocyanide was present with the anode set to the reduction potential of ferricyanide. Under these conditions, no oxidised mediator existed for algae to reduce, and the anode was not set at a potential where oxidation of the reduced mediator

could occur. However, a light induced oxidation current was measured. Again, this inferred the algae could oxidise ferrocyanide; not thought possible from p-MFC theory.

Figures 8 shows measured photocurrent magnitudes; importantly, these were largely unaffected by the potential applied to the anode during chronoamperometry. Similar to with the background currents shown in figure 7, this was in stark contrast to that expected from a p-MFC governed by the accepted theory outlined previously. Photocurrents are explained in the literature by extra reducing equivalents such as NADPH being produced in photosynthesis, which reduce extra mediator. This diffuses to the anode, resulting in extra current being produced in light (a photocurrent). However, this can only happen if an oxidised mediator is present, and if the potential of the anode is set to the oxidation potential of the reduced species. Figure 7 highlights measured outcomes not explained by p-MFC theory with black circles. One example of unexplained results is the photocurrents gained where 9mM ferrocyanide (reduced) mediator was present at the reduction potential for ferricyanide. Similarly, photocurrents were gained with 9 mM ferricyanide at the reduction potential for ferricyanide. Both of these photocurrents inferred that extra ferricyanide was being reduced at the electrode, hence the algae could oxidise ferrocyanide. Oxidation of a ferricyanide mediator is not thought possible by the algae, leading to the inference that photocurrent measurements were not related to algal reduction activities. Note that the relatively large background currents obtained when 9 mM ferricyanide was present and the oxidation potential of ferrocyanide was applied (and 9 mM ferrocyanide and the reduction potential of ferricyanide) also did not appear logical. Although these could have been due to the photochemistry of ferricyanide/ferrocyanide solutions leading to measureable amounts of the opposite redox species being formed previous to experiments, as they were not seen to the same extent in backgrounds, this was unlikely.

The fact that the photocurrents could not be explained by p-MFC theory implied that the algae were either not wholly responsible for p-MFC output, or the accepted p-MFC theory was incorrect. From studying the whole p-MFC device, it was virtually impossible to deduce which explanation was correct. This is because the p-MFC device is complicated, with differing reactions occurring at cathode and anode and a

junction potential present. Consequently, the current output of the p-MFC device could depend on whichever process was rate limiting. This made it impossible to directly relate algal activities to device output.

In addition to the confusion with the photocurrent, overall the current output from the device was unstable. Many explanations can be suggested to explain the device instability. Due to the fact that anodic and cathodic chambers were not sealed, the electrolyte in each chamber dried up rapidly (within 30 minutes). Additionally, the Ag wire provided a pseudo reference, from which the potential of the anode could be measured and controlled. However, as the concentration of ferricyanide and ferrocyanide changed in the anodic chamber, the potential of the Ag wire would also change (according to the Nernst equation). Consequently, the potential of the anode would shift. The cathode potential was not fixed and hence allowed to drift with any change in concentration of species in the cathodic chamber. The drifting of cathode and anode potentials meant the cell voltage would continuously shift, with the current fluctuating as a result. The cell voltage presented a further issue, as occasionally the direction of the cell voltage switched (data not shown). This phenomenon is also reported in the literature, and although not well understood, is thought to relate to the presence of the PEM.

## 3.4 Conclusions

In this chapter the basic p-MFC device as developed by collaborators at Cambridge was tested. It was found that photocurrents and background currents obtained with increased with algal cell concentration (with 9 mM ferricyanide present and the anode set at the oxidation potential for ferrocyanide). This seemed to be explained according to p-MFC theory, whereby reducing equivalents such as NADPH are produced in respiratory processes in dark and light, with additional reducing equivalents produced in photosynthesis in light. These then reduce an oxidised redox mediator, which can diffuse to the anode to become reoxidised.

However, when background and photocurrents were measured at different potentials (reduction potential for ferricyanide or oxidation potential for ferrocyanide) and with either 9 mM ferricyanide, 9 mM ferrocyanide or 4.5 mM ferricyanide/ 4.5 mM

ferrocyanide, results were surprising. Photocurrents were gained under conditions where no oxidised mediator existed for algae to reduce, and the anode was not set at a potential to reoxidised reduced mediator. This was in contrast to p-MFC theory, and inferred that ferrocyanide was somehow being reoxidised.

The basic p-MFC device is extremely complicated. Overall current outputs are as a result of the different processes occurring at the anode and cathode, with the membrane providing a junction potential and complicating the device further. Measured currents and potentials were extremely unstable as a result of drifting anode and cathode potentials. Additionally, due to the device design, the anode and cathode chambers dried out within 30 minutes, also affecting the current. This situation meant that it was impossible to deduce whether the device output was due to algal activities or a combination of factors; in contrast to what the p-MFC theory suggests.

The fact that these investigations gave results not explainable by p-MFC theory was pivotal to the direction of the rest of the thesis. Before further study of the whole p-MFC device, the activity of *C. vulgaris* cells in the presence of a ferricyanide redox mediator was required to be quantified (akin to the study of the anodic chamber alone). Without this understanding, the p-MFC device as a whole could not be understood.

## 3.5 References

1. Ryu, W., Bai, S.J., Park, J.S., Huang, Z.B., Moseley, J., Fabian, T., Fasching, R.J., Grossman, A.R., and Prinz, F.B., *Direct Extraction of Photosynthetic Electrons from Single Algal Cells by Nanoprobing System.* Nano Letters, 2010. **10**(4): p. 1137-1143.
2. Yagishita, T., Sawayama, S., Tsukahara, K., and Ogi, T., *Effects of glucose addition and light on current outputs in photosynthetic electrochemical cells using Synechocystis sp PCC6714.* Journal of Bioscience and Bioengineering, 1999. **88**(2): p. 210-214.
3. Chiao, M., Lam, K.B., and Lin, L.W., *Micromachined microbial and photosynthetic fuel cells.* Journal of Micromechanics and Microengineering, 2006. **16**(12): p. 2547-2553.

4. Yagishita, T., Sawayama, S., Tsukahara, K.I., and Ogi, T., *Effects of intensity of incident light and concentrations of Synechococcus sp. and 2-hydroxy-1,4-naphthoquinone on the current output of photosynthetic electrochemical cell.* Solar Energy, 1997. **61**(5): p. 347-353.
5. Powell, E.E., Mapiour, M.L., Evitts, R.W., and Hill, G.A., *Growth kinetics of Chlorella vulgaris and its use as a cathodic half cell.* Bioresource Technology, 2009. **100**(1): p. 269-274.
6. Rosenbaum, M., Schröder, U., and Scholz, F., *Utilizing the green alga Chlamydomonas reinhardtii for microbial electricity generation: a living solar cell.* Applied Microbiology and Biotechnology, 2005. **68**(6): p. 753-756.
7. Melis, A., Zhang, L.P., Forestier, M., Ghirardi, M.L., and Seibert, M., *Sustained photobiological hydrogen gas production upon reversible inactivation of oxygen evolution in the green alga Chlamydomonas reinhardtii.* Plant Physiology, 2000. **122**(1): p. 127-135.
8. Berk, R.S. and Canfield, J.H., *Bioelectrochemical energy conversion.* Applied Microbiology, 1964. **12**(1): p. 10-&.
9. He, Z., Kan, J., Mansfeld, F., Angenent, L.T., and Nealson, K.H., *Self-Sustained Phototrophic Microbial Fuel Cells Based on the Synergistic Cooperation between Photosynthetic Microorganisms and Heterotrophic Bacteria.* Environmental Science & Technology, 2009. **43**(5): p. 1648-1654.
10. Croft, M.T., Lawrence, A.D., Raux-Deery, E., Warren, M.J., and Smith, A.G., *Algae acquire vitamin B-12 through a symbiotic relationship with bacteria.* Nature, 2005. **438**(7064): p. 90-93.
11. Nishio, K., Hashimoto, K., and Watanabe, K., *Light/electricity conversion by a self-organized photosynthetic biofilm in a single-chamber reactor.* Applied microbiology and biotechnology, 2010. **86**(3): p. 957-964.
12. Malik, S., Drott, E., Grisdela, P., Lee, J., Lee, C., Lowy, D.A., Gray, S., and Tender, L.M., *A self-assembling self-repairing microbial photoelectrochemical solar cell.* Energy & Environmental Science, 2009. **2**(3): p. 292-298.
13. Cao, X.X., Huang, X., Liang, P., Boon, N., Fan, M.Z., Zhang, L., and Zhang, X.Y., *A completely anoxic microbial fuel cell using a photo-biocathode for cathodic carbon dioxide reduction.* Energy & Environmental Science, 2009. **2**(5): p. 498-501.

14. Zou, Y., Pisciotta, J., Billmyre, R.B., and Baskakov, I.V., *Photosynthetic microbial fuel cells with positive light response.* Biotechnology and Bioengineering, 2009. **104**(5): p. 939-946.
15. Zou, Y.J., Pisciotta, J., and Baskakov, I.V., *Nanostructured polypyrrole-coated anode for sun-powered microbial fuel cells.* Bioelectrochemistry, 2010. **79**(1): p. 50-56.
16. Bard, A.J., Parsons, R., and Jordon, J., *Standard potentials in aqueous solutions.* . 1985: Marcel Dekker.
17. Middlemiss, J.K., Anderson, A.M., Stratilo, C.W., and Weger, H.G., *Oxygen consumption associated with ferric reductase activity and iron uptake by iron-limited cells of Chlorella kessleri (Chlorophyceae).* Journal of Phycology, 2001. **37**(3): p. 393-399.
18. Lynnes, J.A., Derzaph, T.L.M., and Weger, H.G., *Iron limitation results in induction of ferricyanide reductase and ferric chelate reductase activities in Chlamydomonas reinhardtii.* Planta, 1998. **204**(3): p. 360-365.

# Chapter 4. Basic Interaction of Algae with Potassium ferricyanide

# Chapter 4 - Basic interaction of Algae with Potassium ferricyanide

## 4.1 Introduction

The previous chapter outlines the fact that although p-MFC device output can be studied through simple methods such as chronoamperometry, deducing how the photosynthetic material is actually behaving in the anodic chamber is virtually impossible due to the complexity of the device. This problem is not well addressed in the literature. In the literature, the pathways of mediator reduction by eukaryotic cells have not always been well elucidated, with relatively few studied examples [1]. There has additionally been no full assessment of the behaviour of *Chlorella vulgaris*; mostly other species have been investigated. Although potassium ferricyanide (ferricyanide) is one of the few examples of an artificial redox mediator used in p-MFC studies whose reduction pathway by photosynthetic organisms has been well studied in microbiology, there is a large absence of knowledge transfer between microbiological and p-MFC studies. This chapter explores the interaction of this mediator with *C. vulgaris* in detail, attempting to bridge the knowledge gap. By understanding the behaviour of *C. vulgaris* with ferricyanide, the p-MFC device as a whole can be better understood.

It must first be understood why *C. vulgaris* interacts with the ferricyanide mediator. Iron is an essential element for photosynthetic organisms and there is good evidence that iron availability limits primary productivity in parts of the ocean and other aquatic environments [2]. In aerobic aquatic environments non colloidal Fe(III) is in the order of 0.3 nM [3, 4], with most typically found in the form of insoluble Fe(III) oxides which exhibit low biological activity. Photosynthetic microorganism iron acquisition mechanisms must therefore be able to cope with low free levels of total aquatic iron and the fact that Fe(III) must be released/solubilised from complexes to be transported across the algal plasma membrane [4]. To this end, numerous studies have shown that plants and algae (particularly those grown in iron deficient conditions) can interact with chelated Fe(III) and reduce it [2, 4-8]. The reduction process creates solvated Fe(II) that can be transported across the cell membrane and subsequently re-oxidised for use by the cell. Two pathways for iron reduction are known, strategy I

which occurs in non-vascular plant roots and several algal species including *C. vulgaris* [9, 10]; and strategy II common to grasses and cyanobacteria [11]. This is not a definitive rule; some reports of strategy II use by eukaryotic algae exist, although they are rare [2], and other studies show evidence for macromolecular algal exudates which can assimilate iron [12].

In strategy I Fe(III) is reduced by ferric reductases in the plasma membrane, with studies showing an increase in the concentration of ferric reductase in the membranes of algae grown under iron deficient conditions [7]. In one study, increased ferric reductase activity in iron-limited conditions was five fold [6]. The ferric reductase reduces extracellular Fe(III) chelates to Fe(II) and free chelator ('chelate splitting'); Fe(II) is subsequently transported across the plasma membrane by an Fe(III) transporter [4, 13]. In strategy II, iron uptake is controlled by the release (in response to iron limitation) of siderophores; organic ligands (such as hydroxamates) that chelate and solubilise Fe(III), and in some cases reduce it. The Fe(II)/(III)-siderophore complex is then transported across the plasma membrane into cells [2, 11].

The majority of the p-MFC literature concentrates on the reduction of a mediator (such as ferricyanide) under illumination, with polarisation curves invariably reported under light conditions. In contrast the microbiological literature reports reduction of ferricyanide (and other iron species) both in the dark and under illumination [2]. Illumination has been found to increase the rate of iron reduction in iron deficient *Chlorella kessleri* [6] and iron sufficient and deficient *C. reinhardtii* [2, 7], although the increase was much greater in the iron deficient case [2]. Ferric reductase activity was investigated in *C. reinhardtii*, and was found to be powered by NADPH provided by the oxidative pentose phosphate pathway in dark, and a combination of NADPH provided by the oxidative pentose phosphate pathway and photosynthetic electron transport chain activity in light [2]. The rate of Fe(III) reduction has been measured colourmetrically by the chelation of the resulting Fe(II) with bathophenanthroline disulfonate [4].

Cellular effects due to mediator interactions are also often neglected in MFC/p-MFC literature. These are crucial to understanding the behaviour and viability of *C. vulgaris* cells in the p-MFC device. These have been studied in the microbiological literature using fluorescence and oxygen electrodes [4, 6, 14] [15] [16]. Studies suggest that the reduction of Fe (III) chelates is closely linked to oxygen consumption, with an increased consumption of oxygen in the dark, and a decrease in net oxygen evolution in the light [4, 6, 14]. As only ~20 % of the reduced iron appears to be taken in by the cells, the external concentration of Fe(II) increases [4, 17]. The suggested mechanism for this Fe(II) removal involves its rapid reoxidation in the presence of oxygen. However, Middlemiss *et al.,* [6], did not observe any change in the oxygen concentration in the presence of ferricyanide (Fe(III)) or ferrocyanide (Fe(II)) as the ferro complex was thought to be stable once formed, not assimilated by cells, and not re-oxidised back to ferricyanide. Other less-adopted explanations are a role for oxygen as the terminal acceptor in mitochondrial respiration [6], or the reduction of $O_2$ to $O_2^-$ by ferric reductase activity, which is then the reducing agent for Fe(III) [6]. Evidence for this comes from the fact that $O_2$ can be directly reduced by ferric reductase in algal plasma membranes [6, 18], $O_2$ can compete with Fe(III) for reduction by ferric reductase, and anaerobic conditions may lead to increased rates of ferric reduction compared to a control [6].

Fluorescence and synchronous scan fluorescence studies have been performed on solutions of algal cells and artificial compounds such as herbicides which can cross cell membranes; this means they have a direct interaction and hence effect on cell machinery [15, 19-22]. The measurement of *in vivo* chlorophyll a fluorescence of green algae has been found to be one of the most sensitive tools for the rapid detection of compounds and environmental conditions that inhibit photosynthesis [20]. An increase in chlorophyll a fluorescence has been linked to the presence of a photosystem II inhibitor such as atrazine [20, 21]; these are thought to enter cells, and bind to the $Q_B$ binding site of PSII with high affinity, blocking photosynthetic flow and increasing chlorophyll a fluorescence activity at 690 nm and 730 nm [21]. Conversely, a decrease in fluorescence has been linked with PSI inhibition [20, 22], as well as other factors. For example, glyphosphate, an inhibitor of 5-enolpyruvylshikimate-3-phosphate (EPSP) synthase (involved in amino acid synthesis

after dark photosynthetic reactions), is thought to decrease fluorescence by decreasing chlorophyll turnover [21]. Some studies also showed that PSII inhibitors were much faster acting than PSI inhibitors [20].

The artificial compound ferricyanide has also been shown to have an effect on fluorescence, even though it cannot cross cell membranes (is impermeant) to directly act as a quencher. Davey *et al.,* [15], studied the reduction of ferricyanide in a range of diatoms, and measured fluorescence using a Waltz XE-PAM pulse amplitude modulated fluorimeter. They found ferricyanide (and not ferrocyanide), induced an immediate and reversible decrease in fluorescence yields ($F_o$ and $F_m$ relating to fluorescence in absence of photosynthetic light and maximum fluorescence in the absence of any photochemical quenching respectively), which they related to ferricyanide reductase activity levels. They suggested that consumption of electrons at the plasma membrane competed directly with $CO_2$ fixation for electrons, altering cytosolic redox poise, and inducing a redox-signalling cascade altering photosynthetic metabolism [15]. Additionally, in PAM fluorescence studies of ferricyanide and *C. reinhardtii* in light by Weger *et al.,* [16], reduction of ferricyanide led to a large increase in non-photochemical quenching. This suggested that reduction of extracellular ferricyanide in light interacts with both photosynthesis and respiration, resulting in a partial inhibition of photosynthetic carbon dioxide fixation [16].

### 4.11 Chapter Aims

The understanding of how and why microbes reduce a mediator in the p-MFC is crucial for the furthering of p-MFC technology. Without this knowledge, whole p-MFC device outputs cannot be understood. However, this is often vastly neglected in p-MFC literature. The previous chapter outlining testing of the basic p-MFC device (utilising C. *vulgaris* and a ferricyanide mediator) gives results unexplainable from p-MFC literature, where it appears *C. vulgaris* could oxidise a reduced mediator. Consequently, the rate and mode of interaction of *C. vulgaris* with both ferricyanide and ferrocyanide was critical to improving understanding of p-MFC device output, and hence improve future device efficiency.

In this chapter the rate of reduction of ferricyanide by a range of concentrations of *C. vulgaris* in light and dark is measured directly by UV-Vis spectrophotometry (referred

to as UV-Vis). It is also investigated whether *C. vulgaris* could oxidise ferrocyanide. The *C. vulgaris* is grown in iron-sufficient conditions, as this is thought to represent the long-term sustainable conditions it would be grown in inside a p-MFC. The effect of ferricyanide on chlorophyll fluorescence from the algae is studied and used as an indicator of the rate of photosynthetic reactions. Finally, the link between oxygen concentration and ferricyanide is considered to give further information on the mode of reduction, and long-term ferricyanide toxicity towards *C. vulgaris* is determined.

## 4.2 Experimental

### 4.21 Proof of principle UV-Vis with potassium ferricyanide and potassium ferrocyanide

UV-Vis experiments allowed bulk quantification of the reduction of ferricyanide when mixed with the alga *C. vulgaris*. It was also determined whether *C. vulgaris* could oxidise ferrocyanide. A bulk solution of Fe in 10 mL *C. vulgaris* (at a concentration of $7x10^7$ cells $mL^{-1}$ in fresh media) was made up. 1mL aliquots of the solution were taken every hour, centrifuged for 3 minutes at $13.2x10^3$ rpm, and supernatant removed. Absorbance of the supernatant at 420 nm was then measured in a spectrometer (type Helios gamma from Thermo electron corporation), which allowed the concentration of ferricyanide to be calculated from calibration curves. This procedure was performed on equivalent samples of algae in light (light at 620 nm from an optical fibre at intensity $1.25x10^{-3}$ W $cm^{-2}$) and dark, and containing either 1 mM ferricyanide, 1 mM ferrocyanide or a 50:50 mix of 0.5 mM ferricyanide: 0.5 mM ferrocyanide. Experiments were run twice, averages calculated, and errors generated. A further experiment investigated the effect of using half the number of algae cells, this time using three equivalent sets in light and dark.

### 4.22 Long term toxicity testing of potassium ferricyanide to *C. vulgaris*

*C. vulgaris* was cultured with ferricyanide (procedure as outlined in appendix) to identify any long term toxicity this chemical species represented. Three identical culture flasks were inoculated with 0.001 mM, 0.01 mM or 0.1 mM ferricyanide. Cell counts were performed every 2 or 3 days using a haemocytometer, and a control containing 0 mM ferricyanide was monitored for comparison.

### 4.23 Cellular Effects resulting from the presence of potassium ferricyanide

To determine the cellular effects resulting from cell-ferricyanide interactions, fluorescence measurements were undertaken. 3.0 mL *C. vulgaris* solution was first put in a cuvette, before the auto-fluorescence of the chlorophyll at 685 nm and 732 nm (when excited by a blue light at 480 nm) were measured using an Ocean Optics USB4000 fluorimeter. Auto-fluorescence of *C. vulgaris* was measured with increasing concentrations of either ferricyanide or ferrocyanide, between 1 and 7 mM, over ten minutes. To study fluorescence reversibility, *C. vulgaris* solutions with 7 mM ferricyanide were washed three times in fresh 3N-BBM+V media, and remeasured. To determine any changes in fluorescence over time, the auto-fluorescence of *C. vulgaris* solutions with 1 mM ferricyanide were measured over 24 hours.

In all experiments, cuvettes were always kept under ambient lab-light conditions between measurements and the cells were always re-suspended with a pipette before every measurement. Five repeats of each measurement were taken (with fresh algae), averages calculated and errors generated.

### 4.24 Oxygen consumption

The oxygen evolution capability of a *C. vulgaris* sample inoculated with 1 mM ferricyanide was studied by illuminating at 620 nm using an optical fibre, and measuring oxygen content using a Clark type oxygen electrode (ISO2 from WPI) connected to a pico-logger ADC-24. These contain a two-electrode configuration cell, immersed in a KCl electrolyte. Oxygen diffuses through a permeable membrane where it is reduced at the cathode, creating a measurable electrical current. As there is a linear relationship between the oxygen concentration and the electrical current, with a two-point calibration, it was possible to measure the oxygen in a sample.

The algal sample was subjected repeatedly to five minutes illumination, then five minutes dark, for approximately forty five minutes. A control sample of *C. vulgaris* with 0 mM ferricyanide, as well as media controls, were also studied. Experiments also measured the amount of oxygen evolved under illumination with increasing concentrations (between 1 and 7 mM) of ferricyanide.

### 4.25 Control experiments

To ensure that algae alone interact with ferricyanide, with no other species involved, control UV-Vis experiments were run. Oxygen, a product of photosynthesis, and $H_2O_2$, a product which builds up in fuel cells and MFCs, were bubbled/added respectively to 1 mM media solutions of ferricyanide or ferrocyanide. Similar to previous experiments, aliquots were taken every hour and absorbance at 420 nm measured in a UV-Vis spectrometer. Concentrations of ferricyanide were calculated from calibration curves as outlined in section 4.21.

## 4.3 Results and Discussion

### 4.31 Proof of principle UV-Vis with potassium ferricyanide and potassium ferrocyanide

UV-Vis spectrophotometry was used as a simple method for investigating the interaction of *C. vulgaris* with both ferricyanide and ferrocyanide. To investigate the reduction of ferricyanide by *C. vulgaris*, a given concentration of ferricyanide and algae suspended in 10 mL media was left either in the dark or illuminated. Every hour 1 mL samples were removed, centrifuged and the supernatant was analysed. Ferricyanide shows a distinct absorption peak centred on 420 nm (absent in ferrocyanide) and this was used to measure the total ferricyanide concentration. An identical experiment was carried out both in the absence of any redox acceptor (media control) and in the presence of ferrocyanide. According to p-MFC and microbiological theory, the ferrocyanide complex should not act as a terminal electron acceptor for the algae; if however ferrocyanide could be re-oxidised in the presence of oxygen the ferricyanide concentration should increase with time in the presence of algae.

Typical UV-Vis curves are shown below in figure 1, showing the ferricyanide absorbance peak at 420 nm. As expected, the absorption at 420 nm decreased over time corresponding to a decrease in solution concentration of ferricyanide. It was thought that this reduction in peak intensity occurred as ferricyanide was reduced to ferrocyanide, which does not absorb at 420 nm, and so was not measured by the UV-Vis. Ferric reductase proteins in the algal membranes aim to reduce extracellular Fe(III) chelates to Fe(II) and free chelator. In this case, due to the strong bonding

involved in ferricyanide, it is unlikely the Fe-CN bond is being split and free ligand is formed [6], therefore the algae are not likely to be taking-up any ferrocyanide. However, the reduction mechanisms continued nonetheless. A calibration curve was constructed by measuring the absorption of known concentrations of ferricyanide in 3N-BBM+V media at 420 nm (figure 2). Using the calibration curve, absorptions could be translated into concentrations of ferricyanide, using the Beer-Lambert law.

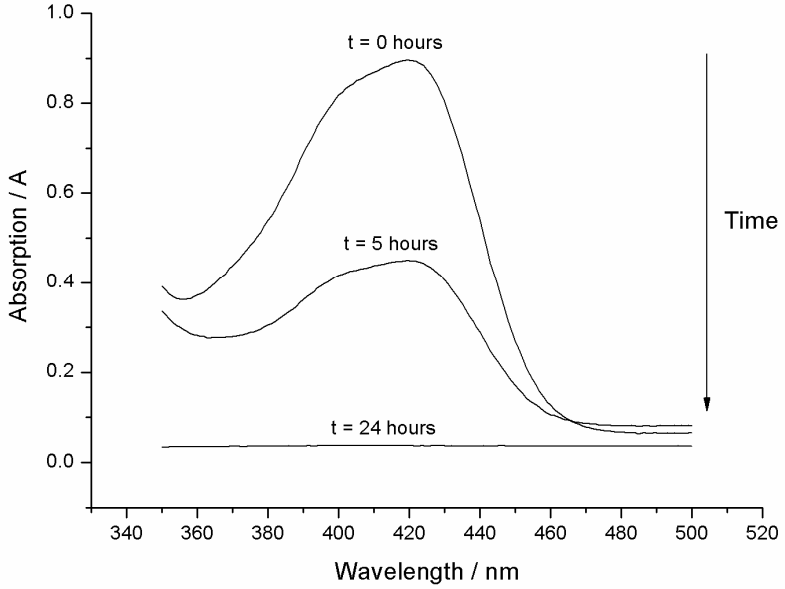


**Figure 1 Typical UV-Vis curves for a solution of *C. vulgaris* and ferricyanide, at selected time points after mixing**

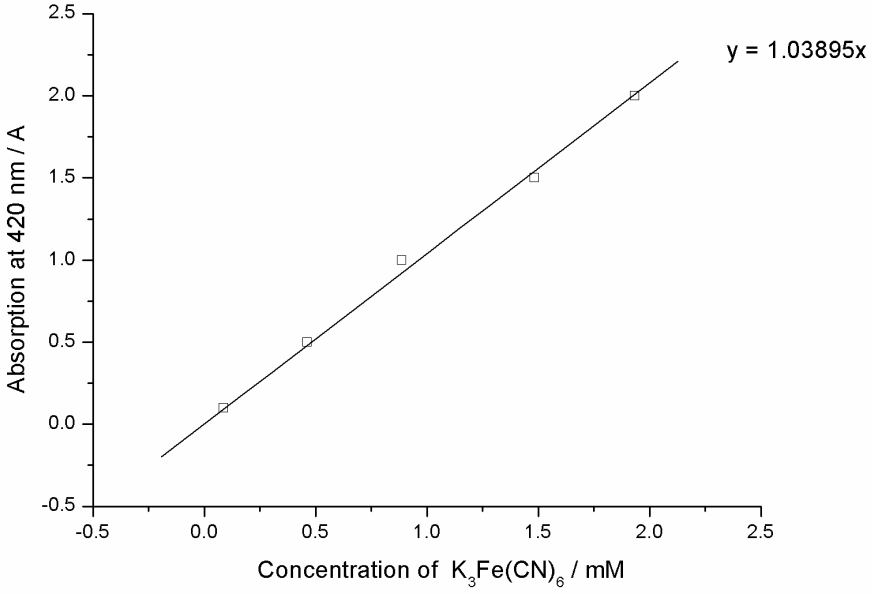


**Figure 2 Calibration curve of ferricyanide in 3N-BBM+V media**

Figure 3 shows the reduction of ferricyanide in the presence of 7.69 x $10^7$ algal cells $cm^{-3}$. In the case of *C. vulgaris* cultured in an iron sufficient environment (2.15 x $10^{-4}$ mol $dm^{-3}$ $FeCl_3$) no statistically relevant difference between dark and illuminated conditions was observed. Many studies show reduction is increased in light, as both respiratory and photosynthetically derived reductants act as cytosolic electron donors for the plasma membrane reductase [15]. However, studies showing large differences in reduction rates between light and dark conditions were performed on iron deficient cells [6, 7]. It was likely that in this study with iron replete algae, UV-Vis was not sensitive enough to detect any small difference in reduction rates between light and dark. In the absence of redox mediator or the presence of ferrocyanide no change was observed, confirming that ferrocyanide does not interact with the algae and that it is also not oxidised by dissolved oxygen in the cell. These findings show that the implications in chapter 3 that the algae were oxidising ferrocyanide were incorrect. The large background and photocurrents obtained with 9 mM ferrocyanide and the anode set to the reduction potential for ferricyanide must have been due to other factors resulting from the device complexity.

To investigate the reduction of ferricyanide in more detail experiments were carried out with a lower ferricyanide concentration and a lower algal concentration. The results are shown in figure 4. Again, little difference in ferricyanide reduction was observed between light and dark conditions. By fitting the initial dark reduction rates (which were linear; first 5 points taken), the initial reduction rates of ferricyanide in the presence of *C. vulgaris* could be calculated. Table 1 shows initial rates of ferricyanide reduction in the dark.

| Concentration Algae / cells $dm^{-3}$ | Concentration Ferricyanide / mmol $dm^{-3}$ | Half-life / h | Initial rate / μmol Fe(III) $dm^{-3}$ $h^{-1}$ | Initial rate/ nmol Fe(III) $10^{-6}$ cells $h^{-1}$ |
|---|---|---|---|---|
| 7.69 x $10^{10}$ | 1 | 4.3 | 110 | 1.43 |
| 7.69 x $10^{10}$ | 0.5 | 6.2 | 80 | 1.08 |
| 3.56 x $10^{10}$ | 1 | 28.0 | 23 | 0.56 |

**Table 1 values of the half-life of ferricyanide and the initial rate of ferricyanide reduction in the dark**

It was established that with a *C. vulgaris* concentration of 7.69 x$10^{10}$ cells $dm^{-3}$ (extrapolated from 10 mL), and an initial ferricyanide concentration of 1 mM, the initial reduction rate was 1.43 nmol Fe(III) $10^{-6}$ cells $h^{-1}$. This decreased with halved cell concentration (0.56 nmol Fe(III) $10^{-6}$ cells $h^{-1}$), and halved initial ferricyanide concentration (1.08 nmol Fe(III) $10^{-6}$ cells $h^{-1}$). These rates are comparable to those published by Middlemiss *et al.*, using *C. kessleri* [6]. However there does not appear to be a straightforward linear relationship between the algal concentration and the initial reduction rate. Reducing the algal concentration by half reduced the initial rate threefold, whereas decreasing the ferricyanide concentration by half created only a small change in rate. This demonstrated that the ferricyanide was likely present in excess.

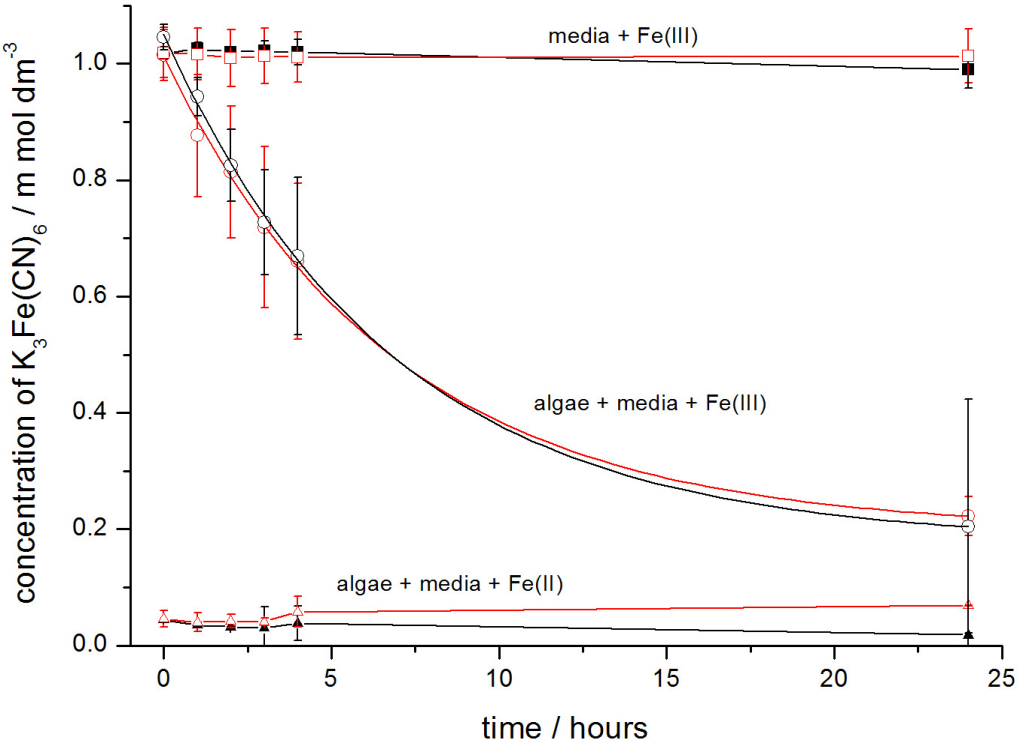


**Figure 3. Change in the concentration of ferricyanide in media (squares) and in the presence of 7.69 x $10^7$ algal cells $mL^{-1}$ (circles). Measurements were taken under illumination (red points) and in the dark (black points). Algae in the presence of ferrocyanide was also monitored (triangles). The error bars show one standard deviation (n=2).**

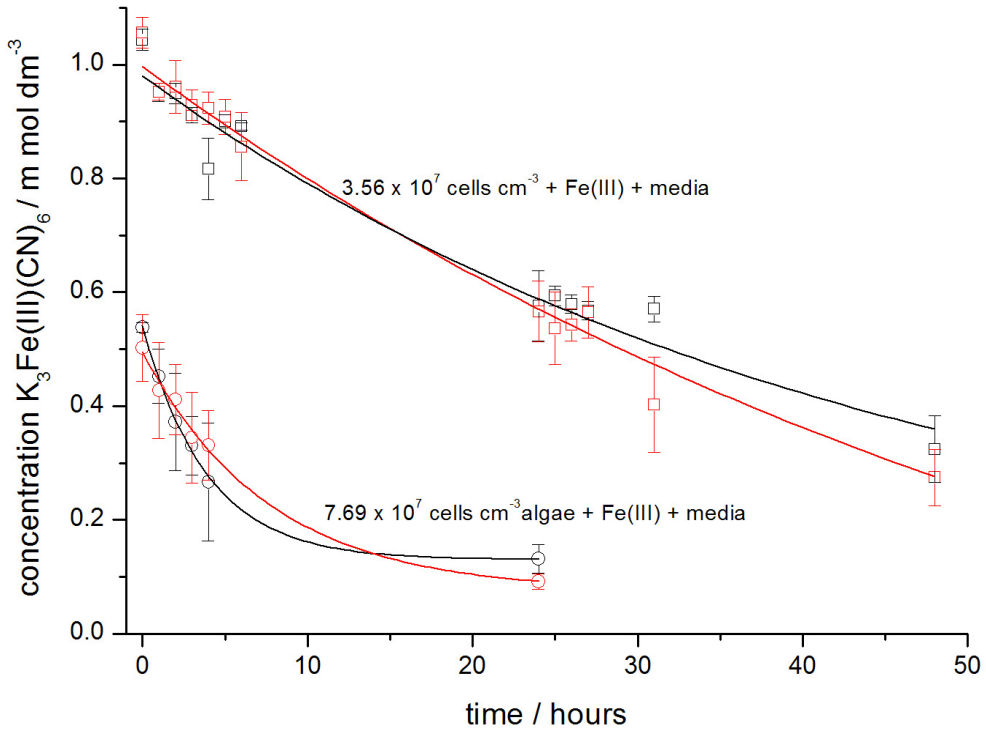


**Figure 4 Change in the concentration of ferricyanide in the presence of 3.56 x $10^7$ algal cells $cm^{-3}$. Measurements were taken under illumination (red squares) and in the dark (black squares) (n=3 for 3.56 x $10^7$ cells and n=2 for 7.69 x $10^7$ cells). The error bars show one standard deviation (n=3).**

These UV-Vis experiments therefore show the reductive (and not oxidative) capabilities of the ferric reductase proteins in the membranes of *C. vulgaris*. No difference was observed between light and dark reduction, but it is unclear as to whether this was due to the lack of sensitivity of the technique, or the fact that the cells were iron sufficient.

### 4.32 Longterm toxicity of potassium ferricyanide to *C. vulgaris*

It was important to quantify any toxicity the ferricyanide represented to *C. vulgaris*. This was to provide any concentration or time limits upon which a p-MFC could be viably operated. Figure 5 shows cell counts over time of cultures containing varying amounts of ferricyanide. Although cell counts did not distinguish between alive and dead cells, any growth inhibition effects could be seen, and these could be attributed to toxicity.

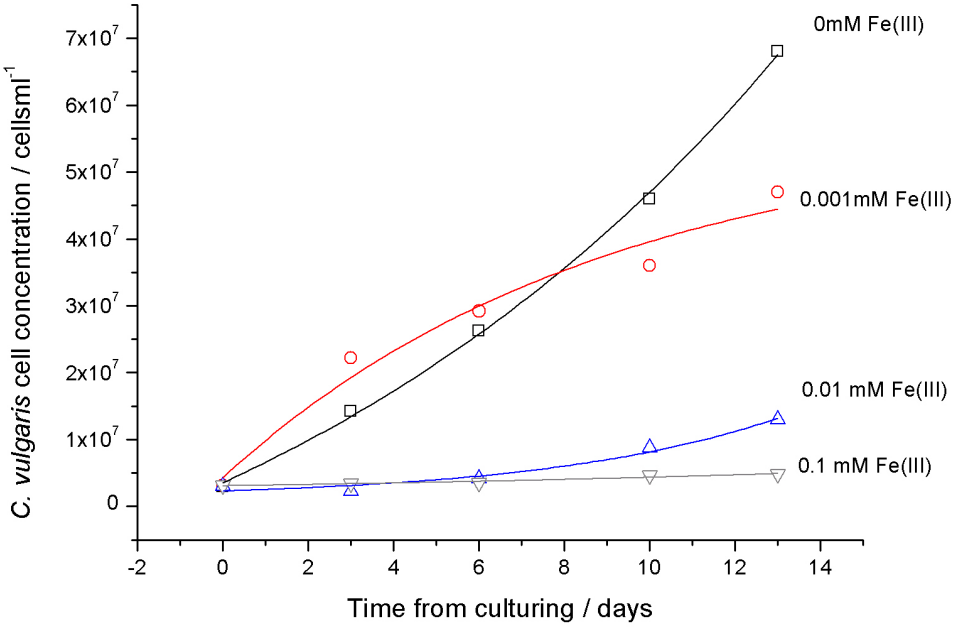


**Figure 5 Cell counts over time of *C. vulgaris* cultures containing varying amounts of ferricyanide**

As figure 5 shows, ferricyanide strongly inhibited growth of algal cells at any concentration above 0.001 mM. It was therefore apparent that for any long term experiments, a concentration of 0.001 mM ferricyanide or below needed to be used, or another mediator (or more toxicity tolerant species) found. The toxicity can be explained as evidence suggests that reduction of extracellular ferricyanide in the light interacts with both photosynthesis and respiration, and results in a partial inhibition of photosynthetic carbon dioxide fixation [16]. Consequently, fewer carbohydrates could be made and used as a store of cellular energy. An interesting point to note is that if stock cultures are grown in 0.001 mM ferricyanide over long periods of time, which largely unaffected cell growth, they could potentially develop extra reducing power via an increase in cellular plasma membrane ferric reductase capacity [13], as well as increased toxicity resistance.

### 4.33 Cellular effects resulting from the presence of potassium ferricyanide

Fluorescence was used to monitor cellular effects caused by the cell impermeable mediator ferricyanide. Using a standard fluorimeter, the auto fluorescence of the algal species *C. vulgaris* was measured by exciting at 480 nm. Light energy absorbed by chlorophyll molecules can undergo three fates, it can drive photosynthesis, be

dissipated as heat, or re-emitted as light (fluorescence). As the processes are competitive, by measuring the yield of chlorophyll fluorescence, information about photochemical efficiency and heat dissipation can be obtained.

Figure 6 shows a typical fluorescence spectrum for *C. Vulgaris*, with two peaks at 684 nm and 732 nm related principally to the response of PSII and PSI respectively in chlorophyll a (although at room temperature, the variable fluorescence is known to originate almost exclusively from PSII) [20]. When inoculated with the impermeant redox species ferricyanide, both peaks reduced dramatically, even though no direct photosystem interaction was possible (as ferricyanide cannot cross cell membranes).

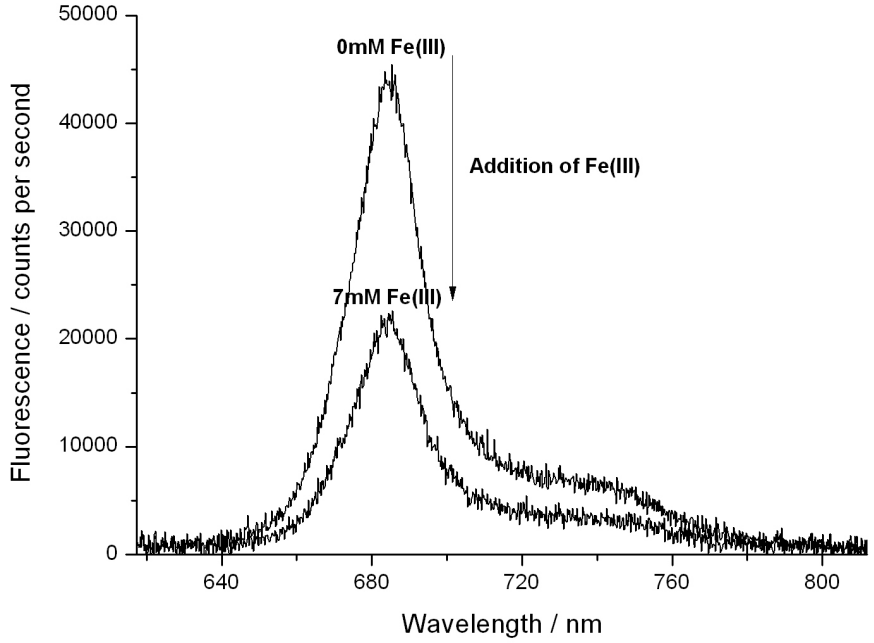


**Figure 6 Auto fluorescence pattern of chlorophyll when excited by 480 nm light. Samples contained 0 or 7 mM ferricyanide**

To determine if the effect of ferricyanide on algal cells changed over time, fluorescence of an algal sample inoculated with 1 mM ferricyanide was measured at various points over time for 24 hours at 684 nm and 732 nm, whilst excited with a 480 nm light. Plots showed that aside from an initial decrease in fluorescence intensity due to the presence of the 1 mM ferricyanide, no further decrease was seen (data not shown). Additional experiments whereby cells inoculated with 7 mM ferricyanide

were washed and fluorescence re-measured showed that fluorescence quenching was reversible; showed in figure 7.

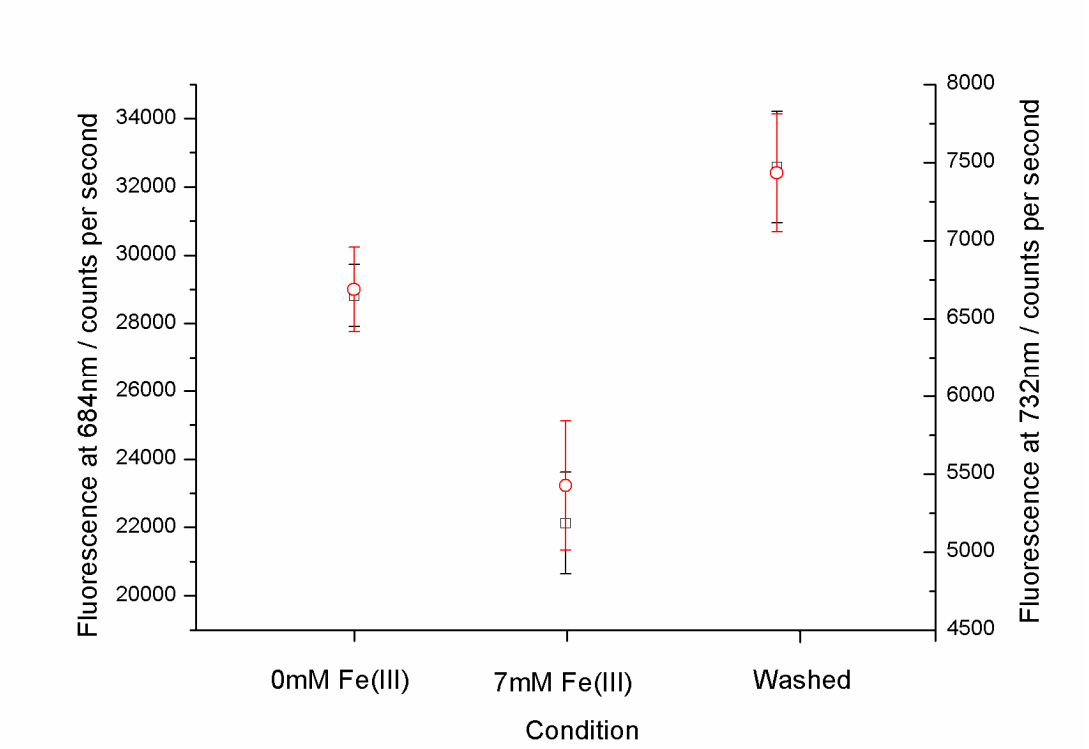


**Figure 7 Auto-fluorescence of *C. vulgaris* at 684 nm (black squares) and 732 nm (red circles) before addition of 7 mM ferricyanide, after addition of 7 mM ferricyanide and after washing. The error bars show one standard deviation (n=5).**

Figures 8 and 9 show the auto-fluorescence of *C. vulgaris* at 684 nm and 732 nm respectively with increasing concentration of ferricyanide and ferrocyanide. A virtually identical decrease in fluorescence at both 684 nm and 732 nm was seen as ferricyanide concentration is increased, whilst ferrocyanide did not affect fluorescence.

Fe(III) induced reversible fluorescence quenching has been shown in PAM fluorescence studies on Fe-limited diatoms [15], and in Fe-limited *C. reinhardtii*l [16]. Ferricyanide reduction proceeds via an immediate oxidation of pools of NADPH (not NADH) [2], and any metabolic process that causes a significant consumption of reduced pyridine nucleotides is likely to impact photosynthetic metabolism [23]. This is due to cellular redox poise being a regulator of the interaction between photosynthesis and respiration, as found in *C. reinhardtii* [24]. At saturating and sub-

saturating photon fluence rates (PFR), ferricyanide addition to Fe-limited *C. reinhardtii* cells resulted in a large increase in non-photochemical quenching (NPQ) involving dissipation of excess energy as heat, with photochemical quenching (PQ) (photosynthesis) much less pronounced [16].

A similar effect was seen for the Fe-limited diatoms [15]. Weger *et al.,* [16], suggested that the inhibition of $CO_2$ fixation during extracellular ferricyanide reduction was the major cause of increased levels of non-photochemical quenching. Inhibition of the Calvin cycle would result in lowered chloroplastic ATP demand, leading to lowered dissipation of the trans-thylakoid $H^+$ gradient, and thus an increase in non-photochemical quenching [16]. Interestingly, they only saw an increase in non-photochemical quenching in Fe deficient cells. In Fe replete cells no non-photochemical quenching was observed when ferricyanide was added. Their result contrasts with these findings for *C. vulgaris*, where a clear decrease was seen, even for Fe replete cells.

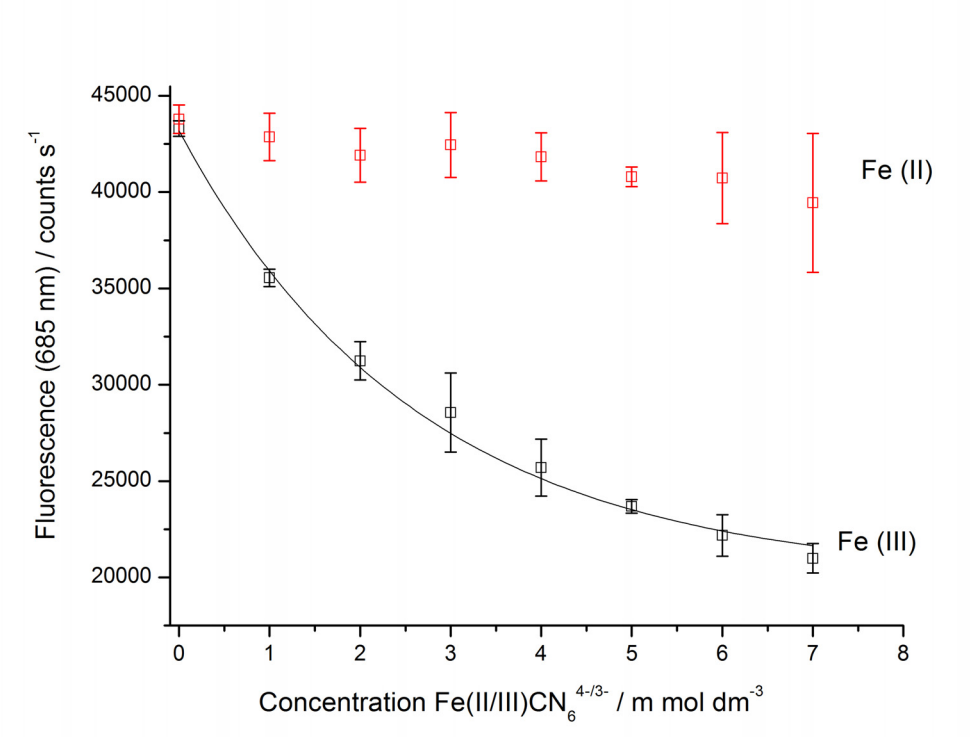


**Figure 8 Auto-fluorescence of C. vulgaris at 684 nm with increasing concentrations of ferricyanide or ferrocyanide. The error bars show one standard deviation (n=5).**

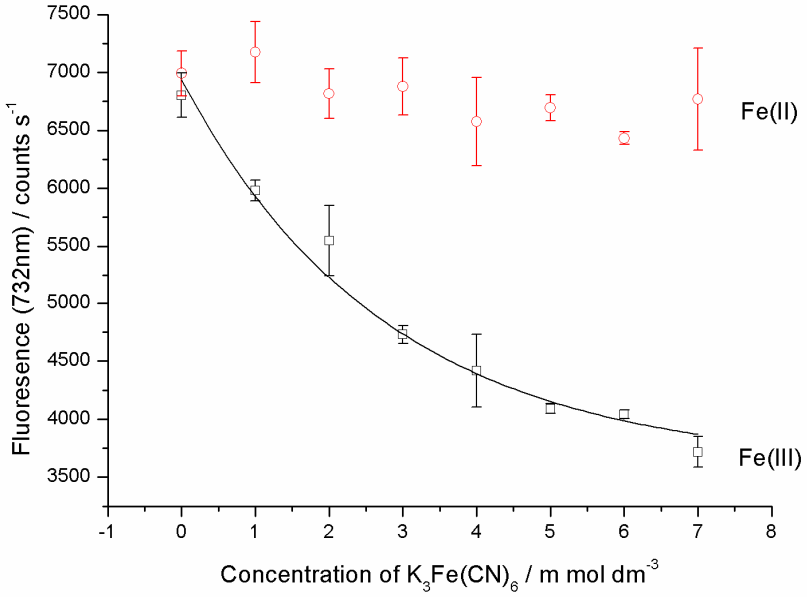


**Figure 9 Auto-fluorescence of C. vulgaris at 732 nm with increasing concentrations of ferricyanide or ferrocyanide. The error bars show one standard deviation (n=5).**

The ratio of absorbance at 684 nm to 732 nm decreased linearly with increasing ferricyanide concentration, but stayed constant with ferrocyanide concentration (figure 10). The reason for this was unknown, but could infer that the activity of PSII increased in relation to PSI (due to increased PSII activity or decreased PSI activity).

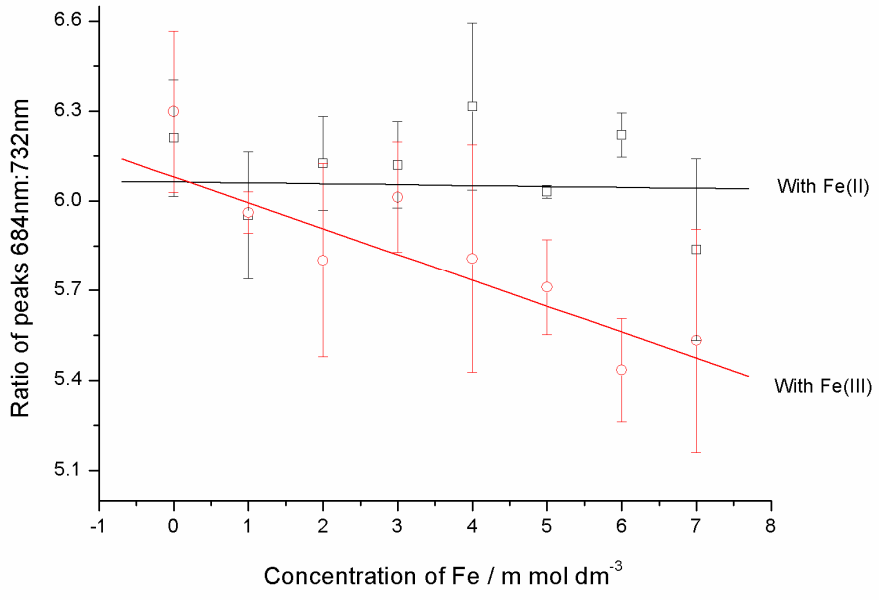


**Figure 10 Ratio of 684 nm to 732 nm fluorescence peaks (taken from averages), with increasing ferricyanide or ferrocyanide. The error bars show one standard deviation (n=5).**

Plotting $I_0/I - 1$ VS [Fe(III)] as shown in figure 11 allowed the determination of the Stern-Volmer coefficient ($K_{SV}$), which related any decrease in fluorescence intensity at each peak to the addition of a quenching species. This was determined to be 0.16055, with a standard error of 0.30118 (r-Sq = 0.99624) for the peak at 684 nm, and 0.12181 with a standard error of 0.20471 (r-Sq = 0.98937) for the peak at 732 nm. Both calculations are for ferricyanide in mM. No other $K_{SV}$ values were found by the author relating to quenching of algae with a redox mediator, but values are useful to compare with future experiments.

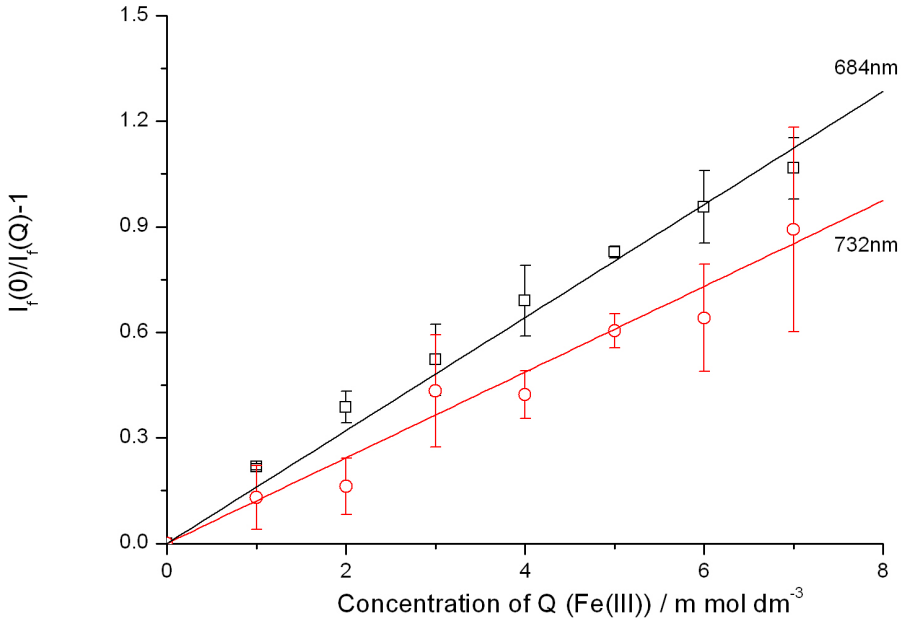


**Figure 11 Effect of ferricyanide concentration on $I_0/I - 1$ of *C. vulgaris* at both peaks.. The error bars show one standard deviation (n=5).**

### 4.34 Oxygen Evolution

Another cellular effect characterised was oxygen production by *C. vulgaris* when in solution with ferricyanide. Oxygen was evolved photosynthetically in periods of light, as shown in figure 12. The magnitude of oxygen produced could be directly related to the amount of photosynthetic activity. Oxygen evolution of a sample of algae containing either 0 mM or 1 mM ferricyanide was measured over 10000 seconds, whilst illuminating with a 620 nm optical fibre light source switched on and off every 500 seconds. Although the amount of oxygen evolved dropped upon addition of 1

mM ferricyanide, the amount of oxygen evolved over time from each illumination cycle remained constant (data not shown). This demonstrated that 1 mM ferricyanide was not acutely toxic over the timescale of 10000 seconds; if so, oxygen evolved in light over time would decrease as photosynthetic activity decreased. Photosynthetic oxygen evolution was measured as the percentage change of the solution oxygen content in light compared to dark, with increasing concentrations of ferricyanide present (figure 13).

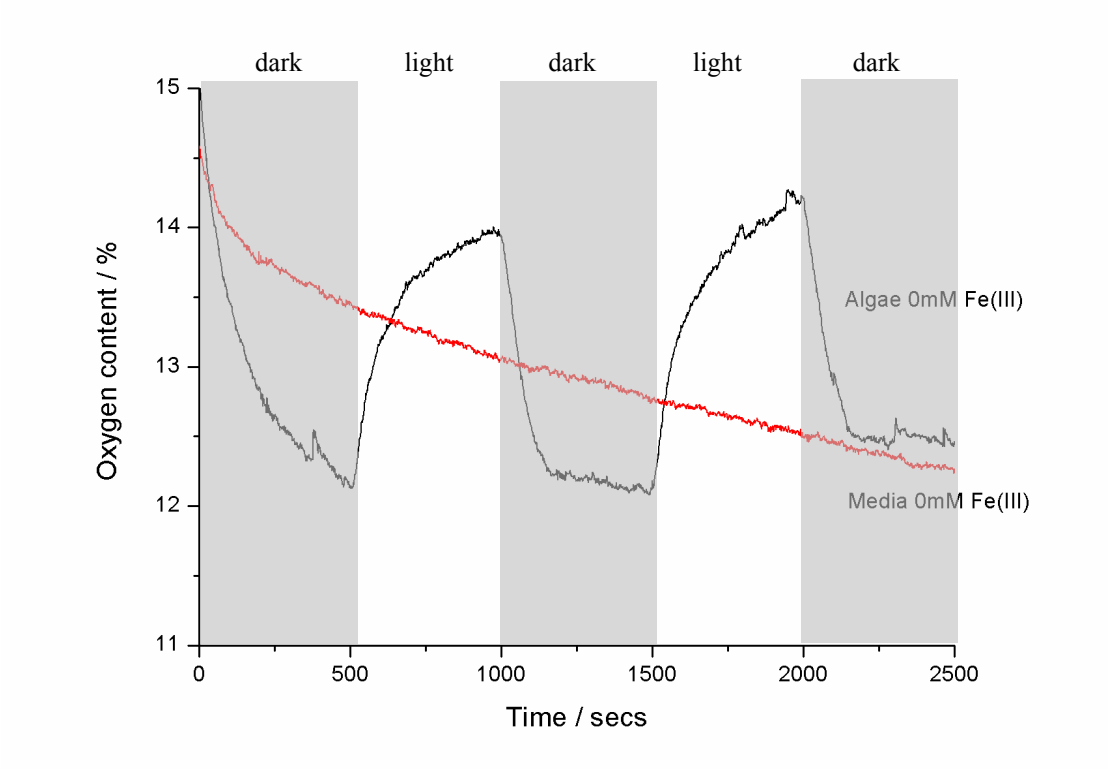


**Figure 12 Oxygen content in samples of *C. vulgaris* or media controls, in light and dark. Unshaded areas represent periods of dark, and shaded areas represent periods of illumination**

Figure 13 shows that as expected, with more cells present, more oxygen was photosynthetically evolved. Additionally, in both cases, oxygen evolution in light decreased with increasing concentrations of ferricyanide. This could be due to toxicity, but previous studies have inferred that ferricyanide was not toxic over the short time-scale of these experiments. This could therefore have been due to interactions of ferricyanide with the oxygen evolving photosynthetic machinery. Middlemiss *et al.,* [6], observed this trend with other iron mediators, and correlated it to the reoxidation of Fe(II) by $O_2$ (as reduction rates by ferric reducatase membranes are greater than Fe(II) uptake rates). However, oxygen was not observed to react with

ferrocyanide, due to its stability [6]. This was confirmed from UV-Vis studies. An alternative explanation is that the oxygen evolving machinery was inhibited by the presence of ferricyanide. Weger *et al.,* [16], suggested that competition existed for photo-generated reductants between photosynthesis and iron reduction, and iron reduction led to an inhibition of $CO_2$ fixation. Although not directly related to the oxygen evolution reactions, perhaps there are feedback mechanisms in place.

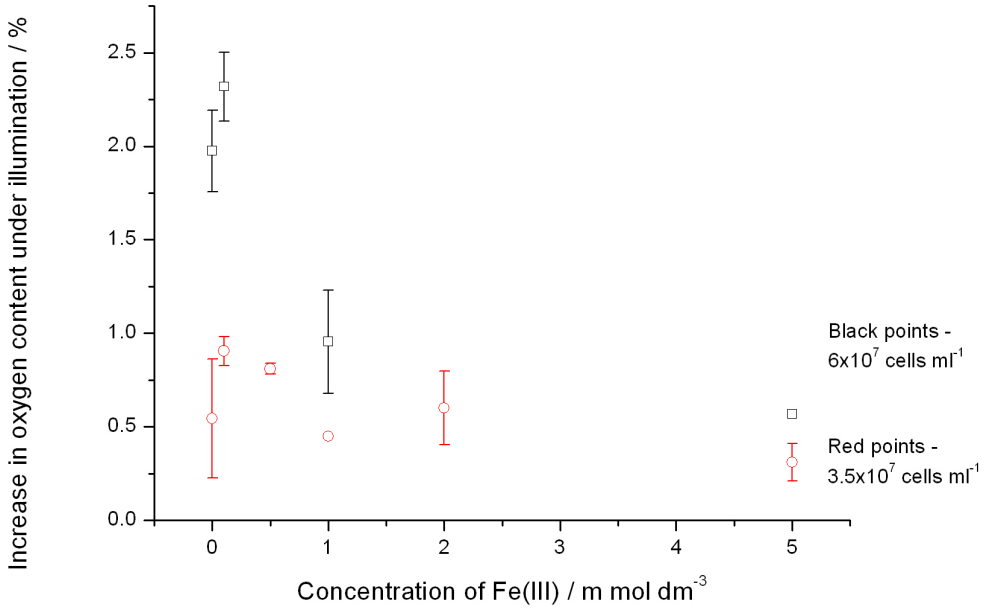


**Figure 13 Photo-oxygen evolution in solutions of *C. vulgaris* with varying cells, and increasing concentrations of ferricyanide. Error bars show one standard deviation (n=2)**

### 4.35 Control experiments

Both oxygen and $H_2O_2$ were added to solutions of 1 mM ferricyanide and ferrocyanide in light and dark, with absorbance measured every hour at 420nm to determine interactions (figures 14 and 15 respectively). This was important to determine if all reactions occurring in a p-MFC device are between algal cells and ferricyanide, or if other products (oxygen from photosynthesis and $H_2O_2$ as an intermediate of oxygen reduction/oxidation to/from water) could interact.

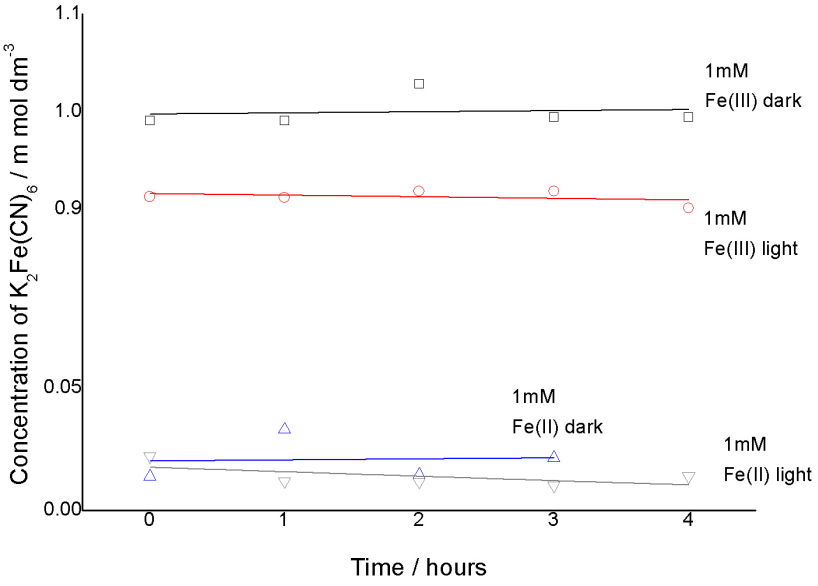


**Figure 14 Concentration of ferricyanide over time in solutions of 1 mM ferricyanide and 1 mM ferrocyanide in 3N-BBM+V media, in dark and light, with constant oxygen bubbling**

Figure 14 shows that oxygen had no effect on the concentration of ferricyanide, when bubbled through 1 mM ferricyanide or ferrocyanide in either light or dark. This corroborated the UV experiments previous, and the finding from Middlemiss *et al.,* [6], that ferrocyanide reoxidation was not seen due to the strength of its Fe-CN bond.

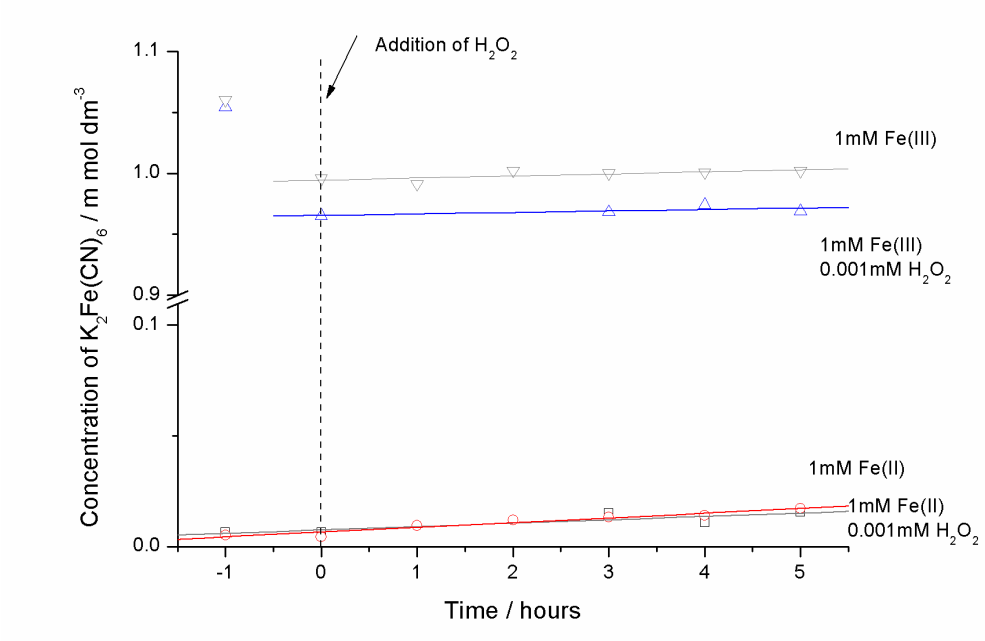


**Figure 15 Concentration of ferricyanide over time in solutions of 1mM ferricyanide and 1mM ferrocyanide in media, in light, with addition of 0.001 mM $H_2O_2$**

Figure 15 also shows that $H_2O_2$ had no effect on the measureable concentration of ferricyanide. Aside from an initial decrease in concentration, which was attributed to dilution, the concentration of ferricyanide remained constant. It is also important to note that the concentration of $H_2O_2$ produced in a p-MFC is likely to be in the nanomolar region, so this test represented extreme conditions probably not attainable in a working device. These findings meant that any products produced in p-MFC devices were unlikely to interact with mediator reactions.

## 4.4 Conclusions

This chapter demonstrated the reductive behaviour of the algal species *C. vulgaris* towards a ferricyanide redox mediator. Additionally, it was shown from UV-Vis studies that *C. vulgaris* cannot oxidise a ferrocyanide mediator. This proved the large background and photocurrents obtained in the p-MFC device in chapter 3 with 9 mM ferrocyanide and the anode set to the reduction potential for ferricyanide were not as a result of cellular activity. This demonstrated that in the p-MFC, the output does not relate entirely to cellular activity in the anodic chamber. Instead, the device output is extremely complex, and must come from a variety of factors.

The reductive behaviour of *C. vulgaris* was thought to be due to ferric reductase in algal cell membranes, which attempt to reduce extracellular Fe(III) to Fe(II) and free chelator. In the case of ferricyanide, the Fe-CN bond is too strong to be broken, but the iron was reduced regardless. With other weakly chelated iron species, Fe(II) can be taken up into algal cells by an Fe transporter, although this process is slower than the rate of reduction.

UV-Vis experiments with differing numbers of algal cells in solution showed that the rate of the reduction process depended upon the number of cells, with more cells giving faster reduction rates. This could be potentially explained due to the increased concentration of ferric reductase membranes (reductive machinery) in solution. It was also shown that reduction rates were limited by the concentration of ferricyanide in solution, with higher concentrations of ferricyanide giving higher rates of reduction.

Importantly, it was determined that the reduction of ferricyanide occurred at a similar rate in light and dark, inferring most of the reducing power used by the ferric reductase membranes was respiratory derived rather than photosynthetic. Previous literature showed illumination increased the rate of iron reduction [2, 6, 7], although the increase was greater in iron deficient cells [2]. It is likely that due to the fact that cells in this study were iron replete, differences between dark and reduction rates were small, and the sensitivity of the UV-Vis technique used in this chapter was too low to distinguish between them.

Cellular interactions were studied. With regards long term toxicity, it was shown that ferricyanide was toxic to *C. vulgaris* cells in the long term at concentrations over 0.001 mM, but not toxic in the short term (under 24 hours) at concentrations under 7 mM. These results had important implications for future work as they provided a time scale during which experiments should be performed. Fluorescence showed ferricyanide and not ferrocyanide induced a reversible quenching effect, which increased with concentration. Weger *et al.*, [16], suggested that the inhibition of $CO_2$ fixation during extracellular ferricyanide reduction was the major cause of the non-photochemical quenching. Inhibition of the Calvin cycle would result in lowered chloroplastic ATP demand, leading to lowered dissipation of the trans-thylakoid $H^+$ gradient, and thus an increase in non-photochemical quenching. Although this effect was only observed with iron deficient cells, the decrease in $CO_2$ fixation could explain the long term toxicity presented by potassium ferricyanide, observed in culturing studies.

Oxygen monitoring experiments also showed that the presence of ferricyanide decreased the amount of photosynthetic oxygen evolved during illumination. This effect increased with ferricyanide concentration. Similar results with other iron mediators were found in studies by Middlemiss *et al.,* [6], and explained as the reoxidation of bulk reduced Fe(II). However, this was not the case for ferrocyanide, as it is too stable for reoxidation. This was confirmed in UV-Vis controls where no change in concentration of ferrocyanide was observed over 5 hours with constant oxygen bubbling. Therefore the reason for the decrease in oxygen evolution is not known, but could be due to a possible feedback mechanism from the inhibition of $CO_2$ fixation.

## 4.5 References


1. Lovley, D.R., *Bug juice: harvesting electricity with microorganisms.* Nature Reviews Microbiology, 2006. **4**(7): p. 497-508.
2. Xue, X.P., Collins, C.M., and Weger, H.G., *The energetics of extracellular Fe(III) reduction by iron-limited Chlamydomonas reinhardtii (Chlorophyta).* Journal of Phycology, 1998. **34**(6): p. 939-944.
3. Liu, X.W. and Millero, F.J., *The solubility of iron in seawater.* Marine Chemistry, 2002. **77**(1): p. 43-54.
4. Weger, H.G., Walker, C.N., and Fink, M.B., *Ferric and cupric reductase activities by iron-limited cells of the green alga Chlorella kessleri: quantification via oxygen electrode.* Physiologia Plantarum, 2007. **131**(2): p. 322-331.
5. Moog, P.R. and Bruggemann, W., *Iron reductase systems on the plant plasma membrane - A review.* Plant and Soil, 1994. **165**(2): p. 241-260.
6. Middlemiss, J.K., Anderson, A.M., Stratilo, C.W., and Weger, H.G., *Oxygen consumption associated with ferric reductase activity and iron uptake by iron-limited cells of Chlorella kessleri (Chlorophyceae).* Journal of Phycology, 2001. **37**(3): p. 393-399.
7. Lynnes, J.A., Derzaph, T.L.M., and Weger, H.G., *Iron limitation results in induction of ferricyanide reductase and ferric chelate reductase activities in Chlamydomonas reinhardtii.* Planta, 1998. **204**(3): p. 360-365.
8. Bauer, P. and Bereczky, Z., *Gene networks involved in iron acquisition strategies in plants.* Agronomie, 2003. **23**(5-6): p. 447-454.
9. Allnutt, F.C.T. and Bonner, W.D., *Characterisation of iron uptake from ferrioxamine-B by Chlorella vulgaris.* Plant Physiology, 1987. **85**(3): p. 746-750.
10. Allnutt, F.C.T. and Bonner, W.D., *Characteristics of iron uptake from hydroxamate siderophores by Chlorella vulgaris and the correlation between uptake and reduction.* Journal of Plant Nutrition, 1984. **7**(1-5): p. 427-435.
11. Wilhelm, S.W. and Trick, C.G., *Iron-limited growth of cyanobacteria - Multiple siderophore production is a common response.* Limnology and Oceanography, 1994. **39**(8): p. 1979-1984.

12. Trick, C.G. and Wilhelm, S.W., *Physiological changes in the coastal marine cyanobacterium Synechococcus Sp. PCC-7002 exposed to low ferric ion levels.* Marine Chemistry, 1995. **50**(1-4): p. 207-217.
13. Schmidt, W., *Iron solutions: acquisition strategies and signaling pathways in plants.* Trends in Plant Science, 2003. **8**(4): p. 188-193.
14. Weger, H.G., *Ferric and cupric reductase activities in the green alga Chlamydomonas reinhardtii: experiments using iron-limited chemostats.* Planta, 1999. **207**(3): p. 377-384.
15. Davey, M.S., Suggett, D.J., Geider, R.J., and Taylor, A.R., *Phytoplankton plasma membrane redox activity: Effect of iron limitation and interaction with photosynthesis.* Journal of Phycology, 2003. **39**(6): p. 1132-1144.
16. Weger, H.G. and Espie, G.S., *Ferric reduction by iron-limited Chlamydomonas cells interacts with both photosynthesis and respiration.* Planta, 2000. **210**(5): p. 775-781.
17. Volker, C. and Wolf-Gladrow, D.A., *Physical limits on iron uptake mediated by siderophores or surface reductases.* Marine Chemistry, 1999. **65**(3-4): p. 227-244.
18. Nespurkova, L., Jirasek, M., Janacek, K., and Rybova, R., *Plasmalemma redox system in the alga hydrodictyon-reticulatum.* Studia Biophysica, 1989. **130**(1-3): p. 95-98.
19. Liu, X.L., Tao, S., and Deng, N., *Synchronous-scan fluorescence spectra of Chlorella vulgaris solution.* Chemosphere, 2005. **60**(11): p. 1550-1554.
20. Fai, P.B., Grant, A., and Reid, B., *Chlorophyll a fluorescence as a biomarker for rapid toxicity assessment.* Environmental Toxicology and Chemistry, 2007. **26**(7): p. 1520-1531.
21. Naessens, M., Leclerc, J.C., and Tran-Minh, C., *Fiber optic biosensor using Chlorella vulgaris for determination of toxic compounds.* Ecotoxicology and Environmental Safety, 2000. **46**(2): p. 181-185.
22. Nguyen-Ngoc, H., Durrieu, C., and Tran-Minh, C., *Synchronous-scan fluorescence of algal cells for toxicity assessment of heavy metals and herbicides.* Ecotoxicology and environmental safety, 2009. **72**(2): p. 316-20.
23. Peltier, G. and Cournac, L., *Chlororespiration.* Annual Review of Plant Biology, 2002. **53**: p. 523-550.

24. Cournac, L., Latouche, G., Cerovic, Z., Redding, K., Ravenel, J., and Peltier, G., *In vivo interactions between photosynthesis, mitorespiration, and chlororespiration in Chlamydomonas reinhardtii.* Plant Physiology, 2002. **129**(4): p. 1921-1928.

# Chapter 5. Electrochemical Studies of Algae with Potassium ferricyanide

# Chapter 5 – Electrochemical Studies of *C. vulgaris* and Potassium Ferricyanide

## 5.1 Introduction

Due to the complexity of the basic p-MFC (shown in chapter 3), the interaction of *Chlorella vulgaris* with the ferricyanide mediator can only be understood from separate studies away from the whole p-MFC device. The previous chapter explores the rate and mode of potassium ferricyanide (ferricyanide) reduction by *C. vulgaris* using basic analytical methods, and demonstrates that algal cells could not oxidise ferrocyanide. However, electrochemical techniques also have an essential role in understanding mechanisms (microbial, physiological, chemical and electron transport) involved in MFCs and p-MFCs, and in identifying limitations with each component. Consequently, this chapter continues the work begun in chapter 4, but using electrochemistry to study algal/ferricyanide mediator interactions. Previous electrochemical studies of cells used in MFCs and p-MFCs are first explored

Mechanisms of electron transfer to an electrode can be studied through cyclic voltammetry. Cyclic voltammetry has obvious applications in detecting naturally produced microbial redox shuttles from microbes such as *Geothrix fermentans* [1] and those in the *Proteobacteria* family [2]. For example, Chung *et al.,* [3], used the technique on supernatant from their MFC, searching for redox products. It has also been used to study extracellular electron transfer to the electrode from electrogenic biofilms, for example those containing *Geobacter* and *Shewanella spp* [4]. Biofilms of *Geobacter sulfurrectucens* grown on graphite at 0.24 V produced a sigmoidal catalytic wave, with an onset potential near -0.2 V vs.. SHE, a maximum limiting current near -0.05 V and a small reversible peak at -0.08 V [5]. At early time points, the first derivative of the cyclic voltammetry data showed a symmetrical maximum near -150 mV, which shifted slightly more negative as biofilms grew. This information supports a model where the dominant mechanism (rate controlling step) in electron transport was not significantly changing during biofilm growth 0.24 V. To date, only microbial extracellular cytochromes have been detected [4]. However, some cyclic voltammetry of MFC systems showed characteristics of inter-conversion

between active-inactive states, typically inactivation during the positive potential sweep, and activation upon the negative sweep. This would not be expected of cytochromes; instead the activation/inactivation of other enzymes such as hydrogenases was thought to be occurring [4]. The shapes of these voltammograms therefore indicated that multi-enzyme systems may contribute to the anodic current.

Other types of voltammetry, including square wave and differential pulse, have also been implemented. Marsili *et al.,* [5], used these techniques to investigate if different redox proteins were used for charge transfer in biofilms grown at different potentials. Although it was noted that damage to the biofilms was possibly occurring due to the frequencies and pulse heights used, no additional peaks could be elucidated, making different pathways unlikely.

Rates of reduction in solutions containing photosynthetic species and exogeneous electron acceptors have been studied electrochemically in the literature, both at stationary and at rotating disk electrodes [6, 7]. At stationary electrodes, cyclic voltammetry was used by Martens *et al.,* [8], to determine the second order rate constant for the reduction of diaminodurene (DAD) by the photosynthetic electron transport chain of *Synechococcus* cells immobilised on glassy carbon electrodes. The voltammetric response under continuous illumination was different to the dark response. Upon illumination, the anodic peak increased and reached a plateau at slow scan rates (5 mV $s^{-1}$), whilst the cathodic peak decreased and was virtually lost This behaviour was typical of the catalytic regeneration of reduced DAD by the photosynthetic bacteria [8]. Second order rate constants were calculated by following the work of Nicholson and Shain [9]. Davey *et al.,* [10], also measured the reduction of ferricyanide in solution by a range of diatoms, by measuring current at carbon fibre microelectrodes poised at an overpotential of 400 mV w.r.t Ag/AgCl. In this way, the positive potential ensured any ferrocyanide (reduced couple) was reoxidised, and they saw higher currents in light than in dark [10]. However, measurements at stationary electrodes are carried out under non-steady state conditions whereby the concentration of the reduced mediator at the surface of the electrode does not remain constant. Therefore it is difficult to validate findings of these systems due to the complex thermodynamics and kinetics involved.

In contrast, amperometry using a rotating disk electrode can be used for kinetic analysis of redox reactions and is highly reproducible even in cell suspensions [11, 12], minimising catalytic effects which occur near the electrode surface [11]. This was first used to study the kinetics of electron transfer in the reduction of 1,4-Benzoquinone (BQ) and 2,6-dimethyl-1,4-benzoquinone (DCBQ) by *Synechococcus* cells. When rotating disk was performed at 0.6 V w.r.t Ag/AgCl, the oxidation current increased linearly under illumination and was constant in the dark; taken to represent the oxidation of hydroquinone generated by *Synechoccocus sp.* cell catalysed photoreduction of BQ (or DNBQ). The slope of the increase in the oxidation current was assumed to signify the steady-state rate of electron transfer to the mediators. The reaction followed Michaelis-Menten type kinetics. Torimura *et al.* did not observe photo-dependent currents with anthraquinone-2,7-disulfonate (AQS), 2-hydroxy-1,4-napthaquinone (HNQ) or 2-methyl-1,4-napthaquinone (vitamin $K_3$). This was thought to have been due to the lower redox potentials of these chemicals, which may have made it energetically difficult to accept electrons [11]. Photoreduction with 2,6-dichloroindolphenol (DCIP) and ferricyanide was also scarcely observed, thought to be due to limited membrane permeability of the negatively charged compounds [11]

Kasuno *et al*., [12], also used rotating disk electrochemistry to investigate the kinetics of the photo-induced electron transfer reaction from chromatophore vesicles and intact cells of *Rhodobacter sphaeroides,* a representative purple bacterium, to the exogeneous electron acceptor DCBQ. Using a fixed potential of 0.5 V, optimum for the oxidation of reduced DCBQ, the rate of photoinduced electron transfer from chromatophores or intact cells was determined as the increase in the slope of the current over time. The concentration of reduced DCBQ upon illumination was determined by measuring the limiting current for reoxidation at the rotating disk. Both reactions were found to follow Michaelis-Menten kinetics, with two phases identified in the current-time curve (figure 1). It was suggested that the *R. spaerodes* chromatophores or intact cells were adsorbed onto the surface of the WE upon application of a positive potential. This resulted in an initial abrupt increase in the positive current. In the second phase, there was a gradual and linear increase in the positive current, which appeared to be due to the transfer of electrons from the chromatophores or intact cells in the bulk solution to the WE [12].

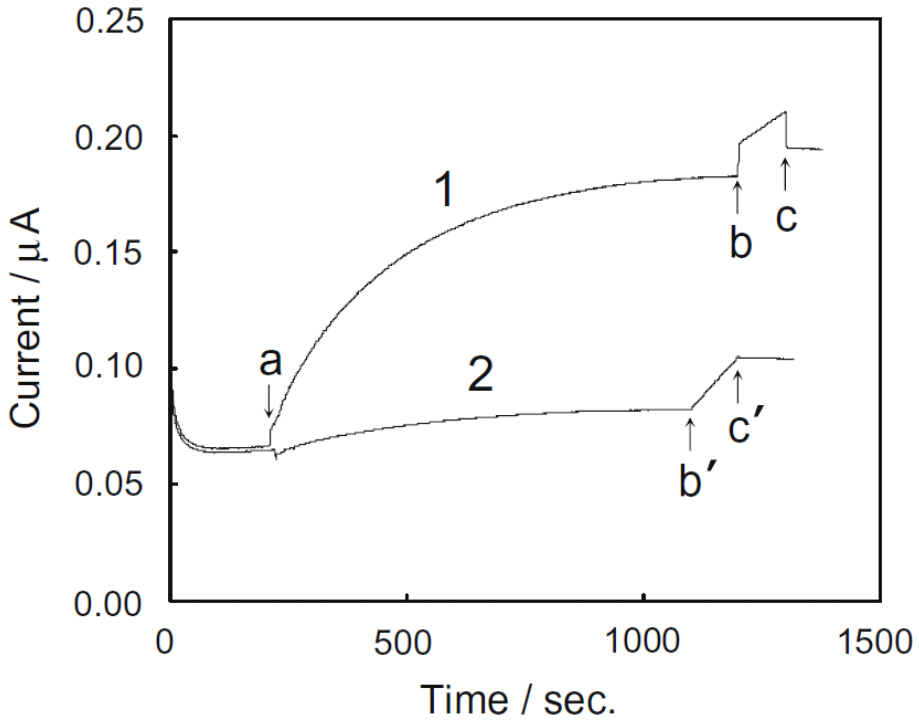


**Figure 1 Reproduced from [12] The amperometric response of a cell containing 0.1 mM DCBQ in pH 8 phosphate buffer. At point a, 23 µg mL$^{-1}$ *R. sphaeroides* chromatophores (curve 1) or 4.6 µg mL$^{-1}$ intact cells (curve 2) were added. Illumination occurred between points b and c.**

### 5.11 Chapter Aims

Electrochemical measurements have proved complementary to those used in chapter 4, to determine rates and mechanism of interactions between *C. vulgaris* and ferricyanide. In this chapter, voltammetry is used to determine if all reduction of ferricyanide occurred through ferric reductive proteins in the cell wall, or if there are additional redox (or siderophore) products that could be detected. Rates of reduction are studied using chronoamperometry, and compared to previous UV-Vis spectrophotometry data (shown in chapter 4). Although UV-Vis gave an initial rate value, due to the continuous depletion of ferricyanide in the bulk, there could have been considerable error involved.

Rate limiting factors for the ferricyanide reduction are determined in this chapter using rotating disk electrochemistry (and the Koutecky-Levich equation). Possible rate limiting steps are shown in figure 2, and could broadly be split into mass transport or kinetics. If the rate of electron transfer at the electrode surface is considered faster than the rate of electron transfer at the algal cell surface, then the

possible rate limiting steps involve the rate of electron transfer at the algae ($k_{et}$), or the diffusion (mass transport) of ferricyanide to the algal cells, and ferrocyanide to the electrode. The diffusion coefficients of ferricyanide and ferrocyanide are assumed to be equal. Determining the rate limiting step is important as if mass transport was found to be rate limiting, measured algal rates of reduction would simply equate to the mass transport limited rate.

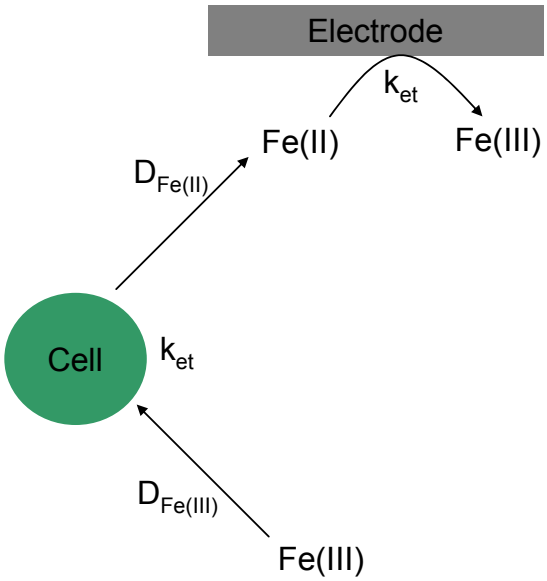


**Figure 2 The possible rate limiting steps (classified broadly into D (diffusion) and k (kinetic)) involved in current generation from the reduction of ferricyanide by algal cells. Assumptions involved; Fe diffuses faster than algal cells, which are subsequently stationary relative to the Fe; $D_{Fe(III)}$ and $D_{Fe(II)}$ are equal and $k_{et}$ at electrode is extremely fast compared to $k_{et}$ at cell**

## 5.2 Experimental

### 5.21 Voltammetry – cyclic and square wave of *C. vulgaris*

All electrochemistry was carried out on an Autolab PGSTAT 12 with a built-in frequency response analyser. Voltammetry was used to determine if redox products were produced by *C. vulgaris*. A standard three electrode set up was assembled in a 10 mL solution of *C. vulgaris* culture, using a Pt counter, Ag/AgCl reference, and either an Au (area 0.03 $cm^2$), boron doped diamond (BDD) (0.07 $cm^2$) or Pt working electrode (area 0.015 $cm^2$). Cyclic voltammetry from -0.7 to 0.7 V was run at different scan rates and different time periods on samples taken from a developing culture, with square wave additionally performed from -0.7 to 0.7 V. A nitrogen purge was applied for use with the Pt WE. Biofilms were additionally grown on FTO

glass working electrodes (area 1 $cm^2$), and tested with cyclic voltammetry from -0.7 to 0.7 V.

### 5.22 Chronoamperometry of *C. vulgaris* and potassium ferricyanide

To study more quantitatively the reduction of ferricyanide by *C. vulgaris*, and determine reduction rates, chronoamperometry at 100 mV past the oxidation potential of ferrocyanide (as determined by cyclic voltammetry) was performed in solutions of algae and ferricyanide. A range of concentrations of algae and ferricyanide were tested; algal concentrations of $7x10^7$ and $1.4x10^8$ cells $mL^{-1}$ were chosen along with concentrations of ferricyanide between 1 mM and 7 mM. This took place in a specially designed chamber utilising a fluorine doped tin oxide (FTO) working electrode (area 1.33 $cm^2$), which allowed light to easily reach the cells, as shown in figure 3a. Once the experiment was running, the sample was illuminated periodically using a 620 nm optical fibre, at $5x10^{-3}$ W $cm^{-2}$. Background 3N-BBM+V media controls were performed, and it could be assumed that once subtracted, any currents were due to the reoxidation of ferrocyanide to ferricyanide at the electrode, which in turn directly corresponded to the rate of reduction of ferricyanide to ferrocyanide by *C. vulgaris* cells in the first place. Rates were normalised for cell numbers and electrode area. Three repeats were taken, approximately 20 minutes apart, to ensure the system was at equilibrium, and the ferricyanide was not damaging the algae in any way.

### 5.23 Rotating Disk Electrochemistry

Rotating disk was additionally employed to further study reduction rates, and determine if the rate was determined by electron transfer kinetics or mass transport. The rotating disk electrode was held at a potential 100 mV positive of the oxidation potential for ferrocyanide, and used to sense the production of ferrocyanide (from ferricyanide) by the algae. A Pt working electrode was used (area 0.07$cm^2$), and the schematic is shown in figure 3b. Experiments involved keeping the ferricyanide concentration constant at 2.78 mM, before increasing the cell concentration (taking dilutions into account) between $2.40x10^7$ to $1.15x10^8$ cells $mL^{-1}$. In a second set of experiments, algal cell concentration was held constant, and the ferricyanide concentration increased. Taking into account dilutions, ferricyanide concentrations were between 2.78 mM to 22.22 mM. Finally, the ferricyanide concentration was held constant at 22.22 mM, and cells again increased from $9.26x10^7$ to $1.79x10^8$ cells $mL^{-1}$.

At each set of values, the rotation speed of the working electrode was increased from 100 rpm to 600 rpm, and currents allowed to stabilise briefly before the spin speed was again increased. Controls with 0 mM ferricyanide or 0 cells $mL^{-1}$ were performed, and three repeats performed for each experiment. After media control average current values were subtracted from averages of the repeats, plots were produced of 1/ current vs. 1/ spin speed (rad). Using the Koutecky-Levich equation, gradients were used to calculate the total ferrocyanide in bulk solution (equation 1), per $1x10^6$ cells $mL^{-1}$, and intercepts used to calculate reduction rates per hour (normalised for electrode area and cell numbers).

$$Gradient = \frac{1}{0.62nFAD_O^{2/3}v^{-1/6}C_O}$$

**Equation 1 The relationship between gradient of 1/ current vs. 1/ square root spin rate (rpm) plots and the diffusion coefficient of ferrocyanide**

Diffusion coefficients for ferrocyanide were calculated in solutions containing 1 mM ferrocyanide and increasing concentrations of algal cells, by performing chronoamperometry at 100 mV past the oxidation potential for ferrocyanide. In this way, ferrocyanide was oxidised to ferricyanide at the electrode, and as the algal cells were merely present (and not interacting) in the reaction, their effect on the diffusion coefficient of ferrocyanide could be measured.

After the averages of media controls were subtracted, the diffusion coefficient for ferrocyanide in differing concentrations of algae could be calculated from the gradient of plots of 1/ current vs. 1/ spin speed (rad), using the Koutecky-Levich equation.

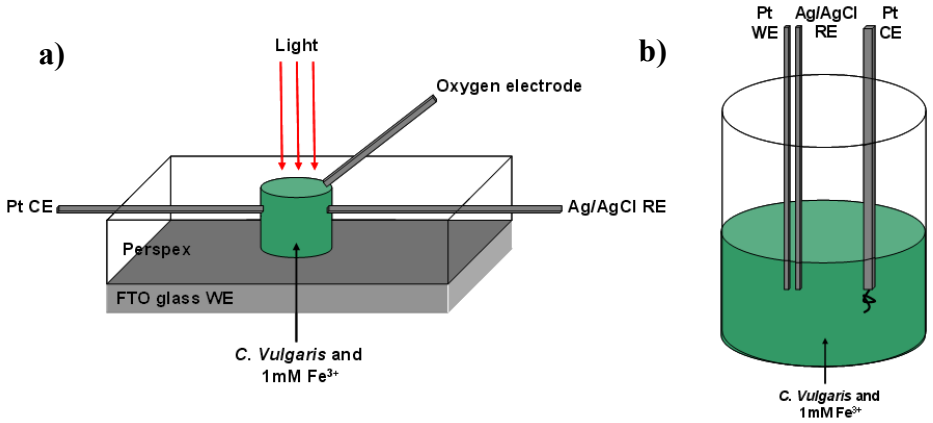


**Figure 3 Schematics of the set-ups used for a) Chronoamperometry and b) rotating disk measurements**

## 5.3 Results and Discussion

### 5.31 Voltammetry – cyclic and square wave of *C. vulgaris*

Cyclic voltammetry was performed on *C. vulgaris* solutions to determine if any redox species were produced in solution. Figures 4 and 5 show cyclic voltammetry on a Au electrode, w.r.t Ag/AgCl.

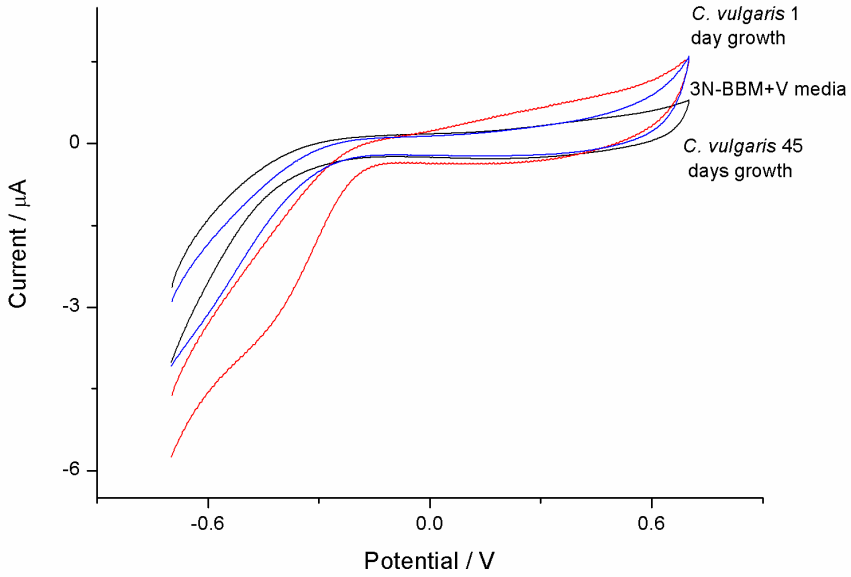


**Figure 4 Cyclic voltammetry at 100 mV $s^{-1}$ of *C. vulgaris* media, one day *C. vulgaris* culture, and fully established 45 day old *C. vulgaris* culture on Au disk electrode (area 0.03$cm^2$) w.r.t Ag/AgCl**

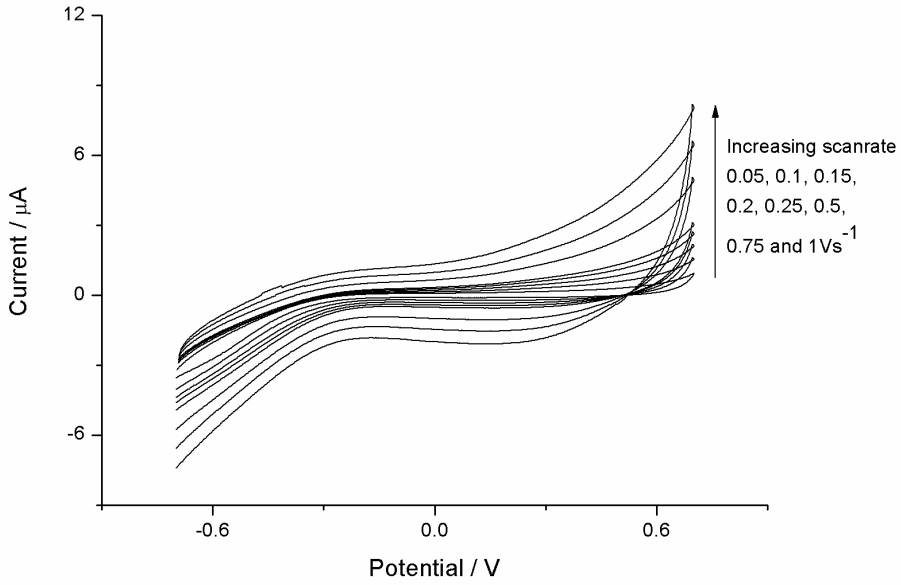


**Figure 5 Cyclic voltammetry of 45 day old *C. vulgaris* culture at a range of scan rates, on Au disk electrode (area 0.03$cm^2$) w.r.t Ag/AgCl**

Figures 4 and 5 show that no redox species other than oxygen were detected using an Au electrode, irrespective of culture age or scan rate used. This pattern was the same using other electrodes, including boron doped diamond, platinum, and biofilms grown on FTO electrodes (data not shown). Aliquots of supernatant were sequentially added to KCl. A nitrogen purge was applied, and electrodes were cleaned in between measurements. However, no other redox species could be detected. Similar results were obtained with square wave voltammetry, between -0.7V and 0.7 w.r.t Ag/AgCl.

This means that no redox products (aside from photosynthetically produced oxygen) seem to be produced by *C. vulgaris*. This corroborates previous literature which suggests that this algal species uses a strategy 1 mechanism for the uptake of Fe(III), whereby ferric reductase proteins in algal membranes reduce Fe(III) to Fe(II).

### 5.32 Chronoamperometry of *C. vulgaris* and potassium ferricyanide

The rate of ferricyanide reduction was measured in a three electrode electrochemical cell with a FTO working electrode (area 1.33cm$^2$). The electrode was polarised to 100 mV positive of the oxidation potential for the ferri/ferro redox couple, and the current was measured under illumination and in the dark for a range of algal and ferricyanide concentrations.

Cyclic voltammograms used to obtain the potential values, with increasing ferricyanide, are shown in figure 6. The value 100 mV positive of the oxidation potential of ferrocyanide was determined as approximately 0.4 V w.r.t Ag/AgCl. This value was chosen for chronoamperometry measurements to ensure that any ferrocyanide reaching the electrode would be immediately oxidised back to ferricyanide. It was assumed that if the electrodes were reducing ferrocyanide to ferricyanide; as only ferricyanide was present initially, the oxidation currents at the electrode were approximately equal to the reduction currents by the algae.

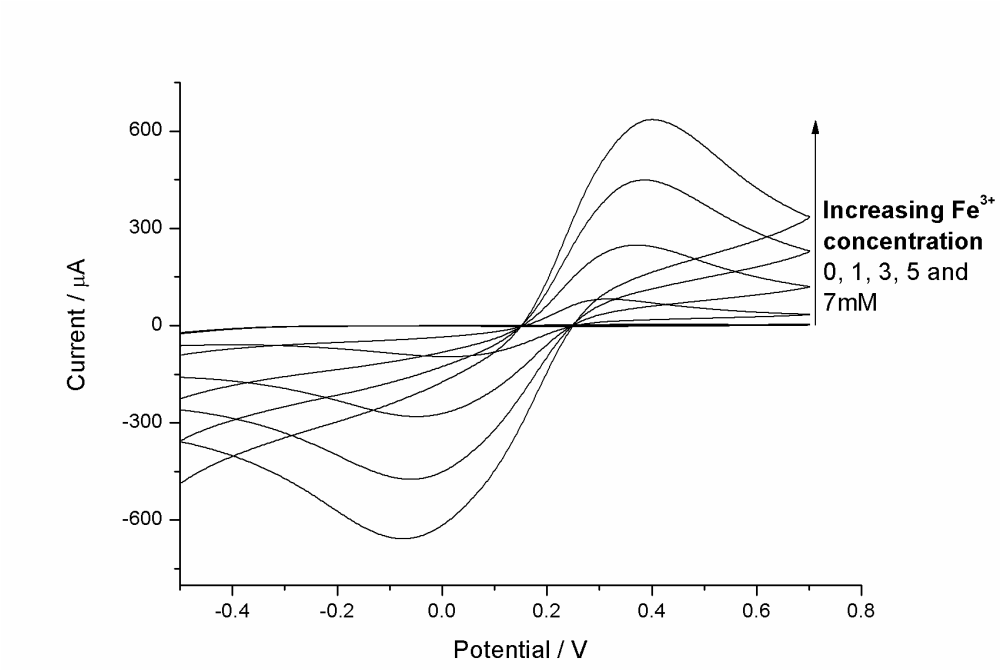


**Figure 6 Typical CVs. obtained from a solution of *C. vulgaris* and increasing ferricyanide concentration, on a FTO glass electrode (area 1.33cm$^2$) w.r.t Ag/AgCl, with 1.51x10$^8$ cells mL$^{-1}$ and 1 mL total volume, at a scan-rate of 0.05 V s$^{-1}$**

Typical chronoamperometry results are shown in figure 7. Photocurrents were observed under illumination, but they were small when compared to overall background current magnitudes (figure 8), especially at the lowest cell concentration tested. With the higher concentration of cells (1.4x10$^8$ cells mL$^{-1}$), photocurrents increased with ferricyanide concentrations to 3 mM, and then decreased at higher ferricyanide concentrations. This suggested small amounts of extra reducing power were produced within the algae in light which could reduce extra ferricyanide, leading to higher reoxidation currents of ferrocyanide to ferricyanide at the electrode. This corroborates previous literature studies, whereby this effect was observed in *C. reinhardtii* [13, 14] and a range of diatoms [10], although the effect was much greater in Fe-deficient cells [14-18]. The fact that photocurrents were small likely meant that UV-Vis was not sensitive enough to detect the change in absorbance (A) between light and dark. The expected change in A was calculated for a photocurrent of 4μA. 4μA= 2.5x10$^{13}$ e s$^{-1}$ = 9 x 10$^{16}$ e hr$^{-1}$ = 1.5x10$^{-4}$ mmol extra ferricyanide reduced hr$^{-1}$ mL$^{-1}$. As 10mL solution was used in UV-Vis, the expected extra ferricyanide reduced was 1.5x10$^{-3}$ mmol hr$^{-1}$. Using the Beer-Lambert law (l=1 cm, ε=1.04 M$^{-1}$ cm$^{-1}$), expected change in absorbance in light compared to dark conditions was 0.0016 A hr$^{-1}$

(unlikely to be detected by UV-Vis). However, this value ignores any mass transport limitations imposed by the electrode compared to conditions experienced in UV-Vis.

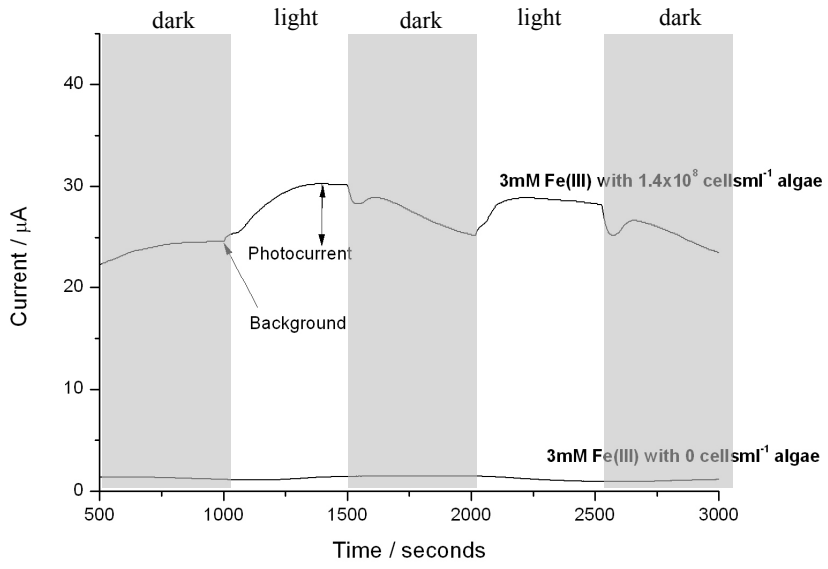


**Figure 7 Typical chronoamperometry (at 100 mV past the oxidation potential for ferricyanide at FTO electrode area 1.33 cm$^2$) of solutions containing ferricyanide mediator with or without *C. vulgaris*. Shaded areas represent darkness, whilst unshaded areas represent illumination**

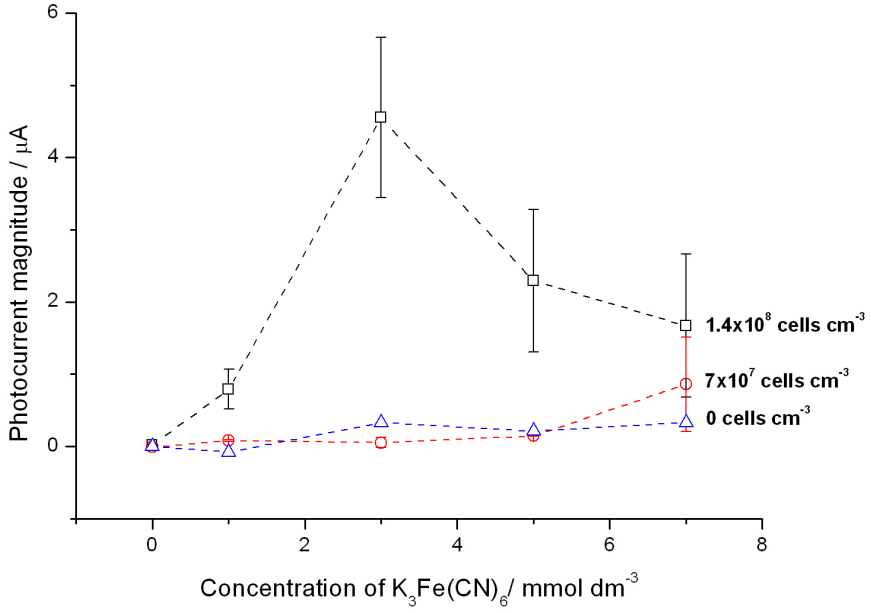


**Figure 8 Photocurrents produced from chronoamperometry experiments (at 100 mV past the oxidation potential for ferrocyanide), using FTO working electrode of area 1.33 cm$^2$ with increasing concentration of ferricyanide and at two algal concentrations. The error bars show one standard deviation (n=3)**

Equilibrium (dark) currents measured at the working electrode increased linearly with increasing amounts of ferricyanide. Although controls showed small current increases with ferricyanide concentration, in the presence of algae a large increase in dark current relative to the control was observed. Using the background (dark) equilibrium currents measured at the working electrode for increasing amounts of ferricyanide, and at two different algal concentrations, background corrected rates of algal ferricyanide reduction were calculated. Once background currents were subtracted (when no algal cells were present), all oxidation currents of ferrocyanide to ferricyanide were considered equal to all ferricyanide reduction rates by the algae. Rates (as shown in figure 8) were calculated by relating current to charge, dividing by charge on one electron, and calculating how many moles of ferricyanide were being reduced to ferrocyanide in one hour, per $1x10^6$ cells.

As figure 9 shows, the normalised rate of ferricyanide reduction appeared to increase linearly with ferricyanide concentration. Doubling the algae concentration gave approximately a threefold increase in rate (3.235, SD =0.79733), as was also approximately measured with UV-Vis. It was interesting that no saturation of current was seen either with increasing ferricyanide or increasing algae. At the same conditions as those used for UV-Vis spectrophotometry (1 mM ferricyanide and $7x10^7$ cells $mL^{-1}$), reduction rates measured with chronoamperometry were approximately three times less than those previously calculated from UV-Vis (0.5 nmol Fe(III) $cm^2$ $hr^{-1}$ $10^{-6}$ cells compared to 1.43 nmol Fe(III) $hr^{-1}$ $10^{-6}$ cells. This difference could be explained as UV-Vis measurements only measured initial rates (often an over-estimation of total rates). Additionally, chronoamperometry experiments were mass transport limited by the use of an electrode (and normalised for electrode area), whereas UV-Vis measured instantaneous bulk reduction. The averages of rates measured from both methods were very comparable to rates calculated previous for Fe replete *C. kessleri* [18] with Fe-replete cells found to have a rate of 0.99 +/- 0.30 nmol $10^{-6}$ cells $hr^{-1}$ in the dark. Additionally, rates in *C. reinhardtii* Fe-replete cells were found to be 5 nmol $10^{-6}$ cells $hr^{-1}$ in dark, and 8 nmol $10^{-6}$ cells $hr^{-1}$, in light [14].

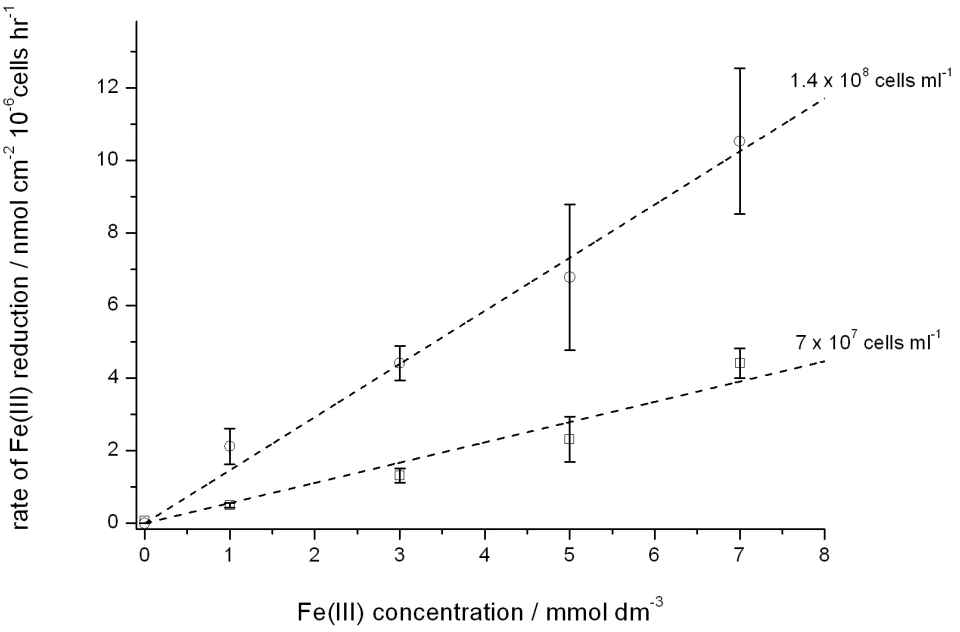


**Figure 9 Rates for the reduction of ferricyanide by *C. vulgaris*, with increasing concentration of ferricyanide and at two different algal concentrations. The error bars show one standard deviation (n=3). Rates were normalised for number of cells per mL and for electrode area**

### 5.33 Rotating Disk Electrochemistry

Rotating disk electrochemistry (RDE) was carried out in the dark and proved to be a simple and reproducible method of studying ferricyanide reduction by *C. vulgaris*. During RDE the Pt working electrode (area 0.07cm$^2$) was rotated (in this case at rotation speeds between 100 and 600 rpm) pulling the solution in to the electrode surface and ensuring efficient mixing in the bulk. The electrode was held at a potential 100 mV positive of the oxidation peak for ferrocyanide, as determined by cyclic voltammetry prior to the RDE experiment. This ensured that any ferrocyanide reaching the electrode surface would immediately be oxidised to ferricyanide.

A calibration measurement was first carried out in a mixture of algae and ferrocyanide to assess whether the presence of algae would change the mass transport of ferrocyanide to the surface. Previous studies have shown that the presence of suspended particles (such as 12.7 μm diameter calcite crystals) could substantially increase the rate of mass transfer of a dissolved redox species to a surface resulting in larger than expected currents. Using the Koutecky-Levich equation, and the gradient of plots of 1/ current vs. 1/ square root spin rate (shown in figure 10), the relationship

between the diffusion coefficient of ferrocyanide and algal concentration was calculated (shown in figure 11). Surprisingly the presence of increasing amounts of algae caused a linear decrease in the diffusion coefficient for ferrocyanide, possibly because the ferri/ferro species spent some of their time complexed to the algae and were not free to move around in solution. In all results, small, negative media control averages were subtracted.

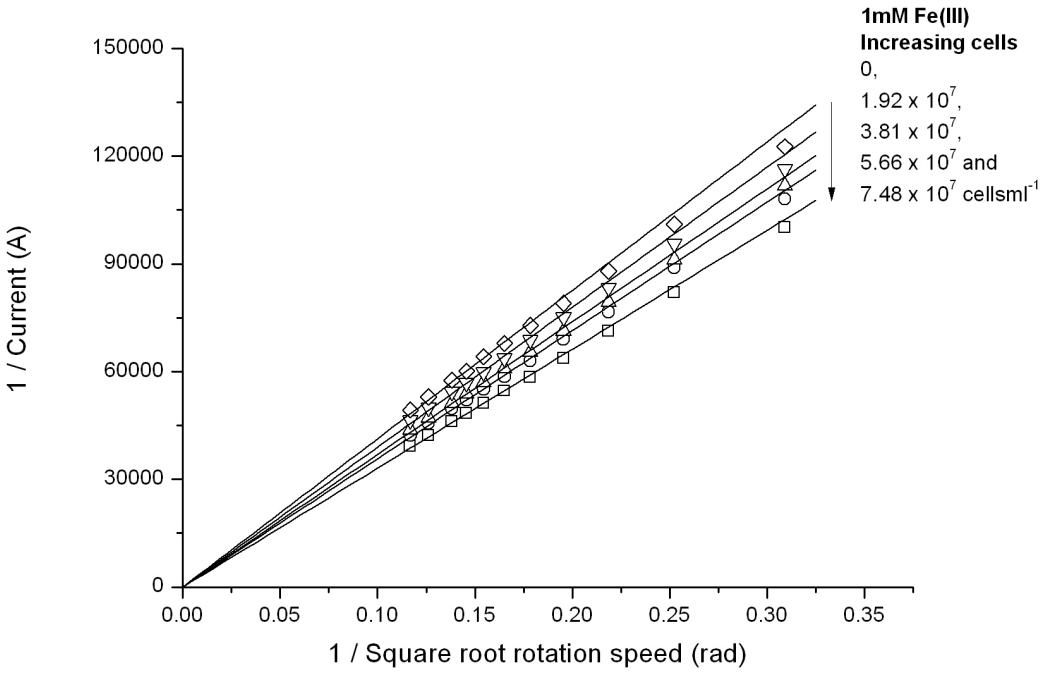


**Figure 10 Plots of 1/ Current VS. 1/ square root rotation speed (rad) with 1 mM ferrocyanide and increasing cells $mL^{-1}$, at a potential 100 mV past the oxidation potential of ferrocyanide. Note that media control currents have been subtracted.**

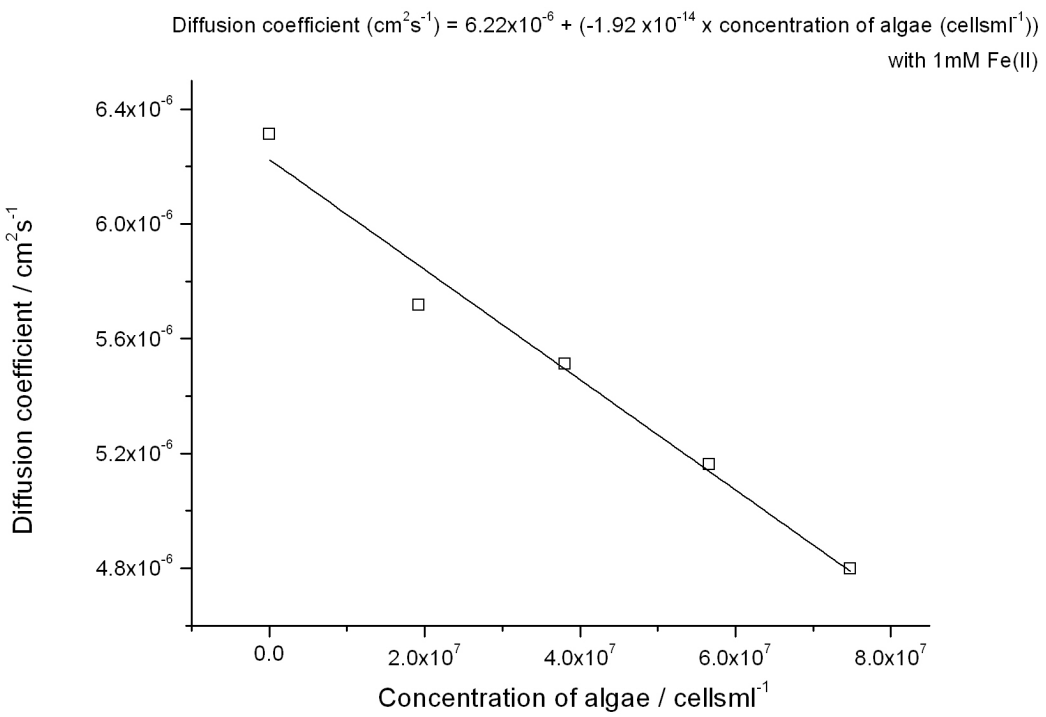


**Figure 11 Diffusion coefficient of ferrocyanide with increasing concentrations of cells, as calculated from the gradients of plots in figure 10 using the Koutecky-Levich equation.**

Rotating disk electrochemistry was then performed with algal cells and ferricyanide in solution, to further study the reduction, and determine if the rate was limited by electron kinetics or mass transport (see figure 2). This took place again at 100 mV past the oxidation potential of ferrocyanide. Experiments involved keeping the ferricyanide concentration constant at 2.78 mM, before increasing the algal cell concentration, then holding cell concentrations constant whilst increasing ferricyanide concentration. Finally, the ferricyanide concentration was held constant at 22.22 mM, and cells again increased. During each experiment, rotation speed was increased step-wise from 100 rpm to 600 rpm. Three repeats were taken, averages calculated, and background media controls subtracted. Then plots were produced of 1/ current vs. 1/ square root rotation speed (figures 12, 13 and 14)

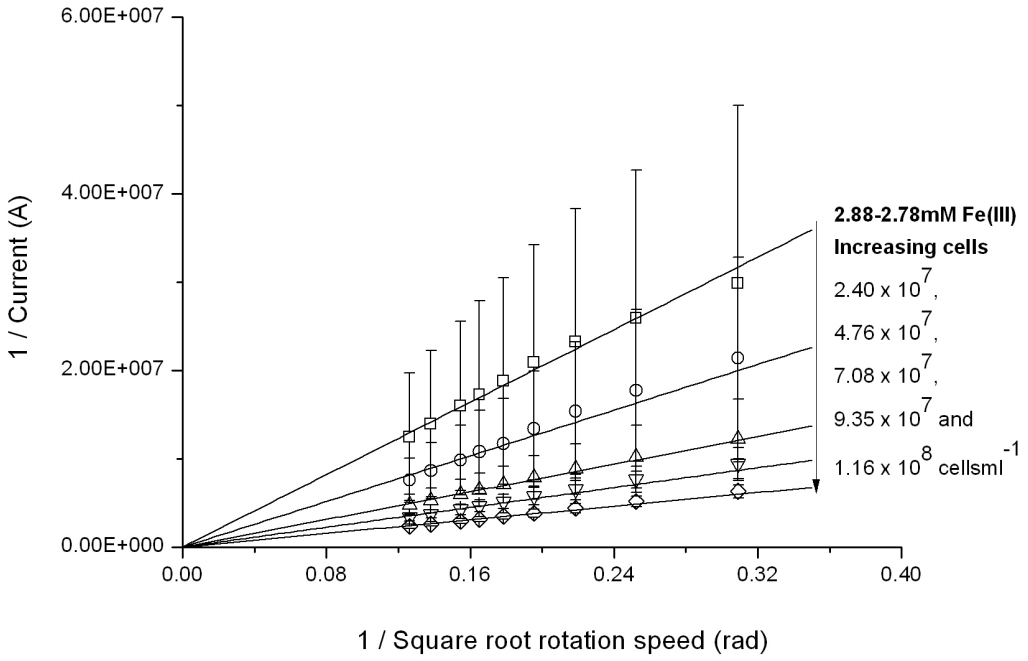


**Figure 12 Plots of 1/Current vs. 1/square root rotation speed (rad) with 2.88 mM ferricyanide and increasing cells in solution from $2.40x10^7$ to $1.16x10^8$ cells $mL^{-1}$, at a potential 100 mV past the oxidation potential of ferrocyanide. The error bars show one standard deviation (n=3). Background controls (with no cells present) have been subtracted**

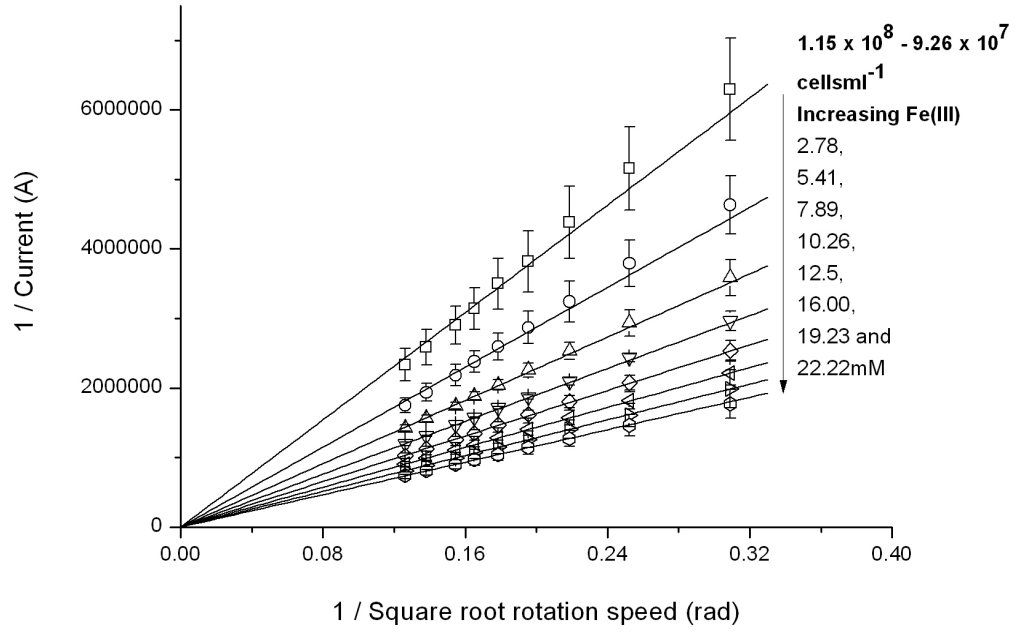


**Figure 13 Plots of 1/ Current vs. 1/ square root rotation speed (rad) with $1.15x10^8$ cells $mL^{-1}$ algae in solution and increasing ferricyanide from 2.78 to 22.22 mM, at a potential 100 mV past the oxidation potential of ferrocyanide. The error bars show one standard deviation (n=3) Background controls (with no cells present) have been subtracted**

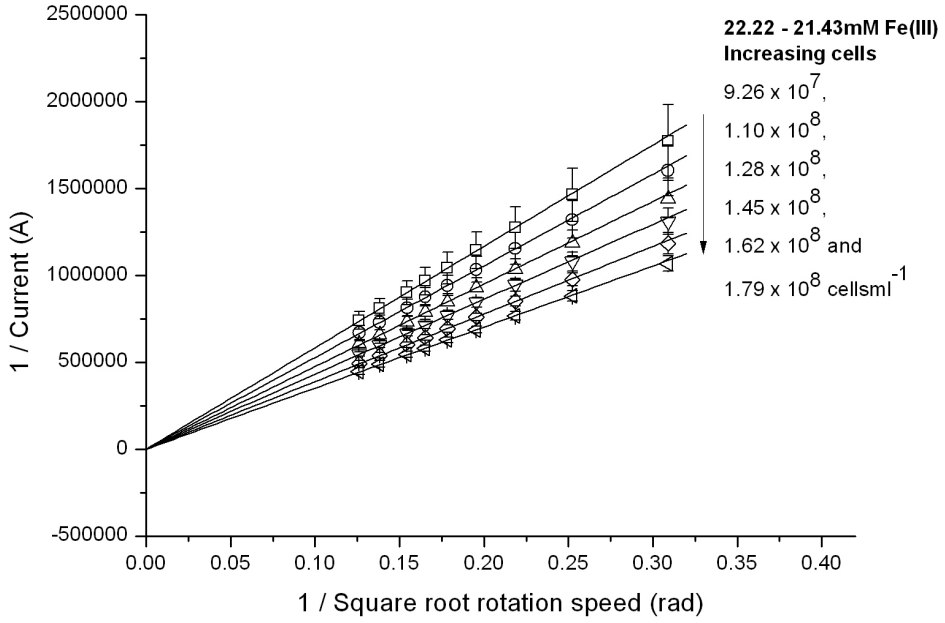


**Figure 14 of 1/Current vs. 1/square root rotation speed (rad) with 22.22 mM ferricyanide and increasing cells in solution from $9.26x10^7$ to $1.79x10^8$ cells $mL^{-1}$, at a potential 100 mV past the oxidation potential of ferrocyanide. The error bars show one standard deviation (n=3). Background controls (with no cells present) have been subtracted**

As can be seen in figures 12-14, the intercept of all linear fits on Koutecky-Levich plots was zero. An intercept of zero showed that the reduction rate of ferricyanide by the algae was mass transport controlled. This meant that the reduction rate of the ferricyanide was only controlled by how fast ferricyanide could diffuse to the algal cells, and ferrocyanide could diffuse to the electrode, meaning the kinetics of algal reduction were extremely quick.

Using the gradients of the Koutecky-Levich plots (figures 12-14), the total bulk concentration of ferrocyanide was calculated per $1x10^6$ cells $mL^{-1}$, which also correlated to the total ferricyanide reduced by the algae. This was calculated according to equation 1. Values were normalised for number of cells.

Figure 15 shows that with increasing ferricyanide concentration, total ferrocyanide in the bulk increased, whereas figure 16 shows that with a constant ferricyanide concentration, and increasing cells, ferrocyanide in the bulk only increased slightly. This makes sense, as it appeared the algal cells turned over ferricyanide at a constant

rate, with the mediator reduction rate depending on the mass transport of the ferricyanide to and from the cells. Increasing the concentration of ferricyanide increased interactions between algae and ferricyanide, therefore increasing the rate of reduction. This differed to that found in chronoamperometry (as discussed previously) and UV-Vis (chapter 3), where it was observed that increasing the concentration of *C. vulgaris* increased the rate of ferricyanide reduction. Due to the stationary conditions in UV-Vis and chronoamperometry, the difference in trends when compared to rotating disk could be explained from cells settling on the bottom of the beaker/electrode respectively. As cells settle, they could have the effect of bringing associated iron with them, so overall the iron concentration would be effectively increased.

Rates of reduction (as calculated for the background currents from chronoamperometry in section 4..32) could not be calculated from the intercepts of the Koutecky-Levich plots. This was because the intercepts of the Koutecky-Levich plots were zero (relating to the mass transport limited currents at infinite diffusion), preventing any data from being obtained about algal kinetics.

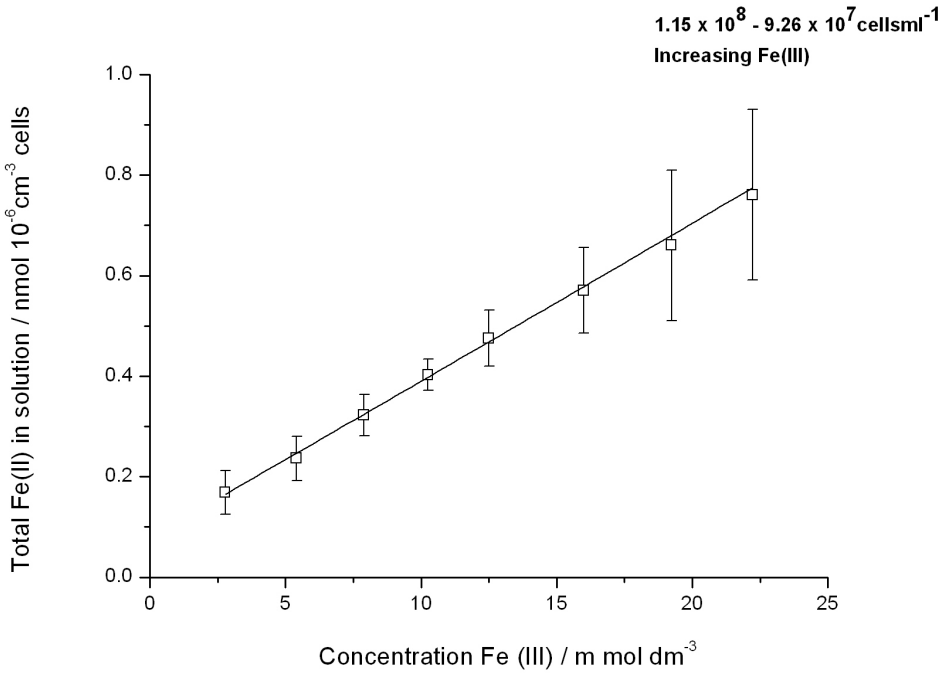


**Figure 15 Bulk concentration of ferrocyanide per 1x10$^6$cellsmL$^{-1}$, with increasing ferricyanide and 1.15x10$^8$ cells mL$^{-1}$ present. Values were calculated using slopes of Koutecky-Levich plots (with backgrounds subtracted) shown in figure 13.**

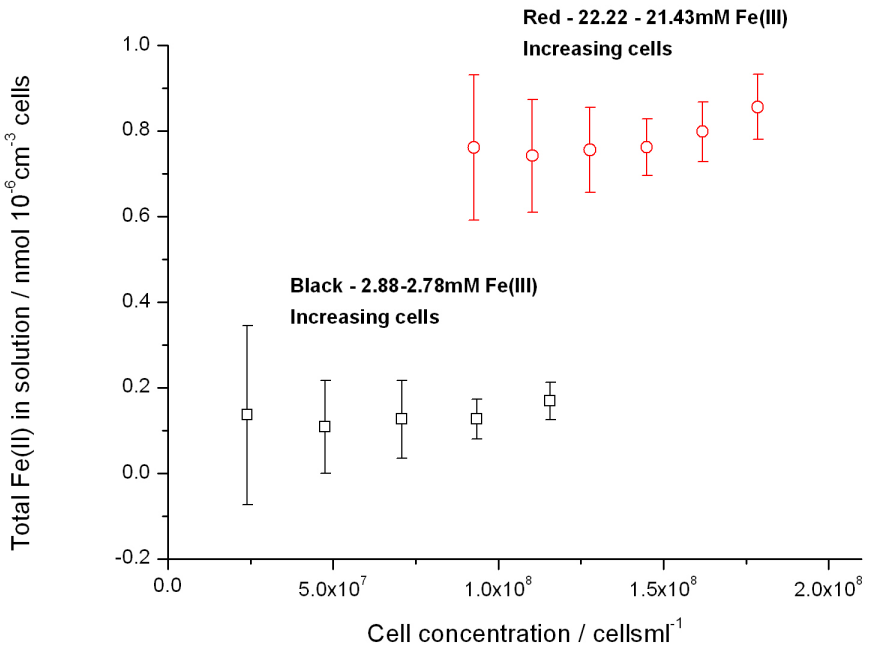


**Figure 16 Bulk concentration of ferrocyanide per 1x10$^6$ cells mL$^{-1}$ with increasing cells mL$^{-1}$ and either 2.88 mM or 22.22 mM ferricyanide present. Values were calculated using slopes of Koutecky-Levich plots (with backgrounds subtracted) shown in figure 12 and 14.**

## 5.4 Conclusions

This chapter set out to electrochemically discover more about the process by which *C. vulgaris* reduce ferricyanide, and the mechanisms behind it. With regards how they reduced ferricyanide, no redox products (or siderophore type molecules) produced by *C. vulgaris* could be identified from voltammetry other than oxygen. This suggested that *C. vulgaris* interacted with ferricyanide via ferric reductase proteins in its cell membrane, as postulated in a strategy 1 mechanism for the uptake of iron.

Chronoamperometry of solutions of algae and ferricyanide at 100 mV past the oxidation potential for ferrocyanide showed photocurrents under illumination, but they were small when compared to overall background current magnitudes, especially at the lowest cell concentration tested. It appeared small amounts of extra reducing power (NADPH) were produced within the algae under illumination, leading to slightly higher reoxidation currents of ferrocyanide to ferricyanide at the electrode. Unlike in *C. reinhardtii* where light has a dramatic increase on cell reductive power, perhaps in *C. vulgaris* only small changes are observed. However, the correlation of cell or ferricyanide concentration with photocurrents was complex.

Equilibrium (dark) currents measured at the working electrode increased with increasing amounts of ferricyanide and cell concentration, with no visible saturation of current occurring. Background dark currents increased with cell and ferricyanide concentration presumably because the NADPH from the oxidative pentose phosphate pathway powering the ferric reductase proteins was in excess to the amount of ferricyanide to be reduced. Consequently ferricyanide concentration was the limiting factor, and the linear relationship was observed. Doubling cell concentration doubled the NADPH produced in the dark, and also the reducing power of the ferric reductase. The more ferricyanide reduced by the *C. vulgaris* cells, the higher the currents seen at the electrode. Rates were calculated, and at the same conditions as those used for UV-vis spectrophotometry (1 mM ferricyanide and $7x10^7$ cells $cm^{-3}$), reduction rates were around three times lower than for UV-Vis at approximately 0.5 nmol $cm^{-2}$ Fe(III) reduced per $10^6$ cells per hour compared to 1.43 nmol Fe(III) $hr^{-1}$ $10^{-6}$ cells. This could be due to higher mass transport limitations in chronoamperometry experiments (as-well as the fact that rates in chronoamperometry were normalised for electrode area), compared to UV-Vis measurements which simply measure instantaneous bulk reduction. Additionally, UV-Vis only measured initial rates, known as an over-estimation of total rates. Table 1 summarises all the work performed to determine rates and limitations on the reduction of ferricyanide by *C. vulgaris*.

| **[Fe(III)] (mM)** | **[cellsmL$^{-1}$] (x$10^7$)** | **Rate from UV-Vis (nmol Fe(III) $hr^{-1}$ $10^{-6}$ cells)** | **Rate from Chronoamperometry (nmol Fe(III) $cm^{-2}$ $hr^{-1}$ $10^{-6}$ cells)** | **Total bulk Fe(II) from RDE (nmol Fe(II) $hr^{-1}$ $10^{-6}$ cells)** | **Mass transport or kinetic limited?** |
|---|---|---|---|---|---|
| 0.5 | 7 | 1.08 | - | - | |
| 1 | 3.5 | 0.56 | - | - | |
| 1 | 7 | 1.43 | 0.5 (increases linearly with [Fe(III)]) | - | |
| 1 | 14 | - | 1.8 (increases linearly with [Fe(III)]) | - | |
| ~3 | 2.5-11 | - | - | 0.1 | MT |
| ~22 | 9-16 | - | - | 0.75 | MT |
| 3-22 | ~10 | - | - | Increase linearly with [Fe(III)] | MT |

**Table 1 Summary table of all work performed to study rates of ferricyanide reduction by *C. vulgaris* (all in the dark)**

Studies with rotating disk electrochemistry showed the reduction rate of ferricyanide by the algae was mass transport controlled under all conditions tested. This meant that the reduction rate of the ferricyanide by the algal cells was only controlled by how fast the ferricyanide could diffuse to the cells and ferrocyanide could diffuse to react at the electrode (these rates can be assumed to be equal). This meant the kinetics of reduction at the algae were extremely fast (see figure 2 for diagrammatic representation of steps involved). With increasing ferricyanide concentration, total ferrocyanide in the bulk increased, whereas with a constant ferricyanide concentration and increasing cells, ferrocyanide in the bulk stayed relatively constant. This makes sense; it would be expected if the rate was mass transport limited that higher concentrations of ferricyanide would increase the mass transport limited rate, whilst with increased algae, although higher currents would be observed in total, per cell the same rate would be seen (assuming Fe is not deficient).

These results imply other experiments (such as the UV-Vis and chronoamperometry) could also be under mass transport limitation. However, as UV-Vis and chronoamperometry were performed with slightly different conditions (lower concentrations of ferricyanide, this cannot be confirmed. With chronoamperometry, higher reduction rates per $10^6$ cells were observed with higher cell concentrations. Although this seems in contrast to the results obtained from rotating disk electrochemistry (where total bulk ferrocyanide remained constant with increasing cells), it could be explained as during the time in which measurements took place, cells settled to the bottom of the chamber onto the electrode. This movement could also draw ferricyanide molecules to the bottom of the chamber, leading to a localised increase in concentration of ferricyanide. As this effect would be increased with higher concentrations of algae, reduction rates of Fe(III) per $10^6$ cells would be higher with higher concentrations of cells. The increase in rates of reduction observed in UV-Vis experiments with an increase in cells was harder to explain. A final important implication was that other measurements in the literature could have measured the mass transport limited rate of reduction and not rates limited by electron transfer at the algae themselves. This means that the kinetics of electron transfer at the algae need much further study.

## 5.5 References


1. Bond, D.R. and Lovley, D.R., *Evidence for involvement of an electron shuttle in electricity generation by Geothrix fermentans.* Applied and Environmental Microbiology, 2005. **71**(4): p. 2186-2189.
2. Lovley, D.R., *Bug juice: harvesting electricity with microorganisms.* Nature Reviews Microbiology, 2006. **4**(7): p. 497-508.
3. Chung, K. and Okabe, S., *Continuous power generation and microbial community structure of the anode biofilms in a three-stage microbial fuel cell system.* Applied Microbiology and Biotechnology, 2009. **83**(5): p. 965-977.
4. Zhao, F., Slade, R.C.T., and Varcoe, J.R., *Techniques for the study and development of microbial fuel cells: an electrochemical perspective.* Chemical Society Reviews, 2009. **38**(7): p. 1926-1939.
5. Marsili, E., Sun, J., and Bond, D.R., *Voltammetry and Growth Physiology of Geobacter sulfurreducens Biofilms as a Function of Growth Stage and Imposed Electrode Potential.* Electroanalysis, 2010. **22**(7-8): p. 865-874.
6. Tamura, T., Sato, A., Ajiki, S., Sugino, H., Hara, M., and Miyake, J., *A photocell based on a high concentration of chromatophore.* Bioelectrochemistry and Bioenergetics, 1991. **26**(1): p. 117-122.
7. Erabi, T., Matsumoto, K., Itoh, H., Takahashi, N., Fujimura, K., Hayase, S., and Wada, M., *Generation of cathodic photocurrent by photosynthetic reaction center complexes from Rhodospirillum rubrum at a Pt electrode.* Denki Kagaku, 1997. **65**(1): p. 26-32.
8. Martens, N. and Hall, E.A.H., *Diaminodurene as a mediator of a photocurrent using intact cells of cyanobacteria.* Photochemistry and Photobiology, 1994. **59**(1): p. 91-98.
9. Nicholson, R.S. and Shain, I., *Theory of stationary electrode polarography - Single scan and cyclic methods applied to reversible, irreversible and kinetic systems.* Analytical Chemistry, 1964. **36**(4): p. 706-&.
10. Davey, M.S., Suggett, D.J., Geider, R.J., and Taylor, A.R., *Phytoplankton plasma membrane redox activity: Effect of iron limitation and interaction with photosynthesis.* Journal of Phycology, 2003. **39**(6): p. 1132-1144.
11. Torimura, M., Miki, A., Wadano, A., Kano, K., and Ikeda, T., *Electrochemical investigation of cyanobacteria Synechococcus sp PCC7942-catalyzed*

*photoreduction of exogenous quinones and photoelectrochemical oxidation of water.* Journal of Electroanalytical Chemistry, 2001. **496**(1-2): p. 21-28.

12. Kasuno, M., Torimura, M., Tsukatani, Y., Murakami, D., Hanada, S., Matsushita, T., and Tao, H., *Characterization of the photoinduced electron transfer reaction from the photosynthetic system in Rhodobacter sphaeroides to an exogenous electron acceptor.* Journal of Electroanalytical Chemistry, 2009. **636**(1-2): p. 101-106.
13. Weger, H.G., Walker, C.N., and Fink, M.B., *Ferric and cupric reductase activities by iron-limited cells of the green alga Chlorella kessleri: quantification via oxygen electrode.* Physiologia Plantarum, 2007. **131**(2): p. 322-331.
14. Weger, H.G. and Espie, G.S., *Ferric reduction by iron-limited Chlamydomonas cells interacts with both photosynthesis and respiration.* Planta, 2000. **210**(5): p. 775-781.
15. Lynnes, J.A., Derzaph, T.L.M., and Weger, H.G., *Iron limitation results in induction of ferricyanide reductase and ferric chelate reductase activities in Chlamydomonas reinhardtii.* Planta, 1998. **204**(3): p. 360-365.
16. Weger, H.G., *Ferric and cupric reductase activities in the green alga Chlamydomonas reinhardtii: experiments using iron-limited chemostats.* Planta, 1999. **207**(3): p. 377-384.
17. Xue, X.P., Collins, C.M., and Weger, H.G., *The energetics of extracellular Fe(III) reduction by iron-limited Chlamydomonas reinhardtii (Chlorophyta).* Journal of Phycology, 1998. **34**(6): p. 939-944.
18. Middlemiss, J.K., Anderson, A.M., Stratilo, C.W., and Weger, H.G., *Oxygen consumption associated with ferric reductase activity and iron uptake by iron-limited cells of Chlorella kessleri (Chlorophyceae).* Journal of Phycology, 2001. **37**(3): p. 393-399.

# Chapter 6. Comparisons of Algal Interaction with Potassium ferricyanide with a Cyanobacterial Species

# Chapter 6 – Comparisons with *Synechocystis*

## 6.1 Introduction

The selection of the photosynthetic species is an important factor for optimising efficiencies in a p-MFC [1]; those that have higher rates of reduction of a mediator and are less susceptible to mediator toxicity would potentially give the most efficient and self-sustainable p-MFC device. Many types of photosynthetic species have been utilised in the literature, with more p-MFCs using cyanobacteria than algae. The previous chapters go some way towards improving the understanding of the basic p-MFC device. In this chapter, many of the same techniques are used to investigate the interaction of the cyanobacterium *Synechocystis PCC 6803* with potassium ferricyanide (ferricyanide), and draw comparisons of behaviour against the alga *Chlorella vulgaris*. This is with the aim to improve p-MFC efficiency.

### 6.11 Use of cyanobacteria in p-MFCs

The most basic p-MFC in the literature used cyanobacteria cells in solution with a mediator in the anodic chamber. *Synechocystis* [2, 3] and *Synechococcus* [4] have been used with 2-Hydroxy-1,4-napthoquinone (HNQ), with photocurrents of 1mA and a maximum power density of 50 mW $m^{-2}$ produced [4]. Other studies used *Phylum Cyanophyta* and methylene blue [5]. In this study, power densities were low under a 10 Ω load, approximately 0.0004 mW $m^{-2}$ (~0.04 nW $cm^{-2}$) in both light and dark, and an open circuit voltage of 300-500 mV was measured. Both mediators were understood to diffuse into cells, siphon electrons and diffuse out the cells again [5]. For HNQ, the main coupling sites with the electron transport chain were thought to be ferredoxin-$NADP^+$ reductase in the light and NAD(P)H dehydrogenase in the dark [6]. However, neither study gave further specifics such as how the mediator actually crossed the cell outer membrane.

Cells and mediator have also been immobilised directly onto an electrode. *Synechococcus*-carbon paste electrodes containing the mediator diaminodurene in the electrode material, and *Synechococcus* cells in a polymer matrix have been constructed [7]. Other *Synechococcus* carbon paste electrodes contained the mediator 2,6-dimethyl-1,4-benzoquinone [8]. In the former study the mediator was

hypothesised to cross the cell membrane and accept electrons from the reduction site at PSII, and also through interaction with PSI [7]. Additionally, electron transfer from cyanobacteria to electrodes coated in conducting polymers such as polyaniline and polypyrrole has been reported (within the electrodes electron transfer through polaron hopping is important) [23, 24]. It is not clear if direct electron transfer to the polymer is occurring, or whether the polymer acts as a catalyst to oxidise redox products produced by the micro-organisms. In p-MFCs containing polyaniline anodes coated with *Synechococcus* biofilms [9], electrons were thought to be extracted from bacterial cells through the polyaniline surface, although no further details were given as to how the process takes place and how electrons crossed outer membranes.

Others suggested cells could undergo electrogenic activity, whereby cells release electrons directly to the anode without utilising electron mediators[10]. This was observed for a diverse genera of cyanobacteria including *Calothrix, Pseudoanabaena, Synechococcus, Anabaena, Phormidium, Nostoc, Lyngbya, Spirulina, Synechocystis and Leptolyngba* [10]. Due to inhibitor studies, and the fact that electrogenic activity was observed only with blue or red light, it was assumed that the electrons responsible for electricogenic activity originated from the photosynthetic electron transport chain. Plastoquinone, present in large amounts in thylakoid and cellular membranes, was thought crucial for electron transport between the electron transport chain and extracellular environment. It was additionally demonstrated that despite mucilaginous sheaths, direct contact was the primary method for electron transfer [10] possibly via conductive nanowires [11]. However, at the time of this thesis, to the author's knowledge few other studies corroborate this finding.

In summary, although one study suggested direct electron transfer was possible from cyanobacteria to an electrode, most p-MFC devices use an artificial redox mediator for this electron transfer step. Often the method of electron transfer has not been well elucidated in the studies, with no clear understanding of cell/mediator interactions. This chapter focuses on the comparison of *Synechocystis* to the algal species *C. vulgaris* in relation to their interaction with ferricyanide. Similar to *C. vulgaris*, studies of the interactions of *Synechocystis* with ferricyanide are based on iron uptake strategies (reviewed below).

**6.12 Cyanobacteria interactions with iron**

When under iron-stressed conditions ($5x10^{-9}$ M $FeCl_3$ [12]), most algae are thought to increase the concentration of ferric reductase proteins expressed on their cell membranes to reduce Fe(III) chelates for uptake. In contrast, iron acquisition by iron limited cyanobacteria has been typically considered to be mediated by siderophores [13-16]. Siderophores are low molecular weight organic compounds which have high binding affinities for ferric iron, and are in some cases thought to facilitate a photochemical reduction of the bound ferric ion [17]. Subsequently, the organism imports the entire iron-siderophore complex into cells through ferrisiderophore-specific proteins, before the iron is released. [13, 15, 16].

Siderophore production has been shown in several cyanobacterial species [14] with transport mechanisms studied in detail for *Anabaena sp.* strain PCC 7120. This strain secreted the siderophore schizokinen and internalised FeSchizokinen via SchT, a tonB dependent transporter in the outer membrane. Transport of the ferrisiderophore complex through the plasma membrane was thought to occur via an unidentified ABC transporter. Other types of siderophores produced by other species included hydroxamate, catecholate, citrate-based siderophores and ferrioxamines [14] One type isolated in an axenic culture of the marine cyanobacterium *Synechococcus* PCC 7002 was a hydroxamic acid-type siderophore [18]. Other molecules have been isolated, but not termed siderophores due to the fact that they were produced in response to iron addition. Siderophores have been detected using a modified CAS assay [19], thin layer chromatography (TLC)[13] and genome studies [14]. Siderophore-iron complexes are also known to be redox active with a highly negative redox potential (<-300 mV) [16]. Thus they should also be detectable via electrochemical methods.

Despite the fact that most literature reviews cite siderophore production as the main way cyanobacteria uptake iron [13, 15], many cyanobacterial species do not produce siderophores. For example, in contrast to early reports by Wilhelm *et al.,*[13, 15], genes for the biosynthesis of siderophores were not found in many *Synechocystis* and *Synechococcus* species [14, 20]. This meant alternative cyanobacterial iron acquisition mechanisms must exist. Initial reports suggested that in iron sufficient ($4x10^{-5}$ M $FeCl_3$ [12]) environments iron uptake was driven primarily by diffusion. In this process, Fe(III) is hypothesised to diffuse along a gradient into the cells via porin

channels in the outer membrane [13]. More recently there have been numerous suggestions for extracellular reduction of Fe(III) species before transport in various cyanobacteria [14, 21], similar to that reported for non-photosynthetic prokaryotes [22, 23] and eukaryotic algae and plants [24, 25]

*Synechocystis* sp PCC 6803, a typical cyanobacterial species where little evidence existed for siderophore production and ferrisiderophore transport, has been focussed on in many literature studies to elucidate alternative mechanisms of iron transport. In a study by Kranzler *et al.* [26], it was found that the species was capable of acquiring iron from exogeneous ferrisiderophores, and unchelated, inorganic Fe was a highly available source of iron. It was also indicated, through inhibition of iron uptake by the Fe(II) specific ligand ferrozine, that reduction of both inorganic iron and ferrisiderophore complexes occurred before transport through the plasma membrane. It was thought iron reduction either occurred outside of the cell on the surface of the outer membrane or in the periplasmic space [26]. This reduction before transport through the plasma membrane would eliminate the need for ferrisiderophore transporters. For internalisation of Fe, only free ion transporters in the plasma membrane would be needed. Following reduction, iron would then be transported as Fe(II), or in some cases reoxidised to Fe(III) and transported. These strategies are consistent with the two transport systems identified in the plasma membrane of *Synechocystis* 6803; FutABC and FeoB, suggested to transport Fe(II) and Fe(III) respectively [27-29]. This strategy has many parallels to the strategy 1 reductive method for iron uptake as thought to occur in *C. vulgaris.*

Few studies in the literature have focused on the effect of light on iron uptake. One study on *Synechococcus* PCC 7002 suggested that light enhanced iron uptake for both iron replete and iron deficient cyanobacteria [13]. It was simply suggested that the increase in iron uptake for iron replete cells resulted from increased solubility of extracellular iron, and in iron deficient cells resulted from an ‘active high affinity transport system’ [13]. A more recent study by Fujii *et al.,* [30], corroborated the first finding, as they observed visible light induced the reductive dissociation of organically complexed Fe. However, it is evident that iron uptake by cyanobacteria is much less characterised than for an algal species such as *C. vulgaris*. Additionally,

cellular effects resulting from iron uptake are much less characterised, with no literature found specifically addressing this.

### 6.13 Chapter Aims

Optimisation of the photosynthetic species used in a p-MFC is important for maximising output efficiencies. As such, this chapter investigates differences between algal and cyanobacterial reduction of ferricyanide, the redox mediator used in the basic p-MFC system this thesis is based on. *Synechocystis* was chosen as the cyanobacteria studied, as it (similar to *C. vulgaris*) represents a well studied example of its phylum.

Main experiments from chapters 4 and 5 are repeated and compared with *Synechocystis*. The rate of reduction of ferricyanide by *Synechocystis* in light and dark is measured directly by UV-Vis spectrophotometry, with control experiments undertaken to investigate any interaction with ferrocyanide. Similar to *C. vulgaris, Synechocystis* is grown in iron-sufficient conditions, both to make it comparable and as this was thought to represent the long-term sustainable conditions it would experience if grown inside a p-MFC. Although fluorescence of *Synechocystis* can not be studied, due to lack of *Synechocystis* auto-fluorescence when excited by 480 nm light, other cellular effects resulting from ferricyanide interaction are investigated. Ferricyanide toxicity is determined, as it is an important factor for consideration when choosing the species for a p-MFC.

In this chapter, rates and mechanism of interactions between *Synechocystis* and ferricyanide are also further studied electrochemically and compared to the findings with *C. vulgaris*. Voltammetry is used to search for redox (or siderophore) products that could be detected. Rates of reduction of ferricyanide are studied using chronoamperometry and rate limiting factors (mass transport or kinetics) of the reduction are determined by rotating disk electrochemistry using the Koutecky-Levich equation. Possible rate limiting steps are shown in figure 1, and include mass transport or kinetics. As with *C. vulgaris* (chapter 5), the possible rate limiting steps involve the rate of electron transfer at the cyanobacteria ($k_{et}$), or the diffusion (mass transport) of ferricyanide to the cyanobacterial cells, and ferrocyanide to the electrode. Determining the rate limiting step is important as if mass transport is found to be rate

limiting, measureable rates of reduction simply equate to the mass transport limited rate.

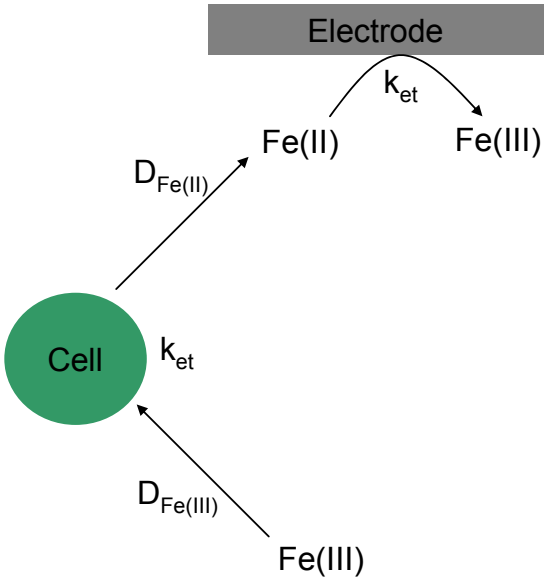


**Figure 1 The possible rate limiting steps involved in current generation from the reduction of ferricyanide by cyanobacterial cells. Assumptions involved; Fe diffuses faster than cyanobacterial cells, which are subsequently stationary relative to the Fe; The diffusion of ferricyanide to the algal cells and diffusion of ferrocyanide to the electrode ($D_{Fe(III)}$ and $D_{Fe(II)}$ respectively) are equal; and $k_{et}$ at electrode is extremely fast compared to $k_{et}$ at cell**

## 6.2 Experimental

### 6.21 Proof of principle UV-Vis with potassium ferricyanide

UV-Vis experiments allowed bulk quantification of the reduction of ferricyanide when mixed with the cyanobacterium *Synechocystis*. A bulk solution of 1 mM ferricyanide in 10 mL *Synechocystis* (at a concentration of $7x10^7$ cells $mL^1$ in fresh BG11 media) was made up. 1ml aliquots of the solution were taken every hour, centrifuged for 3 minutes at $13.2x10^3$ rpm, and supernatant removed. Absorbance of the supernatant at 420 nm was then measured in a spectrometer (type Helios gamma from Thermo electron corporation), which allowed the concentration of ferricyanide to be calculated from calibration curves. This procedure was performed on equivalent samples of cyanobacteria in light (light at 620 nm from an optical fibre at intensity $1.25x10^{-3}$ W $cm^{-2}$) and dark, with BG11 media and 1 mM ferrocyanide controls performed.

### 6.22 Long term toxicity testing of potassium ferricyanide to *Synechocystis*

*Synechocystis* was cultured with ferricyanide (procedure as outlined in appendix) to identify any long term toxicity this chemical species represented. Three identical culture flasks were inoculated with 0.001 mM, 0.01 mM or 0.1 mM ferricyanide. Cell counts were performed every two or three days using a haemocytometer, and a control containing 0 mM ferricyanide was monitored for comparison.

### 6.23 Voltammetry – cyclic and square wave of *Synechocystis*

Voltammetry was used to determine if redox products were produced by *Synechocystis*. A standard three electrode set up was assembled in a 10ml solution of *Synechocystis* culture, using a Pt counter, Ag/AgCl reference, and either an Au (0.03 $cm^2$), boron doped diamond (BDD) (0.07 $cm^2$) or Pt working electrode (area 0.015 $cm^2$). Cyclic voltammetry from -0.7 to 0.7 V was ran at different scan rates and different time periods on samples taken from a developing culture, with square wave additionally performed from -0.7 to 0.7 V. A nitrogen purge was applied for use with the Pt WE due to its reactivity with oxygen. Biofilms were additionally grown on FTO glass working electrodes (area 1 $cm^2$), and tested with cyclic voltammetry from -0.7 to 0.7 V.

### 6.24 Chronoamperometry of *Synechocystis* and potassium ferricyanide

To study more quantitatively the reduction of ferricyanide by *Synechocystis*, and determine reduction rates, chronoamperometry at 100 mV past the oxidation potential for ferrocyanide (as determined by cyclic voltammetry) was performed in solutions of cyanobacteria and ferricyanide. A range of concentrations of cyanobacteria and ferricyanide were tested; cyanobacterial concentrations between $5x10^7$ cells $mL^{-1}$ and $4x10^8$ cells $mL^{-1}$ were chosen along with ferricyanide at a concentration between 0 and 7 mM ferricyanide. Additionally the effect of culture age was studied, with both a 14 and 45 day old cell culture tested.

Chronoamperometry took place in a specially designed chamber utilising a fluorine doped tin oxide (FTO) working electrode (area 1.33 $cm^2$), which allowed light to easily reach the cells, as shown in figure 2a. Once the experiment was running, the sample was illuminated periodically using an optical fibre at 620 nm at $5x10^{-3}$ W $cm^{-2}$. Background BG11 media controls were performed, and it could be assumed that once

subtracted, any currents were due to the reoxidation of ferrocyanide to ferricyanide at the electrode, which in turn directly corresponded to the reduction of ferricyanide by *Synechocystis* cells in the first place. Three repeats were taken, approximately 20 minutes apart, to ensure the system was at equilibrium, and the ferricyanide was not damaging the cells in any way.

**6.25 Rotating Disk Electrochemistry – Limiting factors on current**

Rotating disk electrochemistry was additionally employed to further study reduction rates, and determine if the rate was determined by electron kinetics or mass transport. This took place again at 100 mV past the oxidation potential for ferrocyanide, using a Pt working electrode of area 0.07 $cm^2$ (schematic given in chapter 5, figure 3). Experiments involved keeping the ferricyanide concentration constant at 2.78 mM, before increasing the cell concentration (taking dilutions into account) from $2.40x10^7$ to $1.15x10^8$ cells $mL^{-1}$. Second, the cell concentration was held constant, and ferricyanide concentration increased. Taking into account dilutions, this was from between 2.78 mM to 22.22 mM. Finally, the ferricyanide concentration was held constant at 22.22mM, and cells again increased from $9.26x10^7$ to $1.79x10^8$ cells $mL^{-1}$. At each set of values, the rotation speed of the working electrode was increased from 100 rpm to 600 rpm, and currents allowed to stabilise briefly before the spin speed was again increased. Controls with 0 mM ferricyanide or 0 cells $mL^{-1}$ were performed, and three repeats performed for each experiment. After media control average current values were subtracted from averages of the repeats, plots were produced of 1/current VS 1/ spin speed (rad). Using the Koutecky-Levich equation, gradients were used to calculate the total ferrocyanide in solution (equation given in chapter 5), per $1x10^6$ cells $mL^{-1}$, and intercepts used to calculate reduction rates per hour (normalised for electrode area and cell numbers). Ferrocyanide diffusion coefficients with varying concentrations of *C. vulgaris* cells (experimental outlined in chapter 5) were used in the calculations.

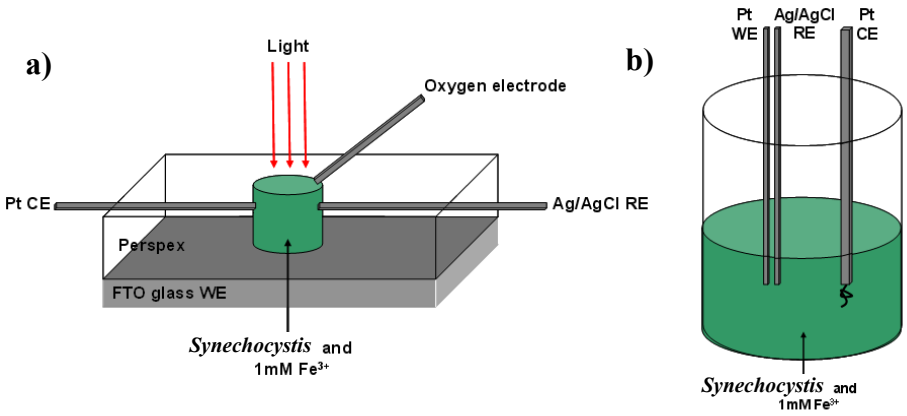


**Figure 2 Schematics of the set-ups used for a) Chronoamperometry and b) rotating disk measurements**

## 6.3 Results and discussion

### 6.31 Proof of principle UV-Vis with potassium ferricyanide

UV-Vis spectrophotometry was used as a simple method for investigating the reduction of ferricyanide in the presence of *Synechocystis*. A given concentration of 1mM ferricyanide and cyanobacteria suspended in 10 mL media was left either in the dark or illuminated, with UV-Vis performed every hour on the supernatant to measure total ferricyanide concentration. An identical experiment was carried out in the absence of any redox acceptor (media control) and with ferrocyanide to ensure that *Synechocystis* had no oxidative capacities.

Typical UV-Vis curves are shown in figure 3. As in solutions of *C. vulgaris* and ferricyanide, the concentration of ferricyanide depleted over time, as shown by the decreasing absorbance at 420 nm. *Synechocystis* represents a species of cyanobacteria thought to have similar iron uptake abilities to the algal species *C. vulgaris*, where machinery in cell membranes and/or periplasmic space reduce ferricyanide to ferrocyanide before uptake commences [26]. Very little is known about the reduction process (for example, the type or location of proteins involved), as until recently most cyanobacteria were thought to use a method of iron uptake involving the release of siderophores. Little evidence for siderophores exists in *Synechocystis,* but if they were present, they would be unlikely to be detectable by UV-Vis; siderophores could also cause the measureable depletion of ferricyanide in solution. However, due to the overwhelming lack of evidence for siderophore production by *Synechocystis,*

reductive abilities were assumed. A calibration curve was constructed by measuring absorption of known concentrations of ferricyanide in BG11 media at 420 nm (figure 4). Absorption could then be translated into concentrations of ferricyanide, using the Beer-Lambert law.

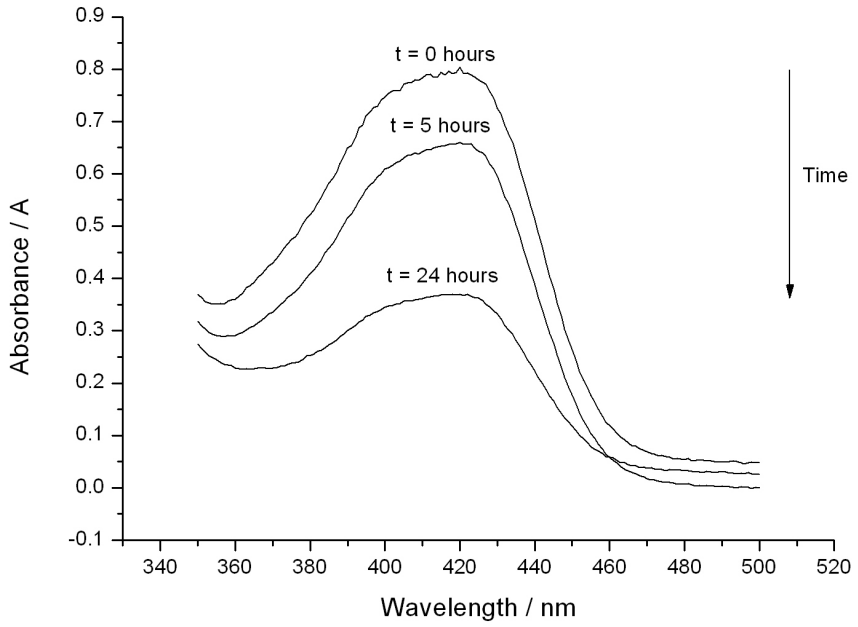


**Figure 3 Typical UV-Vis curves for a solution of *Synechocystis* and ferricyanide, at selected time points after mixing**

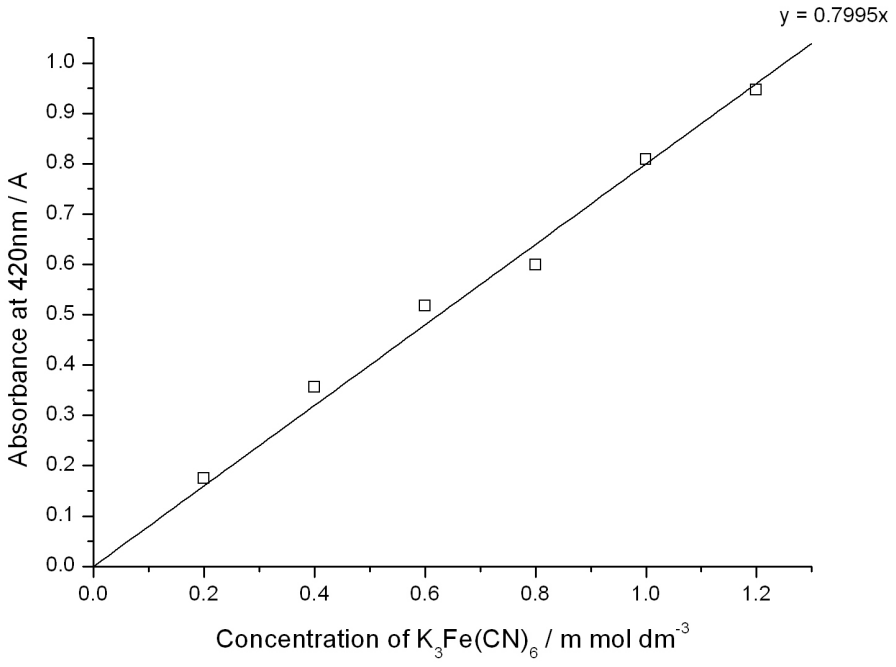


**Figure 4 Calibration curve of ferricyanide in BG11 media**

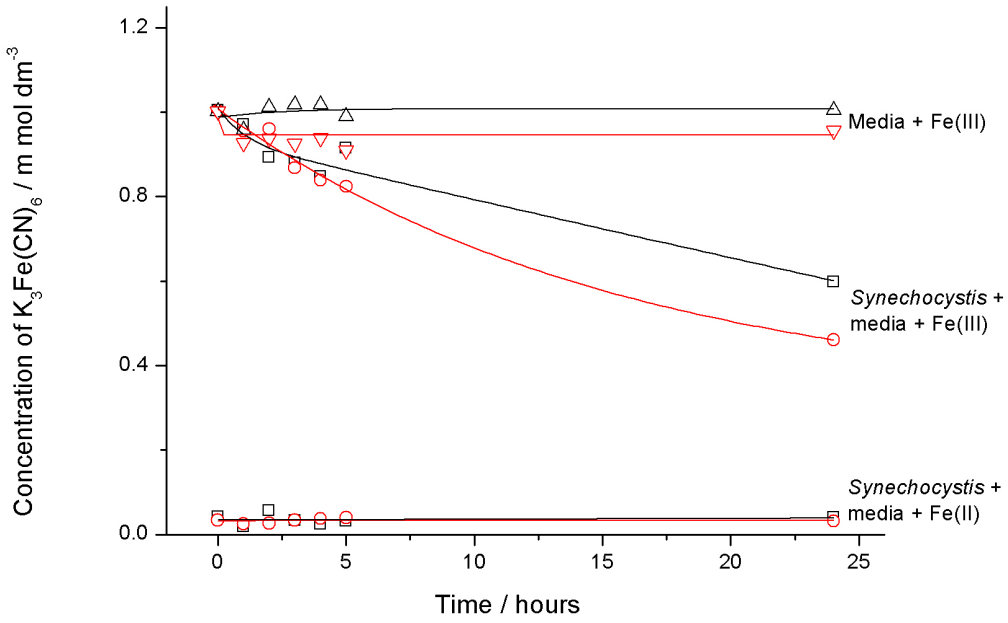


**Figure 5 Change in the concentration of ferricyanide and ferrocyanide in media and in the presence of 7.69 x $10^7$ algal cells $ml^{-1}$. Measurements were taken under illumination (red points) and in the dark (black points).**

Figure 5 shows the reduction of ferricyanide in the presence of 7 x $10^7$ cyanobacterial cells $mL^{-1}$ over time. In contrast to *C. vulgaris*, where illumination was not observed to affect reduction rates (thought possibly due to low sensitivity of the technique), a final difference in concentration of ~0.15 mM could be seen between light and dark repeats. This corroborated other studies whereby in light both respiratory and photosynthetically derived reductants acted as electron donors for the reduction process, increasing reduction rates compared to dark [31]. Although the difference between light and dark reduction was relatively small, studies showing large differences in rates were performed on iron deficient cells [24, 32], whereas cells in this study were cultured in an iron sufficient environment (2.15 x $10^{-4}$ mol $dm^{-3}$ $FeCl_3$). However, more repeats were needed to confirm this difference was not due to experimental error. As with *C. vulgaris*, oxidation of ferrocyanide by *Synechocystis* was not seen to occur.

By fitting the initial dark reduction rates (which were linear; first five points taken), reduction rates of ferricyanide in the presence of *Synechocystis* in the light and dark

were calculated. Table 1 shows values of the half-life of ferricyanide and the initial rate of ferricyanide reduction in the light and dark

| Concentration Synechocystis / cells $dm^{-3}$ | Concentration Ferricyanide / mmol $dm^{-3}$ | Half-life / h | Initial rate / µmol Fe(III) $dm^{-3}$ $h^{-1}$ | Initial rate/ nmol Fe(III) $10^{-6}$ cells $h^{-1}$ |
|---|---|---|---|---|
| $7x10^{10}$ LIGHT | 1 | 12.13 | 42 | 0.42 |
| $7x10^{10}$ DARK | 1 | 12.29 | 41 | 0.41 |

**Table 1 Values of the half-life of ferricyanide and the initial rate of ferricyanide reduction in the dark and dark**

It was established that with a *Synechocystis* concentration of $7x10^{10}$ cells $dm^{-3}$ (extrapolated from 10 mL), and an initial ferricyanide concentration of 1 mM, the initial reduction rate was 0.41 nmol Fe(III) $10^{-6}$ cells $h^{-1}$ in dark and 0.42 nmol Fe(III) $10^{-6}$ cells $h^{-1}$ in light. This makes it almost certain that the difference in reduction of ferricyanide observed after 24 hours was due to error.

When compared to the reduction rates obtained using similar conditions with *C. vulgaris,* 1.43 nmol Fe(III) $10^{-6}$ cells $h^{-1}$ with 7.69 $x10^{10}$ cells $dm^{-3}$ and 1 mM ferricyanide (in dark), the initial reduction rate with *Synechocystis* was approximately 3.5 times lower per $10^{-6}$ cells. These results could infer that *C. vulgaris* was more efficient at reducing ferricyanide. However, comparisons per cell are not ideal, as *Synechocystis* cells are known to be much smaller in size than *C. vulgaris.* When the chlorophyll content of 7 x $10^7$ cells *C. vulgaris* or *Synechocystis* was compared (procedure outlined in the appendix), *C. vulgaris* had 0.03 µg Chl, compared to *Synechocystis* with 0.0068 µg Chl (a difference of 4.4). The difference in reduction rates may therefore have been due to the difference in cell reduction capacity (as measured by chlorophyll content).

### 6.32 Toxicity tests

It was important to quantify any toxicity the ferricyanide represented to *Synechocystis* and compare it to that found in *C. vulgaris*. Finding a photosynthetic species more tolerant to the presence of ferricyanide is an important consideration for p-MFC species selection. Figure 6 shows cell counts over time of cultures containing varying

amounts of ferricyanide. Although cell counts did not distinguish between alive and dead cells, any growth inhibition effects could be seen, attributable to toxicity.

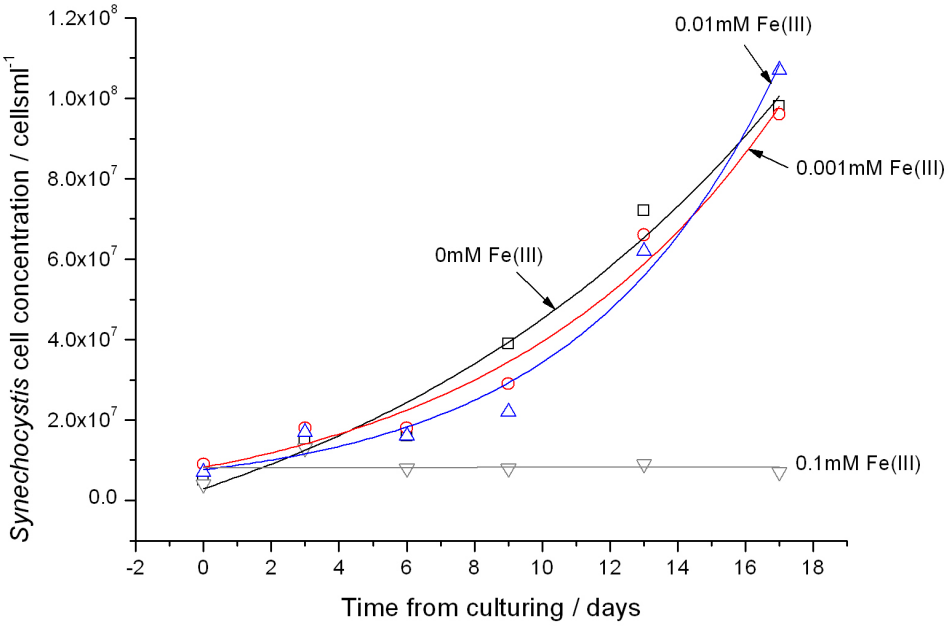


**Figure 6 Toxicity testing of *Synechocystis* and ferricyanide**

The toxicity of ferricyanide to *Synechocystis* (as shown in figure 6) was different to that determined for *C. vulgaris*. It appeared *Synechocystis* was more tolerant to the presence of ferricyanide, as shown by the fact that concentrations of 0.001 mM and 0.01 mM ferricyanide seemed to exhibit no major effects on growth. This would be an advantage if *Synechocystis* was employed in the basic p-MFC device. Only at 0.1mM ferricyanide was the growth of cells prevented. In comparison, with *C. vulgaris,* even 0.001 mM seemed to partially inhibit growth. As with *C. vulgaris,* growth inhibition could be due to over stress of cells resulting from reduction activity. It was interesting to note that both *C. vulgaris* and *Synechocystis* grew at approximately equal rates, with approximately $7x10^7$ cells present in the control after 13 days.

### 6.33 Voltammetry – cyclic and square wave of *Synechocystis*

Cyclic voltammetry was performed on a cyanobacterial culture to determine if any redox species were being produced in solution. Figures 7 and 8 show cyclic voltammetry on a Au electrode (area $0.03cm^2$), w.r.t Ag/AgCl.

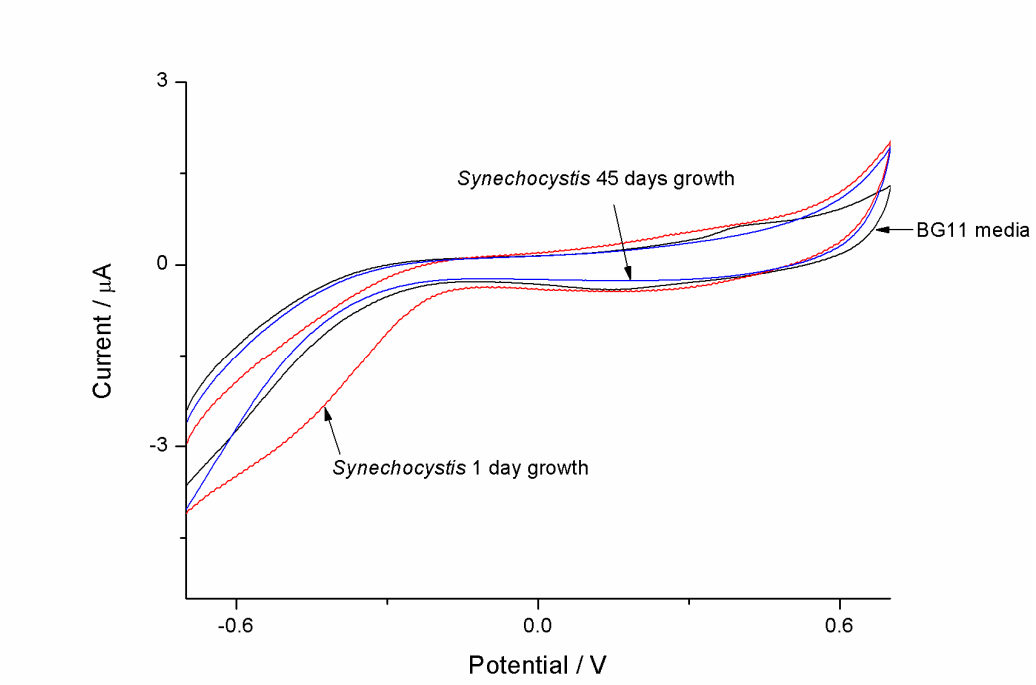


**Figure 7 Cyclic voltammetry at 100 mV $s^{-1}$ of *Synechocystis* media, one day *Synechocystis* culture, and fully established 45 day old *Synechocystis* culture on Au disk electrode (area 0.03 $cm^2$) w.r.t Ag/AgCl**

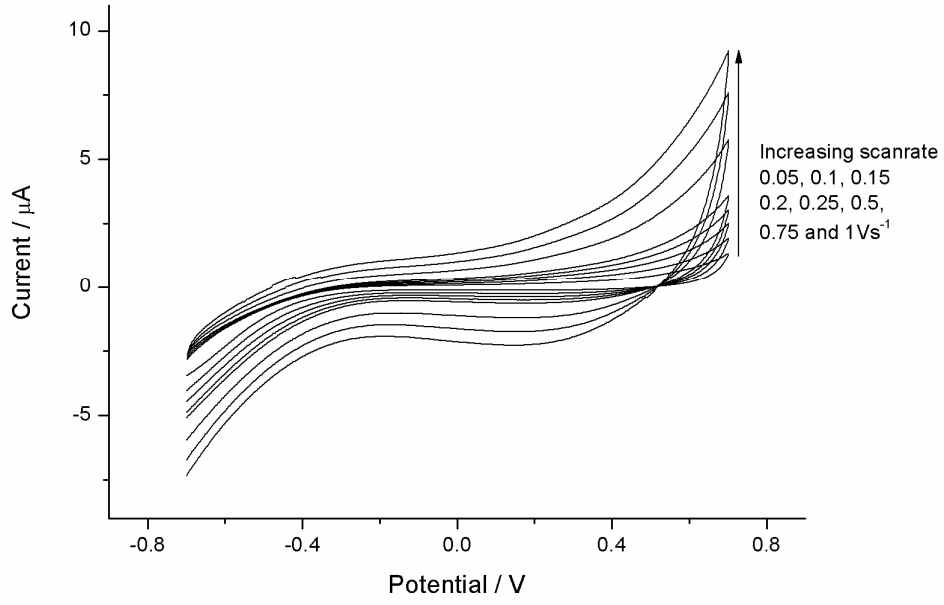


**Figure 8 Cyclic voltammetry of 45 day old *Synechocystis* culture at a range of scanrates, on Au disk electrode (area 0.03 $cm^2$) w.r.t Ag/AgCl**

Figures 7 and 8 show that no redox species (other than oxygen) were detected using an Au electrode, irrespective of culture age or scan rate used. This pattern was the

same using other electrodes, including boron doped diamond and platinum. Aliquots of supernatant were sequentially added to KCl. A nitrogen purge was applied, and electrodes were cleaned in between measurements. However, no redox species were detected using either cyclic or square wave voltammetry (data not shown), other than oxygen (despite the nitrogen purge). This means that no redox products or redox active-siderophore type molecules seem to have been produced by Synechocystis, as was also found with C. vulgaris. If presumed that siderophores would be redox active, this corroborated previous literature which suggests that this cyanobacterial species, similar to C. vulgaris, uses a strategy 1 mechanism for the uptake of Fe(III), whereby reductive machinery (possibly on membranes or in the cytosol) reduce Fe(III) to Fe(II). Cyclic voltammetry was not performed on biofilms as Synechocystis cells would not attach and grow on any substrates used (FTO glass and ITO plastic). This is a serious drawback for the long-term use of Synechocystis in the basic p-MFC device.

### 6.34 Chronoamperometry of *Synechocystis* and potassium ferricyanide

The rate of ferricyanide reduction was measured in a three electrode electrochemical cell with a FTO working electrode (area 1.33 $cm^2$). The electrode was polarised to 100 mV positive of the oxidation potential for ferrocyanide, and the current was measured under illumination and in the dark for a range of cyanobacterial and ferricyanide concentrations. The effect of culture age on reduction was also investigated.

Cyclic voltammograms used to obtain the potential values, with increasing ferricyanide, are shown in figure 9. From figure 9, 0.4 V w.r.t Ag/AgCl was chosen for chronoamperometry measurements to ensure that any ferrocyanide reaching the electrode would be immediately oxidised back to ferricyanide. This form was in the correct oxidation state to accept electrons from *Synechocystis*, allowing quantification of the reduction reaction. It was assumed that if the electrodes were reducing any ferrocyanide to ferricyanide; as only ferricyanide was present initially, after background subtraction, the oxidation currents at the electrode would be approximately equal to the reduction currents by the cyanobacteria. In contrast to UV-Vis measurements, these experiments were able to discriminate between different mechanisms of ferricyanide uptake. Although unlikely as undetected in voltammetry,

if siderophore complexes were produced and utilised, no reoxidation currents of ferrocyanide to ferricyanide would be observed. Instead, currents would drop as when complexed, the effective concentration of ferricyanide in solution would drop.

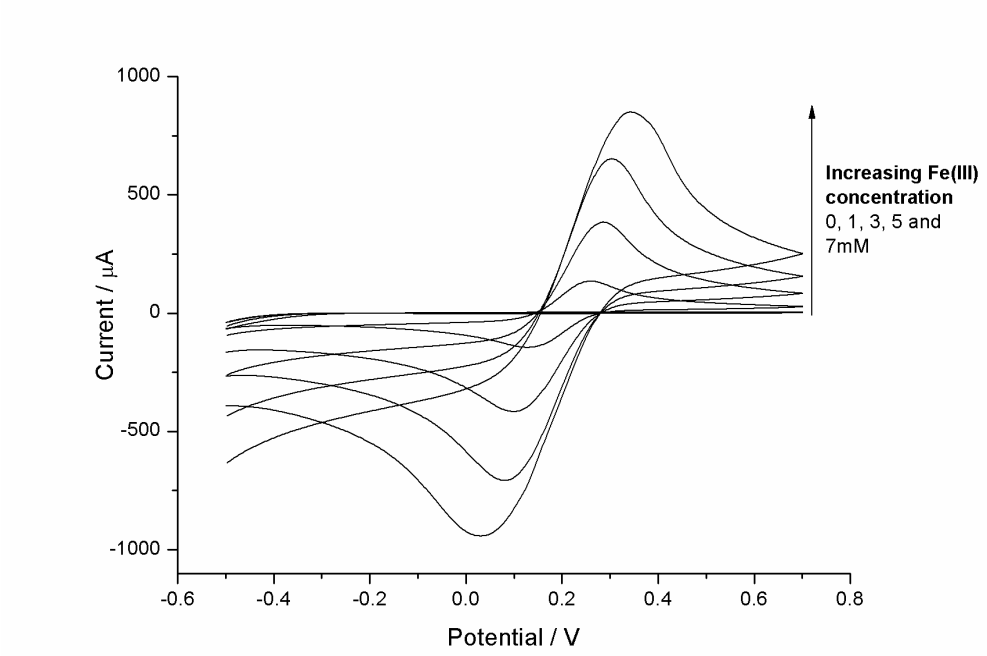


**Figure 9 Typical Cyclic voltammetry at 100 mV $s^{-1}$ obtained from a solution of *Synechocystis* and increasing ferricyanide concentration, on FTO glass electrode (area 1.33$cm^2$) w.r.t Ag/AgCl**

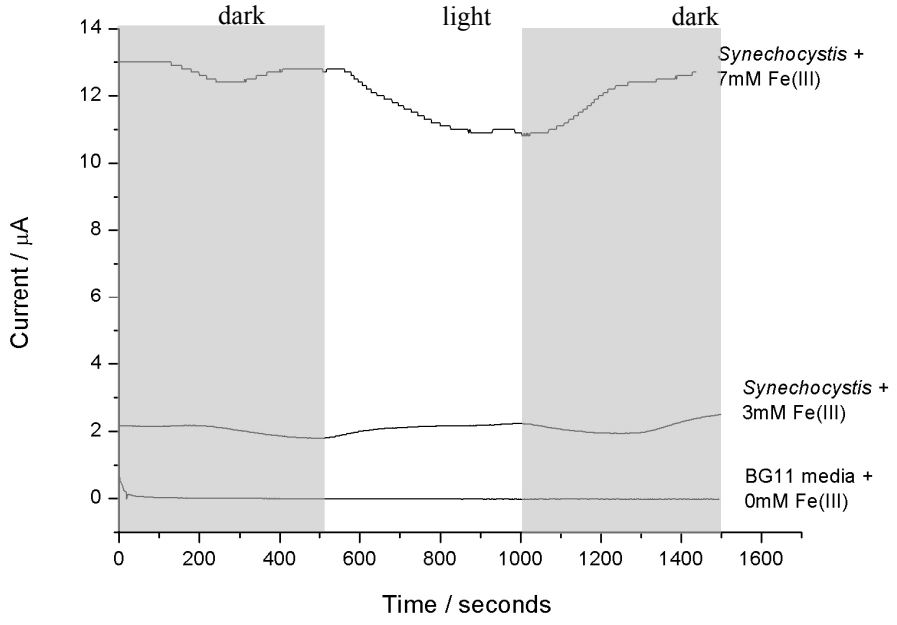


**Figure 10 Typical background and light currents measured during chronoamperometry at 100mV past the oxidation potential for ferrocyanide, at a FTO working electrode (area 1.33 $cm^2$). Shown on the diagram are photocurrents measured with *Synechocystis* and 3 mM or 7 mM ferricyanide. A media control is also shown with 0mM ferricyanide**

Typical chronoamperometry results are shown in figure 10. As with *C. vulgaris,* currents with cyanobacteria and mediator in solution were far higher than those with no mediator and cyanobacteria present. With cyanobacteria, when illuminated, various patterns were seen, as illustrated in the figure with two concentrations of mediator. With 3 mM ferricyanide, when illuminated a small rise in current was observed, with the current dropping back to the previous background value in the dark. In contrast, the opposite photocurrent (negative) was also observed (for example, with 7 mM ferricyanide shown in figure 10). In this case, when illuminated, the current decreased to a relatively stable value before increasing to previous levels in dark. The negative photocurrent inferred that illumination caused a decrease in the reduction of ferricyanide (or even an oxidation of ferrocyanide), although UV-Vis results do not corroborate this. The reason for these pattern discrepancies is unknown. In any case, both patterns contrasted to the positive, double peaked photocurrent patterns seen with *C. vulgaris*, shown in chapter 5.

Photocurrent summaries with increasing ferricyanide or cells are shown in figures 11 and 12. With increasing ferricyanide (figure 11), photocurrents gradually became more positive with both cell culture ages, before becoming large and negative at the highest ferricyanide concentration tested. No negative photocurrents were seen with *C. vulgaris*. The reason for this negative photocurrent was not known, but must have represented a decrease in the total ferrocyanide being oxidised at the electrode. Although this could have represented the result of a complexing agent (such as a siderophore) produced only in light which decreased the total bulk concentration of ferrocyanide, due to fact that siderophores are produced equally in dark and light conditions, and the lack of evidence for any production of siderophores by *Synechocystis* cells, this was unlikely.

With increasing cell concentration (figure 12), different patterns of photocurrents were observed with the differing culture ages. With the 14 day culture, photocurrents became increasingly negative with increasing cell concentration, whilst with the 45 day culture, photocurrents were small and positive. The reason for this discrepancy was not known, but could have represented differences in cell metabolism with age. This was an important finding for p-MFC device use.

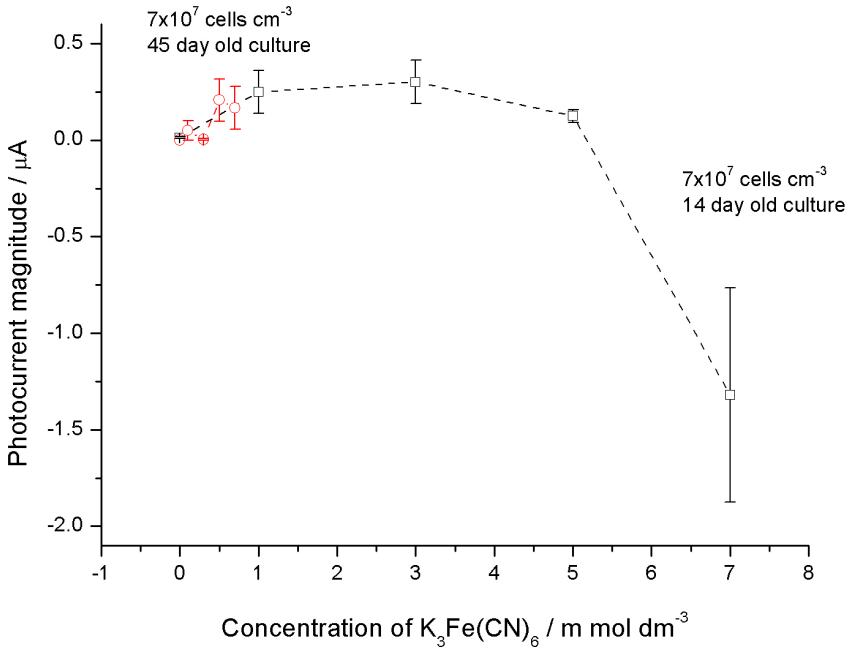


**Figure 11 Photocurrents calculated from the background subtracted change in current during illumination. Currents were measured during chronoamperometry at a FTO electrode (1.33cm$^2$ set to 100 mV past the oxidation potential for ferrocyanide. Solutions contained 7x10$^7$ cells mL$^{-1}$ (of two culture ages) and varying concentrations of ferricyanide in 1 mL total volume**

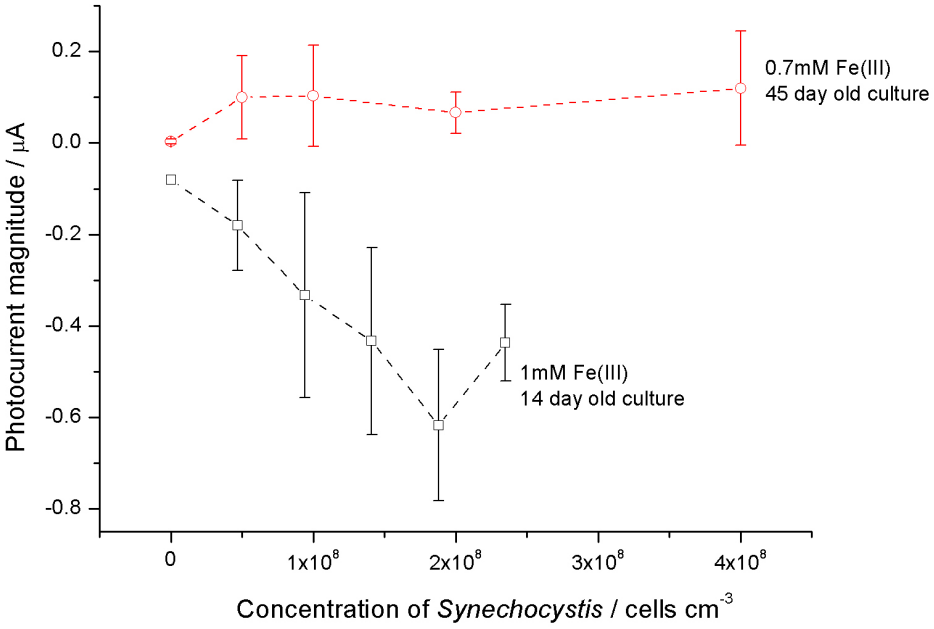


**Figure 12 Photocurrents calculated from background subtracted change in current during illumination. Currents were measured during chronoamperometry at a FTO electrode (1.33cm$^2$ set to 100 mV past the oxidation potential for ferrocyanide. Solutions contained 1 mM ferricyanide and varying concentrations of cells (of two culture ages) in total volume 1 mL)**

Using the background (dark) equilibrium currents measured at the working electrode for increasing amounts of ferricyanide and increasing cell concentrations (at both culture ages), background corrected rates of cyanobacterial ferricyanide reduction were calculated. Once background currents were subtracted for each concentration of ferricyanide (when no cyanobacterial cells were present), all oxidation currents of ferrocyanide were considered equal to all ferricyanide reduction rates by the cyanobacteria. Rates were calculated by relating current to charge, dividing by charge on one electron, and calculating how many moles of ferricyanide were being reduced to ferrocyanide in one hour, per $1x10^6$ cells.

Figures 13 and 14 show that the rate of ferricyanide reduction changed depending on the age of the cells utilised. With increasing ferricyanide (figure 13), rates increased exponentially with 14 day old cells, whilst with 45 day old cells, rates plateaued. In contrast, with *C. vulgaris,* rates increased linearly with ferricyanide concentration at both cell concentrations tested, although the age of the *C. vulgaris* cells was not precisely known.

In agreement with UV-Vis studies, the rate of ferricyanide reduction by *C. vulgaris* was larger than *Synechocystis* (three times higher as measured by chronoamperometry compared to 3.5 times higher as measured with UV-Vis). In figure 13, using the value of the 14 day old cells, the ferricyanide reduction rate with 1 mM ferricyanide and $7x10^7$ cellsml$^{-1}$ was approximately 0.1 nmol Fe(III) cm$^{-2}$ hr$^{-1}$ $10^{-6}$ cells compared to 0.3 nmol Fe(III) cm$^{-2}$ hr$^{-1}$ $10^{-6}$ cells with *C. vulgaris*. As with *C. vulgaris,* ferricyanide reduction rates calculated with 1mM ferricyanide and $7x10^7$ cells mL$^{-1}$ starting conditions were lower calculated from chronoamperometry than UV-Vis. This could be due to the fact that rates calculated from chronoamperometry are normalised for electrode area and additionally UV-vis only measured initial rates (generally known to be overestimating).

With increasing cells and 1mM ferricyanide (figure 14), rates increased to $1x10^8$ cellsml$^{-1}$, before plateauing and decreasing slightly. Rates with the 14 day old cells were approximately 4.5 times greater at $1x10^8$ cells mL$^{-1}$ than the 45 day old cells (0.9 nmol Fe(III) cm$^{-2}$ $10^{-6}$ cells hr$^{-1}$ compared to 0.2 nmol Fe(III) cm$^{-2}$ $10^{-6}$ cells hr$^{-1}$ respectively). It was interesting that whereas with *C. vulgaris,* no saturation of

current was seen either with increasing ferricyanide or increasing algae, with *Synechocystis,* the rate became saturated with respect to cells. One explanation is that as higher concentrations of cells were used in the *Synechocystis* experiments, perhaps the rate saturation point of *C. vulgaris* cells was not discovered as concentrations were not high enough. Additionally, due to smaller mass (and presumably lower ferric reductase capacity) of *Synechocystis* cells, lower saturation points were expected compared to *C. vulgaris.*

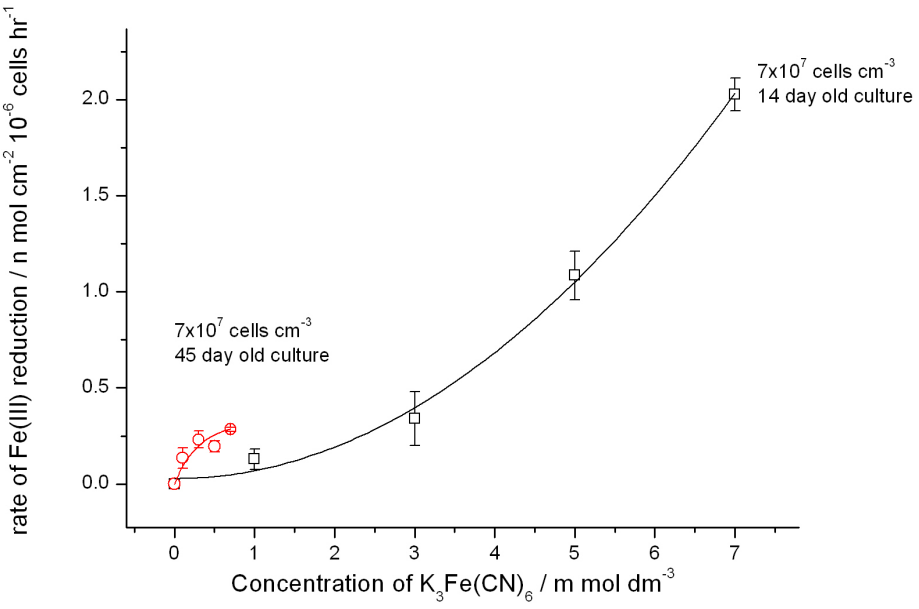


**Figure 13 Rates of ferricyanide reduction normalised for cell numbers and electrode area, calculated from background subtracted dark currents measured during chronoamperometry at a FTO electrode (1.33cm$^2$ set to 100 mV past the oxidation potential for ferrocyanide. Solutions contained 7x10$^7$ cells, with varying concentration ferricyanide (total volume 1 mL). Cells of two ages were used for comparison.**

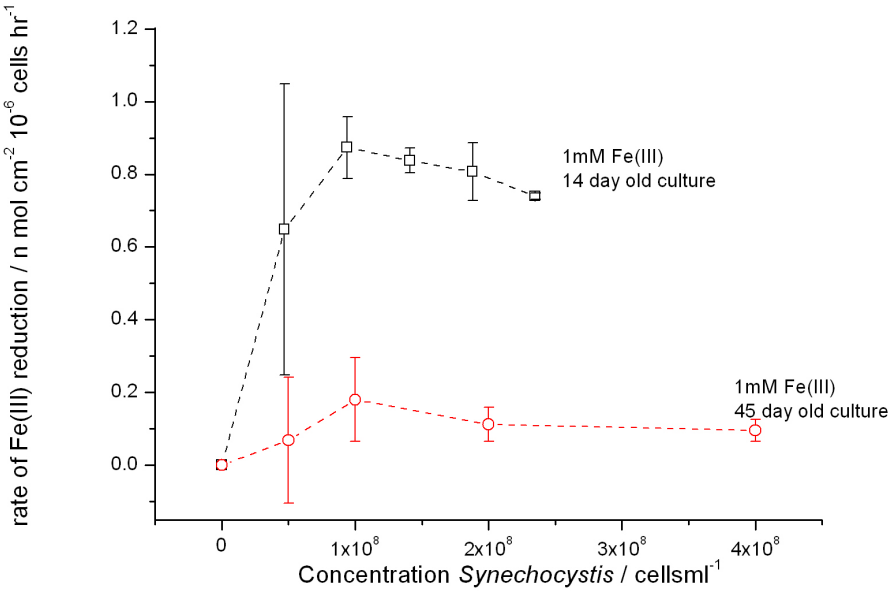


**Figure 14 Rates of ferricyanide reduction normalised for cell numbers and electrode area, calculated from background subtracted dark currents measured during chronoamperometry at a FTO electrode (1.33cm$^2$ set to 100 mV past the oxidation potential for ferrocyanide. Solutions contained 1 mM ferricyanide and varying concentrations of cells (total volume 1 mL). Cells of two ages were used for comparison.**

### 6.35 Rotating Disk Electrochemistry

Rotating disc electrochemistry (RDE) was carried out in the dark with cyanobacterial cells and ferricyanide in solution, to further study the reduction, and determine if the rate was determined by electron kinetics or mass transport (figure 2). During RDE the working electrode was rotated (in this case at rotation speeds between 100 and 600 rpm) pulling the solution in to the electrode surface and ensuring efficient mixing in the bulk. The electrode was held at a potential 100 mV positive of the oxidation peak for ferrocyanide, as determined by cyclic voltammetry prior to the RDE experiment. This ensured that any ferrocyanide reaching the electrode surface would immediately be oxidised to ferricyanide. Experiments involved keeping the ferricyanide concentration constant at 2.78 mM, before increasing the cell concentration, then holding cell concentrations constant whilst increasing ferricyanide concentration. Finally, the ferricyanide concentration was held constant at 22.22 mM, and cells again increased. Three repeats were taken, averages calculated, and media controls subtracted. Then plots were produced of 1/ current vs. 1/ square root rotation speed (figures 15, 16 and 17)

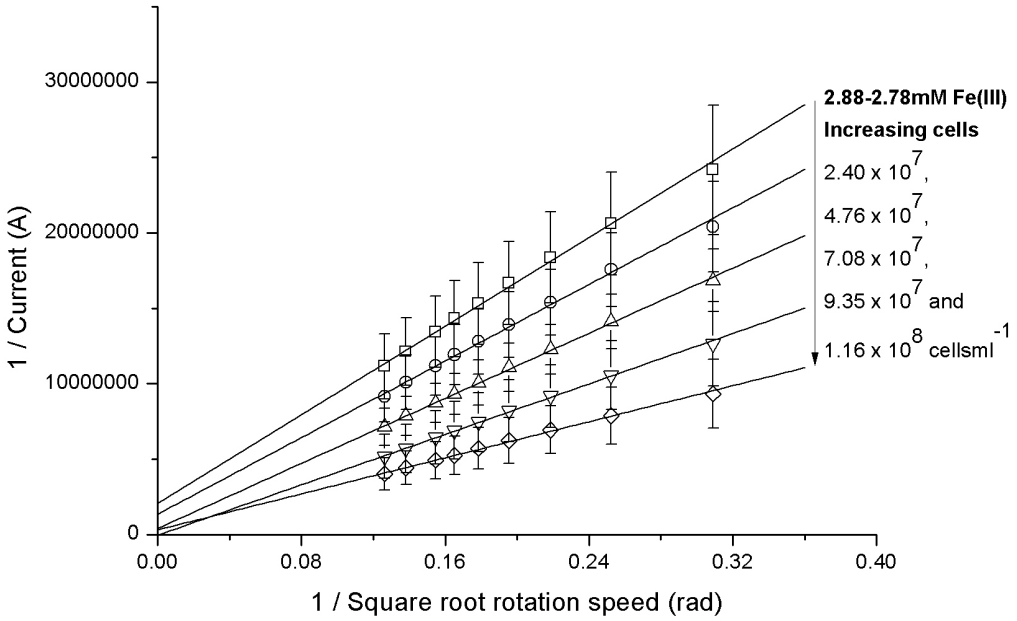


**Figure 15 Plots of 1/Current vs. 1/square root rotation speed (rad) with 2.88 mM ferricyanide and increasing cells in solution at a potential 100 mV past the oxidation potential of ferrocyanide. The error bars show one standard deviation (n=3)**

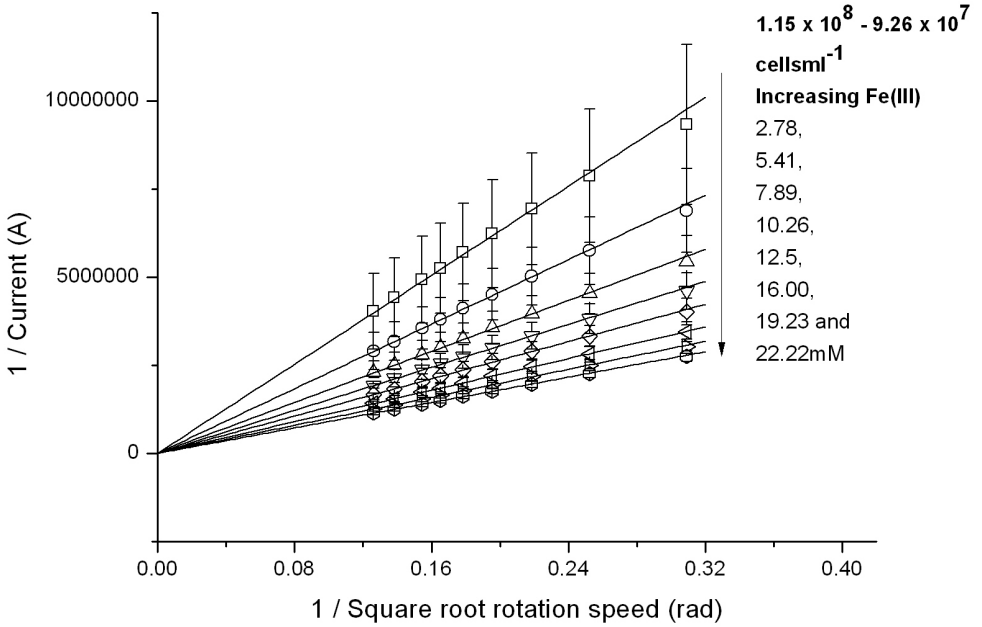


**Figure 16 Plots of 1/Current vs. 1/square root rotation speed (rad) with $1.15x10^8$ cells $ml^{-1}$ cells in solution and increasing ferricyanide, at a potential 100 mV past the oxidation potential of ferrocyanide The error bars show one standard deviation (n=3)**

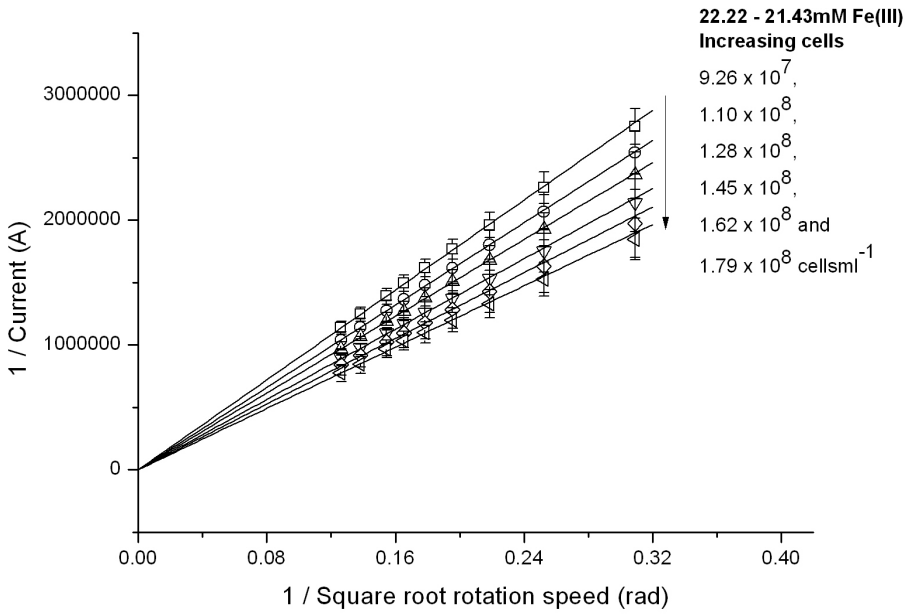


**Figure 17 Plots of 1/ Current vs. 1/ square root rotation speed (rad) with 22.22 mM ferricyanide and increasing cells in solution, at a potential 100 mV past the oxidation potential of ferrocyanide. The error bars show one standard deviation (n=3)**

Linear fits from the Koutecky-Levich plots shown in figures 16 and 17 had intercepts of zero, showing that, as with *C. vulgaris,* the reduction rate of ferricyanide by the cyanobacteria was mass transport controlled. However, in the Koutecky-Levich plots shown in figure 15 (with 3mM ferricyanide), lines of best fit had positive intercepts (excluding experiments with $9.35 \times 10^7$ cells $mL^{-1}$ which averaged a negative intercept). This inferred that under these conditions, kinetic limitations applied, meaning the rate of ferricyanide reduction was limited by the rate of electron transfer at the cells.

Using the positive intercepts of the Koutecky-Levich plots with 3 mM ferricyanide (and cell concentrations of $2.40 \times 10^7$, $4.76 \times 10^7$, $7.08 \times 10^7$ and $1.16 \times 10^8$ cells $mL^{-1}$), probable kinetic limited rates of reduction were calculated. This was by calculating current from the intercept, (normalised for 1 $cm^2$ electrode area), calculating currents passed in one hour, calculating mol ferricyanide reduced, before normalising for $1 \times 10^6$ cells. In order of increasing cell calculation, rates were 1.04 nmol 0.80 nmol, 1.78 nmol and 1.39 nmol Fe(III) $cm^{-2}$ $hr^{-1}$ $10^{-6}$ cells. These rates of reduction were virtually identical to the plateau reached in chronoamperometry (with 14 day old cells), of approximately 0.9 nmol Fe(III) $cm^{-2}$ $hr^{-1}$ $10^{-6}$ cells (figure 14). The

similarity in reduction rates makes it likely that the chronoamperometry was additionally measuring kinetic limited currents. Perhaps as the cells settled onto the electrode surface (possibly bringing ferricyanide molecules), diffusion distances of ferricyanide to the cells and ferrocyanide to the electrode surface were minimised. If mass transport increased, the rate limiting step could then have switched to the kinetics of the ferricyanide reduction at the cyanobacteria. The heterogeneous rate constant, $k^0$, was then calculated according to equation 1. In order of increasing cell concentration, calculated $k^0$ were 0.08, 0.06, 0.12 and 0.05 cm $s^{-1}$. These large values meant the redox centres responsible for the electron transfer in *Synechocystis* cells were reversible (as larger than 0.02 cm $s^{-1}$ [33]), with correspondingly large reorganisation energies.

$$i_K = nFAk^0C$$

**Equation 1 The relationship of $k^0$ to $i_K$**

No kinetic rates were measured under any conditions tested using *C. vulgaris* (chapter 5). This could be due to the larger size of *C. vulgaris* cells compared to *Synechocystis*, meaning more reductive machinery could be present. This would effectively speed up the $k_{et}$ step at the cell surface, meaning much lower cell conditions of *C. vulgaris* would be required for kinetic limitations to become evident over mass transport.

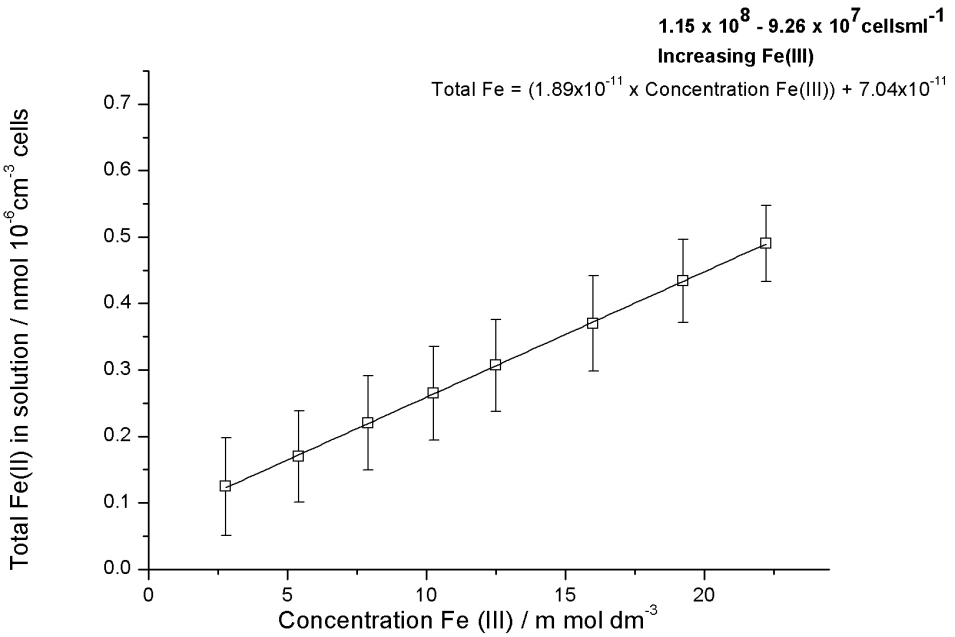


**Figure 18 Bulk concentration of ferrocyanide per $1x10^6$cells $mL^{-1}$, with increasing ferricyanide and $1.15x10^8$ cells $mL^{-1}$ present.**

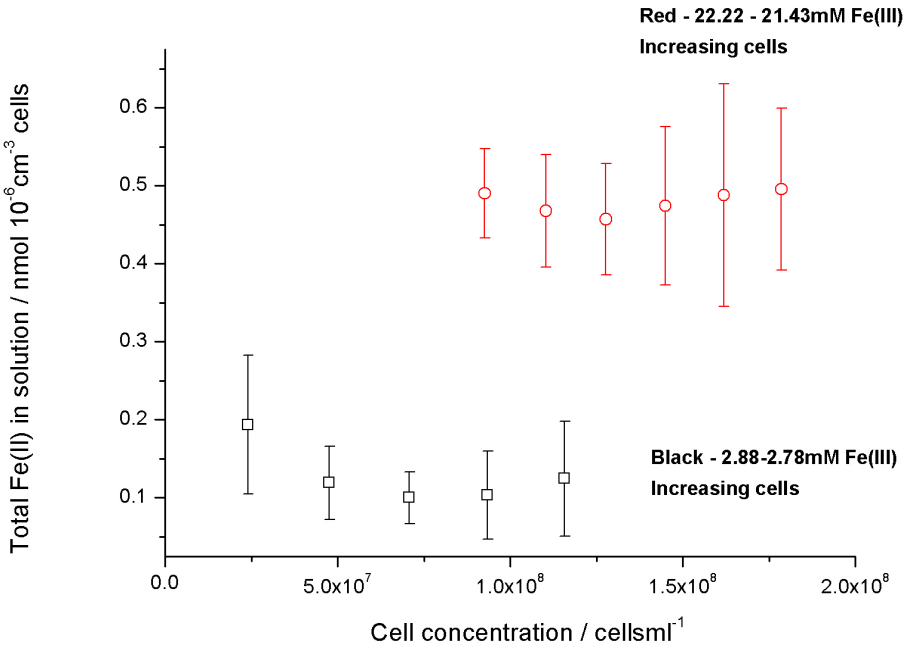


**Figure 19 Bulk concentration of ferrocyanide per 1x10$^6$cells mL$^{-1}$ with increasing cellsmL$^{-1}$ and either 2.88 mM or 22.22 mM ferricyanide present.**

Using the gradients of the Koutecky-Levich plots (figures 15-17), the total bulk concentration of ferrocyanide was calculated per 1x10$^6$ cells ml$^{-1}$, which also correlated to the total ferricyanide reduced by the cyanobacteria. This was according to equation 1. Values were normalised for number of cells.

*Synechocystis* exhibited the same patterns as *C. vulgaris.* Figure 18 shows that with increasing ferricyanide concentration, total ferrocyanide in the bulk increased. With a constant ferricyanide concentration and increasing cells (figure 19), ferrocyanide in the bulk stayed relatively constant. Similar to *C. vulgaris*, it appeared the cyanobacterial cells generally turned over ferricyanide at a constant rate, with the mediator reduction rate depending on the mass transport of the ferricyanide to and from the cells. Increasing the concentration of ferricyanide increased interactions between cyanobacteria and ferricyanide, therefore increasing the rate of reduction (and consequently bulk ferrocyanide concentration). Increasing total cells increased currents overall, but when normalised per cell, the same bulk ferrocyanide was observed. When total ferrocyanide in solution was compared between *Synechocystis* and *C. vulgaris* experiments, it was seen that higher concentrations of ferrocyanide were gained with *C. vulgaris*. This corroborated other experiments performed

whereby *C. vulgaris* had higher reduction rates than *Synechocystis*. For example, with ~22M ferricyanide and $9.26x10^7$cells $ml^{-1}$, total bulk ferrocyanide was ~0.5 nmol $10^{-6}$ $cm^{-3}$ $10^{-6}$ cells with *Synechocystis*, and ~0.75 nmol $10^{-6}$ $cm^{-3}$ $10^{-6}$ cells with *C. vulgaris* (a difference of 1.5).

## 6.4 Conclusions

This chapter aimed to compare the cyanobacterial species *Synechocystis* with the algal species *C. vulgaris* for suitability in a p-MFC. This was in terms of rates and mechanisms of ferricyanide reduction, and tolerance to ferricyanide induced toxicity. With regards how it reduced ferricyanide, no redox products from *Synechocystis* were identified from voltammetry. This corroborated previous research that redox active siderophore compounds were not produced by this cyanobacterial species, with ferricyanide uptake via strategy 1 using reduction membranes (possibly similar to the ferric reductase membranes in *C. vulgaris*).

Table 1 summarises all the work performed to determine rates and limitations on the reduction of ferricyanide by *Synechocystis.* Rates of reduction were studied via UV-Vis, chronoamperometry and rotating disk. In all cases, lower rates of reduction were observed per cell with *Synechocystis* than with *C. vulgaris*. With 1 mM ferricyanide and $7x10^7$ cells $ml^{-1}$, UV-Vis gave initial dark *Synechocystis* rates of ferricyanide reduction of 0.41 nmol Fe(III) $10^{-6}$ cells $hr^{-1}$, compared to 1.43 nmol Fe(III) $10^{-6}$ cells $hr^{-1}$ with *C. vulgaris*; a difference of a factor of ~3.5. Chronoamperometry gave dark *Synechocystis* ferricyanide reduction rates as 0.1 nmol Fe(III) $cm^{-2}$ $10^{-6}$ cells $hr^{-1}$ (with 14 day old cells) compared to 0.5 nmol Fe(III) $cm^{-2}$ $10^{-6}$ cells $hr^{-1}$ with *C. vulgaris*. This was a difference of a factor of five. Using rotating disk in the dark with 22 mM ferricyanide and $9.26x10^7$ cells $mL^{-1}$, total bulk ferrocyanide was ~0.38 nmol $10^{-6}$ $mL^{-1}$ cells with *Synechocystis*, and ~0.7 nmol $10^{-6}ml^{-1}$ cells with *C. vulgaris* (a difference of a factor of two). Higher ferricyanide reduction rates in *C. vulgaris* compared to *Synechocystis* could be due to differences in cell mass. When the chlorophyll content of 7 x $10^7$ cells *C. vulgaris* or *Synechocystis* was compared, *C. vulgaris* had a factor of 4.4 more chlorophyll. The difference in reduction rates may therefore have been partly due to the difference in cell reduction capacity (as measured by chlorophyll content).

| [Fe(III)] (mM) | [cells] (x$10^7$) | Rate from UV-Vis (nmol Fe(III) $hr^{-1}$ $10^{-6}$ cells) | Rate from Chronoamperometry (nmol Fe(III) $cm^{-2}$ $hr^{-1}$ $10^{-6}$ cells) | Total bulk Fe(II) from RDE (nmol Fe(II) $hr^{-1}$ $10^{-6}$ cells) | Mass transport (MT) or kinetic (K) limited? |
|---|---|---|---|---|---|
| 1 | 7 (unknown age culture) | 0.41 | - | - | |
| 1 | 7 (14 day culture) | - | 0.1 (exponential increase with [Fe(III)]) | - | |
| 1 | 7 (45 day culture) | - | 0.3 (plateaued out with [Fe(III)]) | - | |
| 1 | 10 (14 day culture) | - | 0.9 (plateaued out with [cells]) | | |
| 1 | 10 (45 day culture) | - | 0.2 (plateaued out with [cells]) | | |
| ~3 | 2.5-11 | - | - | 0.125 | KL – rate from intercept ~ 1 nmol Fe(III) $cm^{-2}$ $hr^{-1}10^{-6}$ |
| ~22 | 9-16 | - | - | 0.5 | MT |
| Varying | ~10 | - | - | Increase linearly | MT |

**Table 2 Summary table of ferricyanide reduction by *Synechocystis* (all in the dark) rate work**

As with *C. vulgaris*, most Koutecky-Levich plots showed that mass transport and not kinetics was found to limit rates of reduction of ferricyanide by *Synechocystis* (due to intercepts of zero on Koutecky-Levich plots). This meant that the reduction rate of the ferricyanide by the cyanobacterial cells was only controlled by how fast the ferricyanide could diffuse to the cells and ferrocyanide could diffuse to react at the electrode (see figure 2 for more detail). Higher concentrations of ferricyanide increased the mass transport limited rate, whilst with increased cyanobacteria, once normalised (for cell numbers) the same rate was seen (assuming Fe is not deficient). However, with the lowest numbers of cells tested and 3 mM ferricyanide, positive intercepts of Koutecky-Levich plots showed that kinetic limitations applied to the rate. Kinetic limited rates of reduction were calculated from the intercepts, and averaged at 1nmol Fe(III) $cm^{-2}$ $hr^{-1}10^{-6}$ cells. This was very close to the maximum plateaued rate

of reduction seen in chronoamperometry with 1mM ferricyanide and increasing cells (14 day old culture). The similarity makes it likely that the chronoamperometry measured kinetic limited rates. Calculated heterogeneous rate constants were large, and averaged around 0.08 cm $s^{-1}$. This showed the redox centres responsible for the electron transfer in *Synechocystis* cells were reversible (as $k^0$>0.02 cm $s^{-1}$ [33]), with correspondingly large reorganisation energies.

Photocurrents in light were complex. With increasing ferricyanide, *Synechocystis* photocurrents increased gradually before becoming large and negative at the highest ferricyanide concentration tested. With increasing cells, both negative and positive photocurrents were observed depending on the culture age. The reason for the negative photocurrents (not seen with *C. vulgaris*) was unknown, but must have represented a decrease in the total ferrocyanide being oxidised at the electrode. This could have indicated a decrease in reduction rates by *Synechocystis,* but this effect was not observed during UV-Vis experiments in light and dark and so is unlikely. Although the photocurrent trends were complicated, as with *C. vulgaris*, they demonstrated that light can have an effect on the system.

Cell growth was studied. It appeared *Synechocystis* growth was more resilient to the presence of ferricyanide than *C. vulgaris*. However, in contrast to *C. vulgaris,* cells were not able to be grown in biofilms on FTO glass; a drawback for a potential p-MFC species. The culture age was also found to have a large influence on rates of reduction by *Synechocystis* cells, with the 14 day old culture generally presenting higher reduction rates than the 45 day old culture. This could represent the different stages of growth the cells were in; the 14 day old cells were likely entering an exponential growth phase, whilst the 45 day old cells were likely in a stationary phase of growth. As this was not studied in *C. vulgaris*, comparisons could not be drawn.

In summary, *Synechocystis* has some features such as a high resilience to ferricyanide toxicity which make it suitable for use as a species in a p-MFC. However, due to lower rates of reduction, the complexity of some of the photocurrent patterns observed and the fact that it was unable to form biofilms on simple electrode materials, *C. vulgaris* is more useful as a model system.

## 6.5 References


1. Du, Z.W., Li, H.R., and Gu, T.Y., *A state of the art review on microbial fuel cells: A promising technology for wastewater treatment and bioenergy.* Biotechnology Advances, 2007. **25**: p. 464-482.
2. Yagishita, T., Sawayama, S., Tsukahara, K., and Ogi, T., *Effects of glucose addition and light on current outputs in photosynthetic electrochemical cells using Synechocystis sp PCC6714.* Journal of Bioscience and Bioengineering, 1999. **88**(2): p. 210-214.
3. Yagishita, T., Sawayama, S., Tsukahara, K., and Ogi, T., *Behavior of glucose degradation in Synechocystis sp. M-203 in bioelectrochemical fuel cells.* Bioelectrochemistry and Bioenergetics, 1997. **43**(1): p. 177-180.
4. Yagishita, T., Sawayama, S., Tsukahara, K.I., and Ogi, T., *Effects of intensity of incident light and concentrations of Synechococcus sp. and 2-hydroxy-1,4-naphthoquinone on the current output of photosynthetic electrochemical cell.* Solar Energy, 1997. **61**(5): p. 347-353.
5. Chiao, M., Lam, K.B., and Lin, L.W., *Micromachined microbial and photosynthetic fuel cells.* Journal of Micromechanics and Microengineering, 2006. **16**(12): p. 2547-2553.
6. Yagishita, T., Horigome, T., and Tanaka, K., *Effects of light, $CO_2$ and inhibitors on the current output of biofuel cells containing organism Synechococcus Sp.* Journal of Chemical Technology and Biotechnology, 1993. **56**(4): p. 393-399.
7. Martens, N. and Hall, E.A.H., *Diaminodurene as a mediator of a photocurrent using intact cells of cyanobacteria.* Photochemistry and Photobiology, 1994. **59**(1): p. 91-98.
8. Torimura, M., Miki, A., Wadano, A., Kano, K., and Ikeda, T., *Electrochemical investigation of cyanobacteria Synechococcus sp PCC7942-catalyzed photoreduction of exogenous quinones and photoelectrochemical oxidation of water.* Journal of Electroanalytical Chemistry, 2001. **496**(1-2): p. 21-28.
9. Furukawa, Y., Moriuchi, T., and Morishima, K., *Design principle and prototyping of a direct photosynthetic/metabolic biofuel cell (DPMFC).* Journal of micromechanics and microengineering : structures, devices and systems, 2006. **16**(9): p. S220-S225.

10. Pisciotta, J.M., Zou, Y., and Baskakov, I.V., *Light-Dependent Electrogenic Activity of Cyanobacteria.* Plos One, 2010. **5**(5).
11. Gorby, Y.A., Yanina, S., McLean, J.S., Rosso, K.M., Moyles, D., Dohnalkova, A., Beveridge, T.J., Chang, I.S., Kim, B.H., Kim, K.S., Culley, D.E., Reed, S.B., Romine, M.F., Saffarini, D.A., Hill, E.A., Shi, L., Elias, D.A., Kennedy, D.W., Pinchuk, G., Watanabe, K., Ishii, S., Logan, B., Nealson, K.H., and Fredrickson, J.K., *Electrically conductive bacterial nanowires produced by Shewanella oneidensis strain MR-1 and other microorganisms.* Proceedings of the National Academy of Sciences of the United States of America, 2006. **103**(30): p. 11358-11363.
12. Trick, C.G. and Wilhelm, S.W., *Physiological changes in the coastal marine cyanobacterium Synechococcus Sp. PCC-7002 exposed to low ferric ion levels.* Marine Chemistry, 1995. **50**(1-4): p. 207-217.
13. Wilhelm, S.W. and Trick, C.G., *Iron-limited growth of cyanobacteria - Multiple siderophore production is a common response.* Limnology and Oceanography, 1994. **39**(8): p. 1979-1984.
14. Hopkinson, B.M. and Morel, F.M.M., *The role of siderophores in iron acquisition by photosynthetic marine microorganisms.* Biometals, 2009. **22**(4): p. 659-669.
15. Wilhelm, S.W., *Ecology of iron-limited cyanobacteria: A review of physiological responses and implications for aquatic systems.* Aquatic Microbial Ecology, 1995. **9**(3): p. 295-303.
16. Hider, R.C. and Kong, X., *Chemistry and biology of siderophores.* Natural Product Reports, 2010. **27**(5): p. 637-657.
17. Borer, P.M., Sulzberger, B., Reichard, P., and Kraemer, S.M., *Effect of siderophores on the light-induced dissolution of colloidal iron(III) (hydr)oxides.* Marine Chemistry, 2005. **93**(2-4): p. 179-193.
18. Armstrong, J.E. and Vanbaalen, C., *Iron transport in microalgae - Isolation and biological activity of a hydroxamate siderophore from the blue-green alga Agmenellum quadruplicatum.* Journal of General Microbiology, 1979. **111**(APR): p. 253-262.
19. Schwyn, B. and Neilands, J.B., *Universal chemical assay for the detection and determination of siderophores.* Analytical Biochemistry, 1987. **160**(1): p. 47-56.

20. Ehrenreich, I.M., Waterbury, J.B., and Webb, E.A., *Distribution and diversity of natural product genes in marine and freshwater cyanobacterial cultures and genomes.* Applied and Environmental Microbiology, 2005. **71**(11): p. 7401-7413.

21. Rose, A.L., Salmon, T.P., Lukondeh, T., Neilan, B.A., and Waite, T.D., *Use of superoxide as an electron shuttle for iron acquisition by the marine cyanobacterium Lyngbya majuscula.* Environmental Science & Technology, 2005. **39**(10): p. 3708-3715.

22. Schröder, I., Johnson, E., and de Vries, S., *Microbial ferric iron reductases.* Fems Microbiology Reviews, 2003. **27**(2-3): p. 427-447.

23. Vartivarian, S.E. and Cowart, R.E., *Extracellular iron reductases: Identification of a new class of enzymes by siderophore-producing microorganisms.* Archives of Biochemistry and Biophysics, 1999. **364**(1): p. 75-82.

24. Middlemiss, J.K., Anderson, A.M., Stratilo, C.W., and Weger, H.G., *Oxygen consumption associated with ferric reductase activity and iron uptake by iron-limited cells of Chlorella kessleri (Chlorophyceae).* Journal of Phycology, 2001. **37**(3): p. 393-399.

25. Weger, H.G., *Ferric and cupric reductase activities in the green alga Chlamydomonas reinhardtii: experiments using iron-limited chemostats.* Planta, 1999. **207**(3): p. 377-384.

26. Chana Kranzler, H.L., Yeala Shaked, Nir keren, *The role of reduction in iron uptake processes in a unicellular, planktonic cyanobacterium.* Environmental Microbiology, 2011.

27. Badarau, A., Firbank, S.J., Waldron, K.J., Yanagisawa, S., Robinson, N.J., Banfield, M.J., and Dennison, C., *FutA2 is a ferric binding protein from Synechocystis PCC 6803.* Journal of Biological Chemistry, 2008. **283**(18): p. 12520-12527.

28. Koropatkin, N., Randich, A.M., Bhattacharyya-Pakrasi, M., Pakrasi, H.B., and Smith, T.J., *The structure of the iron-binding protein, FutA1, from Synechocystis 6803.* Journal of Biological Chemistry, 2007. **282**(37): p. 27468-27477.

29. Katoh, H., Hagino, N., Grossman, A.R., and Ogawa, T., *Genes essential to iron transport in the cyanobacterium Synechocystis sp strain PCC 6803.* Journal of Bacteriology, 2001. **183**(9): p. 2779-2784.

30. Fujii, M., Dang, T.C., Rose, A.L., Omura, T., and Waite, T.D., *Effect of Light on Iron Uptake by the Freshwater Cyanobacterium Microcystis aeruginosa.* Environmental Science & Technology, 2011. **45**(4): p. 1391-1398.

31. Davey, M.S., Suggett, D.J., Geider, R.J., and Taylor, A.R., *Phytoplankton plasma membrane redox activity: Effect of iron limitation and interaction with photosynthesis.* Journal of Phycology, 2003. **39**(6): p. 1132-1144.

32. Lynnes, J.A., Derzaph, T.L.M., and Weger, H.G., *Iron limitation results in induction of ferricyanide reductase and ferric chelate reductase activities in Chlamydomonas reinhardtii.* Planta, 1998. **204**(3): p. 360-365.

33. Harvey, D., *Analytical Chemistry 2.0-Analytical Chemistry, the Basic Concepts*. 1999, McGraw-Hill.

# Chapter 7. Other Redox Mediators

# Chapter 7 – Other Redox Mediators

## 7.1 Introduction

So far this thesis has solely focussed on the artificial mediator potassium ferricyanide (ferricyanide), as it was utilised in the basic p-MFC device. Importantly, due to its toxicity at high concentrations, and effects on growth, ferricyanide is not an ideal mediator [1]. Artificial mediators in solution are not commercially viable in general, due to their cost, and their constant need for replacing [2]. A mediator is required which is cheap, non toxic and does not need replacing [2]. In practice, this is likely to take the form of a natural mediator (such as quinone), or a tethered mediator such as a conductive polymer. This chapter explores whether *Chlorella vulgaris* can interact with other such mediators. Optimisation of the mediator component of the basic p-MFC device is crucial to improve efficiency and long-term operation capacity.

Good mediators should possess several features [3, 4]; they need to be able to cross the cell membrane easily, and easily accept electrons from the electron carriers of the electron transport chains, with a high reaction rate. They need to have good solubility, be non-biodegradable, non-toxic and have low cost. A mediator with a low redox potential would in theory maximize the redox difference between anode and cathode giving the highest voltage difference. However, it would not necessarily be most efficient at extracting electrons from reduced intracellular systems (NADH, NADPH or reduced cytochromes) within the microbes [3, 4]. An ideal redox mediator would have a standard redox potential just slightly lower in energy than the redox energy of the protein / redox system in the micro-organism [3].

Mediators in a passive cell can be natural or artificial. Metabolic products produced by microbes themselves can act as reducing agents [2]. For example, hydrogen sulphide is a reduced product of anaerobic metabolism that will readily react with electrodes. Although fuel cells containing sulphate reducers have generated power, efficiencies are low as only two of the eight electrons used to reduce sulphate to sulphide are released at the electrode surface [5]. Furthermore, the *Desulfovibrio* species typically used in these systems only incompletely oxidise their organic electron donors to acetate, further limiting efficiency. Although it is possible to

modify the composition of anodes to increase their reactivity with other metabolic end products [6], these electrodes tend to foul with oxidation products.

Redox shuttles can also be produced by microbes, which can be reduced by the producer microbe, or other microbes acting in a symbiosis. Natural shuttles used as an electron transfer mechanism to reduce Fe(III) were first discovered in the bacterial species *Shewanella oneidensis* [7]. However, biosynthesising an electron shuttle is energetically expensive, requiring shuttles to be recycled many times to regain the energy investment [2]. Indeed, a one time replacement of medium in a pure culture fuel cell of *Geothrix* reduced power production by 50 %, as this eliminated the vast majority of electron mediators in solution produced by the microorganisms [8]. For this reason, microbes that produce electron shuttles are at a competitive disadvantage in environments where the shuttle is rapidly lost from the release site [9]. Coupled with the incomplete oxidation of organic fuels performed by many species producing electron shuttles [10], efficiencies are limited. In any case, *C. vulgaris* was not found to produce any redox active species, as determined in chapter 5.

Artificial mediators, for example iron chelates and neutral red, offer the possibility for microorganisms in a microbial fuel cell to overcome the metabolic energy losses associated with producing electron shuttles [5]. In many cases the reduced cellular constituents that interact with artificial mediators have not been determined, but there are many mechanisms by which mediators might intercept electrons. In the case of neutral red (one of the most effective mediators [11]) studies have demonstrated that it accepts electrons from NADH and can be enzymatically reduced by a hydrogenase and possibly formate dehydrogenase [12]. However, the ability of a microbe to conserve energy to support growth has yet to be demonstrated [2]. This is significant for long-term operations, as the microbes catalysing the oxidation of organic fuels require some energy for maintenance and growth. Furthermore, many artificial electron shuttles are expensive and toxic both to humans and the environment [2], and so are not a suitable choice for sustainable MFC electricity generation.

| Type | Mediator |
|---|---|
| Solution/ Synthetic | Methyl Viologen (MV) [13] |
| | Neutral red (NR) [4, 11] |
| | Methylene Blue [4, 6] |
| | Fe(III)EDTA [3] |
| | Fe(III) NTA/Fe(II) NTA [3] |
| | Fe(CN)6 3−/Fe(CN)6 4− [3] |
| | Benzyl Viologen [3] |
| | Brilliant Cresyl Blue [3] |
| | Meldolas blue [4, 14] |
| | Resezurin [15] |
| Fixed/ Synthetic | Sulphonated anthaquinone in polymer [16] |
| | Covalent functionalisation of gold and carbon with an osmium coordination complex [17] |
| | Polypyrrole [18, 19] |
| | Polyaniline [19] |
| | Neutral red and metals (such as Mn(IV) and Fe(III) incorporated into graphite electrodes [20, 21] |
| Solution/ Natural | Phenazine [22] |
| | 2-amino-3 carboxy-1,4-naphthoquinone [22] |
| | 1,2-dihydroxynaphthalene [22] |
| | 2,6-di-tert-butyl-p-benzoquinone [22] |
| | flavin mononucleotide [23] |
| | Riboflavin [23] |
| | Anthraquinone-2,6-disulfonic acid [23] |
| | Pyocyanin [24] |
| | Thionine [4, 15] |
| | humic acids [23] |
| | Quinones [25] |
| | 1-hydroxy-4-aminoanthraquinone [22] |
| | 2-hydroxy-1,4-naphtoquinone [23] |
| | phenazine-1-carboxamide [24] |

**Table 1 various mediators known to have been used in MFCs**

Although table 1 demonstrates that many mediator types have been used in MFCs and p-MFC, with the majority studied artificial, in the most efficient devices no non-natural redox mediators are added [1, 3]. Bacterial colonies that secrete naturally occurring redox mediators are used. Alternatively some bacteria have been shown to

transfer electrons to electrodes directly [9, 26-30]. Various cyanobacteria have also been suggested to have the ability to perform direct electron transfer to electrodes [31], although no other studies have been found which corroborate this finding. Direct electron transfer is thought to be protein mediated, possibly via cytochromes in the extra-cellular matrix (ECM) or bacterial pili.

### 7.11 Conducting polymers

In recent years, conducting polymers such as polyaniline (PANI) and polypyrrole (POLYP) have been used in MFCs as surface attached mediators [32]. One of the benefits of surfaced attached mediators is that when a biofilm is grown on an anode with a surfaced attached mediator, the anodic reaction is confined to the anodic surface. This means that the PEM of a device would not be needed to separate anodic and cathodic chambers, lowering the internal resistance of a p-MFC and increasing $E_{cell}$. Pietron *et al.*, [33], used PANI coated carbon foams as anodic materials in small scale microbial fuel cells. Scott *et al.*, [34], prepared graphite felt anodes modified with Carbon/PANI composites (26.5 mW $m^{-2}$ for Carbon/PANI composite compared to 9.5 mW $m^{-2}$ for plain graphite felt). In this study, improvement was hypothesised to be as a result of the increase in surface area which multiplied the number of sites for microbial colonization, as well as biocompatibility. Also, by doping, special morphology with a high nanofibrous structure was developed [32, 35].

Less attention has been given to conducting polymers in p-MFCs. Zou *et al.*, [19], developed a p-MFC using naturally growing freshwater photosynthetic biofilms, which gave an increase in cell voltage upon illumination. When the p-MFC anodes were coated with electrically conducting polymers such as PANI and POLYP, the voltage magnitude increased and the amplitude of light response improved significantly (0.95 mW $m^{-2}$ for PANI coated and 1.3 mW $m^{-2}$ for POLYP coated anodes). Zou *et al.,* [18], also compared the difference of using nanostructured or granular POLYP anodes in p-MFCs. They determined that nanostructured fibrillar POLYP showed better performance, which cyclic voltammetry and impedance spectroscopy inferred was due to improvement in electrochemical properties including higher redox current and lower electron-transfer resistance. Coating the anode in fibrillar POLYP at a loading density of 3 mg $cm^{-2}$ resulted in a 450 %

increase in the power density compared to those reported in previous studies on p-MFCs that used the same photosynthetic culture [18].

The electrons producing the positive voltage response under illumination seen in [19] and [18] were thought to come directly from the photosynthetic electron transport chain. It was speculated that due to the long chains, PANI and POLYP could physically interact with photosynthetic cell membranes, enabling direct discharge of electrons onto the anodic surface [18, 19]. Evidence for a photosynthetic (rather than respiratory) source of electrons in polymer p-MFCs came from the perfect coincidence between the light cycles and oscillation in cell voltage, the immediate response to light and the sharpness in change in cell voltage [18, 19]. An alternate scenario was that the polymer acted as a catalyst to oxidise extracellular products produced by the micro-organisms during photosynthesis. However, if this was correct, a delay would be expected between illumination and cell voltage rise, and the cell voltage rise would be gradual. A third unlikely mechanism to account for the electricity was that heterotrophs consumed organic compounds released by phototrophs. This would not explain the perfect coincidence between light cycles and voltage oscillation, and would also result in a negative voltage response (rather than positive) [19].

Conducting polymers such as PANI (shown in figure 1) and POLYP are known to be biocompatible with both cyanobacteria and algae and accelerate biofilm growth [19]. This positive effect on biofilm formation is thought to be due to the fact that positively charged natural surfaces enhance adhesion of bacteria [36]. PANI biocompatibility has also been increased further by surface functionalisation using quinoid groups [34]. In addition to the biocompatibility benefits, the presence of conducting polymers on the anode surface slowed down the anode deactivation caused by interference from bacterial metabolic products, as well as the by-products of any electro-catalytic oxidation process [34, 37]. Other benefits of PANI electrodes include environmentally stability, reversible redox activity in different pHs, easy processing as thin films, particles and fibres, and tuneable hydrophilicity through doping with camphorsulphonic acid [34].

PANI has been extensively characterised, with properties known to depend on the redox and protonation state of films. Current models for the PANI system are based on the three oxidation states, leucoemeraldine, emeraldine and the fully oxidised form of PANI, pernigraniline (see figures 1 and 2). These can be distinguished by UV-Vis (figure 3), where according to Ormecon [38], manufacturers of PANI, emeraldine base (green) absorbs primarily at 800 nm, 440 nm and 330 nm, whilst emeraldine base (blue) primarily absorbs at 320 nm and 640 nm. This latter state can be formed by alkaline treating of emeraldine salt. Leucoemeraldine only absorbs at 330 nm, and is colourless. Emeraldine base is regarded as the most useful form of polyaniline due to its high stability at room temperature and the fact that, upon acid doping it is electrically conducting [39]. In this form, the film is swelled with an influx of ions. Leucoemeraldine and pernigraniline are poor conductors, even when doped with an acid [39].

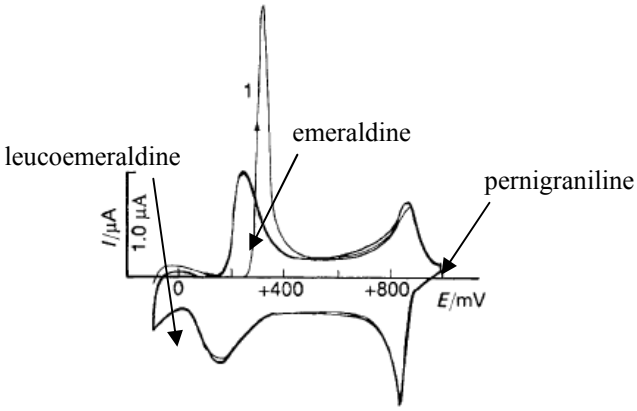


**Figure 1 Reproduced from [39] First-cycle and multicycle cyclic voltammogram recorded at 0.1 V $s^{-1}$ with a 40 nm PANI film w.r.t SCE**

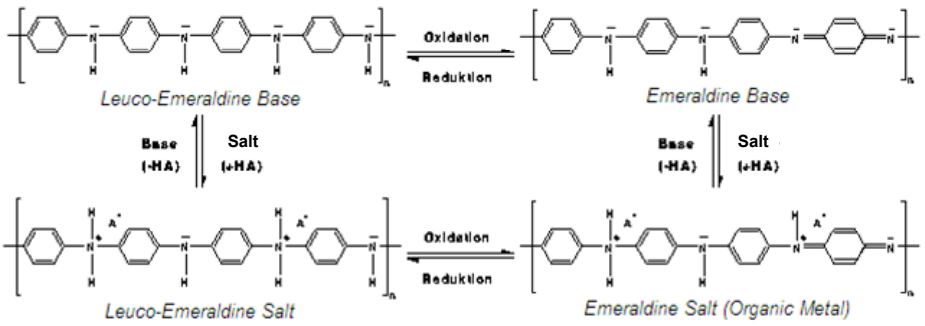


**Figure 2 Reproduced from [38] Leucoemeraldine contains only amine links. Pernigraniline (not shown) is the fully oxidized state with imine links instead of amine links. The emeraldine form has both amine and imine links; if neutral, it is called emeraldine base. If doped it is called emeraldine salt (ES), with the imine nitrogens protonated by an acid.**

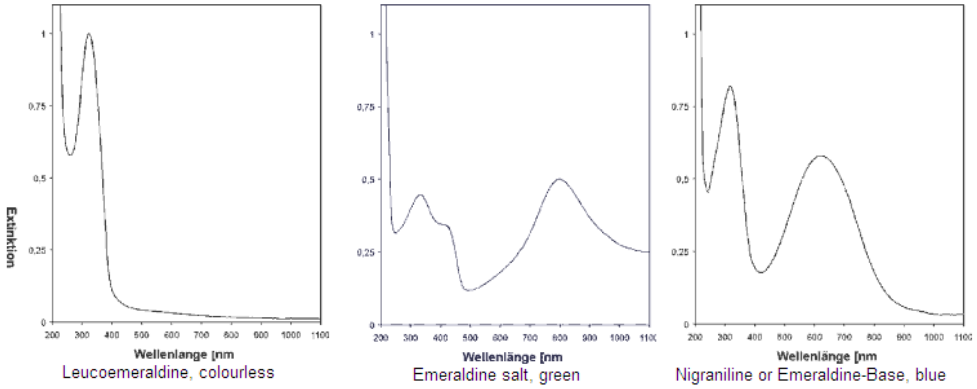


**Figure 3 Reproduced from [38] Typical absorbencies from UV-Vis experiments for leucoemeraldine, emeraldine salt and emeraldine base**

## 7.12 Chapter Aims

Due to many drawbacks (such as long term toxicity), the artificial compound ferricyanide is not ideal as a redox mediator in the basic p-MFC device (tested in chapter 3). Ideally, no mediator would be required for electron transfer from cell to anode, with the utilisation of a photosynthetic species which could easily perform direct electron transfer when grown on an electrode surface. However, as no algae have been found which can perform direct electron transfer (and virtually no evidence exists for direct electron transfer in cyanobacteria), a mediator is required. Finding a mediator to replace ferricyanide is crucial for the improvement of efficiency and long term performance of the basic p-MFC. Natural mediators are generally considered the most attractive option as they are potentially most biocompatible.

In this chapter, the redox mediator cytochrome C (cyt C)) is screened for interaction with *C. vulgaris* by UV-Vis spectrophotometry. The oxidised form of cyt C was chosen for testing as it is a low toxicity redox protein containing a haem center. It is commonly found inside cells, where it plays vital roles in mitochondrial electron transport chains and electron transport in anodophilic bacteria [40]. Consequently it is interesting to determine if it can participate in cell redox reactions external to a cell. Redox state is easily ascertainable by the UV-Vis spectra [41, 42]. Additionally, the surface tethered redox polymer PANI is studied. Although PANI is not natural or based on natural compounds, it offers high biocompatibility and represents the closest thing possible to direct electron transfer by *C. vulgaris*. A method is outlined for the production of PANI coated fluorine doped tin oxide (FTO) coated $TiO_2$ ceramics and

glass (see chapter 8 for the production of $TiO_2$ ceramics and comparisons of PANI against other materials). PANI materials are characterised, before a p-MFC device is assembled and tested using the PANI coated ceramic.

## 7.2 Experimental

### 7.21 UV-Vis Spectrophotometry

To determine whether *C. vulgaris* could reduce cyt C, UV-Vis was performed. A bulk solution of 10mL *C. vulgaris* at a concentration of $7x10^7$ cells $mL^{-1}$ (resuspended in fresh media) with 0.02 mM cyt C (bovine heart (95 % oxidised) from Sigma Aldrich 30398 - BioChemika, ≥95% (GE)). This concentration was chosen according to previous literature and its solubility in water. At certain time periods, 1mL aliquots were drawn from solution, and centrifuged at 13.2 x $10^3$ rpm for three minutes. Without disturbing the pellet of cells the supernatant was pippetted into a cuvette and absorbance measured using a UV-Vis spectrometer (type Helios gamma from Thermo electron corporation). Repeats were executed separately in light (illumination from an optical fibre at 620 nm, with intensity 1.25 x $10^{-3}$ W $cm^{-2}$ and area 2 $cm^2$), and the dark, with media controls performed. Calibration curves to enable cyt C concentration to be calculated from absorption were made.

### 7.22 Polyaniline coating of ceramics

To test the feasibility of tethered mediators, PANI electrodes were created. All electrochemistry in this chapter was carried out on an Autolab PGSTAT 12 with a built-in frequency response analyser. FTO coated $TiO_2$ ceramics were prepared as outlined in chapter 8. PANI was then deposited by performing linear sweep voltammetry from 0 to 1.2 V w.r.t Ag/AgCl at a scan rate of 1 mV $s^{-1}$ in a solution of 1 M $H_2SO_4$ containing 0.1 M aniline. The FTO coated ceramic acted as the working electrode, with a platinum counter. This treatment resulted in a thick layer of PANI on the ceramic – after rinsing; excess PANI not sufficiently bonded to the surface was removed, leaving a stable layer.

Due to the difficulty of characterising the PANI coated porous ceramics (because of their irregular surface area and lack of suitable for UV-Vis), most characterisation

took place on a PANI coated 1x1 $cm^{-2}$ piece of flat FTO coated glass. This was coated using the method outlined above.

**7.23 Polyaniline Characterisation**

Properties of the PANI films grown on FTO glass were measured by cyclic voltammetry and impedance and UV-Vis (at the reduction and oxidation potentials for emeraldine and leucoemeraldine respectively as determined by cyclic voltammetry). This was measured after a 12 hour soak in the 1 M $H_2SO_4$ electrolyte used to grow the films, and also after 12 hours soaking in the media used to grow the *C. vulgaris cells*.

To determine biocompatibility, PANI coated FTO glass cultured in *C. vulgaris* for 45 days was studied by SEM (culturing procedure in appendix). PANI ceramics were additionally cultured in freshly inoculated *C. vulgaris* flasks. After a period of 45 days, cell and chlorophyll loadings were calculated.

**7.24 Polyaniline Use in Device**

An electrochemical cell device was constructed according to figure 4, using 3N-BBM+V media as electrolyte, and the PANI ceramic as the anode. The device was modified from the basic p-MFC design used in chapter 3 to accommodate the new ceramic electrode. The main change to the design was the enlargement of both anodic and cathodic chambers (increasing the volume of each from 100 µl to 1 ml). Not only did this allow the use of the PANI anode, but the issue of the drying electrolyte in the basic p-MFC device (outlined in chapter 3) was solved.

The p-MFC device was initially constructed with *C. vulgaris* present as planktonic cells in solution at a concentration of $7x10^7$ cells $mL^{-1}$. Cyclic voltammetry was performed in the dark, and in the light (light at 620 nm from an optical fibre at intensity $5x10^{-3}$ W $cm^{-2}$). Chronoamperometry was subsequently performed on the assembled PANI p-MFC device at the half wave potential found from the cyclic voltammetry both in the dark and under illumination at 620 nm from an optical fibre (using different intensities of light).

Second, the p-MFC device was constructed with *C. vulgaris* present on the PANI anode as a biofilm (cultured for 45 days as outlined in the appendix - cell loadings

were calculated and compared to other materials for biocompatibility comparisons in chapter 8). Chronoamperometry was repeated on the assembled cultured PANI p-MFC device at the half wave potential found from the cyclic voltammetry both in the dark and under illumination at 620 nm, intensity 5 x 10 W $cm^{-3}$ from an optical fibre. To measure polarisation curves the voltage was measured across a range of resistors that were varied between 10 MΩ and 1 KΩ, the voltage readings were all taken ten minutes after each resistance was chosen and the data was logged using a pico data logger ADC-24. After device use, cell counts and chlorophyll loadings were calculated of biological material used. Polarisation curves were thought a better way of measuring p-MFC device output as they gave the device longer times to reach equilibrium (steady state) than the chronoamperometry measurements used previous. This meant that measurements were more stable and reproducible, as well as being comparable with most p-MFC literature. From the polarisation curves, power output was calculated, and the resistance of the cell giving maximum power for operation could be determined.

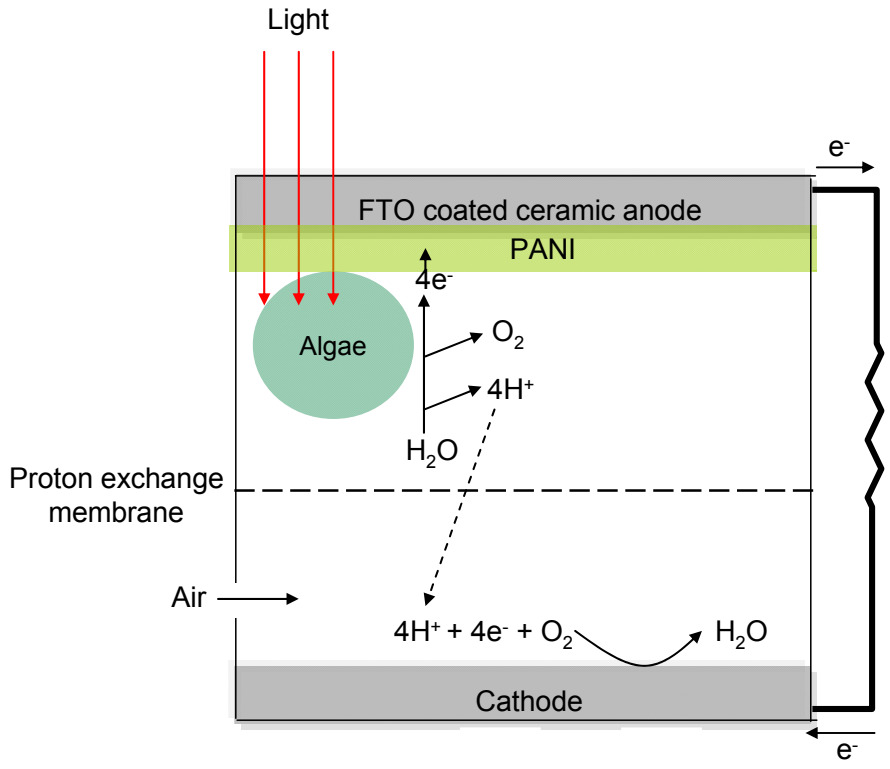


**Figure 4 Schematic of p-MFC device constructed using PANI coated FTO coated ceramic, with algal cells in a biofilm grown on PANI anode or on in solution in the anodic chamber.**

## 7.3 Results and Discussion

### 7.31 UV-Vis Spectrophotometry

UV-Vis was performed over time on solutions of cyt C and *C. vulgaris*. In the oxidised form (as supplied 95 % oxidised), cyt C exhibited two main peaks at 409 nm and 531 nm, whilst in the reduced form peaks at 420 nm, 421 nm and 450 nm were exhibited. A calibration curve for the oxidised form plotting the absorbance at 409 nm and 531 nm for a range of known concentrations is shown in figure 5, which allowed the precise concentration of the oxidised form to be calculated. UV-Vis experiments involved solutions of a starting concentration of 0.02 mM cyt C, in algae and media, in light and dark over time (figure 6).

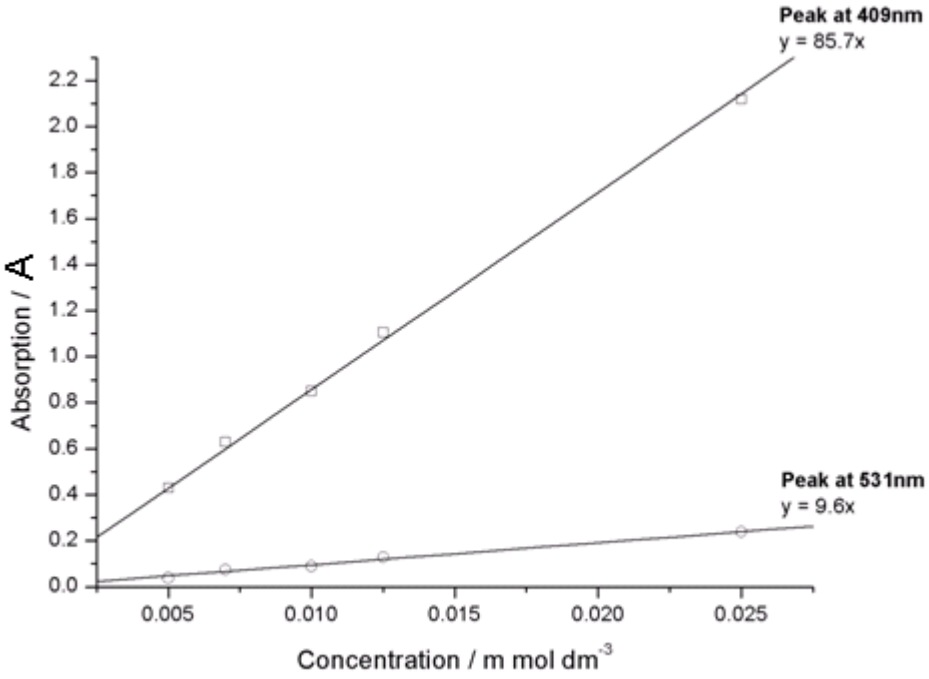


**Figure 5 Calibration curves of the 2 peaks exhibited for cyt C at 409 nm and 531 nm, to calculate the concentration of the oxidised form of cyt C**

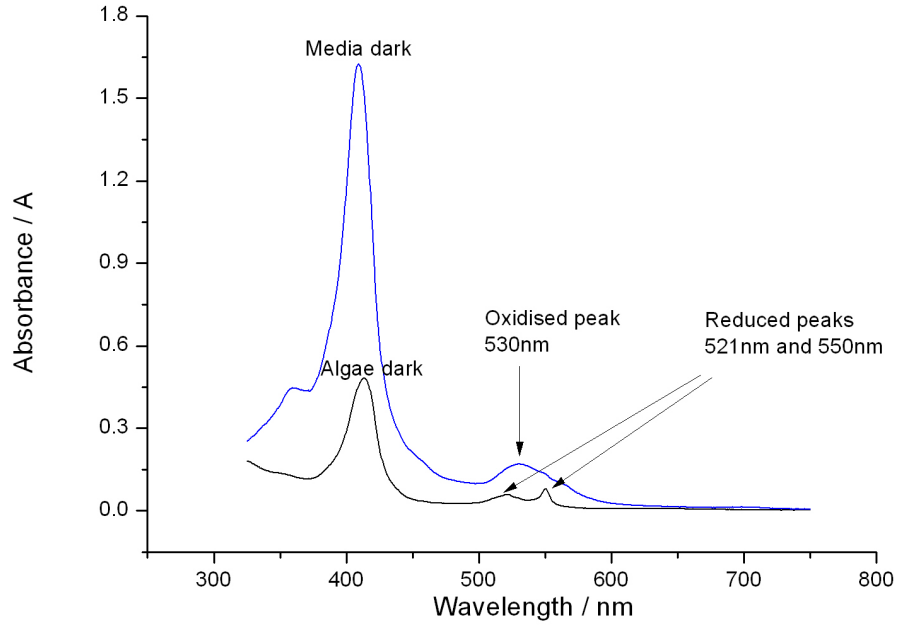


**Figure 6 Absorption spectra of 0.02 mM cyt C, when in solution with algae or media in dark. Upon inoculation in algae all peaks decreased rapidly, with appearance of reduction peaks at 521 nm and 550 nm. The 530 nm peak, indicative of the oxidised form, remained evident in media.**

Upon addition to the algae the cyt C peak at ~409 nm was greatly diminished, both in light and dark compared to spectra in media (figure 6 shows dark absorbance). This could suggest that the protein was denatured. However, due to the fact that over time in light the peak increased, this inferred the cyt C became complexed to the algae, before being slowly released. Using the calibration curve and the measured peaks at ~409 nm (although peaks varied from this wavelength value in the presence of algae, shifting for example from 412 to 407 nm in light and 413 to 412 nm in dark from 0 to 6 hours), the total concentration of cyt C present in solution over time was estimated (figure 7). Although the peak was chosen as it gave the greatest sensitivity, as it only takes into account the oxidised form, some error can be assumed.

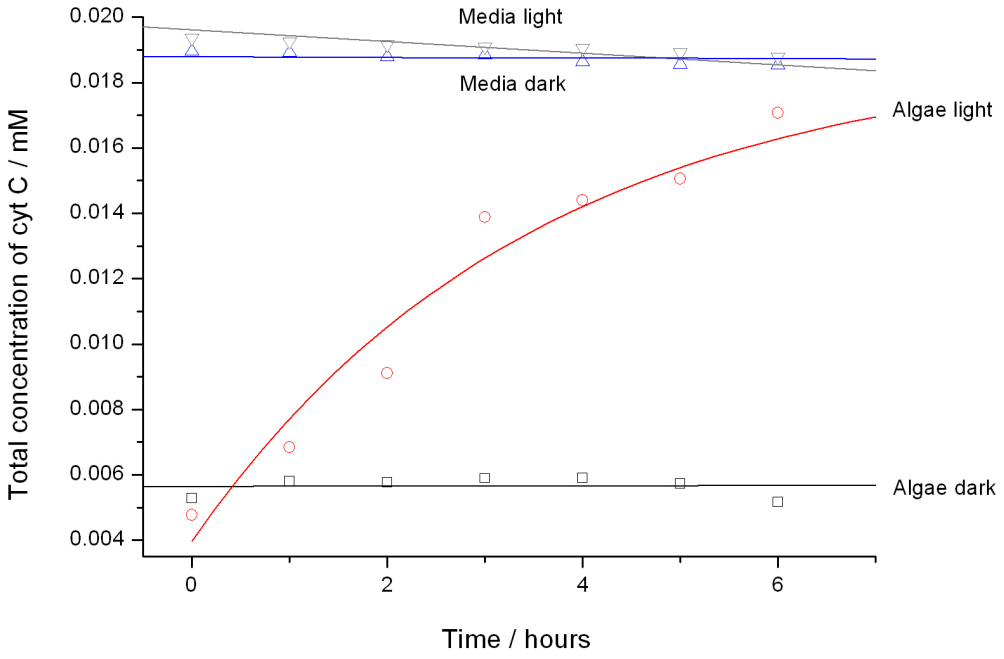


**Figure 7 Estimate of total amount of cyt C in solution, based on the peak at 409 nm exhibited in the oxidised form. NB This is just for use as an indication of total concentration, and does not take into account reduced or oxidised forms.**

As well as the decrease in free cyt C concentration on addition of the algae, it appeared as if cyt C was reduced in algal solutions; shown by the replacement of the peak at 530 nm with twin peaks at 521 nm and 550 nm. This inferred that electrons (for example from the photosynthetic electron transport chain and respiratory sources) were able to be donated to cyt C. These peaks increased in light, but remained constantly low in dark (absorbance given in figures 8 and 9 which respectively show the two main peaks indicative of reduced cyt C). Although this could signify cyt C becoming progressively reduced under illumination, it is more likely that the reduced concentration grew in light as it was progressively released by cells (figure 7). Reasons for differences in light and dark cyt C release were not known.

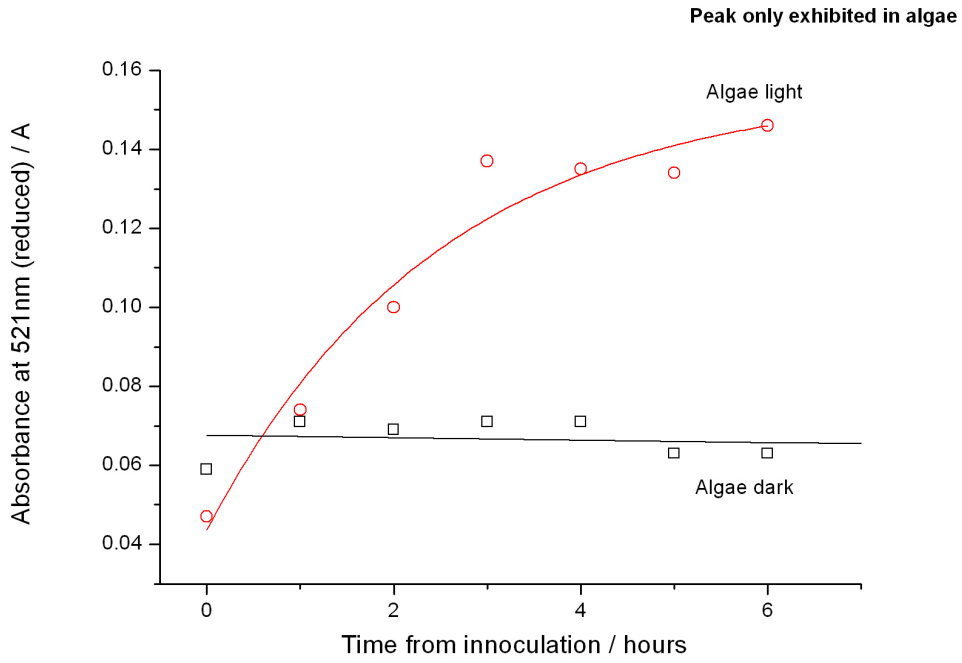


**Figure 8 Change in absorption at 521 nm (indicative of reduced cyt C) of 0.02 mM cyt C, when in solution with algae in light or dark**

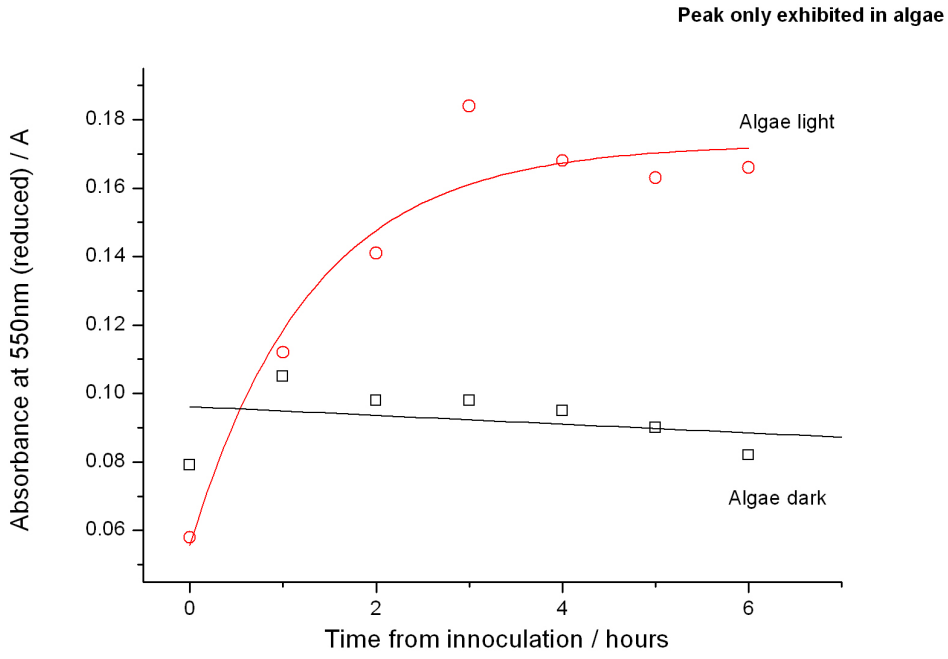


**Figure 9 Change in absorption at 550 nm (indicative of reduced cyt C) of 0.02 mM cyt C, when in solution with algae in light or dark**

In contrast, the media/cyt C solutions retained the broad peak at 530 nm characteristic of the oxidised species which was initially added. Over time this remained relatively stable in light and dark (figure 10).

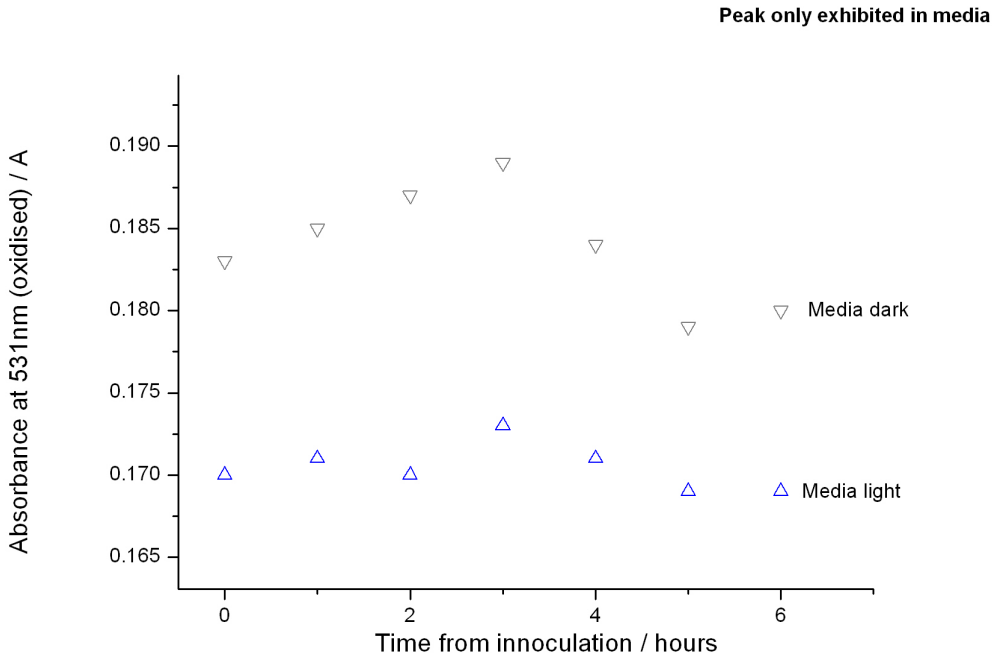


**Figure 10 Change in absorption at 531 nm of 0.02 mM cyt C, when in solution with media in light or dark**

As cyt C could be reduced by algae, it has potential in a p-MFC device as a mediator. However, as the solution concentration of cyt C was somehow reduced when in the presence of algae, its future use in a p-MFC device is unlikely.

### 7.32 Production of polyaniline ceramics

The redox polymer PANI was electrochemically deposited on FTO glass (for characterisation experiments), and on FTO coated $TiO_2$ porous electrodes (for device testing), using linear sweep voltammetry. Using this method, the PANI coating on the $TiO_2$ ceramics seemed homogenous and reproducible. Pictures of the typical substrates obtained are shown below in figure 11.

a)

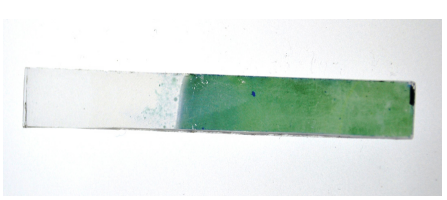

b)

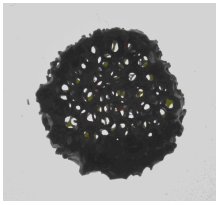

**Figure 11 a) PANI coated FTO coated glass, and b) PANI coated FTO $TiO_2$ ceramic**

### 7.33 Polyaniline Characterisation

The properties of the same PANI film on FTO glass, in first $H_2SO_4$ then 3N-BBM+V media (pH 6.4), were characterised by cyclic voltammetry, after soaking for 12 hours in each. It should be noted that the same film was used throughout the study.

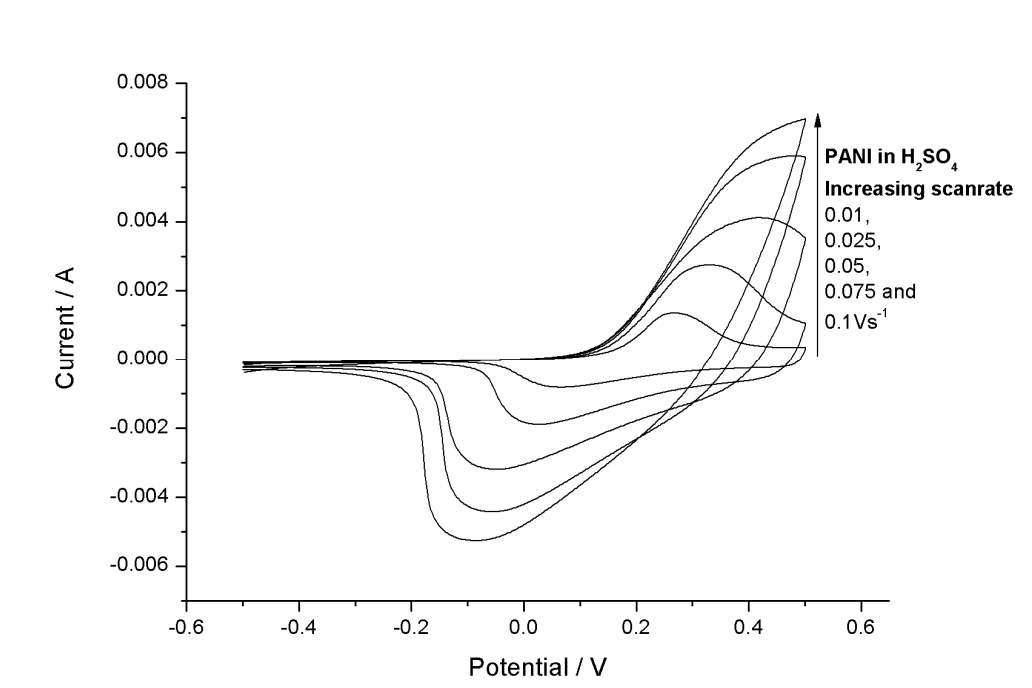


**Figure 12 Cyclic voltammetry at different scan rates w.r.t Ag/AgCl of PANI film of approximate area 2 $cm^2$ in 1 M $H_2SO_4$**

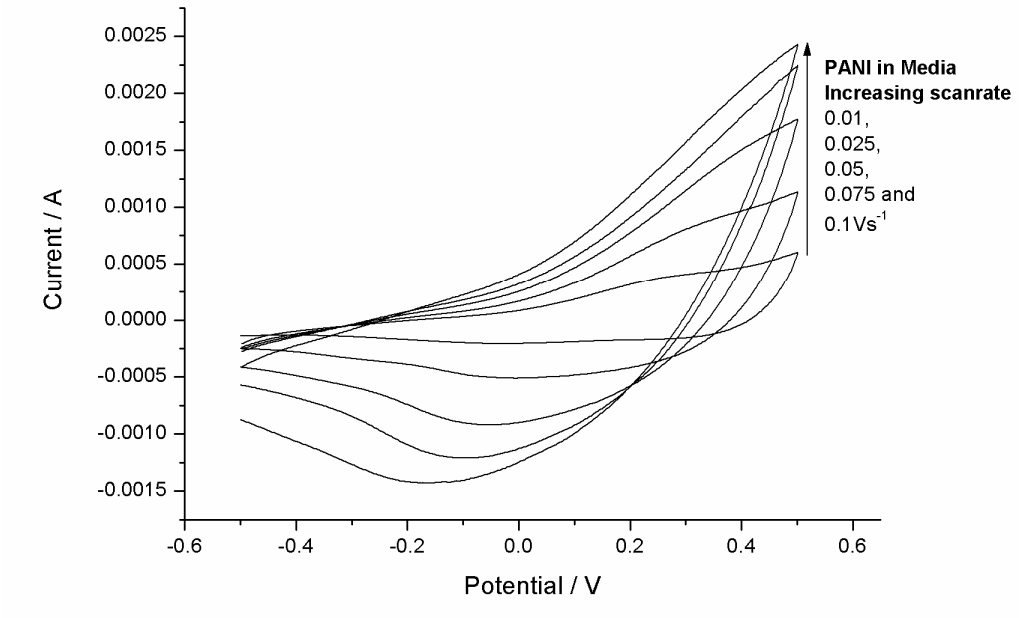


**Figure 13 Cyclic voltammetry at different scan rates w.r.t Ag/AgCl of PANI film of approximate area 2 $cm^2$ in algal media**

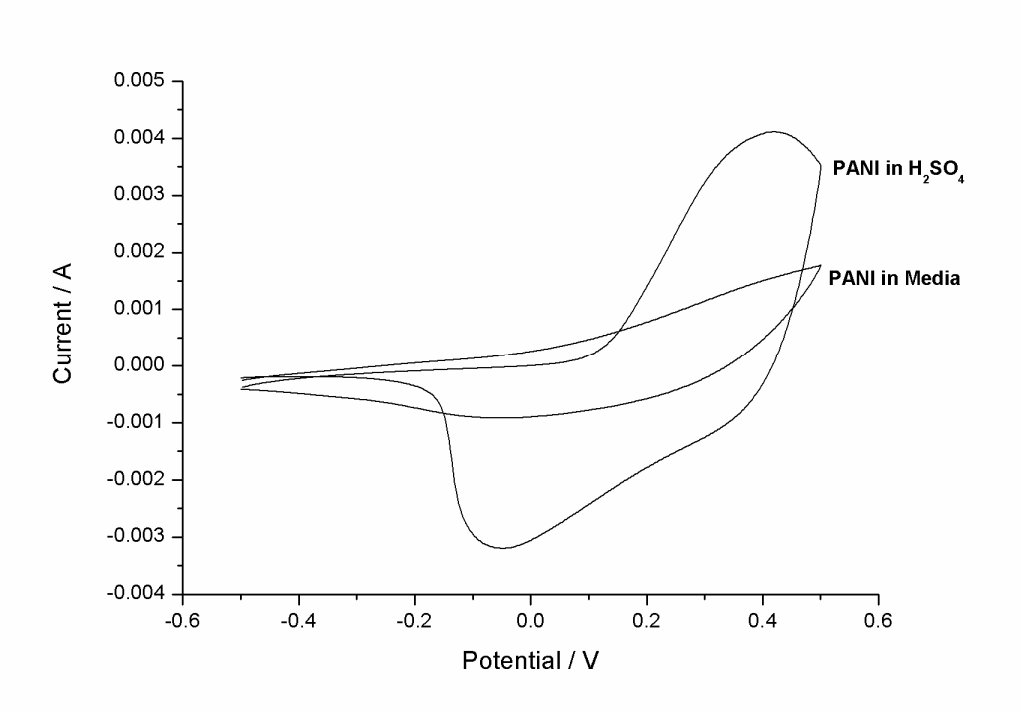


**Figure 14 Cyclic voltammetry w.r.t Ag/AgCl comparing PANI film of approximate area 2 $cm^2$ in 1 M $H_2SO_4$ or algal media, at 0.05 V $s^{-1}$ scanrate**

Figures 12, 13, and 14 show that the reversibility of the cyclic voltammograms changed depending on which solution the PANI has been soaked in. When the film was soaked in $H_2SO_4$, much more of the film could be oxidised and reduced compared to when it was soaked in media, as shown by the higher currents and more reversible peak. This has important implications for use in p-MFCs, where the electrolyte is media.

Impedance was used to study the electrical properties of the films in both $H_2SO_4$ and media, at oxidation and reduction potentials (as determined from cyclic voltammetry). It was found the PANI films in $H_2SO_4$ perfectly fitted to a DX Extended element (type 8; FSW Cap) model, confirming their polymer structure (figure 15).

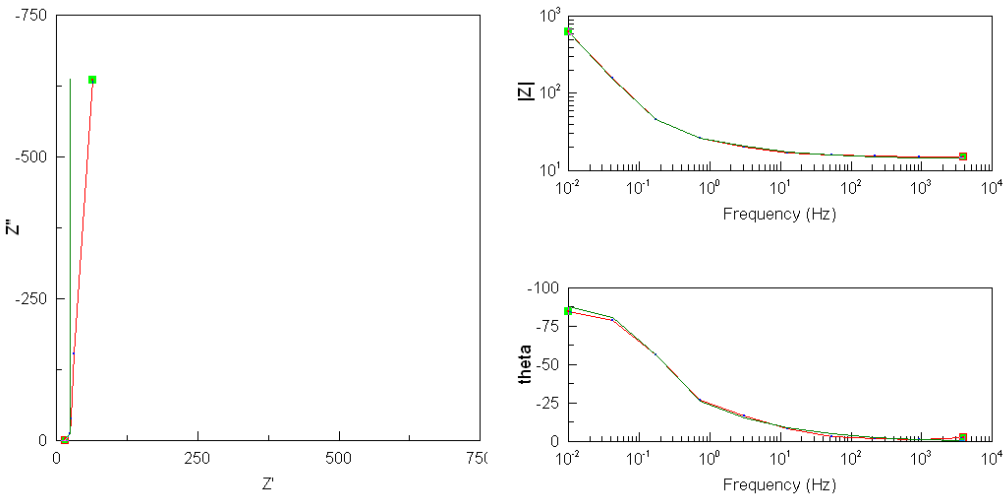


**Figure 15 Nyquist and Bode plots of PANI in $H_2SO_4$ at the oxidation potential, fitted to a distributed element. Experimental data is shown in red, with the fitting shown in green.**

Capacitance of the PANI films in $H_2SO_4$ was estimated at the oxidation and reduction potential values by studying the y intercept of admittance plots (data not shown). At the oxidation potential the film had an approximate chemical capacitance of 0.025 farads, compared to 0.00011 farads at the reduction potential. It was also determined that the reduced PANI film had a much greater resistance than the oxidised film, of approximately 3500 Ω. It was apparent the redox properties of PANI were very different when soaked in media than in $H_2SO_4$, with the apparent redox state in media under all potentials tested comparable (from Bode plots) to the reduced form exhibited in the $H_2SO_4$ (data not shown). Resistance of the films was also higher. At the oxidation potential, the resistance was approximately 50000 Ω, with a smaller resistance at the reduction potential of approximately 7500 Ω (data not shown). The greater resistance at the oxidation potential was unexpected, and is perhaps indicative of the films instability at this redox potential. PANI films soaked in algal solutions for 12 hours showed similar patterns to media alone, but with even higher resistance (data not shown). Impedance was carried out in light and dark, with no real differences found (data not shown).

PANI was additionally characterised with UV-Vis. UV-Vis spectra of the films were measured after a 12 hour soak in either 1 M $H_2SO_4$ or media, at reduction, oxidation and redox potentials as identified by cyclic voltammetry (figure 16). The same film was used for all measurements.

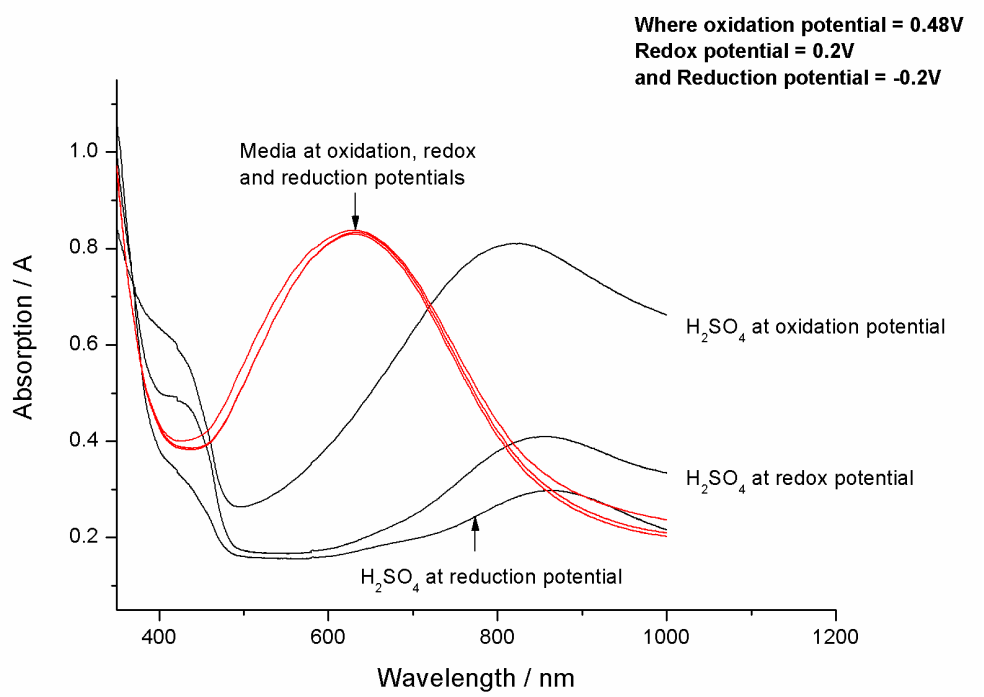


**Figure 16 UV-Vis of PANI film on glass FTO either in $H_2SO_4$ or algal media, at reduction, oxidation and half wave potentials**

When soaked in $H_2SO_4$, the increasing absorbance at 810 nm with increasing potential was indicative of the transition from leucoemeraldine to emeraldine salt [38]. This state is known to be acid doped and highly conducing, as corroborated by the impedance data. The fact that there was some absorbance, even below the reduction potential, inferred not all of the film was responsive. This could be due to thickness.

In media, the main absorbance at 620 nm correlated to that of emeraldine base. This was constant, even with a reduction potential applied to it. This form of PANI is neutral, and less conducting than when acid doped. Impedance studies confirmed the increased resistance when compared to PANI in acid. However, the impedance results showed PANI in media to be more similar to the reduced form in acid, rather than the oxidised form. Structurally, UV-Vis showed this was not the case. It was unknown why this discrepancy existed.

The decreased conductivity and redox activity of PANI films in media presented drawbacks for the long-term use of PANI as a tethered mediator in a p-MFC (where media would be used as an electrolyte for self-sustainable cell growth). It is possible

that the differences in PANI behaviour in media or $H_2SO_4$ were due to pH. The pH of the media was 6.4, and therefore contained less protons than $H_2SO_4$. The media also contained $Na^+/K^+$ ions, which could potentially react with oxidation sites of the PANI.

To determine biocompatibility, PANI coated FTO glass was cultured with the algal species *C. vulgaris*.

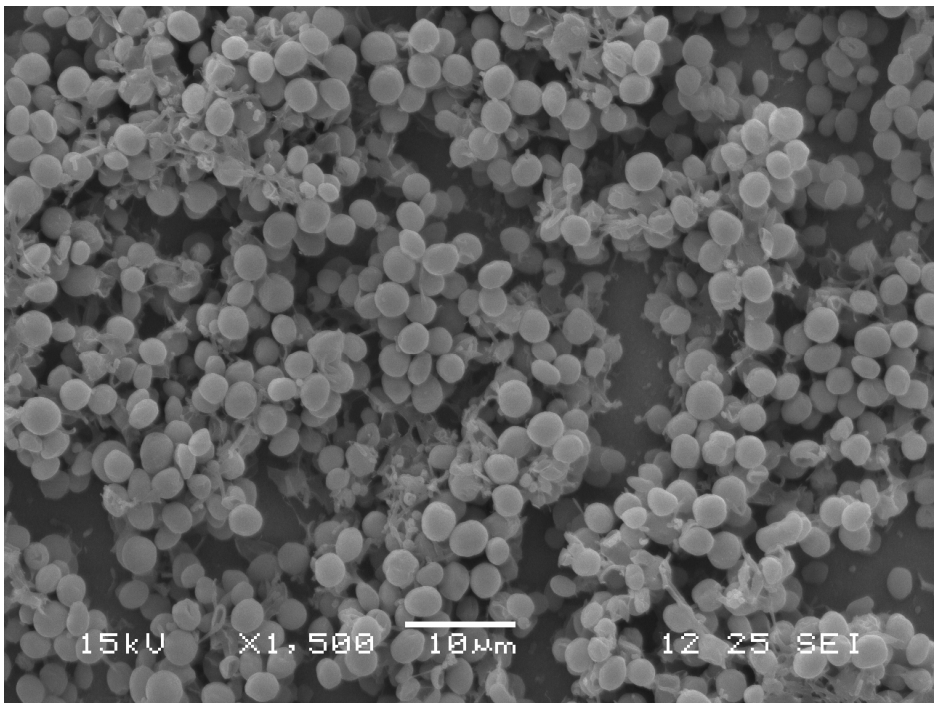


**Figure 17 *C. vulgaris* grown on PANI coated FTO glass**

As shown in figure 17, the PANI surface exhibited high biocompatibility towards *C. vulgaris*. A thick layer of cells was present, all excreting a healthy extracellular matrix. The biocompatibility of PANI was thought to be due to their positively charged structure, which is known to enhance adhesion of bacteria. The potential exists for much more work to be performed on tailoring materials for biofilm formation, for example, using a 'layer by layer' approach. However, this is outside the scope of this thesis.

### 7.34 Polyaniline Use in a Device

A ceramic coated in PANI was utilised in a device. Cyclic voltammetry was performed on the PANI ceramic before and after testing (24 hours apart – figure 18).

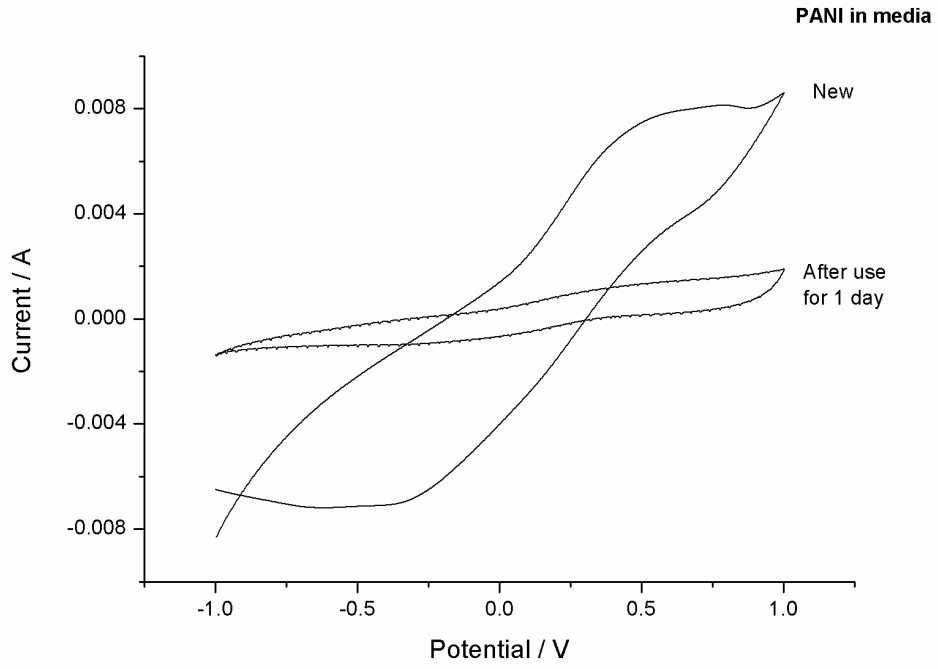


**Figure 18 Cyclic voltammetry at 100 mV $s^{-1}$ of PANI ceramic in device with KCl chamber and CEM in media w.r.t Ag/AgCl.**

As figure 18 shows, redox activity of the PANI electrode dropped considerably from when new, to when used. This correlates with findings from Zou *et al.,* [43], that their p-MFC using a PANI anode dropped in performance (when illuminated) by 60-80%, with the most substantial drop in performance of up to 50% occurring in the first week. Decline in performance of conductive polymer was one reason they suggested as an explanation, with others being gradual accumulation of dissolved oxygen in anodic chamber, an increase in pH that causes insufficient supply of protons to cathodic reaction or a depletion of BG-11 medium. Owing to the cyclic voltammetry and impedance results, it is likely that their loss of performance was due to higher resistivity of their polymer anode.

The p-MFC device was constructed with algal solution in its anodic chamber, and cyclic voltammetry was performed in light and dark (figure 19)

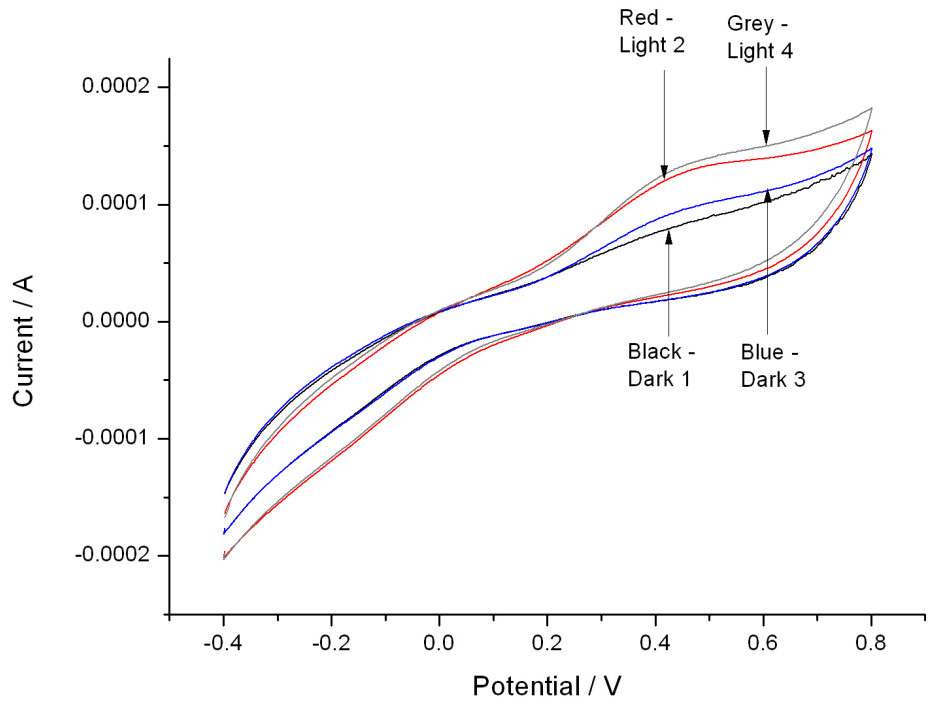


**Figure 19 Cyclic voltammetry of PANI ceramic in device, in *C. vulgaris* solution prepared at a concentration of $7x10^7$ cells $mL^{-1}$ in light and dark. p-MFC device was left to equilibrate to light/dark conditions for 10 minutes before each CV was measured. Potential w.r.t Ag/AgCl. Light intensity at 620nm with an intensity of $5x10^{-3}$ W $cm^{-2}$. The number reflects the order the scans were performed. No difference was observed between light and dark in media (data not shown)**

Figure 19 shows that in light with an algal solution, an increase in the oxidation peak magnitude of the PANI was seen with the first scan, which decreased upon subsequent scanning. This was highly repeatable, and was not seen with the media control (data not shown). This could mean that algae were reducing the PANI surface, meaning there was more to be re-oxidised when the potential was swept up.

From cyclic voltammetry the half wave of PANI was identified as approximately 0.1 V w.r.t Ag/AgCl, which was used for subsequent chronoamperometry measurements. Once stable, the p-MFC device was illuminated with a red light source of varying intensity, with results shown in figure 20. This was to determine if photocurrents were directly related to photosynthesis as postulated by Zou *et al.* [18, 43]

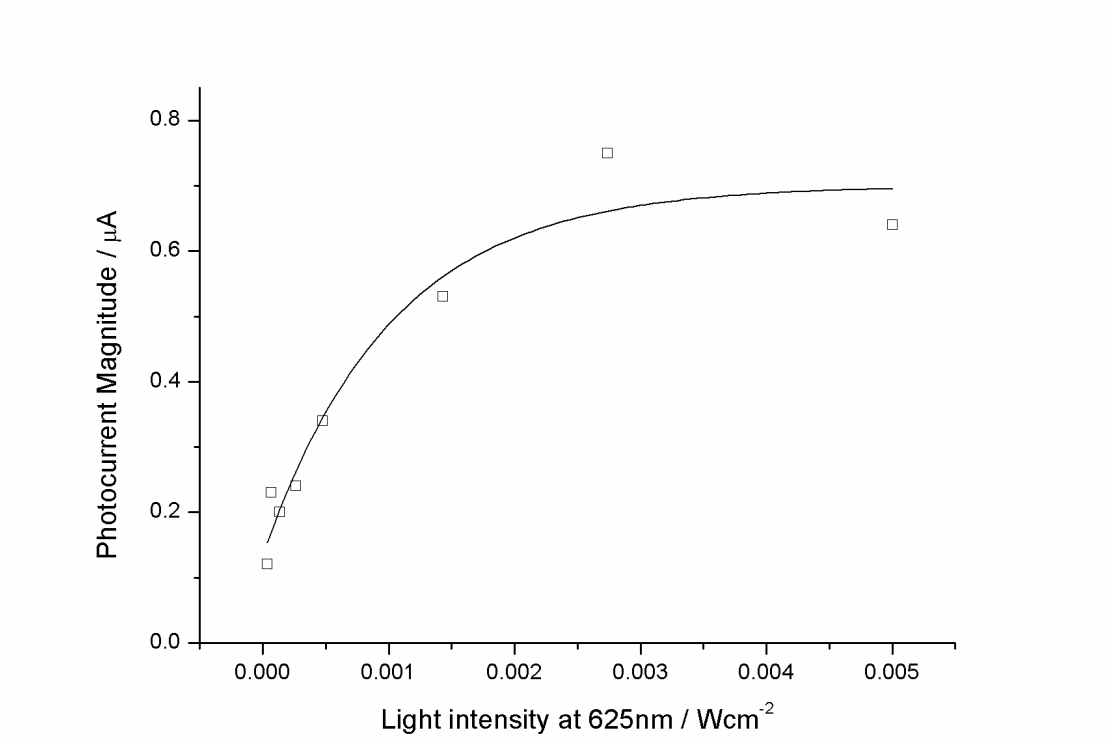


**Figure 20 Photocurrent magnitudes obtained from chronoamperometry measurements at half wave potential and different light intensities, using PANI ceramic device with *C. vulgaris* in solution in a 1 mL chamber, prepared at a concentration of $7x10^7$ cells $mL^{-1}$.**

Figure 20 shows that as the light intensity was increased, photo-current magnitude increased until it reached a reasonable stable current value of approximately 0.65 μA at illumination intensities higher than $1.5x10^{-3}$ W $cm^{-2}$. One possible explanation is with increasing light, the rate of photosynthesis increased as the chloroplasts absorbed more light energy. With increased photosynthesis, more electrons were produced by the photosynthetic transport chain. In a hypothesis by Zou *et al.*, due, electrons from the photosynthetic electron transport chain were thought to be directly accessed by the PANI, due to the interaction of the long chains of with cell membranes. Hence with increased light, increased photocurrents were gained. However, above a certain intensity of light, called photo-saturation, chloroplasts cease absorption of increasing energy to limit damage, potentially leading to the plateau of photocurrents at higher light intensities. An interesting feature was that at the lowest light intensity value tested, $5.2 x10^{-6}$ W $cm^{-2}$, a negative photocurrent of a large magnitude (-1.05 μA) was obtained (not shown on figure 28 for simplicity). This was hard to explain; it was possible that the algal cells themselves underwent different processes depending on the intensity of illumination supplied.

The p-MFC device was then set up with a biofilm cultured on the PANI anode. Chronoamperometry measurements were repeated at the half wave potential, with typical photocurrents shown in figure 27.

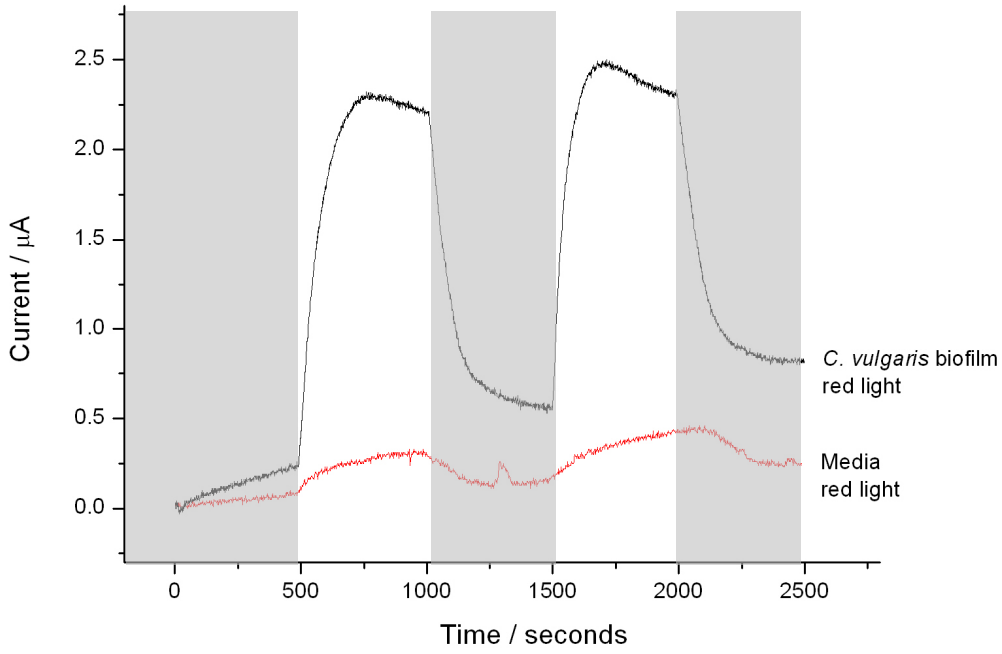


**Figure 21 Chronoamperometry at half wave potential of PANI ceramic p-MFC device with *C. vulgaris* biofilm ($1x10^9$ cells) or a media control. A red light was used for illumination at 620 nm with an intensity of $5x10^{-3}$ W $cm^{-2}$. Note that plots on graph are normalised to 0A. Before normalising, the dark current of each plot was approximately -1.5 µA**

Figures 21 shows the current obtained in dark and red light with and without a biofilm of *C. vulgaris* present on the PANI ceramic. Without an algal biofilm present (media control), a small increase in current was observed with light. However, with the algal biofilm, a much larger increase was observed with light, with currents rising sharply and stabilising at a plateau, before decreasing sharply again in darkness. These photocurrents were larger than those observed with planktonic algae in solutions, possibly due to the higher numbers of cells present ($1x10^9$ cells measured growing on the biofilm compared to $7x10^7$ cells $ml^{-1}$ in planktonic solution). The sharpness in rise and fall of photocurrents with illumination and dark periods is evidence for the photosynthetic source of electrons, as postulated by Zou *et al.* [18, 43]. However, it is hard to envisage how exactly PANI chains would be able to enter cells to interact with photosynthetic membranes, without being detrimental to cell health.

A p-MFC device was also set up containing the PANI anode with *C. vulgaris* biofilm without the proton exchange membrane (PEM). Chronoamperometry measurements were repeated, and under similar conditions to those used in figure 21, photocurrents of approximately the same magnitude and shape to those produced by a p-MFC device with a PEM membrane were observed (data not shown). This was thought possible due to the fact that both the PANI redox mediator and the algal biofilm were tethered to the anode surface, and so unable to interact with the cathode. The fact that a p-MFC device could be made without the PEM could have exciting implications for improving device efficiency. Internal cell resistance would be lowered, increasing $E_{cell}$ as calculated from equation 1 in chapter 3.

Another way used to measure the output of the device was to construct polarisation curves, as shown in figures 22 and 23 (p-MFC device with membrane in place and either a biofilm grown on the PANI anode or media control respectively). When polarisation curves were measured in the device using the polyaniline working electrode ceramic, it was apparent that the potential was constantly falling. This was attributed to the falling redox activity of the polyaniline film, as shown by cyclic voltammetry, which meant that polarisation curves recorded at different times could not be compared. This also explains the results of Zou *et al.,* [19], who achieved power densities of between 0.06 - 0.95 μW $cm^{-2}$ for biofilms grown on PANI or poly(pyrrole) coated electrodes but who also experienced similar issues with unstable falling potentials. The fact that the polarisation curves were changing constantly, and the fact that the actual surface area of the PANI coated ceramic was unknown, makes it difficult to compare results to this (and other) literature. If the surface area of the PANI ceramics was taken to be 7 $cm^2$, as calculated for the FTO coated ceramics in chapter 8, the power output was calculated to be 0.004 μW $cm^{-2}$ anode area. This was far lower than power densities achieved by Zou *et al.,* [19], although Zou *et al.* did not utilise single cultures and did not mention cell density. The falling redox activity and hence unstable potential makes the polyaniline ceramic an interesting concept, but not useable in a long-term p-MFC device.

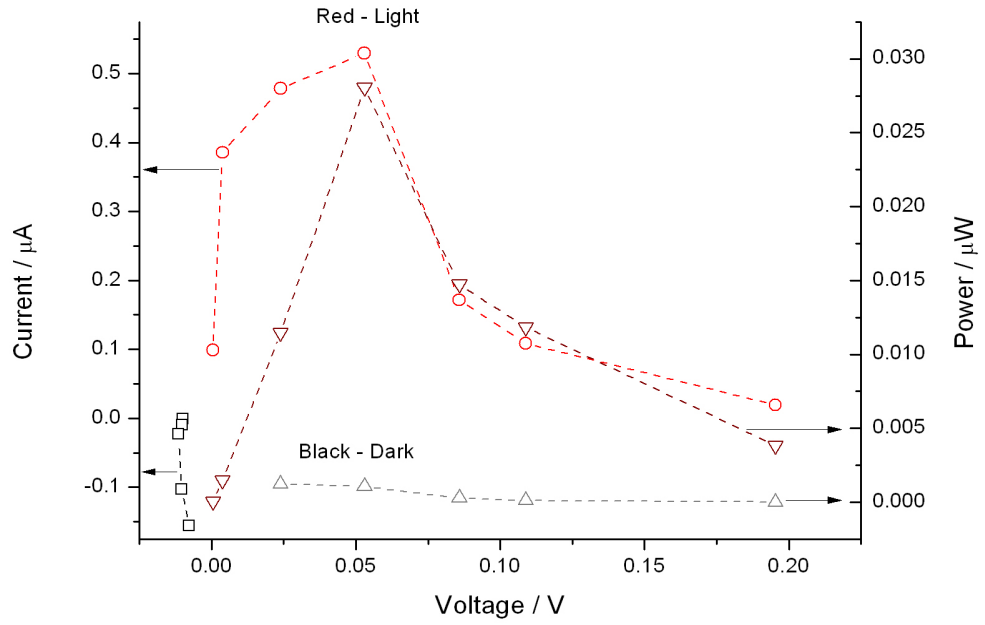


**Figure 22 Polarisation curves of PANI ceramic with a *C. vulgaris* biofilm containing approximately 1x10$^{9}$ cells, in light and dark. Light at 620 nm with an intensity of 5x10$^{-3}$ W cm$^{-2}$. Note that measurements were left for 10 minutes at each resistance point, with an hour between light (first experiment), and dark (second) measurements.**

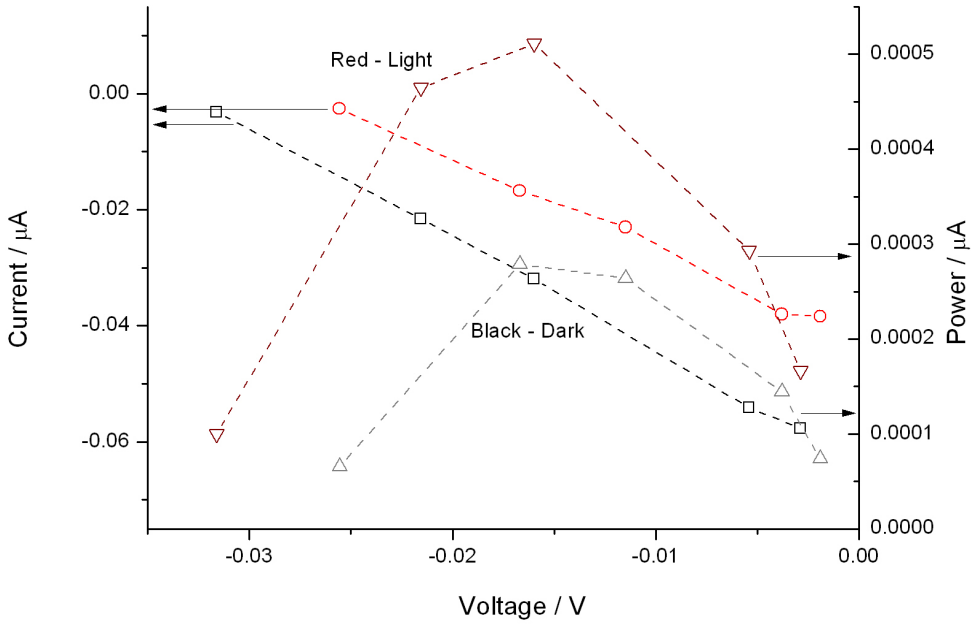


**Figure 23 Polarisation curves of PANI ceramic with no *C. vulgaris* cells present in light and dark. Light at 620 nm with an intensity of 5x10$^{-3}$ W cm$^{-2}$. Note that measurements were left for 10 minutes at each point, and taken one hour after experiments in figure 28. Light was tested first, then dark**

## 7.4 Conclusions

The natural redox mediator cyt C and the immobilised redox polymer PANI were tested for their interaction affinity with *C. vulgaris*. Although a p-MFC device would in theory be most efficient and self sustainable without the use of a redox mediator, as *C. vulgaris* and other algal/cyanobacterial species are not generally known to perform direct electron transfer, a redox mediator presented the only way to pass electrons to the anode. Finding a different redox mediator that, unlike the artificial compound ferricyanide, was biocompatible (for example, based on natural compounds or a tethered redox polymer) was extremely important for improving the efficiency of the basic p-MFC device.

Some interesting results were gained using cyt C in its oxidised form. It appeared as if the *C. vulgaris* immediately reduced this species upon contact. However, results inferred that the vast majority of cyt C in solution was somehow sequestered to the algal cell surface, before being released slowly over time in light. Due to the sequestering of cyt C, it would not be viable in a p-MFC device.

FTO coated ceramics were coated with the conductive redox polymer PANI using a simple method, which resulted in a stable and durable electrode. SEM and culturing studies of similar PANI coated FTO glass confirmed that the PANI surface was biocompatible towards the algae *C. vulgaris*. Electrical properties were tested through a variety of impedance and voltammetry methods. It was shown that upon soaking in media, rather than the $H_2SO_4$ used to make the films, redox performance dropped and resistivity increased. UV-Vis results showed that when soaked in media, the redox state did not change regardless of the potential applied to it, despite the presence of charge balancing counter ions (for example $Na^+$ and $K^+$). It is possible that the ions reacted with oxidised sites on the PANI surface.

When used as the working electrode in the device, it was shown that the PANI could act as a suitable electron acceptor for the electrons produced by the algae *C. vulgaris*. Cyclic voltammetry in light in an algal solution produced higher oxidation currents than when in the dark. Chronoamperometry measurements also showed far higher photocurrent magnitudes in light with algae in solution, than its media alone.

Interestingly, when photocurrent magnitudes over different light intensities were compared, as light intensity increased, photocurrents increased until a relatively stable value was produced. This was evidence for the source of photosynthetic electrons for power output. It has been suggested that PANI chains can inter-calculate with photosynthetic membranes within cells [18, 43], but it is unclear how this process would occur, and how cells would not be damaged. However, at very low light intensities, a negative photocurrent was produced, inferring a different cellular process was occurring.

However, despite the interesting and promising results, due to the fact that the PANI seemed to degrade constantly (as shown by the falling device voltage measured in polarisation curves), the PANI ceramic electrode has no place in the device in the long-term.

## 7.5 References


1. Rosenbaum, M. and Schröder, U., *Photomicrobial Solar and Fuel Cells.* Electroanalysis, 2010. **22**(7-8): p. 844-855.
2. Lovley, D.R., *Bug juice: harvesting electricity with microorganisms.* Nature Reviews Microbiology, 2006. **4**(7): p. 497-508.
3. Du, Z.W., Li, H.R., and Gu, T.Y., *A state of the art review on microbial fuel cells: A promising technology for wastewater treatment and bioenergy.* Biotechnology Advances, 2007. **25**: p. 464-482.
4. Ieropoulos, I.A., Greenman, J., Melhuish, C., and Hart, J., *Comparative study of three types of microbial fuel cell.* Enzyme and Microbial Technology, 2005. **37**(2): p. 238-245.
5. Katz, E., Shipway, A.N., and Wilner, I., *Handbook of Fuel-Cells-Fundamentals, Technology and Application*, ed. W. Vielstich, A. Lamm, and H.A. Gasteiger. 2003, Chichester: John Wiley & Sons, Ltd.
6. Schröder, U., Niessen, J., and Scholz, F., *A generation of microbial fuel cells with current outputs boosted by more than one order of magnitude.* Angewandte Chemie-International Edition, 2003. **42**(25): p. 2880-2883.
7. Newman, D.K. and Kolter, R., *A role for excreted quinones in extracellular electron transfer.* Nature, 2000. **405**(6782): p. 94-97.

8. Bond, D.R. and Lovley, D.R., *Evidence for involvement of an electron shuttle in electricity generation by Geothrix fermentans.* Applied and Environmental Microbiology, 2005. **71**(4): p. 2186-2189.
9. Nevin, K.P. and Lovley, D.R., *Mechanisms for Fe(III) oxide reduction in sedimentary environments.* Geomicrobiology Journal, 2002. **19**(2): p. 141-159.
10. Lovley, D.R., Phillips, E.J.P., and Lonergan, D.J., *Hydrogen and formate oxidation coupled to dissimilatory reduction of iron or manganese by Alteromonas putrefaciens.* Applied and Environmental Microbiology, 1989. **55**(3): p. 700-706.
11. Park, D.H. and Zeikus, J.G., *Electricity generation in microbial fuel cells using neutral red as an electronophore.* Applied and Environmental Microbiology, 2000. **66**(4): p. 1292-1297.
12. McKinlay, J.B. and Zeikus, J.G., *Extracellular iron reduction is mediated in part by neutral red and hydrogenase in Escherichia coli.* Applied and Environmental Microbiology, 2004. **70**(6): p. 3467-3474.
13. Aulenta, F., Catervi, A., Majone, M., Panero, S., Reale, P., and Rossetti, S., *Electron transfer from a solid-state electrode assisted by methyl viologen sustains efficient microbial reductive dechlorination of TCE.* Environmental Science & Technology, 2007. **41**(7): p. 2554-2559.
14. Allen, R.M. and Bennetto, H.P., *Microbial fuel cells - Electricity production from carbohydrates.* Applied Biochemistry and Biotechnology, 1993. **39**: p. 27-40.
15. Lee, S.A., Choi, Y., Jung, S.H., and Kim, S., *Effect of initial carbon sources on the electrochemical detection of glucose by Gluconobacter oxydans.* Bioelectrochemistry, 2002. **57**(2): p. 173-178.
16. Adachi, M., Shimomura, T., Komatsu, M., Yakuwa, H., and Miya, A., *A novel mediator-polymer-modified anode for microbial fuel cells.* Chemical Communications, 2008(17): p. 2055-2057.
17. Ricci, A., Rolli, C., Rothacher, S., Baraldo, L., Bonazzola, C., Calvo, E.J., Tognalli, N., and Fainstein, A., *Electron transfer at Au surfaces modified by tethered osmium bipyridine-pyridine complexes.* Journal of Solid State Electrochemistry, 2007. **11**(11): p. 1511-1520.

18. Zou, Y.J., Pisciotta, J., and Baskakov, I.V., *Nanostructured polypyrrole-coated anode for sun-powered microbial fuel cells.* Bioelectrochemistry, 2010. **79**(1): p. 50-56.
19. Zou, Y., Pisciotta, J., Billmyre, R.B., and Baskakov, I.V., *Photosynthetic microbial fuel cells with positive light response.* Biotechnology and Bioengineering, 2009. **104**(5): p. 939-946.
20. Park, D.H. and Zeikus, J.G., *Impact of electrode composition on electricity generation in a single-compartment fuel cell using Shewanella putrefaciens.* Applied Microbiology and Biotechnology, 2002. **59**(1): p. 58-61.
21. Park, D.H. and Zeikus, J.G., *Improved fuel cell and electrode designs for producing electricity from microbial degradation.* Biotechnology and Bioengineering, 2003. **81**(3): p. 348-355.
22. Tang, X., Du, Z., and Li, H., *Anodic electron shuttle mechanism based on 1-hydroxy-4-aminoanthraquinone in microbial fuel cells.* Electrochemistry Communications, 2010. **12**(8): p. 1140-1143.
23. Velasquez-Orta, S.B., Head, I.M., Curtis, T.P., Scott, K., Lloyd, J.R., and von Canstein, H., *The effect of flavin electron shuttles in microbial fuel cells current production.* Applied Microbiology and Biotechnology, 2010. **85**(5): p. 1373-1381.
24. Rabaey, K., Boon, N., Siciliano, S.D., Verhaege, M., and Verstraete, W., *Biofuel cells select for microbial consortia that self-mediate electron transfer.* Applied and Environmental Microbiology, 2004. **70**(9): p. 5373-5382.
25. Uchimiya, M. and Stone, A.T., *Reversible redox chemistry of quinones: Impact on biogeochemical cycles.* Chemosphere, 2009. **77**(4): p. 451-458.
26. Reguera, G., McCarthy, K.D., Mehta, T., Nicoll, J.S., Tuominen, M.T., and Lovley, D.R., *Extracellular electron transfer via microbial nanowires.* Nature, 2005. **435**(7045): p. 1098-1101.
27. Lovley, D.R., Holmes, D.E., and Nevin, K.P., *Dissimilatory Fe(III) and Mn(IV) reduction.* Advances in Microbial Physiology, Vol. 49, 2004. **49**: p. 219-286.
28. Greenman, J., Ieropoulos, I., and and Melhuish, C., *Perfusion anodophile biofilm electrodes and their potential for computing*, ed. A. Adamatzky and C. Teuscher. 2006.
29. Lovley, D.R., *Extracellular electron transfer: wires, capacitors, iron lungs, and more.* Geobiology, 2008. **6**(3): p. 225-231.

30. McLean, J.S., Wanger, G., Gorby, Y.A., Wainstein, M., McQuaid, J., Ishii, S.I., Bretschger, O., Beyenal, H., and Nealson, K.H., *Quantification of Electron Transfer Rates to a Solid Phase Electron Acceptor through the Stages of Biofilm Formation from Single Cells to Multicellular Communities.* Environmental Science & Technology, 2010. **44**(7): p. 2721-2727.
31. Pisciotta, J.M., Zou, Y., and Baskakov, I.V., *Light-Dependent Electrogenic Activity of Cyanobacteria.* Plos One, 2010. **5**(5).
32. Rinaldi, A., Mecheri, B., Garavaglia, V., Licoccia, S., Di Nardo, P., and Traversa, E., *Engineering materials and biology to boost performance of microbial fuel cells: a critical review.* Energy & Environmental Science, 2008. **1**(4): p. 417-429.
33. Pietron, J.J., Jones-Meehan, J., Little, B., Ray, R., and Ringeisen, B.R., *Polyaniline-coated high-surface-area carbon foams as anode materials in reagentless, aerobic, small-scale microbial fuel cells.* Abstracts of Papers American Chemical Society, 2005. **230**: p. U1680.
34. Scott, K., Rimbu, G.A., Katuri, K.P., Prasad, K.K., and Head, I.M., *Application of modified carbon anodes in microbial fuel cells.* Process Safety and Environmental Protection, 2007. **85**(B5): p. 481-488.
35. Zhang, L.J. and Wan, M.X., *Synthesis and characterization of self-assembled polyaniline nanotubes doped with D-10-camphorsulfonic acid.* Nanotechnology, 2002. **13**(6): p. 750-755.
36. Cheng, S. and Logan, B.E., *Ammonia treatment of carbon cloth anodes to enhance power generation of microbial fuel cells.* Electrochemistry Communications, 2007. **9**(3): p. 492-496.
37. Rosenbaum, M., Schröder, U., and Scholz, F., *In situ electrooxidation of photobiological hydrogen in a photobioelectrochemical fuel cell based on Rhodobacter sphaeroides.* Environmental Science & Technology, 2005. **39**(16): p. 6328-6333.
38. Nanotechnology, O.-O.M. *Technical data - Polyaniline UV-vis-spectra*. 1995; Available from: http://www2.zipperling.de/Products/PAni/datenbla/uvvis_e.html.
39. Nyholm, L. and Peter, L.M., *Wide pH range microelectrode study of the electrochemical behaviour of polyaniline films in buffered solutions.* Journal of the Chemical Society-Faraday Transactions, 1994. **90**(1): p. 149-154.

40. Shi, L.A., Richardson, D.J., Wang, Z.M., Kerisit, S.N., Rosso, K.M., Zachara, J.M., and Fredrickson, J.K., *The roles of outer membrane cytochromes of Shewanella and Geobacter in extracellular electron transfer.* Environmental Microbiology Reports, 2009. **1**(4): p. 220-227.

41. Takeda, T., Sonoyama, T., Takayama, S.I.J., Mita, H., Yamamoto, Y., and Sambong, Y., *Correlation between the Stability and Redox Potential of Three Homologous Cytochromes c from Two Thermophiles and One Mesophile.* Bioscience Biotechnology and Biochemistry, 2009. **73**(2): p. 366-371.

42. Butt, W.D. and Keilin, D., *Absorption spectra and some other properties of cytochrome C and of its compounds with ligands.* Proceedings of the Royal Society of London Series B-Biological Sciences, 1962. **156**(965): p. 429-&.

43. Zou, Y.J., Pisciotta, J., Billmyre, R.B., and Baskakov, I.V., *Photosynthetic Microbial Fuel Cells With Positive Light Response.* Biotechnology and Bioengineering, 2009. **104**(5): p. 939-946.

# Chapter 8. Development and Testing of New Porous Anode

# Chapter 8 - Development of new porous anode

## 8.1 Introduction

Despite the benefits of MFC and p-MFCs as an energy source, technology has not been sufficiently optimised for these systems to operate as large scale applications [1]. A critical factor for optimum operation has been identified as the anodic microorganism population and its interaction with the electrode surface [2, 3]. Improving the anode material to optimise interactions with the microorganisms would improve the efficiency of a p-MFC device, and also its long term operation capacity. In the basic p-MFC device the anode is a piece of indium tin oxide (ITO) with the algae suspended in a filter paper matrix. This offers no long term operation capacity for the p-MFC device as a whole. As such, this chapter investigates the scope for development of a new p-MFC anode material; crucial for improving long term operation capacity and device efficiency.

At present graphite, in forms such as carbon felt, or planar ITO coated glass are popularly used as the anodic material in MFCs, as they can produce large current outputs [1]. Although several new electrode materials have been explored, such as Au and stainless steel anodes, MFC devices using these exhibited low current densities [1, 4]. For reason, and the fact that carbon materials are cheap, robust and have high surface areas on which bacteria can proliferate, carbon materials are still the most common anode material used in MFCs [5]. Recently a range of carbon based anodes were studied (including carbon veil and papers) showing them to develop large amounts of efficient biofilm growth, and when used as anodic material, an efficient MFCs output was produced [6]. Precious metal coatings such as Pt have also been shown to increase the current density of graphite electrodes [1, 7]. Some bacteria have been shown to transfer electrons directly to electrodes [1, 8, 9]. Direct electron transfer is thought to be protein mediated, possibly via cytochromes in the extra cellular matrix (ECM) or bacterial conductive nanowires [10].

p-MFCs containing a range of anode materials have also been reported. As p-MFCs are largely based on MFC studies, carbon materials including graphite felt, carbon cloth and carbon paint have frequently been used as anode materials [11-13]. However, carbon has

several drawbacks when used in p-MFCs, primarily because it is a dense black material and light can only penetrate into the first layer of the photosynthetic biofilm. As a result the majority of the internal surface area is wasted. In addition there have not been many studies into the growth of algal/ cyanobacterial biofilms directly onto carbon felt materials so it is not known if the micro-organisms form healthy biofilms in these materials. Consequently, as Zou *et al.* point out [14], a new three-dimensional porous material is required for p-MFCs to yield higher energy per unit area anode.

Several new materials have already been explored as the anode material for p-MFCs. Indium and fluorine doped tin oxides (ITO and FTO respectively) have been tested [15], which although having the advantage of being highly transparent, lack the high internal surface area of a porous material. This is one of the issues with the basic p-MFC device tested in chapter 3. Electron transfer from cyanobacteria to electrodes coated in conducting polymers such as polyaniline (PANI) and polypyrrole has been reported [16-18], although it is not clear if direct electron transfer to the polymer occurred, or whether the polymer acted as a catalyst to oxidise redox products produced by the micro-organisms. PANI anodes present issues when used in a p-MFC device as shown in chapter 6. Consequently, no newly investigated materials fulfil the requirements for a p-MFC anode material. Required properties of a p-MFC anode include high porosity and/or photo transparency for increased light transmittance/scattering, high conductivity, durability, and most importantly possess some strategy to immobilise cells.

Although many artificial routes have been taken to immobilise cells [19], for longevity, natural routes are preferred. Indirect attachment of cells relies on the natural tendency of many types of microalgae to attach to surfaces and grow on them through the production of extra-cellular polymers (EPS). This produces biofilms, which are completely self sustainable communities that can grow on sediments in a range of environments [20]. When cells are grown on an electrode surface, long term, high efficiency operation of any kind of MFC or p-MFC would be achieved due to enhanced electron transfer to the electrode, orientation of the components relative to the electrode surface and the stabilisation of protein complexes [21]. Cell death would also be reduced as the formation of micro-colonies increases tolerance to toxic

substances [22]. Importantly for p-MFCs, dense biofilms of photosynthetic organisms has been shown to result in the highest rates of photosynthesis [14].

For biofilms to grow on an anode, the anode should satisfy a number of criteria. It should be mechanically and chemically resistant, inert to surroundings and microalgae, nontoxic, photo transparent, and be biocompatible. Adhesion of cells is complex, and can be related to topography and hydrophobicity. Sekar [23] studied the adhesion of *Chlorella vulgaris* and other algal species, and found attachment was higher on rough compared to smooth surfaces, which was corroborated by other research groups [24]. It was thought that rough surfaces could provide increased surface area and convection of nutrients [25], with a greater number of micro-refuges for protection from hydro-dynamic forces [26] The attachment point theory also states that microalga larger than the scale of micro texture have reduced adhesion due to fewer attachment points existing. [27]. Additionally, physico-chemical parameters of the algae and the substratum are believed to contribute to adhesion, with many studies finding adhesion is mainly mediated by hydrophobic interactions [28]. An explanation for this could be that the higher attachment on hydrophobic surfaces is mediated by the water exclusion mechanism [23]; in hydrophilic substrata water is poorly excluded resulting in less attachment.

Substrate materials can be natural or synthetic. Natural carrier materials (such as Loofa sponges) have proved successful as a substrate for biofilm growth [29-31], although problems have often arisen due to lack of structural reproducibility. To overcome these problems, synthetic materials have been widely used for biofilm growth. For example, ceramics such as Biolite® [32] or standard ceramic plates [[33, 34] have been used previously to grow algae biofilms. Other types of ceramics used to immobilise different types of cells include calcium phosphate and aluminium oxide [35]. These have been developed into synthetic bone substitutes that promote bone formation by osteoconduction, and upon which bone marrow cells can be grown [35]. Features such as high pore interconnectivity allows high permeability of fluids and gases through the porous structure (shown in figure 1), allowing nutrients to reach the cells, and waste products to be removed [36].

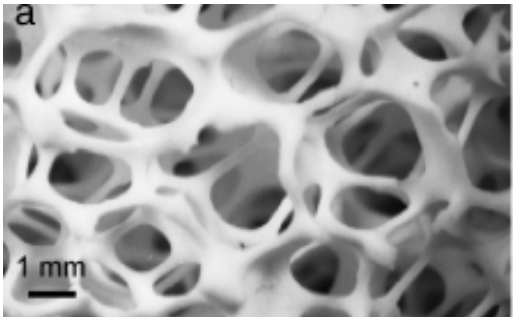


**Figure 1 Reproduced from [36] Microstructure of alumina based open cell structure obtained using polyurethane foam templates with the replica technique**

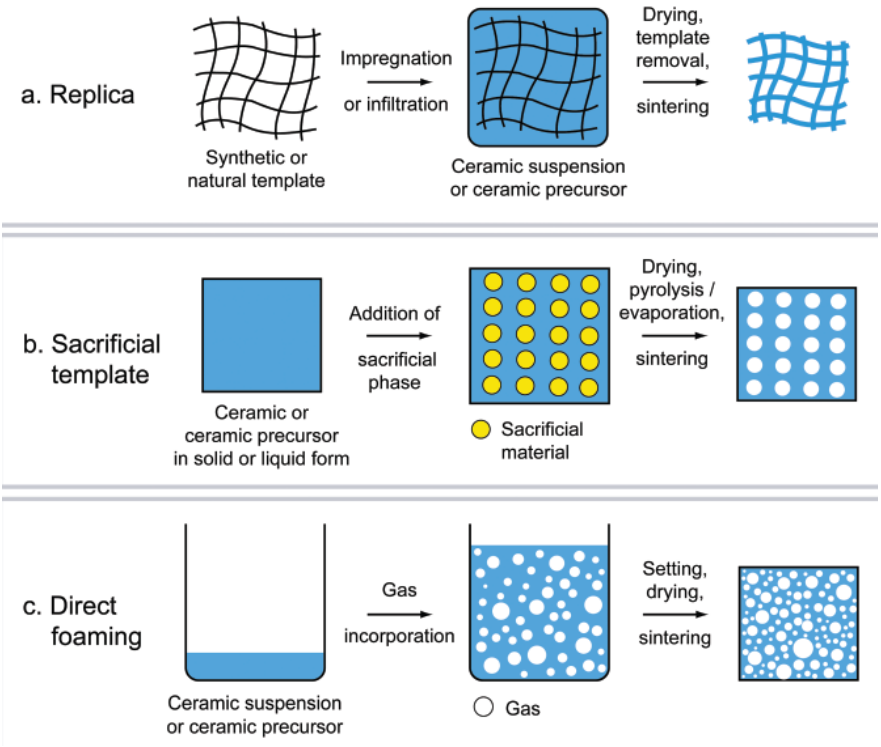


**Figure 2 Reproduced from [37]. The main routes to produce macroporous ceramics; replica, sacrificial template and direct foaming**

The macroporous alumina ceramics shown in figure 1 were produced using a replica method using the synthetic material polyurethane as a template. The replica method, along with the other routes to producing macroporous ceramics, is outlined in figure 2, and is considered the simplest method for macroporous ceramic production [37]. The replica method is based on the impregnation of a structure using a ceramic suspension, in order to produce a macroporous ceramic exhibiting the same morphology as the original porous material. Porous ceramics obtained through the sponge replica

method can reach total open porosity levels within the range 40 %-95 % and are characterised by a reticulated structure of highly interconnected pores with sizes between 200 μm and 3 mm [37].

### 8.11 Chapter Aims

The ITO anode used in the basic p-MFC device is not ideal, in part due to the lack of high surface area for *C. vulgaris* cells to proliferate on. Consequently, in this chapter, the preparation of macroporous ceramic electrodes (and their characterisation) is reported as a replacement material. Although the present use of these types of ceramics is for the growth of bone marrow cell biofilms, it is thought their properties would also make them ideal for use as the base material for the anode in a p-MFC. The ceramics have pores of tailorable size, allowing algae to grow within the pores with adequate nutrient diffusion to and from cells. The high porosity of the ceramics would allow light to scatter through, and it is hoped that enough of the other conditions would be satisfied to make them biocompatible.

The ceramic substrates produced in this chapter are composed of titanium dioxide, with the surface coated by a thin layer of FTO to make them conducting for use as an anode. In this chapter, ceramics are characterised structurally, electrically and for biocompatibility. For the latter, *C. vulgaris* is used as a model organism, with results compared to other commonly used p-MFC anode materials including carbon felt and planar FTO materials. PANI ceramics made in chapter 7 are also compared.

Finally, the assembly and testing (with polarisation curves) of a p-MFC device utilising the FTO coated ceramic electrodes is reported. Polarisation curves were used rather than chronoamperometry measurements as they measure the p-MFC under more steady state conditions and mean no external potential is required to be applied to the anode. p-MFC outputs can also be more easily compared to those recorded in the literature, as most previous studies use the technique.

## 8.2 Experimental

### 8.21 Making the ceramic matrix

Macroporous titanium dioxide ceramics were produced via a replication process that

utilised polyurethane (PU) foam as a template material. This has proven a highly effective route for producing ceramics with well interconnected porosity, at relatively low cost [38]. Cylinders of reticulated PU foam ('RR20', 2.3 – 3.3 mm typical pore size, Sydney Heath & Sons, UK) of dimensions 15 x 15 x 7.5 mm were coated in a thixotropic ceramic slip. The slip was prepared using commercial $TiO_2$ powder (0.3 μm mean particle size, 99.5 % pure, Pi-kem, UK) incorporated into distilled water with binders, plasticisers and surfactants (PVP, PVA and Dispex A40, respectively), shown in table 1. Using this particle size (not nanostructured) meant no photochemistry which could potentially be disruptive to algal cells grown on the sintered ceramics would be seen. In order to avoid agglomeration and provide the desired rheology, the slurry was ball milled with zirconia grinding media for 24 hours. The slip was then used to coat the PU foams. After coating, excess slip was removed from the pores using high velocity compressed air. To improve the stability of the ceramic, an extra layer of $TiO_2$ slip was applied to the sides of the cylinder. The coated foam was left to dry for 24 hours at ambient temperature before sintering in a muffle furnace. The furnace was heated at 1 ˚C $min^{-1}$ and held for 1 hour at 600 $^{o}$C to burn out the PU template, then heated at 2˚C $min^{-1}$ to 1300 ˚C for 4 hours to sinter the ceramic.

To improve electrical conduction, the ceramics were coated with a thin layer of FTO by chemical vapour deposition (Solaronix SA). This is a technique used to deposit thin films onto a substrate, which involves precursors in the vapour phase undergoing a series of chemical reactions [39]. Precursors were first evaporated and transported into the main gas flow, whereupon chemical reactions produced reactive intermediates and gaseous by products. Reactants were then transported to the substrate surface and adsorbed. After diffusion over the surface, nucleation and surface chemical reactions led to solid film formation. Desorption and mass transport allowed remaining fragments to leave the reaction zone.

To obtain a uniform coating of the ceramics, the carrier gas was flowed through the pores and the individual specimens rotated half way through the deposition to ensure both faces of the cylinder were covered. An equivalent deposition on a flat glass substrate resulted in a sheet resistance of 10 Ω square.

| Component | Amount (g or mL) |
|---|---|
| Distilled Water | 125 mL |
| Dispex GA40 | 2.5 mL |
| PVP | 1.5 g |
| PEG 400 | 3 g |
| Methyl Cellulose | 1.5 g |
| PVA | 3 g |
| $TiO_2$ | 300 g |
| Milling Media | 64 g |

**Table 1 Standard ceramic slip recipe, sintered according to standard procedure – Ramp to 600 ˚C at 1 ˚C $min^{-1}$, Hold 1 hour, Ramp to 1300 ˚C at 2 ˚C $min^{-1}$, Hold 4 hours, Ramp to 25 ˚C at 2 ˚C $min^{-1}$**

## 8.22 Other Electrode materials

Untreated carbon felt electrodes were obtained from le Carbone UK Ltd. and (with the exception of sterilization) used as received. FTO glass electrodes were made from TEC 8 Pilkington glass. PANI films were obtained using the method in chapter 6.

### 8.23 Biocompatibility of electrodes

To grow a biofilm on the electrode surfaces, sterilised electrodes were placed in a sterile culture of *C. vulgaris* for 45 days. The only exception was biofilm growth on FTO glass electrodes, agitation prevented attachment of a film to the surface, so the films were grown under static conditions (all culturing procedures outlined in the appendix). After 45 days in the culture medium the electrodes were removed and the total algal loading was measured in two ways. Firstly the cells were removed by sequential vortexing in media and counted using a haemocytometer. Secondly the chlorophyll content was extracted with methanol and quantified by UV-Vis spectrophotometry. In the case of electrochemical measurements, the electrodes were removed from the culture solution and rinsed gently in fresh media before use. Biofilms were grown ex-situ to the p-MFCs as the p-MFC flow dynamics varied in the presence of the each anode materials and could have lead to anomalies in biofilm growth. It was decided that biofilm growth in conical flasks containing identical inoculants and kept under constant agitation would give more comparable results. Although cells grown under load form different biofilms, the main aim of this study

was to investigate the biocompatibility of the various materials and to study the viability of the algae grown on the different electrode surfaces.

Images of biofilms on the electrode surfaces were obtained on a JEOL JSM-6480LV Scanning Electron Microscope (SEM). Before imaging the biofilms were fixed chemically by placing them in a 2.5 % glutaraldehyde solution. They were then post-fixed in 1 % Osmium Tetrachloride for 1 hour. Finally the samples were dehydrated in acetone and air dried.

**8.24 Characterisation of ceramics**

Electrochemistry (cyclic voltammetry and impedance spectroscopy) was carried out on an Autolab PGSTAT 12 with a built-in frequency response analyser. The surface area was estimated by comparing cyclic voltammograms from -0.7 to 0.7 V w.r.t Ag/AgCl of 1 mM potassium ferricyanide (ferricyanide) in 0.1 M KCl of different electrodes, and calculating the background subtracted areas under the oxidation peaks [40]. The total charge passed at the electrodes with known surface areas was then used to estimate the surface areas of the ceramic and carbon felt electrodes. The active surface area of the FTO ceramics was also estimated by measuring the double layer capacitance of the ceramic and comparing it to that of flat pieces of FTO produced using the same deposition technique that had a known surface area. Similarly the internal area of the carbon electrodes was estimated by measuring the double layer capacitance for the carbon felt and comparing it to the capacitance of a glassy carbon electrode of known surface area. Series resistances for the electrodes were measured by impedance spectroscopy in 0.1 M KCl. The contact angle of a 100 µl droplet of deionised water was also measured on the surface of flat FTO coated glass (taken as representative of the FTO coated ceramic), carbon paper and PANI coated glass as a measure of hydrophilicity/ hydrophobicity. Carbon paper was tested as it was difficult to measure the contact angle of carbon felt due to its irregular surface.

Further characterisation was performed on the ceramics. Samples of both un-sintered and sintered $TiO_2$ were tested by XRD diffraction to determine crystal structure. Uncoated and coated ceramics were also imaged in an SEM. Strength tests were performed by crushing the $TiO_2$ ceramics in a vice under a 50 kN load cell, and recording the movement and pressure of the test cell to give the first major break.

The stress experienced by the ceramics was calculated according to equation 1, and strain calculated according to equation 2.

$$\tau = \omega / A$$

**Equation 1 Calculation of stress ($\tau$ in MPa), where ω is the load (N) and A is the area ($mm^2$)**

$$\varepsilon = \frac{\Delta \ell}{\ell_o} \times 100$$

**Equation 2 Calculation of stress ($\varepsilon$ in %), where $\ell_o$ is the original sample length (mm), $\Delta \ell$ is the displacement (mm)**

### 8.25 Assembly of p-MFC device using FTO coated ceramic as anode

A p-MFC device was assembled with the fabricated FTO coated ceramic electrode as the anode. In this system, the p-MFCs consisted of a cylindrical chamber (1.7 (Ø) x 1 cm) into which the ceramic anode fitted. The bottom of the chamber was clamped to a piece of nafion coated activated carbon cloth that acted as the cathode (Nafion membrane 115 heat sealed to FM 10 activated carbon cloth, Chemviron Carbon Ltd). The electrolyte contained 2.5 mM ferricyanide and 2.5 mM ferrocyanide prepared in fresh 3N-BBN+V media. Even though only the oxidised mediator, ferricyanide, acted to accept electrons from the algae, a 50:50 mixture of oxidised: reduced mediator was used to allow the cell to come to equilibrium more quickly at open circuit and to reduce the background currents.

Devices contained algae either in solution, at a concentration of 3.2 μg $ml^{-1}$, or grown on the surface of the ceramic electrodes (as outlined in the appendix for 17 days). Results were compared to a p-MFC device utilising a flat FTO electrode (approximating to the ITO used in the basic p-MFC device tested in chapter 3) and the carbon felt popularly used in other p-MFC devices. For the FTO electrode, biofilms were grown over 11 days. The FTO electrode was cultured for a shorter time than the other materials as, although an algal mat grew on the surface, it became increasingly fragile with increasing thickness. Films left for 17 days tended to fall away from the surface when touched. A schematic of a device is shown in figure 3. It should be noted that PANI films were assembled and tested in a p-MFC device in chapter 7. Device performance

could not be directly compared to the materials in this chapter as PANI p-MFC devices do not use a ferricyanide mediator.

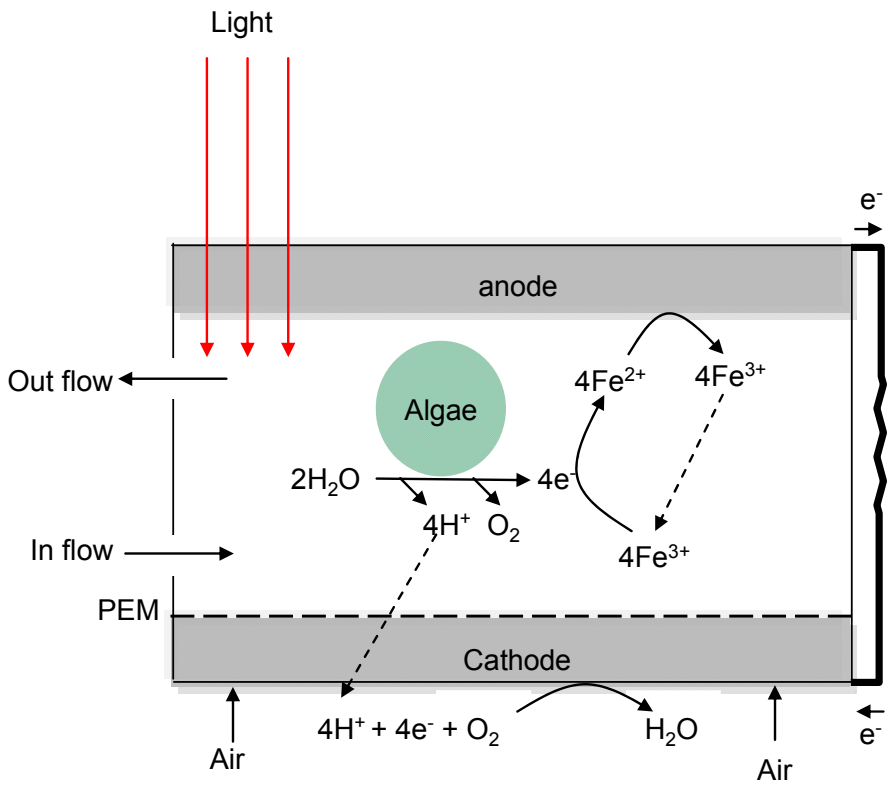


**Figure 3 Schematic of assembled flow cell device, where the anode was either a FTO coated ceramic, flat FTO coated glass or carbon felt, and algae were either planktonic or in a biofilm.**

To measure polarisation curves the voltage was measured across a range of resistors that were varied between 10 MΩ and 1 KΩ, the voltage readings were all taken ten minutes after each resistance was chosen and the data was logged using a pico data logger ADC-24. All polarisation curves were measured under the same constant flow conditions (0.35 mL $min^{-1}$) and under low monochromatic light illumination (12 W $m^{-2}$ at 652 nm). Polarisation curves were thought a better way of measuring p-MFC device output as they gave the device longer times to reach equilibrium than the chronoamperometry measurements used in chapter 3. Flowing conditions were also utilised (*i.e.* the p-MFC device was a flow cell), as they allowed a system to be developed that would not develop localised concentration changes. This meant that measurements would be more stable and reproducible, and the p-MFC device would be under similar conditions utilised for long term operation (ie. algal waste products transported away and fresh media transported in). From the polarisation curves, power output was calculated, and the resistance of the cell giving maximum power for operation could be determined.

## 8.3 Results and Discussion

### 8.31 Ceramic matrix produced

Figures 4 a) b) and c) show the ceramics produced using the replica method. Figure 4a) shows a typical FTO coated ceramic electrode, whilst figure 4b) shows the flexibility of design and scale achievable with the method. Figure 4c) shows the millimetre size pores obtained. The ceramizing foam method allowed the preparation of electrodes of any size and shape. While all initial studies were carried out with small cylindrical electrodes, 7.5 mm thick (as in figure 4a), square electrodes were also produced for use in flow cells (for a colleague's project). The size of the ceramic could also be varied by using different poly(urethane) foam supports. Electrodes with small (10 PPI), medium (20PPI) and large (30PPI) pores were prepared and contrasted (where PPI is pores per inch). The algal loadings in all three types of electrode were similar after 45 days (data not shown) and it was decided to focus on the samples with medium sized pores that gave the best compromise between strength and surface area.

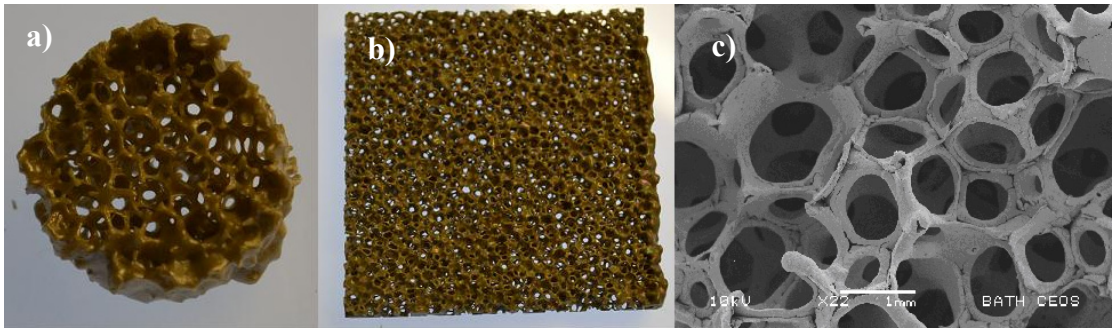


**Figure 4 Images of ceramic made with medium (20PPI) pore size PU foam a) Typical FTO coated ceramic electrode with dimensions 15 x 7.5 mm b) A larger FTO coated ceramic electrode of dimensions 48 x 48 x 7.5 mm. The flexibility of foam templating is that electrodes of almost any size and shape can be prepared. c) A close up of the pore structure.**

### 8.32 Biocompatibility of electrodes

The biocompatibility of the ceramic electrodes was investigated by comparing algal biofilm growth after 45 days on FTO coated ceramic (figure 5), uncoated ceramic, PANI coated ceramic and carbon felt. Cells were removed by sequential vortexing and counted using a haemocytometer before chlorophyll extraction and quantification.

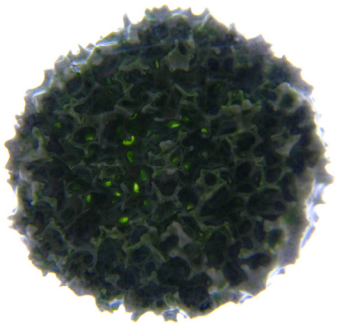

**Figure 5 FTO coated ceramic after culturing in *C. vulgaris***

Figure 6 shows the algal loading as a function of internal surface area (determined in section 8.33). Interestingly the lowest algal loading was observed for the FTO coated sample. Both uncoated ceramic and PANI coated ceramic appeared to be slightly better at promoting biofilm growth. The number of algae growing inside the carbon felt was comparable to the number in the FTO ceramic. In all cases the algae preferred growing inside the electrode to remaining in a planktonic state in the solution; evidenced by much higher algal concentrations measured inside the material compared to free in the supernatant (data not shown).

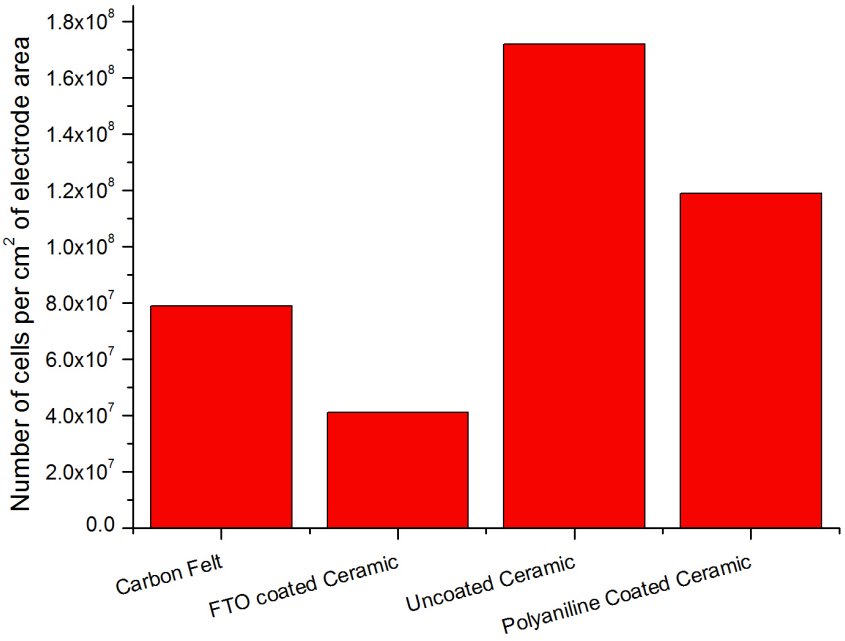


**Figure 6 Cell loadings in a variety of anode materials after culturing in *C. vulgaris* for 45 days**

Untreated fibrous carbon materials are frequently used as anode materials in MFCs and the microbes have been shown to form dense biofilms around the fibres [6].

Despite this and the relatively high loadings in figure 5, carbon felt did not appear to be an ideal matrix for *C. vulgaris*. SEM showed the carbon fibres to be sparsely populated with distorted cells and no extensive extra cellular matrix (ECM) formed (figure 7a). The algae seemed to congregate inside the material but not to attach to the carbon surface. The reason for this was unknown.

In contrast the algae growing on the FTO coated ceramic appeared to form healthy colonies on the surface (figure 7b). The biofilms grown on FTO ceramics showed a fibrous ECM, with fibres directly anchored to the electrode surface. The biofilms on the surface of planar FTO coated glass have been imaged, as shown in figure 7c. The ECM of the biofilms on the FTO glass was quite different to that on the ceramic and showed a much less fibrous and more two dimensional structure. Although dense colonies of algae were seen, they were very poorly attached to the surface. Biofilms were extremely fragile, as shown by the fact that if disturbed, cells came away from the substrate. This makes FTO glass as an anode in long term p-MFC devices not a viable option. Figure 8 shows a single algal cell attached to the FTO ceramic via its ECM. This suggested that the FTO coated ceramic may be a good long term electrode material in p-MFCs and also explained why the biofilms grown on the ceramic attached more strongly than those grown on flat FTO glass. In addition, if algal or cyanobacterial strains capable of direct protein mediated electron transfer to electrodes are discovered, the porous FTO may be useful if the ECM of these strains can also directly attach to the electrode surface.

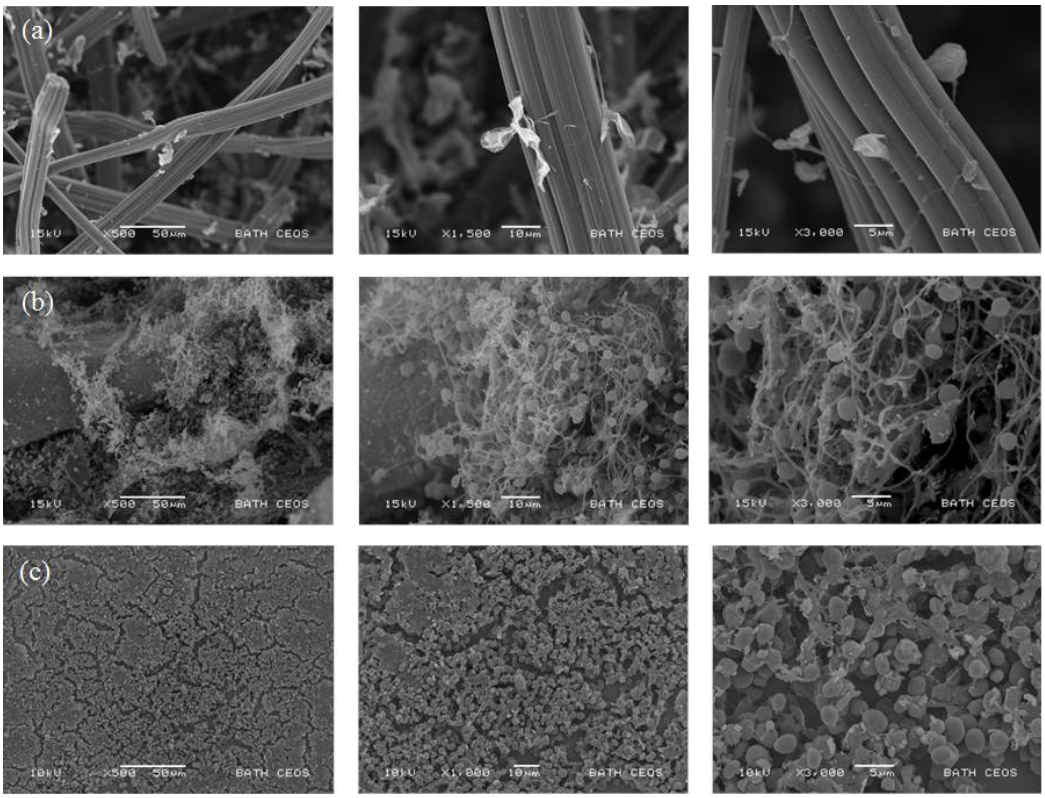


**Figure 7 Left to right shows images at increasing magnification, in all cases the scale bars are 50 µm, 10 µm and 5 µm respectively. a) Images of algae growing on carbon felt. b) algae growing on an FTO ceramic electrode. c) algae growing on flat FTO coated glass.**

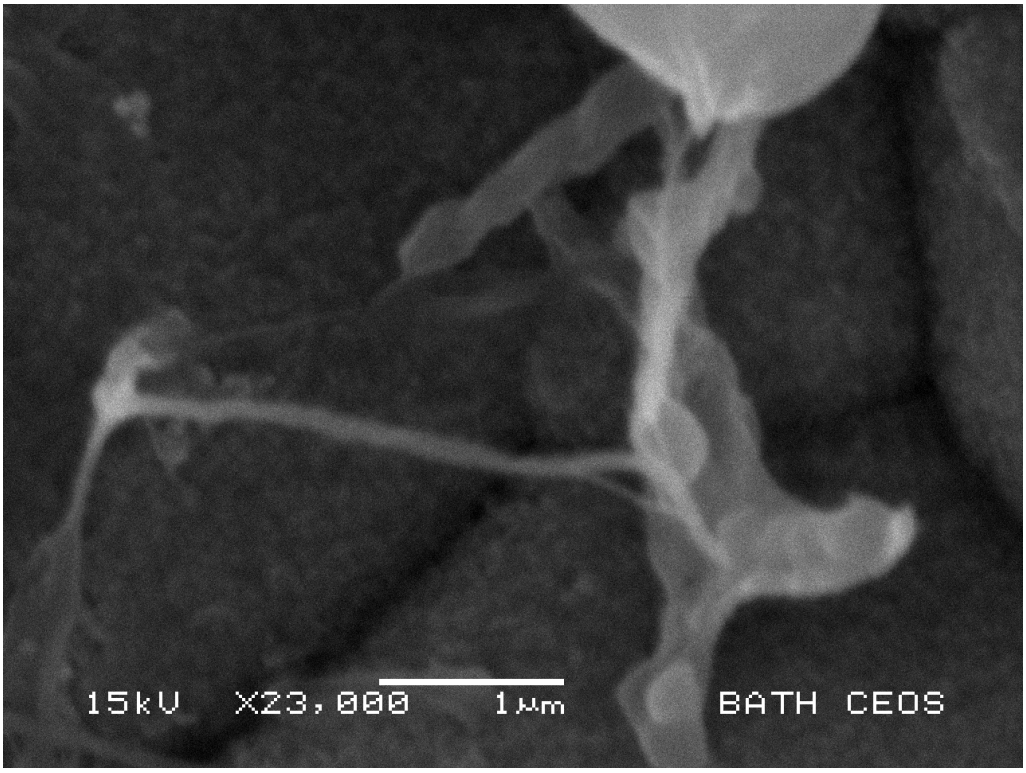


**Figure 8 A close up of the algal ECM on an FTO ceramic, showing direct attachment of the matrix to the FTO surface.**

### 8.33 Characterisation

SEM was performed on the surface of FTO and non FTO coated $TiO_2$ ceramics. Figures 9a) and b). show the uncoated ceramic surface, which appeared quite smooth on the micrometre length scale used. The scale bars are 5 μm and 1 μm respectively. Figures 9c). and d) show the $TiO_2$ ceramic coated with a layer of FTO, with a nanostructured surface. Again the scale bars are 5 μm and 1 μm respectively. Some larger crystalline aggregates were found, in addition to the nanostructured FTO surface that stretched between the aggregates.

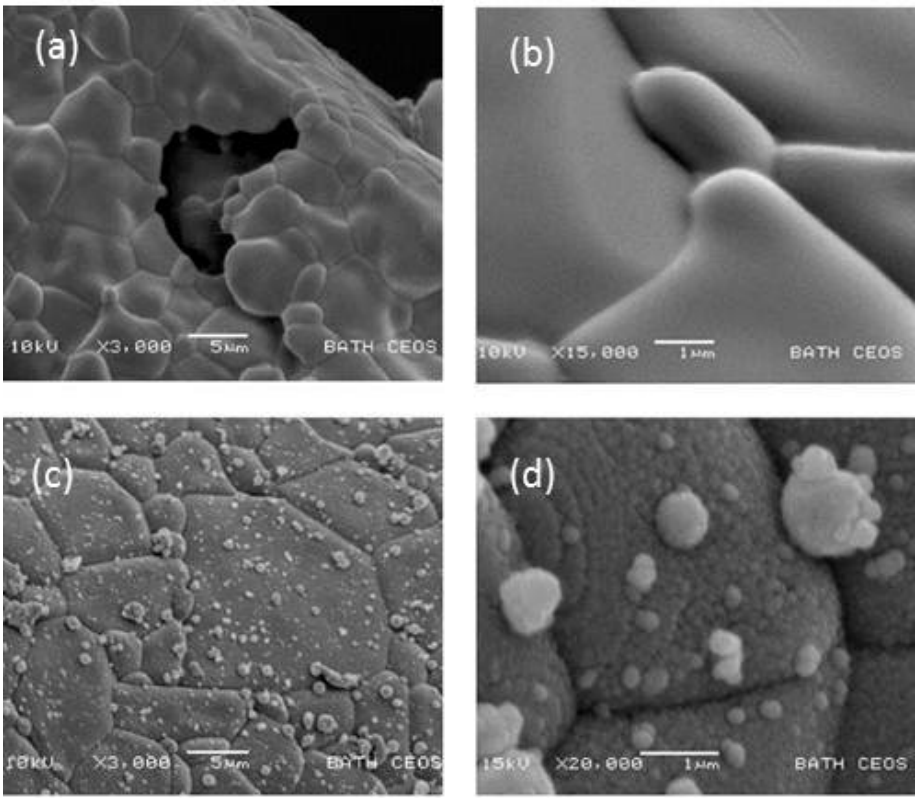


**Figure 9a) and b) SEM images of the surface of uncoated $TiO_2$,; c) The surface of $TiO_2$ ceramic after it had been coated with a layer of FTO by CVD; d.)The nanocrystalline FTO film that stretched between the larger crystalline aggregates**

The sheet resistance of FTO films grown on flat glass using the same deposition conditions was 10 Ω square. The FTO coated ceramics were confirmed to have similar conductivities by impedance spectroscopy which gave series resistances of approximately 10 Ω.

Contact angle measurements were made of PANI coated FTO glass and FTO coated glass. It was impossible to perform contact angle measurements on the various

ceramics due to their irregular shape, but they could be considered analogous to the respectively coated glass. It was also difficult to perform measurements on carbon felt, due to its diffuse boundary when studied with the camera used to record contact angle results. Instead, a similar form of carbon, carbon paper was utilised. Results, shown in figure 10, give the order of hydrophobicity as carbon paper; FTO glass; PANI. In the culturing study described previous which tested for biocompatibility, materials were ranked (in order of cell concentration per $cm^2$); PANI ceramic, Carbon felt, FTO ceramic. Consequently, no direct variation can be seen between these variables.

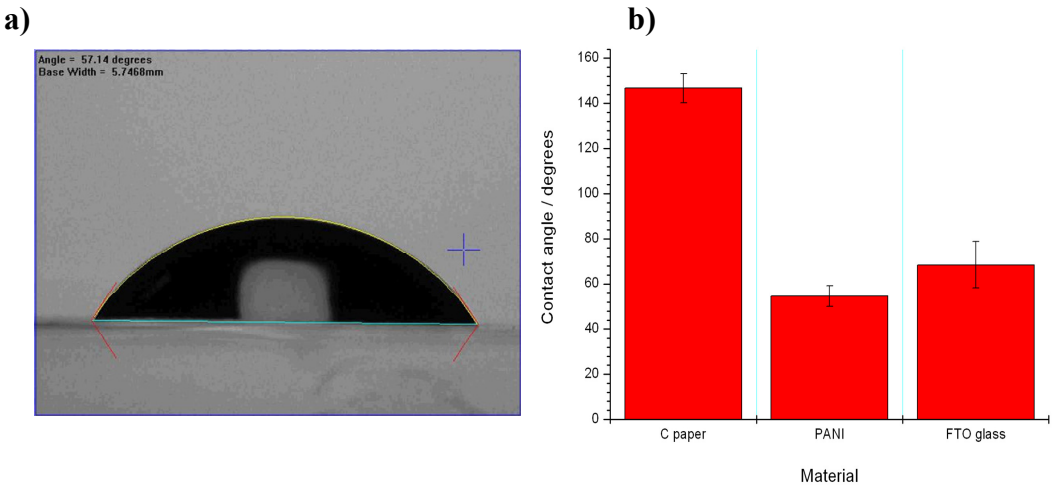


**Figure 10 a) An example of a contact angle measurement on FTO glass using a 100 µl droplet of water b) Summary of contact angle of 100 µl droplets of water onto C paper, PANI and FTO glass. Error bars show one standard deviation (n=6)**

Surface area of electrodes was estimated by comparing cyclic voltammograms of ferricyanide at flat carbon and flat FTO electrodes (both with known surface area) to CVs of carbon felt and ceramic electrodes (data not shown). Additionally, the active surface area of the FTO ceramics was calculated by measuring the double layer capacitance of the ceramic and comparing it to that of flat pieces of FTO of known surface area. After averaging, the 1.5 (Ø) x 0.75 cm ceramics were found to have internal surface areas of between 7 and 8.5 $cm^2$

XRD experiments compared both the $TiO_2$ powder and sintered sample to a rutile standard. Figure 11 shows that the peaks found in both samples exactly matched the standard, confirming both were in rutile form.

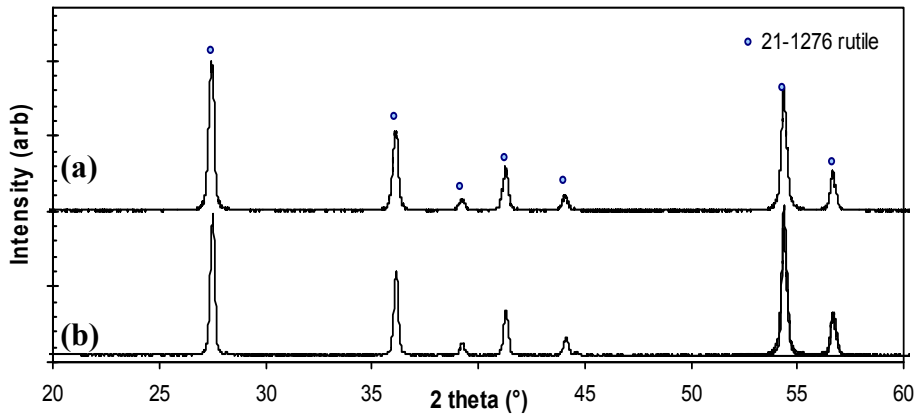


**Figure 11 XRD results comparing a) sintered sample and b) $TiO_2$ powder used to a rutile standard (blue points)**

Strength testing (typical results in figure 12, and summary results in figure 13) showed that the ceramic could withstand approximately 3.5 MPa before first major breakage, depending on density. Density increased with higher ceramic loadings. Although beneficial for strength, this resulted in smaller surface area and pore size. The value of 3.5 Mpa before breakage is a reasonable standard for a porous ceramic, showing ceramics to be reasonably robust.

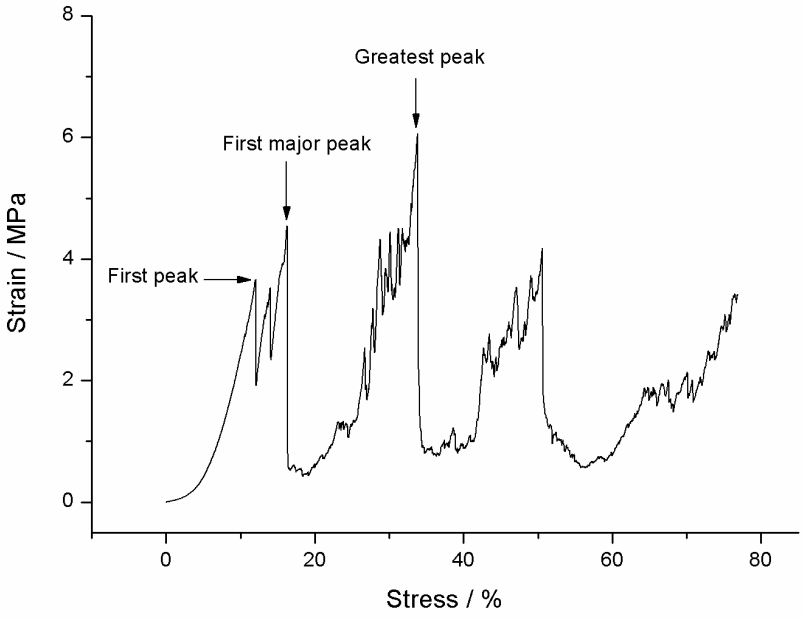


**Figure 12 Typical measurements of stress and strain. As stress was applied, strain increased until breakage. The figure shows the various ways breakage strain can be measured; either to first breakage, first major breakage or greatest breakage (breakage measured as strain release)**

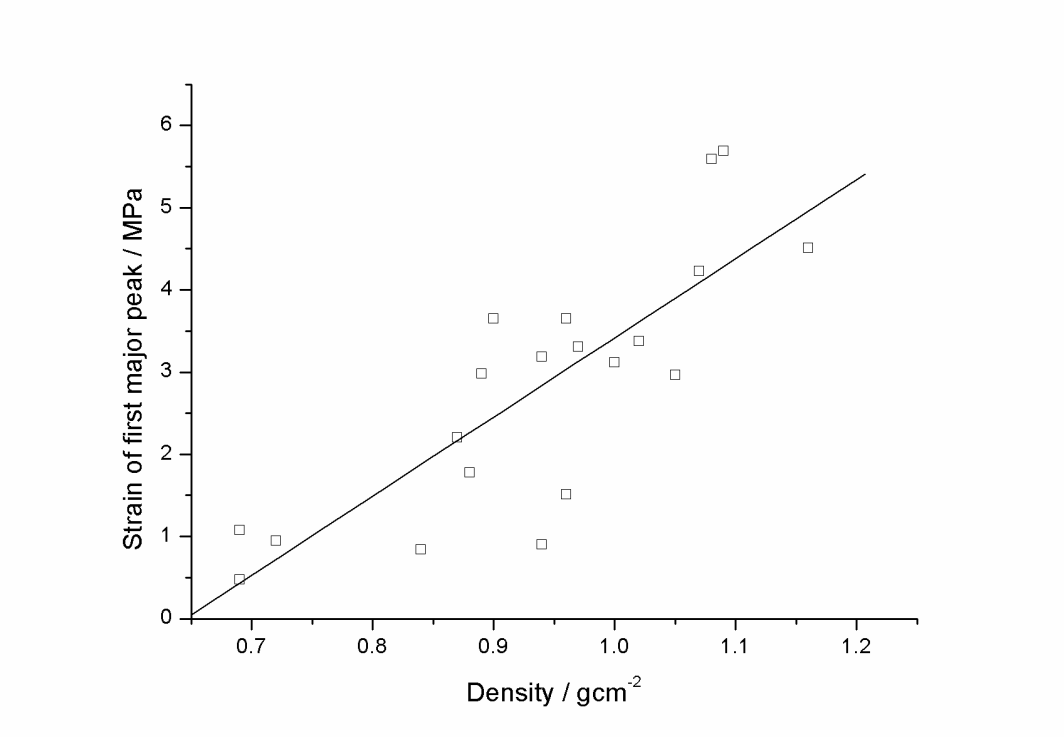


**Figure 13 Summary data of strain applied to ceramic before first major breakage VS density**

## 8.34 Testing of device

Ceramic anodes were investigated in complete p-MFC devices and compared to flat FTO glass anodes and carbon felt anodes. The electrolyte of the p-MFC device contained 2.5 mM ferricyanide and 2.5 mM ferrocyanide (a 50:50 mixture was added to allow the p-MFC to come to equilibrium at open circuit more quickly.) Polarisation curves were measured for p-MFCs with *C. vulgaris* biofilms on ceramic anodes (figure 14a) and biofilms on FTO glass anodes (figure 14b). For comparison polarisation curves have been shown for the ceramic in the presence of planktonic algae (figure 14c). Finally curves are also shown for biofilms on the FTO ceramic and FTO glass anodes in the absence of the 2.5 mM ferricyanide: 2.5 mM ferrocyanide redox mediator (figure 14d). Polarisation curves for the carbon felt were also measured, but as outputs were so low, the data is not shown. All measurements were carried out under illumination from monochromatic light (12 W $m^{-2}$ at 652 nm), and outputs are quoted as current density per $cm^2$ of actual anode surface area to directly compare materials.

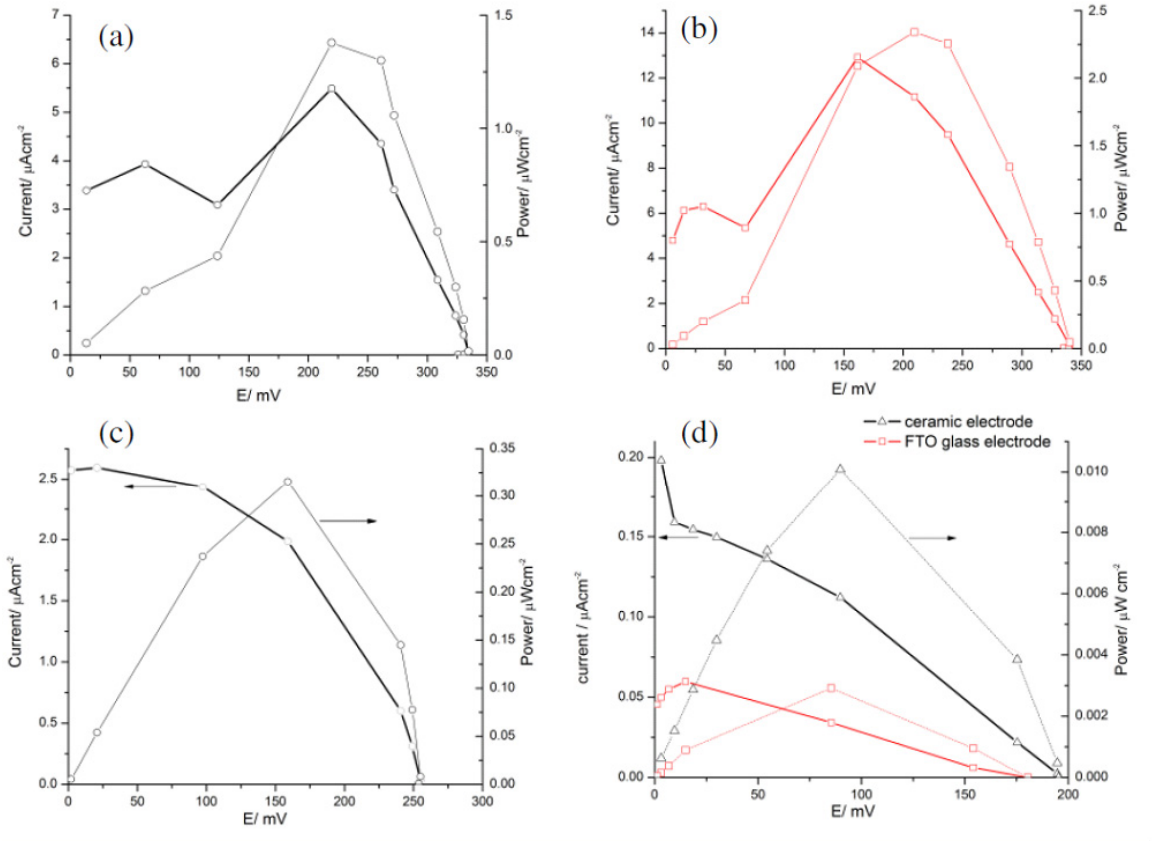


**Figure 14 Polarisation and power curves for a) an algal biofilm in a p-MFC with FTO coated ceramic anode b) an algal biofilm in a p-MFC with an FTO glass anode c) planktonic algae in a p-MFC with an FTO coated ceramic anode d) an algal biofilm on both FTO coated ceramc anode (triangles, black line) and FTO coated glass (squares, red line) with no mediator present.**

From comparing figures 14a and c (FTO ceramic p-MFC with either an algal biofilm or planktonic algae respectively), it was seen that the presence of a biofilm dramatically increased the power output of the device. The maximum power output of the device containing planktonic algae was 0.32 µW $cm^{-2}$. The $i_{SC}$ was 2.6 µA $cm^{-2}$, the $V_{OC}$ was 254 mV and the fill factor was 49 %. In contrast the biofilm covered ceramic anode gave a maximum power density of ~1.4 µW $cm^{-2}$, more than 4 times higher than that for planktonic algae. The open circuit voltage was also about 80 mV higher when there was a biofilm on the surface. Figure 14d demonstrates that a redox shuttle is essential for power production. The biofilm coated FTO ceramic p-MFC device gave roughly 16 times the power density per $cm^2$ to those containing carbon cloth anodes (0.02 µW $cm^{-2}$, data not shown). The maximum power point for cells containing carbon felt anodes was also low

(~0.004 μA $cm^{-2}$). All polarisation curves shown in figures 14 a, b and c show a drop incurrent as the short circuit position is approached. This is likely to be due to mass transport limitations at high current densities [41].

The power density was highest for the p-MFC device where a biofilm was grown on FTO glass directly. The maximum power density for a biofilm on FTO glass was ~2.4 μW $cm^{-2}$ in the presence of redox mediator, which was 100 times higher than that of planktonic algae in contact with FTO glass in the anodic chamber (0.024 μW $cm^{-2}$, data not shown). This was probably due to the fact that these biofilms were grown under stationary conditions allowing a thicker algal film to deposit on the surface. However these films were extremely fragile and very easily removed from the surface, making long-term use of FTO glass anodes in p-MFC devices non-ideal. If the biofilm on the ceramic electrode was allowed to grow further under stationary conditions it is likely higher power densities would be seen.

The maximum powers obtained from p-MFCs with FTO ceramic anodes were similar or better than those reported in the literature. Zou *et al.* [18] reported power densities of between 0.06 - 0.95 μW $cm^{-2}$ for biofilms grown on PANI or poly(pyrrole) coated electrodes. The lowest power output was obtained from biofilms of *Synechocystis PCC-6803.* The highest output from mixed colonies of photosynthetic organisms, where the anode was carbon paint coated with nanostructured poly(pyrrole). Yagishita *et al.* obtained power densities of ~0.14 μW $cm^{-2}$ under illumination at 60 W $m^{-2}$ for *Synechocystis* in the presence of 2-hydroxy-1,4-napthoquinone [42]. The highest power density was reported by Tsujimura *et al.*, who obtained maximum power densities of ~29 μW $cm^{-2}$ under illumination at 15 W $m^{-2}$ in the presence of 2,6- dimethyl-1,4-benzoquinone as the redox acceptor with S*ynechococcus PCC 7942* [12]. The power density is quoted with respect to the geometric surface area of the anode (4.5 $cm^2$ of a 1 mm thick carbon felt anode). It is therefore difficult to compare the result directly with the power outputs for the ceramic electrodes which have been quoted as a function of actual surface area. The fact that comparable power densities are obtained in simple, unoptimized p-MFC devices suggests that porous ceramic electrodes are a promising new anode material for p-MFCs.

## 8.4 Conclusions

Due to the limitations imposed by the anode material in the basic p-MFC device; for

example the lack of a large surface area; a new anode material for long term use in a p-MFC was developed. Macroporous $TiO_2$ ceramics based on bone substitute materials were developed, and coated with a thin layer of FTO to give high conductivity. In this chapter, these were characterised and tested in complete p-MFC devices. p-MFC devices were also developed with other typical anode materials (FTO glass and carbon felt) for comparison.

The developed electrode material contained mm sized pores, as well as a nanostructured high internal surface that appeared to aid algal attachment. Despite higher overall algal loading in carbon felt electrodes, ceramic electrodes had good loading as a function of their surface area. Loading was higher in uncoated $TiO_2$ ceramic electrodes compared to FTO coated ones, meaning there is much scope for optimisation.

In addition the algae form a healthy biofilm on FTO coated $TiO_2$, ceramics whereas on carbon felt the algae remained as far away from the surface as possible. Dense algal biofilms grew on planar FTO glass but were very fragile and not suited for use in p-MFCs. The fragile nature of the FTO glass biofilms could be due to the fact that little extracellular matrix was observed. It is likely that the surface morphology of the FTO coated ceramics requires further micro-texture optimisation, as it was observed from SEM that algal cells tended to congregate in areas of increased roughness.

Further characterisation showed the FTO ceramics to have similar resistivity to that of FTO coated glass (10 Ω square), and a high internal surface area of between 7 and 8.5$cm^2$ per measured 1.5 (Ø) x 0.75 cm sample. The $TiO_2$ was in rutile form, and sintered ceramics had reasonable strength which increased with density. Due to the fact that the particles making up the ceramics were not nanostructured, no photochemistry could occur with the produced substrates.

Studies of complete p-MFCs containing the model organism C. *vulgaris* suggested that porous ceramic electrodes are a promising novel anode material for p-MFCs. Polarisation curves were constructed as these were thought to represent a better method of studying p-MFC devices than chronoamperometry; a potential was not required to be applied to the anode and due to the fact that measurements were far

slower, they were more representative of equilibrium conditions. Power densities better than many literature reports have been shown. In this study the p-MFC devices were not optimised. The ceramic offers a long term sustainable solution, as algae can be grown on the surface in its porous matrix.

## 8.5 References


1. Michaelidou, U., ter Heijne, A., Euverink, G.J.W., Hamelers, H.V.M., Stams, A.J.M., and Geelhoed, J.S., *Microbial Communities and Electrochemical Performance of Titanium-Based Anodic Electrodes in a Microbial Fuel Cell.* Applied and Environmental Microbiology, 2011. **77**(3): p. 1069-1075.
2. Lovley, D.R., *Microbial fuel cells: novel microbial physiologies and engineering approaches.* Current Opinion in Biotechnology, 2006. **17**(3): p. 327-332.
3. Du, Z.W., Li, H.R., and Gu, T.Y., *A state of the art review on microbial fuel cells: A promising technology for wastewater treatment and bioenergy.* Biotechnology Advances, 2007. **25**: p. 464-482.
4. Dumas, C., Mollica, A., Feron, D., Basseguy, R., Etcheverry, L., and Bergel, A., *Marine microbial fuel cell: Use of stainless steel electrodes as anode and cathode materials.* Electrochimica Acta, 2007. **53**(2): p. 468-473.
5. Park, D.H. and Zeikus, J.G., *Electricity generation in microbial fuel cells using neutral red as an electronophore.* Applied and Environmental Microbiology, 2000. **66**(4): p. 1292-1297.
6. Liu, Y., Harnisch, F., Fricke, K., Schroeder, U., Climent, V., and Miguel Feliu, J., *The study of electrochemically active microbial biofilms on different carbon-based anode materials in microbial fuel cells.* Biosensors & Bioelectronics, 2010. **25**(9): p. 2167-2171.
7. Park, H.I., Sanchez, D., Cho, S.K., and Yun, M., *Bacterial communities on electron-beam Pt-deposited electrodes in a mediator-less microbial fuel cell.* Environmental science & technology, 2008. **42**(16): p. 6243-9.
8. Bond, D.R. and Lovley, D.R., *Evidence for involvement of an electron shuttle in electricity generation by Geothrix fermentans.* Applied and Environmental Microbiology, 2005. **71**(4): p. 2186-2189.

9. Reguera, G., McCarthy, K.D., Mehta, T., Nicoll, J.S., Tuominen, M.T., and Lovley, D.R., *Extracellular electron transfer via microbial nanowires.* Nature, 2005. **435**(7045): p. 1098-1101.
10. Gorby, Y.A., Yanina, S., McLean, J.S., Rosso, K.M., Moyles, D., Dohnalkova, A., Beveridge, T.J., Chang, I.S., Kim, B.H., Kim, K.S., Culley, D.E., Reed, S.B., Romine, M.F., Saffarini, D.A., Hill, E.A., Shi, L., Elias, D.A., Kennedy, D.W., Pinchuk, G., Watanabe, K., Ishii, S., Logan, B., Nealson, K.H., and Fredrickson, J.K., *Electrically conductive bacterial nanowires produced by Shewanella oneidensis strain MR-1 and other microorganisms (vol 103, pg 11358, 2006).* Proceedings of the National Academy of Sciences of the United States of America, 2009. **106**(23): p. 9535-9535.
11. Nishio, K., Hashimoto, K., and Watanabe, K., *Light/electricity conversion by a self-organized photosynthetic biofilm in a single-chamber reactor.* Applied microbiology and biotechnology, 2010. **86**(3): p. 957-964.
12. Tsujimura, S., Wadano, A., Kano, K., and Ikeda, T., *Photosynthetic bioelectrochemical cell utilizing cyanobacteria and water-generating oxidase.* Enzyme and Microbial Technology, 2001. **29**(4-5): p. 225-231.
13. Rosenbaum, M. and Schröder, U., *Photomicrobial Solar and Fuel Cells.* Electroanalysis, 2010. **22**(7-8): p. 844-855.
14. Zou, Y., Pisciotta, J., Billmyre, R.B., and Baskakov, I.V., *Photosynthetic microbial fuel cells with positive light response.* Biotechnology and Bioengineering, 2009. **104**(5): p. 939-946.
15. Chiao, M., Lam, K.B., and Lin, L.W., *Micromachined microbial and photosynthetic fuel cells.* Journal of Micromechanics and Microengineering, 2006. **16**(12): p. 2547-2553.
16. Pisciotta, J.M., Zou, Y., and Baskakov, I.V., *Light-Dependent Electrogenic Activity of Cyanobacteria.* Plos One, 2010. **5**(5).
17. Rosenbaum, M., Schröder, U., and Scholz, F., *In situ electrooxidation of photobiological hydrogen in a photobioelectrochemical fuel cell based on Rhodobacter sphaeroides.* Environmental Science & Technology, 2005. **39**(16): p. 6328-6333.
18. Zou, Y.J., Pisciotta, J., Billmyre, R.B., and Baskakov, I.V., *Photosynthetic Microbial Fuel Cells With Positive Light Response.* Biotechnology and Bioengineering, 2009. **104**(5): p. 939-946.

19. Moreno-Garrido, I., *Microalgae immobilization: Current techniques and uses.* Bioresource Technology, 2008. **99**(10): p. 3949-3964.
20. Stal, L., ed. *Cyanobacterial mats and stromatolites. In The ecology of cyanobacteria: Their diversity in time and space*. 1st ed., ed. W.a. Potts. 2000, Kluwer: Dordrecht, London, Boston.
21. Esper, B., Badura, A., and Rogner, M., *Photosynthesis as a power supply for (bio-)hydrogen production.* Trends in Plant Science, 2006. **11**(11): p. 543-549.
22. Rooke, J.C., Meunier, C., Leonard, A., and Su, B.L. *Energy from photobioreactors: Bioencapsulation of photosynthetically active molecules, organelles, and whole cells within biologically inert matrices*. in *3rd International Symposium on Novel Materials and Their Synthesis/17th International Symposium on Fine Chemistry and Functional Polymers*. 2007. Shanghai, China: Int Union Pure Applied Chemistry.
23. Sekar, R., Venugopalan, V.P., Satpathy, K.K., Nair, K.V.K., and Rao, V.N.R., *Laboratory studies on adhesion of microalgae to hard substrates.* Hydrobiologia, 2004. **512**(1-3): p. 109-116.
24. Hunt, A.P. and Parry, J.D., *The effect of substratum roughness and river flow rate on the development of a freshwater biofilm community.* Biofouling, 1998. **12**(4): p. 287-303.
25. Characklis, W.G. and Cooksey, K.E., *Biofilms and microbial fouling.* Advances in Applied Microbiology, 1983. **29**: p. 93-138.
26. Granhag, L.M., Finlay, J.A., Jonsson, P.R., Callow, J.A., and Callow, M.E., *Roughness-dependent removal of settled spores of the green alga Ulva (syn. Enteromorpha) exposed to hydrodynamic forces from a water jet.* Biofouling, 2004. **20**(2): p. 117-122.
27. Scardino, A.J., Harvey, E., and De Nys, R., *Testing attachment point theory: diatom attachment on microtextured polyimide biomimics.* Biofouling, 2006. **22**(1): p. 55-60.
28. Barberousse, H., Brayner, R., Do Rego, A.M.B., Castaing, J.C., Beurdeley-Saudou, P., and Colombet, J.F., *Adhesion of facade coating colonisers, as mediated by physico-chemical properties.* Biofouling, 2007. **23**(1): p. 15-24.
29. Liu, Y.K., Seki, M., Tanaka, H., and Furusaki, S., *Characteristics of loofa (Luffa cylindrica) sponge as a carrier for plant cell mobilization.* Journal of Fermentation and Bioengineering, 1998. **85**(4): p. 416-421.

30. Akhtar, N., Iqbal, J., and Iqbal, M., *Removal and recovery of nickel(II) from aqueous solution by loofa sponge-immobilized biomass of Chlorella sorokiniana: characterization studies.* Journal of Hazardous Materials, 2004. **108**(1-2): p. 85-94.

31. Ogbonna, J.C., Tomiyama, S., and Tanaka, H., *Development of a method for immobilization of non-flocculating cells in loofa (Luffa cylindrica) sponge.* Process Biochemistry, 1996. **31**(8): p. 737-744.

32. Prieto, M.B., Hidalgo, A., Serra, J.L., and Llama, M.J., *Degradation of phenol by Rhodococcus erythropolis UPV-1 immobilized on Biolite((R)) in a packed-bed reactor.* Journal of Biotechnology, 2002. **97**(1): p. 1-11.

33. Doi, H., Katano, I., and Kikuchi, E., *The use of algal-mat habitats by aquatic insect grazers: Effects of microalgat cues.* Basic and Applied Ecology, 2006. **7**(2): p. 153-158.

34. Jacobson, L.M., David, M.B., and Mitchell, C.A., *Algal growth response in two Illinois rivers receiving sewage effluent.* Journal of Freshwater Ecology, 2008. **23**(2): p. 179-187.

35. Toquet, J., Rohanizadeh, R., Guicheux, J., Couillard, S., Passuti, N., Daculsi, G., and Heymann, D., *Osteogenic potential in vitro of human bone marrow cells cultured on macroporous biphasic calcium phosphate ceramic.* Journal of Biomedical Materials Research, 1999. **44**(1): p. 98-108.

36. Innocentini, M.D.M., Sepulveda, P., Salvini, V.R., Pandolfelli, V.C., and Coury, J.R., *Permeability and structure of cellular ceramics: A comparison between two preparation techniques.* Journal of the American Ceramic Society, 1998. **81**(12): p. 3349-3352.

37. Studart, A.R., Gonzenbach, U.T., Tervoort, E., and Gauckler, L.J., *Processing routes to macroporous ceramics: A review.* Journal of the American Ceramic Society, 2006. **89**(6): p. 1771-1789.

38. Bowen, C.R., Gittings, J.P., Dent, A.C.E., Turner, I.G., Baxter, F.R., and Chaudhuri, J.B., *Electrical characterization of hydroxyapatite-based bioceramics.* Acta Biomaterialia, 2009. **5**(2): p. 743-754.

39. Jones, A., *Chemical Vapour Deposition Precursors, Processes and Applications*. 2009, The Royal Society of Chemistry: Cambridge.

40. Ahl, S., Cameron, P., Liu, J., Knoll, W., Erlebacher, J., and Yu, F., *A comparative plasmonic study of nanoporous and evaporated gold films.* PLASMONICS, 2008. **3**(1): p. 13-20.

41. Zhao, F., Slade, R.C.T., and Varcoe, J.R., *Techniques for the study and development of microbial fuel cells: an electrochemical perspective.* Chemical Society Reviews, 2009. **38**(7): p. 1926-1939.

42. Yagishita, T., Sawayama, S., Tsukahara, K.I., and Ogi, T., *Effects of intensity of incident light and concentrations of Synechococcus sp. and 2-hydroxy-1,4-naphthoquinone on the current output of photosynthetic electrochemical cell.* Solar Energy, 1997. **61**(5): p. 347-353.

# Chapter 9. Preliminary Characterisation of *C. vulgaris* Biofilms by Scanning Electrochemical Microscopy

# Chapter 9 – Preliminary characterisation of *C. vulgaris* biofilms by scanning electrochemical microscopy

## 9.1 Introduction

Previous chapters underline the fact that studying whole pMFC devices is complex, and to fully understand device outputs, cellular activity and interactions with a redox mediator in the anodic chamber must first be characterised. As such, chapters 4 and 5 examine the reduction capacity of *Chlorella vulgaris* cells towards a potassium ferricyanide (ferricyanide) mediator outside of the complexity of the pMFC device. A technique that can investigate the behaviour of cells without moving them from steady state conditions, in situ to the pMFC device would be invaluable. To this end, in this chapter scanning electrochemical microscopy (SECM) using ultra-microelectrodes (UMEs) was applied to characterise a *C. vulgaris* biofilm in relation to its ferricyanide reductive capacity. This was performed *ex situ* to the pMFC device. If successful, the capacity exists for further SECM investigations to be executed on biofilms within a working pMFC device. The fact that measurements can be taken whilst the UME is moved relative to the substrate means chemical processes occurring at the solution-substrate interface can be studied and topographic profiles obtained. Previously, the technique has been used to study many other processes; both biological and artificial [1-3]. Applications of SECM in relation to cell studies shall now be reviewed.

Real time information on the cellular status and metabolic activity of living cells, based on the reduction current for oxygen (in substrate generation, tip collection mode) has been well characterised [4-7]. UMEs have been inserted into single algal protoplast cells to determine intracellular reduction currents for oxygen, with the change in reduction current directly correlated to intercellular concentration of oxygen [8, 9]. Here, the rapid increase in oxygen reduction current under illumination correlated to the increase in intracellular oxygen concentration due to photosynthesis; which returned to original levels in dark. An immediate peak after irradiation was caused by the light reaction (photosynthetic electron transport), before a steady state value was reached after oxygen production was limited by the dark reaction (carbon

fixation) [8, 9]. However, inserting a UME is a physical stimulation, and may cause changes to typical cell activity.

Therefore UMEs have also been used to study localised changes in oxygen concentration near intact single cells. Using this concept, Kaya *et al.* monitored the cellular respiratory activity of single human HeLa cells [6], finding oxygen concentration to be a more rapid indicator of respiratory activity than fluorescence. Similarly, Yasukawa *et al.* imaged respiratory and photosynthetic activities of single, algal protoplasts by scanning in constant height mode [4, 7]. In the dark, the image of the protoplast appeared as a spot with lower oxygen concentration due to consumption of oxygen by respiration. Conversely, when irradiated with light, the opposite image appeared due to the photosynthetic generation of oxygen (figure 1). Oxygen generation by photosynthesis and oxygen consumption by respiration at single cell levels could then be calculated from equation 1 [7]

$$f = 4\pi r_s D(C_s - C^*)$$

**Equation 1 Rate of oxygen generation, where D = the diffusion coefficient ($cm^2s^{-1}$), $r_s$ is the radius of protoplast, $C_s$ is oxygen concentration at the protoplast surface and $C^*$ is concentration of oxygen in bulk solution. Oxygen concentrations at the protoplast surface were determined by extrapolating approach curves to 0 distances.**

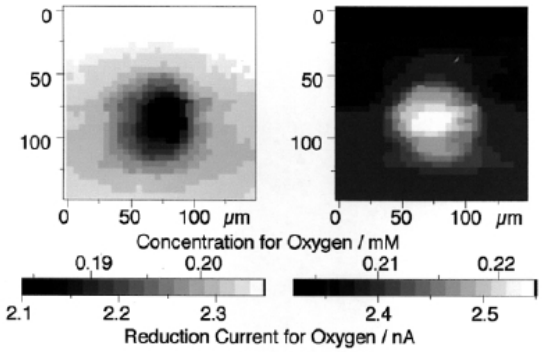


**Figure 1 Reproduced from [7] SECM images of left; a respiring cell and right; a photosynthesising cell. Probe: Pt electrode with radius 1.2µm at -0.5V w.r.t Ag/AgCl**

In addition, permeability coefficients ($P_m$) of a redox species through a cell membrane have been determined by monitoring the change in concentration of particular redox species in the vicinity of the membrane [7]. By placing the UME probe inside the unstirred layer close to the membrane, the change in concentration of hydrophobic

species permeated from the other side of the solution can be monitored in real time (figure 2). Due to hindered diffusion, redox currents are lower than in the bulk; however, the decrease in the redox current correlates with the permeability of the membrane to redox species. Quantitative analysis to give the $P_m$ values for redox mediators passing through the membrane can be performed using digital simulation of redox currents with UME membrane distance. The permeability of a cell membrane is closely related to the hydrophobicity, mass and total charge of a redox mediator species. The protoplast membrane was found to be almost impermeable to ferrocyanide and ferricyanide, with $P_m$ values of $\geq 1.0 \times 10^{-4}$ [7].

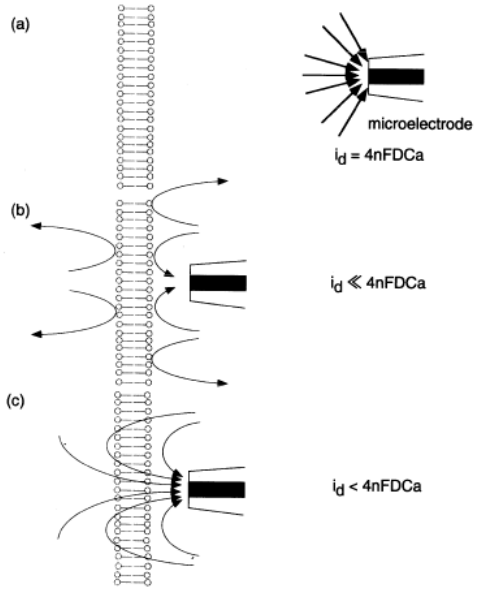


**Figure 2 Reproduced from [7] Redox response at a UME. a) In the bulk solution a steady state current is observed. When the UME is placed close to a membrane, the current becomes lower than in the bulk and depends on whether the membrane is b) impermeable or c) permeable.**

Intracellular redox activity of individual living cells has been probed by measuring the rate of transmembrane charge transfer [10, 11]. Feedback mode was employed in a study by Liu *et al.* to measure kinetics of transmembrane charge transfer in breast cells [10]. Negative feedback was observed with hydrophilic (ferrocyanide and ferrocenecarboxylate) mediators, which could not pass through the cell membrane. In contrast, hydrophobic mediators (medadione and 1,2-napthoquinone) could enter the cell, and be regenerated via bimolecular reactions with intracellular redox centres [10]. Apparent rate constants of mediator regeneration were extracted by fitting approach curves to SECM theory [12]. Similarly, redox activity of individual purple bacteria

(*Rhodobacter sphaeroides*) has been probed [11], with rates and pathways of charge transfer studied. This corroborated the study by Liu *et al.*, finding hydrophobic redox species (for example, menadione and 1,2-napthoquinone) capable of permeating both the outer cell membrane and cytoplasmic membrane. Although exhibiting negative feedback, currents were higher than for a pure insulator. The effective rate constants of redox reactions of such mediators with intracellular redox species were determined from fitting to the theory [12], and shown to correlate with mediator formal potential [11]. From kinetic analysis, total internal concentration of intracellular redox centres capable of oxidising menadiol was 50-100 μM, and the intracellular potential encountered by hydrophobic species was -110+/-90mV vs Ag/AgCl. Hydrophilic ionic species (for example, $Ru(NH_3)_6^{3+}$ and ferricyanide - $Fe(CN)_6^{3-}$), again exhibited negative feedback, and could only cross the outer membrane of a bacterium and react with redox centres in the periplasm, potentially explaining the different intracellular potential encountered by hydrophilic redox species (180+/-70mV vs Ag/AgCl) [11].

Furthermore, effects resulting from the presence of a redox mediator on photosynthesis and respiration have been determined. Yasukawa *et al.* [13] quantitatively investigated the influence of benzoquinone (BQ) on the respiratory and photosynthetic electron transport in a single algal protoplast using SECM, with the UME positioned close to the cell. The cell permeable BQ/*p*-hydroquinone ($QH_2$) redox couple acted as an electron mediator to facilitate reactions of biological molecules [14]. In light the oxidation current of $QH_2$ increased and the reduction current of BQ decreased immediately, before returning to original levels in the dark. In addition, photosynthetic oxygen generation was increased in the presence of BQ. This inferred that BQ functions as an electron acceptor to increase the rate of photosynthetic electron transport, and hence the rate of oxygen production [7, 13]. The electron transfer between ferricyanide was also investigated [13], but no response of the redox current upon light irradiation was exhibited. The authors attributed this to the fact that the membrane permeability for the redox membrane was very low [13]. However, this did not account for the interaction of ferricyanide with ferric reductase proteins on the cell membrane as discussed in chapter 4 and 5.

Finally, cell metabolites can be quantified. Zhou *et al.* used SECM to characterise the peroxidase activity in a single protoplast of the algal species *Bryopsis plumose* [15].

The oxidation reaction requires the enzyme substrate hydrogen peroxide. When ferrocene methanol was added to the solution, it was oxidised to ferriceniummethanol ($FMA^+$) at the protoplast surface due to the peroxidase catalytic reaction, which could be detected by scanning the microelectrode tip close to the sample surface. A plot of the $FMA^+$ generation rates with respect to the hydrogen peroxide concentration could be described by a Michaelis-Menten-type reaction model.

### 9. 11 Chapter Aims

In this chapter, characteristics of a biofilm of *C. vulgaris* are preliminarily investigated by SECM. This technique offers many advantages over other techniques. For example, it minimises changes in cellular environment, and offers the potential for biofilms to be characterised in the future in situ in a pMFC device.

Firstly, the production of oxygen is used as a proof of principle for the sensitivity of SECM to detect cell metabolic activity in light and dark. In dark, the SECM effectively operates in redox competition mode (where tip and substrate both consume oxygen) and in the light, the SECM experiment effectively operates in substrate generation tip collection mode (where the substrate produces oxygen which the tip consumes). Cyclic voltammetry is also used to determine whether any redox active cell metabolites are produced that could be detected at 'close' distances by the UME.

Secondly, the reduction of ferricyanide to ferrocyanide (as outlined in [16-18]) is studied in feedback mode (whereby if cells can turn over ferricyanide to ferrocyanide, tip currents increase) in light and dark, using approach curves and by measuring close to the biofilm. These experiments were complimentary to those performed in chapter 5.

## 9.2 Experimental

In all experiments, the SECM instrument used was a home made system with an Autolab PGSTAT101 (Ecochemie) to control the electrochemistry and three M605 micropositioners driven by three C863 controllers via the PIMikroMove software (all from Physik Instrument). The system also included an electrochemical cell with observation window and a "VCAM2" video microscope viewing system. The

instrument was mounted within a dark box inside a faraday cage, and light was provided from a fibre optic cold light source, directed into the dark box.

The electrochemical cell was created by securing an algal substrate (of various types – see 9.21 and 9.22) into the bottom of a specially designed chamber, before filling with 3N-BBM media. After surrounding with a dark box, and mounting within a Faraday cage, this was operated in 2 electrode mode, using a UME as working electrode and an SCE as reference/counter electrode. UME electrodes were created in house using a Pt microwire sealed in a soda glass body, with a diameter of either 10 μm or 25μm. The glass was ground down with silicon carbide emery paper, and the microdisc electrode polished with progressively smaller diameter, 1 - 0.3 μm, alumina micro polish to achieve a flat surface. Before use, UMEs were re-polished in 0.3 μm alumina micropolish (Buehler).

Once the electrochemical cell components were positioned, 'close', and 'bulk' positions were identified using a microscope camera. The microelectrode was brought down to a minimum distance (by eye) from the substrate; although relatively arbitrary, this was termed 'close' and was approximated as ~50μm from the surface. 'Bulk' was considered 1mm distance out from this value in the z axis. Assessing the tip substrate distance was difficult, and accuracy depended on the substrate used. For example, when an agar substrate was used, a clear interface boundary was evident by eye between solution and electrolyte. However, when using cells (in a biofilm or precipitated), the electrolyte/substrate interface was diffuse and virtually difficult to determine manually.

### 9.21 Initial investigations of oxygen production by *C. vulgaris*

SECM was used to detect oxygen produced by biofilms, as in [4-7], based on a procedure modified from that outlined by Sosna *et al.* [19]. Oxygen can be electrochemically reduced at an electrode (the oxygen reduction reaction, or ORR), at a potential around -0.55V w.r.t SCE. From the limiting current measured at the ORR potential, oxygen concentration at the electrode could be calculated according to equation 2.

$$i_T = 4nFDCa$$

**Equation 2 The tip current $i_T$ (A), as related to the number of electrons in each redox step (for oxygen (n = 2.6 for a 5 µm radius UME [19]), F (Faradays constant), D (oxygen diffusion coefficient in water = $2.2x10^{-5}$ $cm^{-2}$ $s^{-1}$), C (concentration in mol $cm^{-3}$) and a (radius of UME). This equation reflects quasi-hemispherical diffusion and so is only relevant in the 'bulk'.**

Equation 2 reflects quasi-hemispherical diffusion is present at the UME, and so is valid in the 'bulk' but not at very 'close' tip substrate distances where the substrate interacts with the diffusion layer of the UME. 'Close' to the substrate, where the tip-substrate distance is smaller than the radius of the UME (i.e $_{dtip-sub}$<a) the UME tip becomes parallel to the substrate and forms a type of thin layer cell. This can be described by equation 3.

$$i_T = \frac{nF\pi a^2 DC_{sub}}{d_{tip-sub}}$$

**Equation 3 The tip current $i_T$ (A), as related to the number of electrons in each redox step (for oxygen n = 2.6 for a 5 µm radius [19]), F (Faradays constant), D (oxygen diffusion coefficient in water = $2.2x10^{-5}$ $cm^{-2}$ $s^{-1}$), $C_{sub}$ (concentration at substrate in mol $cm^{-3}$), a (UME radius in cm) and $d_{tip-sub}$ (distance between UME tip and substrate in cm). This equation assumes the tip-substrate gap behaves as a thin layer cell when the tip is 'close' to the substrate**

Again, equation 3 is a gross approximation which neglects the fact that the tip-substrate gap is more like a leaky thin layer cell (for example, the cell substrate is porous and consumption of oxygen by the tip alters the metabolism locally).

*C. vulgaris* cultured on agar was initially used as a substrate, as it was thought that the algal cells would be well adhered, creating a system whereby all cells were attached to the substrate with virtually no planktonic cells in the 'bulk'. This would give the most sensitivity to the concentration profile of oxygen over distance away from the algal substrate. Agar was created using 3N-BBM+V media and cultured for 14 days as outlined in the appendix. A 3 x 1 cm section was then secured at the bottom of the electrochemical cell as a substrate. Cyclic voltammetry was performed at close and bulk positions between -1 and 1 V w.r.t SCE at various scan-rates. Effects of light on cyclic voltammetry were additionally determined. Approach curves were also performed whereby chronoamperometry was used to hold the UME at the potential for the ORR to occur as determined by cyclic voltammetry, whilst the UME was

lowered and its current recorded 'on the fly' towards the substrate along the $z$ – axis from 'bulk' (1 mm) to 'close' (0 mm) distances. Current $i_{Tip}$ was recorded with respect to tip position. After the approach curves were measured, retraction curves were subsequently performed to assess reproducibility and hysteresis between approach and retraction. During these experiments, the UME was moved slowly to avoid convective issues at 1 μm $s^{-1}$. Measurements were repeated using uncultured agar as a control.

SECM was then used to detect oxygen evolved from a thick layer of precipitated cells. The electrochemical cell chamber (with electrodes in place) was filled with *C. vulgaris* culture solution (at a cell density of $4.6x10^{-7}$ cells $ml^{-1}$) and left for 12 hours, for the cells to precipitate out under gravitational forces. From the lessons learned with agar, for highest sensitivity, all oxygen concentrations were studied via chronoamperometry at -0.55 V w.r.t SCE, corresponding to a potential 100 mV past the potential where the ORR reaction occurred. This potential was determined by voltammetry. A cleaning procedure was additionally used by applying a 1 second pulse at 0.6 V every n seconds (between 20 seconds and 300) to remove fouling from the surface (which has the effect of forming and stripping oxide from the UME surface). Approach curves were performed between 0 and 1mm of the surface, under illumination and the dark at 10 $\mu ms^{-1}$. Under illumination the SECM effectively operated in substrate generation tip collection mode, and in the dark the SECM operated in redox competition mode, where both substrate and tip consume the same redox species. Additionally, whilst the UME was stationary (at either a 'close' position or a 'bulk' position) effects of illumination on the current were determined.

### 9.2 Potassium ferricyanide reduction by precipitated *C. vulgaris* cells

After proof of principle from the oxygen measurements, SECM was used to detect ferricyanide reduction to ferrocyanide by a thick layer of precipitated cells. The electrochemical cell chamber was filled with *C. vulgaris* culture solution (at a cell density of $4.6x10^{7}$ cells $ml^{-1}$) and 1 mM ferrocyanide and left for 12 hours for the cells to precipitate out under gravitational forces. Due to fouling that had been seen to rapidly occur with ferrocyanide on Pt electrodes, a 25 μm $s^{-1}$ Pt microelectrode was added only directly before experiments were performed.

The reduction of ferricyanide to ferrocyanide by the algal cells was studied using chronoamperometry at 0.4 V w.r.t SCE (as determined by cyclic voltammetry), which corresponded to a potential 100 mV past the oxidation potential for ferrocyanide. Using this potential ensured that ferricyanide was only produced at the UME tip, to give a limiting current. If algae then reduced the ferricyanide, feedback effects would ensue, to increase the current relative to that in the 'bulk'. Approach curves in feedback mode at 0.4 V w.r.t SCE were performed between 0 and 1 mm of the surface, in light and dark. Additionally, whilst the UME was stationary at 0.4 V w.r.t SCE, at either 'close' or 'bulk' positions, effects of light on the current were determined.

Figure 3 summarises the measurements performed in this chapter for both oxygen sensing and ferricyanide reduction experiments.

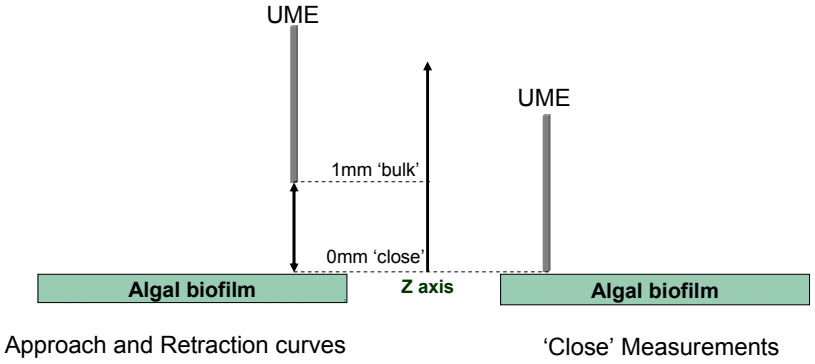


**Figure 3 The different types of measurements performed in SECM, where the current is measured at a potential specific to redox species of interest. The UME therefore acts as a sensor.**

## 9.3 Results and Discussion

### 9.31 Initial investigations of oxygen production by *C. vulgaris*

*Agar substrate*

Cultured agar was first used as a substrate for oxygen detection in a SECM. First, cyclic voltammetry was performed 'close' (0 mm from algal surface (figure 4)), and in the 'bulk' (1 mm away from the surface (data not shown), in light and dark conditions. The concentration of oxygen could be calculated from the limiting current at the peak exhibited at -0.55 Vw.r.t SCE, where the oxygen reduction reaction (ORR) occurred.

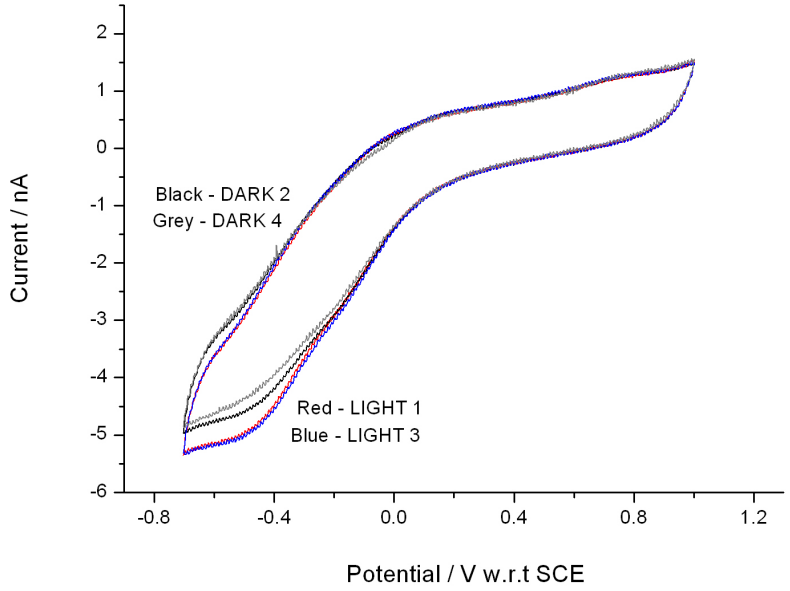


**Figure 4 Cyclic voltammetry at a UME with radius 5µm 'close' to a cultured agar substrate, in light and dark. The number shown represents the order the cyclic voltammograms were performed in. Three scans at scan rate 25 mV $s^{-1}$ were performed under each condition, with the last complete scan shown. Limiting currents (at -0.55 V w.r.t SCE) in the bulk averaged at around -3.75 nA**

Figure 4 shows that limiting currents measured at the potential for the ORR to occur increased very slightly upon illumination and decreased in the dark. When illumination conditions were varied, limiting currents varied from -4.96 nA (DARK), -5.49 nA (LIGHT), -4.82 nA DARK), to -5.46 nA (LIGHT). It is important to note that in this and subsequent analysis, if more than one CV was performed, the last limiting current scan value was taken. The sensitivity to light inferred that oxygen was produced photosynthetically as expected in light, and detected at the microelectrode. The decrease in oxygen concentration in the dark (compared to light) could also have been due to respiratory consumption. It should also be noted that no redox activity other than the oxygen was detected, inferring that no redox active metabolites were produced by the cells (or metabolites were either not reactive with platinum or were too short lived).

When cyclic voltammetry was performed in the 'bulk', 1 mm away from the algal surface, limiting currents were much lower than 'close' to the algal surface (data not shown), around -3.75 nA compared to -5 nA respectively. This was despite the fact

that in the 'bulk' no hindered diffusion from topography would occur. Therefore this can only be explained by the fact that algae must have been producing oxygen, increasing the localised concentration near the surface. Additionally, limiting currents in the 'bulk' did not increase in response to light. Although small increases of limiting current were seen on each subsequent scan, this inferred the electrode became successively cleaner with scanning rather than oxygen increased. When conditions were varied, limiting currents at -0.55 V w.r.t SCE increased from -3.56 nA (DARK) to -3.75 nA (LIGHT), -3.93 nA (DARK) and finally -4.04 nA (LIGHT) as the sample conditions changed. If algal cells were well attached to the agar substrate, photosynthetically produced oxygen would only reach the microelectrode and be detected 'close' to the agar surface due to slow diffusion.

Cyclic voltammetry was also performed within the agar itself, as shown in figure 5.

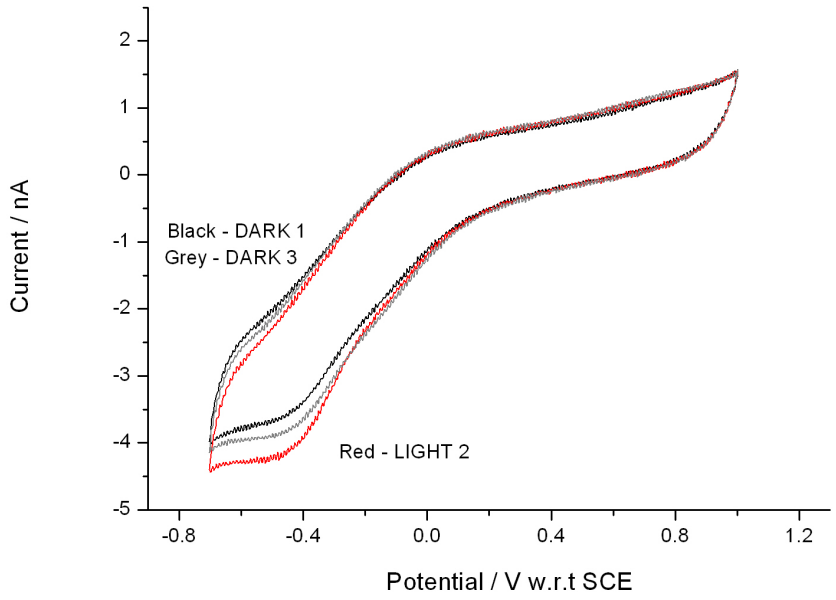


**Figure 5 Cyclic voltammetry with the UME (radius 5 µm) driven 200 µm inside a cultured agar substrate, in light and dark. The number shown represents the order the cyclic voltammograms were performed in. Three scans at scan rate 25 mV $s^{-1}$ were performed under each condition, with the last complete scan shown. Limiting currents (at -0.55 V w.r.t SCE) in the bulk averaged at around -3.75 nA**

The limiting current in figure 5 at -0.55 V w.r.t SCE, performed when the UME was within the cultured agar itself, showed a small response under illumination. As illumination conditions were varied, the limiting current increased from -4 nA

(DARK), to -4.46 nA (LIGHT) and back to -4.12 nA (DARK). The agar itself was extremely unlikely to evolve oxygen under illumination, and it was also unlikely that photosynthetic oxygen produced by algae cultured on the agar surface could diffuse to the electrode within the agar in the times involved. Additionally, algal cells were unlikely to grow within the agar. Therefore the response could be due to algal cells trapped in a thin layer on the surface of the UME pushed into the agar. This could act in a similar manner to a thin layer cell, as mentioned in [12].

When cyclic voltammetry was performed on uncultured agar in the 'bulk' and 'close' to the agar surface, more oxygen was detected 'close' to the agar than in the 'bulk' (data not shown). In the 'bulk' limiting currents at the potential for the ORR reaction to occur (-0.55 V w.r.t SCE) were -3.5 nA, 'close' to the agar currents were -4 nA, and when moved back to the 'bulk' position, currents were -3.8 nA. This trend in oxygen concentration was not expected, and could indicate the UME was not performing well. The magnitudes of these limiting currents were slightly less than with cultured agar, and no light response was seen.

When performing SECM experiments, it was found difficult to determine distances of 'close' and 'bulk' by eye from using the zoom lens video microscope. However, approach curves (measured at -0.55 V w.r.t SCE) performed on uncultured agar from a UME position within the 'bulk' to within the agar itself showed the potential for precise positioning control in future experiments (shown in figure 6). Upon approach of a microelectrode towards the agar surface, the current dropped gradually, with hindered diffusion (visible as a steeper decrease in current) evident directly before agar penetration (ie. the last ~0.05 mm). This was the response expected from an insulating surface, although it would be anticipated that the current would be stable in the 'bulk' until moved to the 'close' position, rather than decreasing continuously from 1 mm to 0 mm. This could be due to fouling of the tip with time. After a steep drop in current associated with the change in oxygen concentration over the agar/solution interface, a new level of oxygen was determined thought to correspond to the level of oxygen within the agar itself. This immediate drop in current could be used for precise control of UME positioning in future experiments (where no algae are present on the agar surface).

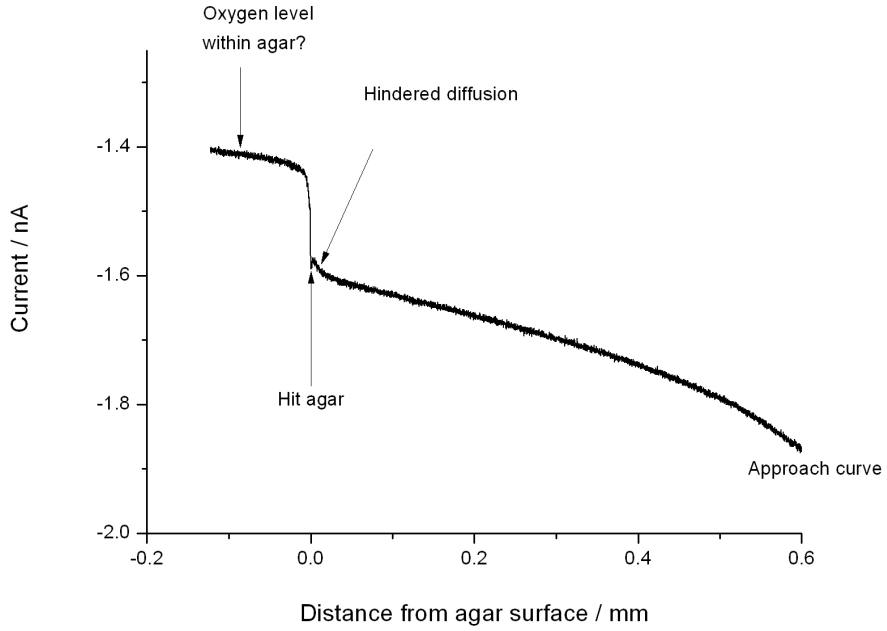


**Figure 6 Currents measured during chronoamperometry with the UME (radius 5 µm) held at -0.55 V w.r.t SCE, whilst approaching and penetrating uncultured agar. Small amounts of hindered diffusion are labelled, as well as the sharp drop in current indicating agar penetration.**

From figures 5 and 6, it was apparent that currents obtained in approach curves were much lower than those obtained at the same potential (-0.55 V w.r.t SCE) during cyclic voltammetry. Experiments were carried out whereby linear sweep voltammetry was performed from 0.25 V to -0.55 V, before the potential was immediately held at -0.55 V (data not shown) in the same measurement. It was found that when scan rates of 100 mV $s^{-1}$ and 10 mV $s^{-1}$ were used to sweep the potential down to -0.55 V w.r.t SCE during linear sweep voltammetry, a large jump in current occurred when chronoamperometry was immediately initiated and the potential was held at -0.55 V w.r.t SCE. This was not evident when a scan rate of 1 mV $s^{-1}$ was used, showing the current discrepancy to be a time-scale problem. This current trend was hard to explain. An advantage of UMEs is that charging currents and mass transport limitations supposedly become negligible. However the cyclic voltammograms shown in figures 3 and 4 did show a large amount of hysteresis usually associated with charging of the double layer. This could indicate the presence of a film on the UME which increased the UME capacitance, possibly caused by bio-fouling. The experiments therefore showed the importance of using slow scan rates to get steady state currents, and future experiments could involve coating the UME tip with a protective film (such as Nafion) to protect against bio-fouling.

*Precipitated cells*

Due to the lessons learned from the agar experiments, namely that high cell densities were required to give high sensitivity, a substrate consisting of a thick sediment of cells was then used. It was also apparent from initial experiments that chronoamperometry performed at the potential for the ORR (-0.55 V w.r.t SCE) was the best method of measuring oxygen concentration. All following results were obtained at that potential.

Approach curves were measured, whereby the current was measured in between cleaning pulses, which acted to reduce fouling on the electrode and prevent current decay whilst the electrode moved in the z axis. Approaches and retractions were performed immediately after one another to prevent hysteresis due to fouling over time. Figure 7 shows an example of ideal chronoamperometry, measured whilst approaching and retracting the precipitated cell substrate over a distance of 0.5 mm at 0.01 mm $s^{-1}$ in the dark. Little hysteresis was exhibited and slopes were similar upon approaching and retracting the UME to/from the algal precipitate.

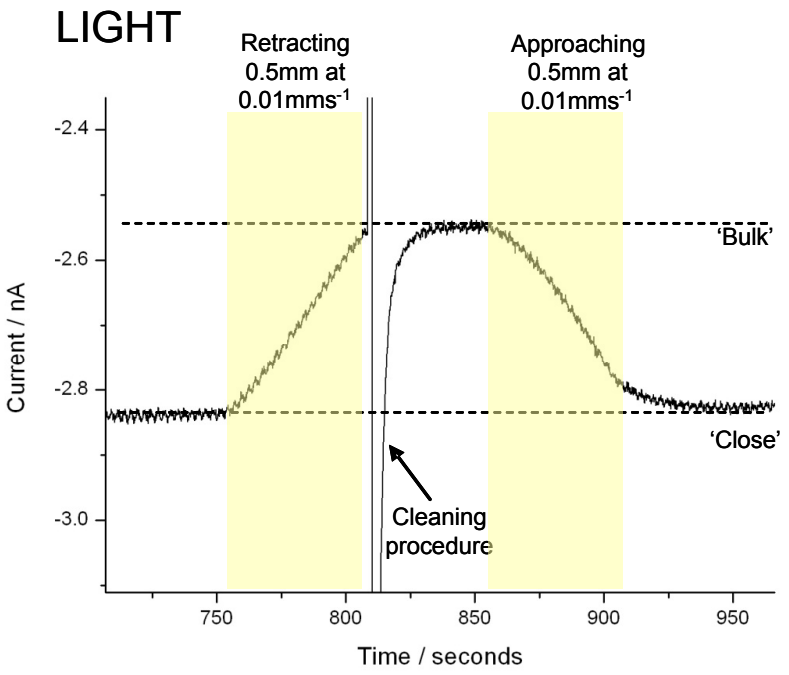


**Figure 7 Chronoamperometry during approach and retraction of a UME (radius 5 µm) held at -0.55 V w.r.t SCE, to a precipitated cell substrate in light. The distance travelled was 0.5 mm at a speed of 0.01 mm $s^{-1}$. Approximate limiting current values in 'bulk' and 'close' positions, and the cleaning procedure, are labelled. Yellow shaded areas indicate time periods of UME movement**

Approach and retraction curves (similar to that in figure 7) were performed over 1 mm, at 0.01 mm $s^{-1}$ in light and dark. Original chronoamperometry in light and dark, and summary curves plotted w.r.t distance are shown in figures 8a and b, and figure 9 respectively. Approach curves were normalised with respect to 'bulk' current values and the radius of the UME, and shown in figure 10.

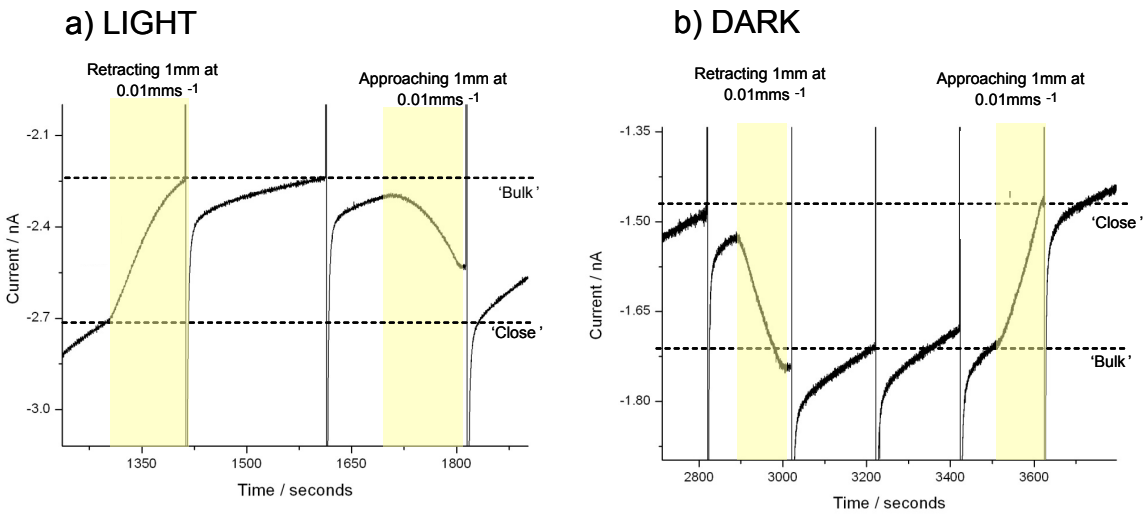


**Figure 8 Chronoamperometry during approach and retraction of a UME (radius 5 µm) held at -0.55 V w.r.t SCE, to a precipitated cell substrate in the light a) and the dark b). The distance travelled was 1mm at a speed of 0.01 mm $s^{-1}$. Approximate limiting current values in 'bulk' and 'close' positions are labelled. Yellow shaded areas indicate time periods of UME movement**

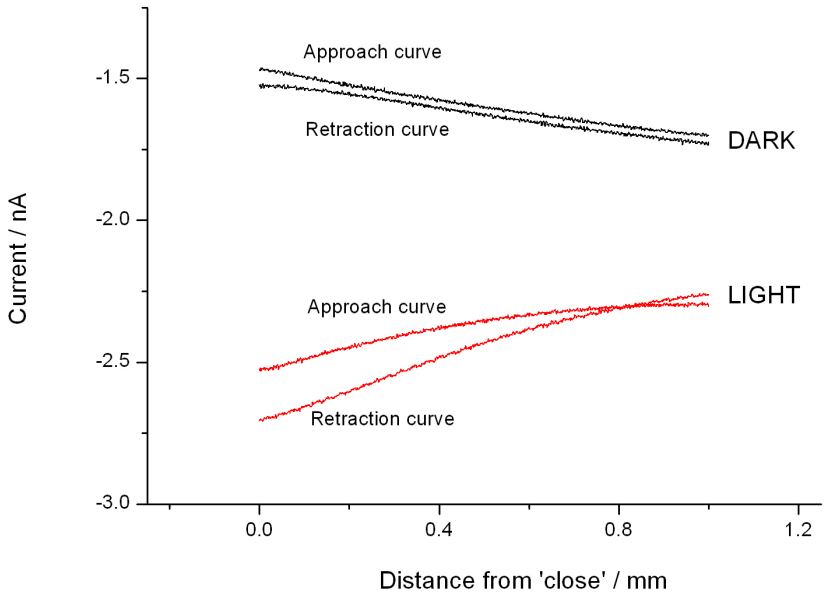


**Figure 9 Summary approach and retraction curves from the chronoamperometry (at -0.55 V w.r.t SCE) shown in figures 8a and 8b, of a UME (radius 5 µm) to a precipitated cell substrate in light and dark. The distance travelled was 1 mm at a speed of 0.01 mm $s^{-1}$.**

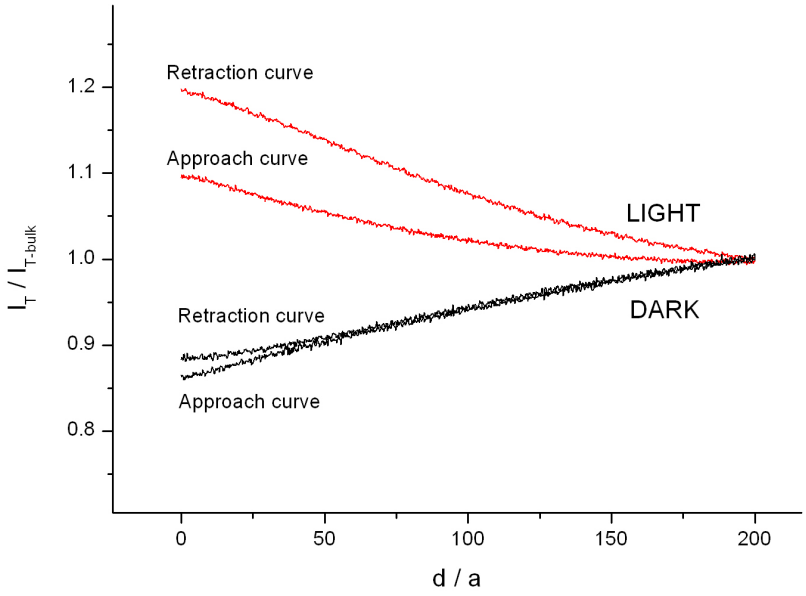


**Figure 10 Normalised approach and retraction curves of a UME (radius 5 µm) to a precipitated cell substrate in light and dark (calculated using the data shown in figure 9). The distance travelled was 1 mm at a speed of 0.01 mm $s^{-1}$, and the UME was held at -0.5 V w.r.t SCE. $i_T$ was divided by $I_{T\text{-bulk}}$ , and d (distance from substrate in cm) was divided by a (UME tip radius in cm)**

Although it was hard to follow the approach and retraction curves to a precipitated cell substrate (shown in figures 8 and 9) as the cleaning pulse changed the shape of the transient, different current trends seem to have been obtained depending on illumination conditions. This is more clearly shown in the normalised currents shown in figure 10, where upon approaching the algal substrate in light normalised currents increased, and in dark decreased, compared to 'bulk' values In the light, the precipitated cells making up the substrate photosynthesised. This meant as the microelectrode approached the surface; $i_T$ increased from around -2.28 nA in the 'bulk', to -2.6 nA 'close' to the substrate. The SECM experiment effectively operated in substrate generation-tip collection mode, with a concentration profile of oxygen apparent between the algal surface and the 'bulk'. 'Close' to the substrate, the flux of oxygen reaching the tip was greater at the electrode than in the 'bulk', making the current correspondingly high.

Conversely, in the dark, the algae consumed oxygen as they respired to produce carbohydrates. As the tip approached the algal substrate, the concentration of oxygen

was not only less as the algae were consuming it, but the micro electrode also would have encountered small amounts of hindered diffusion. Both of these factors decreased the flux of oxygen reaching the electrode, and the current therefore decreased from approximately -1.71 nA in the 'bulk' to -1.49 nA 'close' to the surface. In the dark, the SECM experiment effectively operated in redox competition mode, whereby the tip and the substrate were both competing for the same species.

There was a considerable difference in 'bulk' current between dark and light experiments, with the 'bulk' current in the light much higher than that in the dark. Using equation 2, the concentration of oxygen in the bulk was calculated as 0.15 mmol $dm^{-3}$ in the dark, and 0.19 mmol $dm^{-3}$ in the light. These values were reasonable (although slightly lower than expected), as seawater has an average oxygen concentration of 0.22 mmol $dm^{-3}$. The increase in oxygen concentration in the 'bulk' shown in the approach and retraction curves inferred that cells were not well adhered to the surface, with some present and photosynthesising in the 'bulk'. This was further implied by the fact that the concentration profile of oxygen in light exhibited in figure 9 (and normalised in figure 10) continuously changed when the UME was moved into the 'bulk' rather than rapidly reaching a constant value. A constant 'bulk' current value would be expected due to the fact that substrate-product concentration gradients are usually only found close to the substrate itself because of slow diffusion. As the cells were only precipitated by gravity, it was likely that the very small convection currents in solution (partly caused by the microelectrode movement) caused some mixing of cells with the 'bulk' solution. The presence of algal cells in the 'bulk' was additionally shown by chronoamperometry experiments performed with the UME stationary in the 'bulk', which showed oxygen concentration increased in light and decreased in dark (data not shown).

The light and dark response of the precipitated algal substrate was then investigated by bringing the microelectrode 'close' and stationary next to the surface, and measuring changes in limiting current at the ORR potential using chronoamperometry. This approach was potentially more powerful than approach curves as it allowed current transients to be monitored in real time. Figure 11 shows a typical response in the limiting current to illumination.

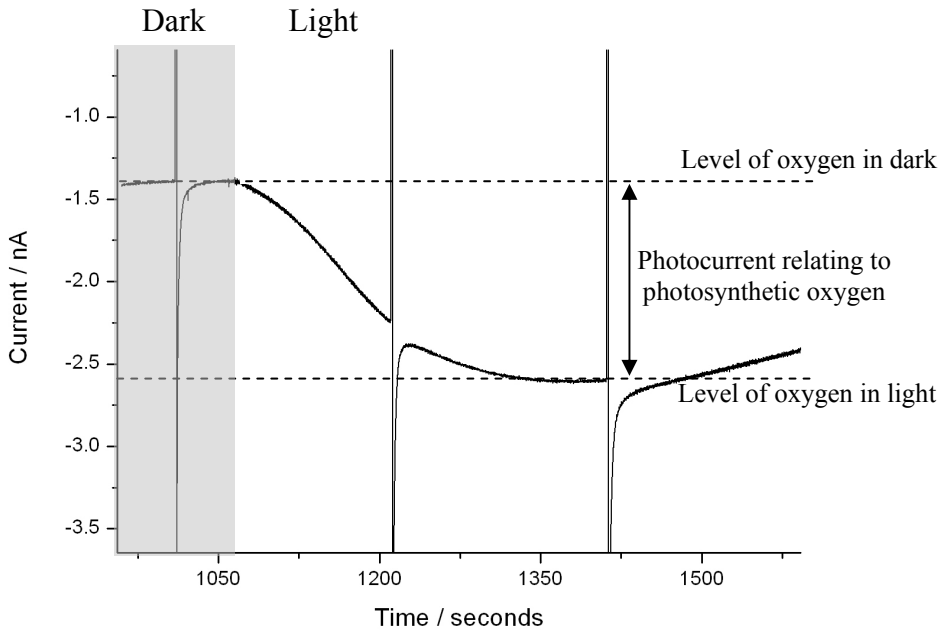


**Figure 11 Typical limiting current measured during chronoamperometry of a UME (radius 5 µm) held at -0.55 V w.r.t SCE, positioned 'close' to a precipitated algal cell substrate. The limiting current response to illumination is shown.. Areas shaded grey represent periods of darkness, whilst unshaded areas represent illumination**

As shown in figure 11, as expected, upon illumination $i_T$ increased. As the algae produced oxygen during photosynthesis, an increased flux of oxygen reached the UME and larger reduction currents were seen. The current reached a peak current within approximately 300 seconds, before decreasing slowly. It would be interesting to correlate this to speed of onset of photosynthesis. It was thought the decrease in $i_T$ was due to a decrease in the rate of photosynthesis, due to a combination of photo-inhibition (due to high light intensities) and possibly product inhibition.

Experiments subsequently explored the relationship between the time period in which the algae were in the dark, and the maximum peak current reached upon illumination (expressed as the difference between max peak current and background dark levels) The results are shown in figure 12. Corresponding concentrations of evolved oxygen were calculated using equation 2, and are shown in figure 13. Although equation 3 describes more accurately the situation when a UME (with 5µm radius) is parallel to a substrate, the 50µm tip-substrate distance was a very large distance to consider the system as analogous to a leaky thin layer cell ($d_{tip\text{-}sub}$=50 µm =10**a;* which is

approximate to the bulk), invalidating its use. Although equation 2 was not perfect, (for example due to the fact that the substrate was not uniform and allowed oxygen to diffuse through it with a diffusion coefficient different to than in the bulk), it allowed oxygen concentration to be calculated to a reasonable degree of accuracy.

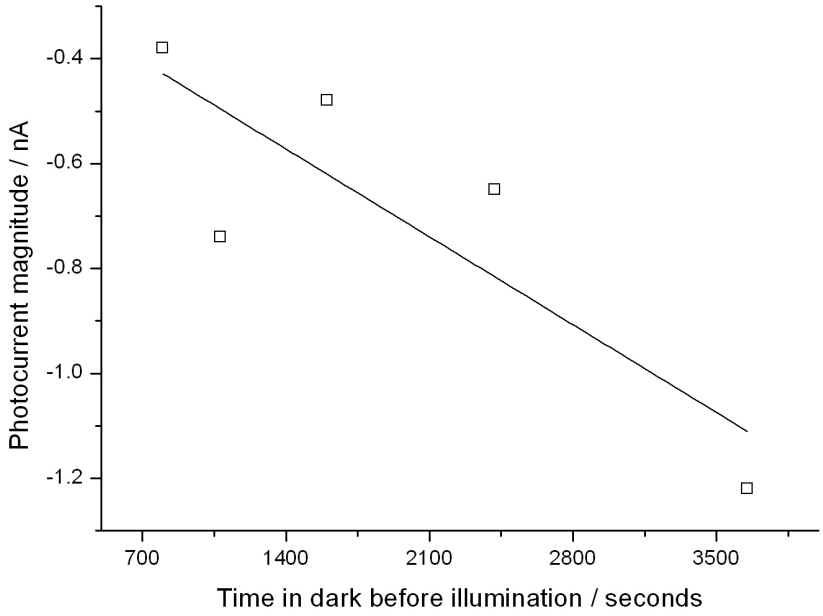


**Figure 12 The change in limiting current measured during chronoamperometry (with a UME of radius 5 µm and held at -0.55 V w.r.t SCE) upon illumination after varying lengths of time in the dark. This therefore related to photosynthetically evolved oxygen**

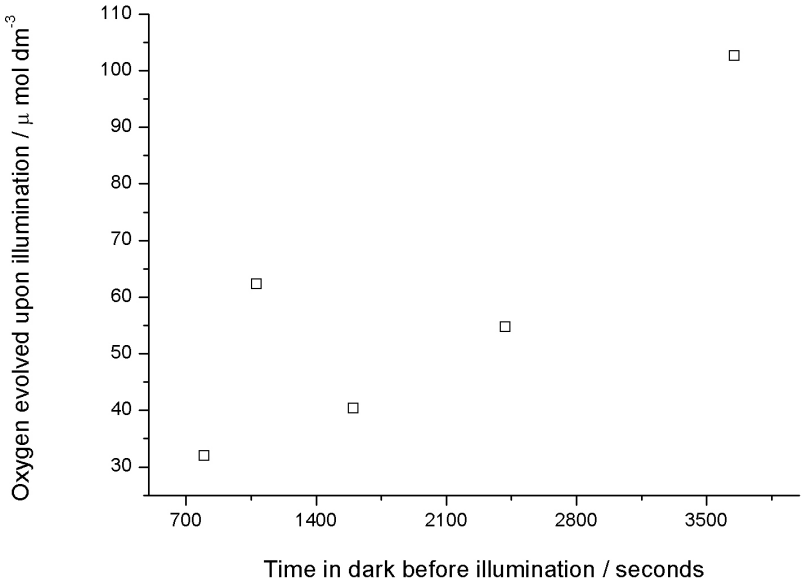


**Figure 13 The oxygen evolved during illumination after varying amounts of time in the dark. Limiting currents were measured during chronoamperometry (with a UME of radius 5 µm and held at -0.55 V w.r.t SCE). Oxygen was calculated from $i_T$=4nFDCa where $i_T$ is tip current (A), n = the number of electrons in one redox step (2.6), F = Faradays constant, D= diffusion coefficient of oxygen in water ($2.20x10^{-5}$ $cm^{-2}$ $s^{-1}$), a= the UME disc radius ($5x10^{-4}$ cm) and C= concentration (mol $cm^{-3}$)**

## 9.33 Potassium ferricyanide reduction detection – precipitated *C. vulgaris* cells

To study the ability of *C. vulgaris* cells to reduce ferricyanide to ferrocyanide, a thick precipitate of cells similar to that used in 9.32 was used as a substrate, with 1 mM ferrocyanide in solution. Cyclic voltammetry in the 'bulk' was then used to identify a potential 100 mV past the oxidation potential for ferrocyanide (results not shown). This value was then used to set the potential of the UME during chronoamperometry. In this way, only ferrocyanide existed in the bulk solution, with ferricyanide produced at the tip of the UME to give a current $i_T$. If the algae reduced ferricyanide to ferrocyanide, $i_T$ should increase with respect to that in the bulk. In this case, the SECM should operate in the feedback mode.

Whilst performing chronoamperometry at 0.4 V w.r.t SCE, approach and retraction curves were recorded between 0 and 1 mm distance from the algal precipitated substrate, at 0.001 mm $s^{-1}$ (note, two hours existed between each measurement, with the UME held at open circuit between them). Figure 14 shows original

chronoamperometry measurements performed in light and dark, with summary approach curves shown in figure 15. Approach curves were normalised with respect to 'bulk' current values and the radius of the UME, and are shown in figure 16.

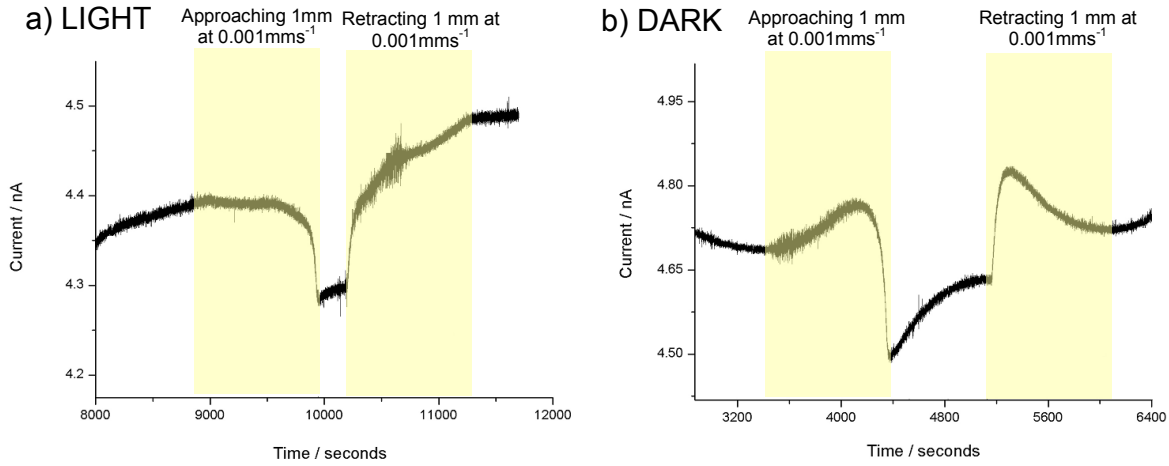


**Figure 14 Chronoamperometry during approach and retraction of a UME (radius 12.5 µm held at 0.4 V w.r.t SCE) to a precipitated cell substrate in a) the light and b) the dark, with 1 mM ferrocyanide in solution. The distance travelled was 1 mm at a speed of 0.001 mm $s^{-1}$. Yellow shaded areas indicate time periods of UME movement**

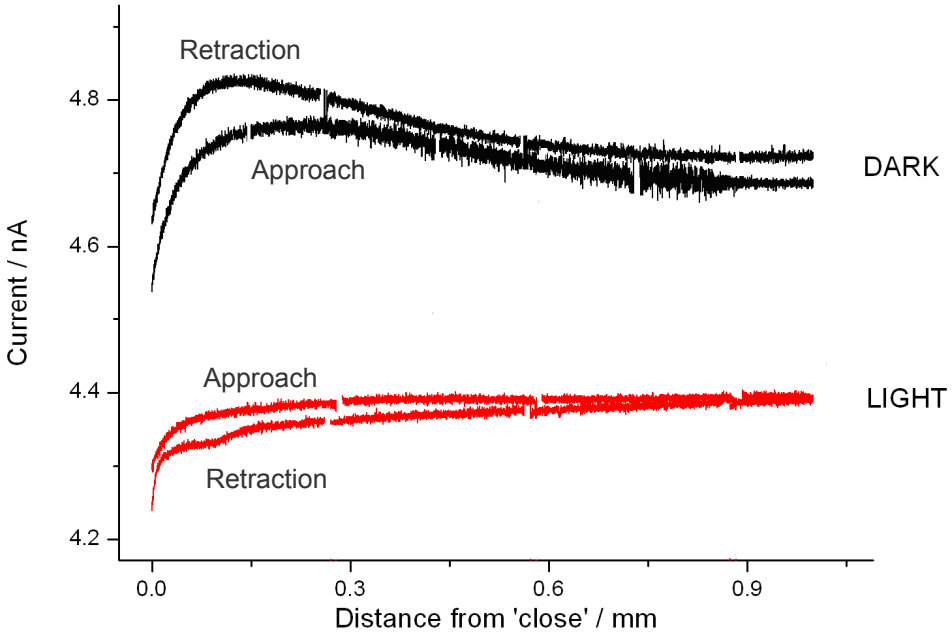


**Figure 15 Approach and retraction curves of a UME (radius 12.5 µm held at 0.4 V w.r.t SCE) to a precipitated cell substrate in light and the dark, with 1 mM ferrocyanide in solution. The distance travelled was 1 mm at a speed of 0.001 mm $s^{-1}$**

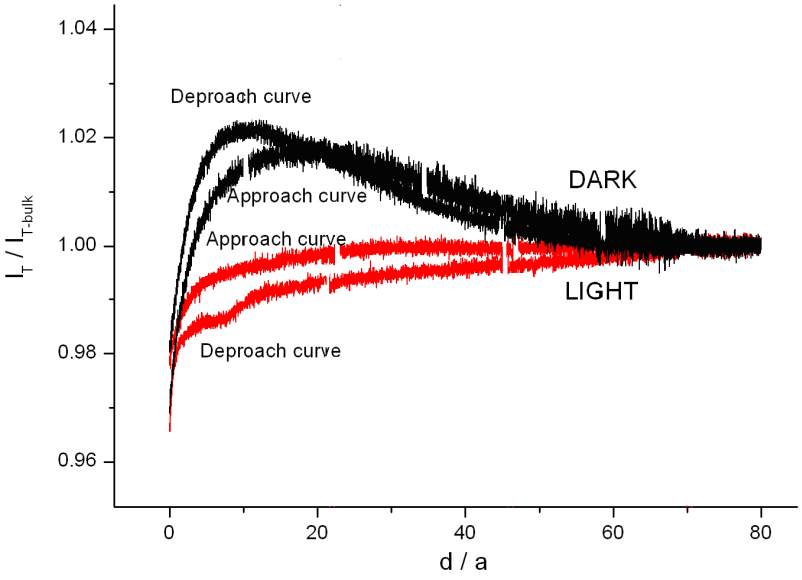


**Figure 16 Normalised approach and retraction curves of a UME (radius 12.5 µm held at 0.4 V w.r.t SCE) to a precipitated cell substrate in light and dark (calculated using the data shown in figure 16), with 1mM ferrocyanide in solution. The distance travelled was 1mm at a speed of 0.001 mm $s^{-1}$. $i_T$ was divided by $I_{T\text{-bulk}}$ , and d (distance from substrate in cm) was divided by a (UME tip radius in cm).**

Figures 15 and 16 show that different feedback effects were observed in light and dark. In the dark, on approaching the algal surface, an increase in the current was seen (similar to positive feedback). In this process, as the UME was brought closer to the algae, ferricyanide produced at the tip began to be reduced to ferrocyanide by the algae, which then increased the reoxidation rates at the tip due to feedback effects. However, true positive feedback can only happen if $d_{tip\text{-}sub}$ is less than the diffusion layer thickness, i.e less than 10 times the tip radius. As dark currents increased far into the 'bulk' in figures 15 and 16 (approximately 0.7 mm away from the surface), and change was not localised to 'close' distances within the diffusion layer, this meant that the algae were floating within the 'bulk'. This situation was not ideal. Conversely, in the light, slight negative feedback was observed. This did not correspond to pure hindered diffusion as seen over insulating substrates, so it could be assumed that some turn over by the algae occurred, although at a slower rate to that in the dark. Similar to in the dark, tip currents changed far into the 'bulk' in the light. Total currents in the 'bulk' were greater in the dark than in the light. Using equation

2, the concentration of ferrocyanide in the bulk was calculated as 1.35 mmol $dm^{-3}$ in the dark, and 1.28 mmol $dm^{-3}$ in light. However, as the measurements were taken within two hours of each other, this may be due to the time difference. Interestingly, at 'close' distances, and after the tip had finished moving, a slow, then rapid drop in the current was observed in both light and dark. This could correlate with the tip touching the algal surface, with hindered diffusion occurring.

The UME was then positioned 'close' to the algal substrate, and the current measured with the substrate illuminated and in the dark (figure 17). Figure 17 shows that although the curve was complex, on the whole, the current was lower in the dark and increased in the light. In contrast to the results shown in figure 15 and 16, this suggested that the feedback effects and rates of algal reduction of ferricyanide were greater in the light than the dark. This would mean that in light, extra electrons can be gained from photosynthesis. The complexity of the curve upon light off could be interpreted as the transition from using reductive equivalents generated in photosynthesis, to using those generated in respiration (in the dark). The decrease in current could be due to the fact that the production of photosynthetic reductive equivalents (electrons) are 'switched off', and it takes some time to switch to using reductive equivalents from other respiratory pathways. The shape of the current transient in light/dark is similar to photocurrents obtained from chronoamperometry in chapter 5, making it likely it represents real patterns.

Figure 18 shows that currents measured in the 'bulk' under illumination and in the dark showed similar patterns. Again the currents decreased in the dark, and increased under illumination. Irrespective of whether the UME was positioned 'close' or in the 'bulk' the maximum current change was approximately 200 pA. This current response in the 'bulk' again inferred that the algae were not firmly attached to the substrate, and were floating in solution. Figures 15 and 16 showed currents to be higher in the 'bulk' solution than 'close' to the algae, as they were taken at the same time as the approach curve in light shown in figure 14. More work is needed to determine if this was a real response, or if it was a time resolved problem.

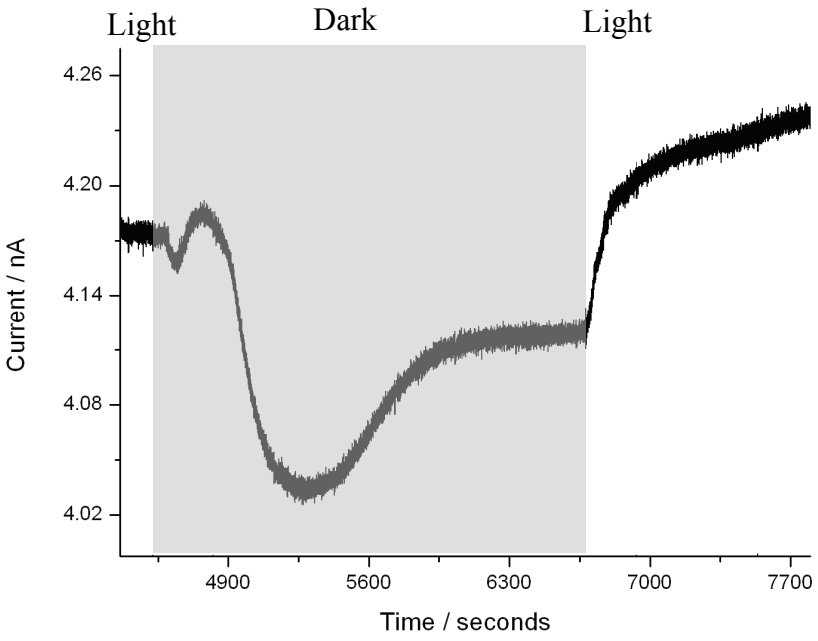


**Figure 17 Chronoamperometry measurements with UME (radius 12.5 µm held at 0.4 V w.r.t SCE), showing current response in light and dark. The UME was positioned 'close' to a precipitated algal substrate, with 1 mM ferrocyanide in solution. Areas shaded grey represent periods of darkness, whilst unshaded areas represent illumination**

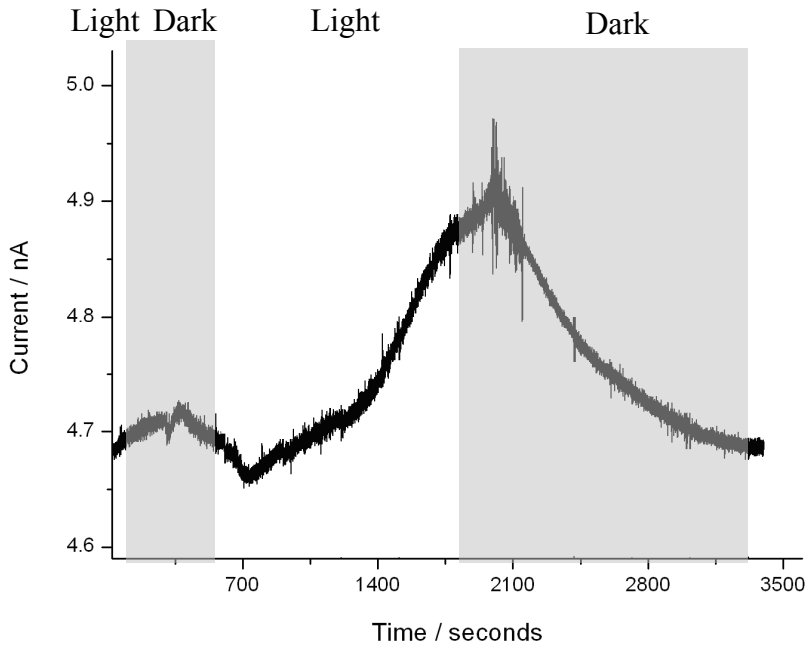


**Figure 18 Chronoamperometry measurements with UME (radius 12.5 µm held at 0.4 V w.r.t SCE), showing current response in light and dark. The UME was positioned in the 'bulk' from a precipitated algal substrate, with 1 mM ferrocyanide in solution. Areas shaded grey represent periods of darkness, whilst unshaded areas represent illumination**

Interestingly, other studies investigating the electron transfer between ferricyanide and the photosynthetic electron transport chain found no response of the redox current upon light irradiation [7]. They ascribed this to the fact that the permeability for the passage of ferricyanide through the algal protoplast membrane is small. However, this explanation did not take into the account the fact that ferricyanide can be reduced on the algal membrane by ferri-reductase proteins (as demonstrated throughout this thesis and especially in chapters 4 and 5). Additionally, topography of a cell was studied by scanning the UME in the presence of 1 mM ferrocyanide, with the UME set 100 mV past the oxidation potential for ferrocyanide (0.4 V w.r.t Ag/AgCl) [7]. The oxidation current decreased over the cell because of blocking of diffusion when the tip approached the protoplast surface measurement; this is in contrast to the positive feedback effects seen in the dark in figure 16.

## 9.4 Conclusions

SECM was applied to study characteristics of *C. vulgaris* biofilms (oxygen production and ferricyanide reduction), with the emphasis that in future health and reductive ability of biofilms in a MFC could be monitored in situ. All work presented represented preliminary experiments; therefore it was difficult to draw conclusions from such initial data.

SECM proved a sensitive technique for the detection of photosynthetic oxygen production and respiratory consumption by the algae, as used in other studies [4-7]. To detect oxygen, a procedure modified from Sosna *et al.* was used [19]. When a potential corresponding to the ORR was applied to the UME tip, a limiting current was reached which directly corresponded to the amount of oxygen in solution. With the onset of photosynthesis, this limiting current increased with the production of oxygen. Conversely, in the dark, the limiting current decreased as oxygen was consumed by the algae. The SECM operated in different modes depending on illumination conditions. In light, where oxygen was produced by the algae, the SECM operated in substrate generation, tip collection mode. In the dark, where both the algae and the UME tip consumed oxygen, the SECM operated in redox competition mode.

Oxygen was measured using cyclic voltammetry and chronoamperometry methods. It was apparent that the sensitivity for oxygen measurements was higher when chronoamperometry was performed. With cyclic voltammetry, although differences between light and dark voltammograms could be seen, (corresponding to photosynthetic production of oxygen in light and respiratory consumption in dark), differences were low. Oxygen concentrations could additionally not be continuously measured using cyclic voltammetry. Conversely, chronoamperometry enabled oxygen concentration to be studied in real time, allowing the photosynthetic production of oxygen to be monitored immediately after cells were illuminated.

Oxygen production of *C. vulgaris* cells prepared by different methods was tested. Initially, cells were cultured on agar as it was thought that this would anchor them to the substrate, giving a maximum concentration gradient of oxygen between 'close' (where the cells were) and 'bulk' solution distances. However, it became apparent that cell density on the agar was too low to give high measurement sensitivity. Due to this, cells were simply allowed to precipitated out into a thick layer over 12 hours prior to measurements. Although not anchored to the surface, providing the UME moved slow enough near the cells so as not to disturb them, reasonably high measurement sensitivity was achieved, with distinction between 'close' and 'bulk' positions.

SECM was also used to investigate the reduction of a ferricyanide mediator by *C. vulgaris* precipitated out into a thick layer. For this, 1 mM ferrocyanide was added to the electrolyte solution and the UME tip was held 100 mV past the oxidation potential for ferrocyanide. In this way, the SECM operated in feedback mode; ferricyanide was created at the UME tip giving a certain limiting current; if the algae reduced it, positive feedback effects occurred and currents increased. Otherwise, negative feedback (hindered diffusion) would occur. Results were slightly conflicting; approach curves showed positive feedback effects occurring in the dark and slight negative feedback effects occurring in light. This inferred algal reduction was greater in dark than light. However, when the SECM was held stationary close to the algal surface (and in the bulk), it was found that currents were higher in light than dark. This suggested that photosynthesis increased the feedback effects, meaning that reduction was increased under illumination. Other results shown in chapter 5, as well

as the vast majority of pMFC literature corroborate (see chapter 5 for details) this latter implication. Interestingly, the complexity of the ferricyanide reduction currents 'close' to the algal substrate in light and dark mirrored chronoamperometry experiments in the 'bulk' performed in chapter 5, whereupon various peaks and troughs occurred before stable current values were reached. This inferred the shape of the current curve represented real patterns of ferricyanide reduction, and not measurement artefacts. The complexity of the curves upon illumination or the dark could be interpreted as the transitional interplay from using photosynthetically produced reductive equivalents to respiratory produced reductive equivalents in differing light conditions.

Overall, SECM experiments offer great potential for future characterisation of MFC biofilms. However, it was apparent when performing the SECM experiments that the algae were not well adhered to the substrate; even when grown on agar. This was evident from the deviation of bulk behaviour from that expected, inferring algae were floating in solution. This led to approach curves exhibiting changing currents far into the 'bulk' away from the algal substrate. Before further experiments are performed, the issue of immobilising algae on a substrate must be well addressed; until then, 'bulk' and 'close' distances are indistinguishable

## 9.5 References

1. Bertoncello, P., *Advances on scanning electrochemical microscopy (SECM) for energy.* Energy & Environmental Science, 2010. **3**(11): p. 1620-1633.
2. Beaulieu, I., Kuss, S., Mauzeroll, J., and Geissler, M., *Biological Scanning Electrochemical Microscopy and Its Application to Live Cell Studies.* Analytical Chemistry, 2011. **83**(5): p. 1485-1492.
3. Edwards, M.A., Martin, S., Whitworth, A.L., Macpherson, J.V., and Unwin, P.R., *Scanning electrochemical microscopy: principles and applications to biophysical systems.* Physiological Measurement, 2006. **27**(12): p. R63-R108.
4. Yasukawa, T., Kaya, T., and Matsue, T., *Imaging of photosynthetic and respiratory activities of a single algal protoplast by scanning electrochemical microscopy.* Chemistry Letters, 1999(9): p. 975-976.

5. Zhu, L.L., Gao, N., Zhang, X.L., and Jin, W.R., *Accurately measuring respiratory activity of single living cells by scanning electrochemical microscopy.* Talanta, 2008. **77**(2): p. 804-808.
6. Kaya, T., Torisawa, Y.S., Oyamatsu, D., Nishizawa, M., and Matsue, T., *Monitoring the cellular activity of a cultured single cell by scanning electrochemical microscopy (SECM). A comparison with fluorescence viability monitoring.* Biosensors & Bioelectronics, 2003. **18**(11): p. 1379-1383.
7. Yasukawa, T., Kaya, T., and Matsue, T., *Characterization and imaging of single cells with scanning electrochemical microscopy.* Electroanalysis, 2000. **12**(9): p. 653-659.
8. Matsue, T., Koike, S., and Uchida, I., *Microamperometric estimation of photosynthesis inhibition in a single algal protoplast.* Biochemical and Biophysical Research Communications, 1993. **197**(3): p. 1283-1287.
9. Matsue, T., Koike, S., Abe, T., Itabashi, T., and Uchida, I., *An ultramicroelectrode for determination of intracellular oxygen-light irradiation-induced change in oxygen concentration in an algal protoplast* Biochimica Et Biophysica Acta, 1992. **1101**(1): p. 69-72.
10. Liu, B., Rotenberg, S.A., and Mirkin, M.V., *Scanning electrochemical microscopy of living cells: Different redox activities of nonmetastatic and metastatic human breast cells.* Proceedings of the National Academy of Sciences of the United States of America, 2000. **97**(18): p. 9855-9860.
11. Cai, C.X., Liu, B., Mirkin, M.V., Frank, H.A., and Rusling, J.F., *Scanning electrochemical microscopy of living cells. 3. Rhodobacter sphaeroides.* Analytical Chemistry, 2002. **74**(1): p. 114-119.
12. Wei, C., Bard, A.J., and Mirkin, M.V., *Scanning electrochemical microscopy 31. Application of SECM to the study of charge-transfer processes at the liquid-liquid interface.* Journal of Physical Chemistry, 1995. **99**(43): p. 16033-16042.
13. Yasukawa, T., Uchida, I., and Matsue, T., *Microamperometric measurements of photosynthetic activity in a single algal protoplast.* Biophysical Journal, 1999. **76**(2): p. 1129-1135.
14. Ikeda, T., Kurosaki, T., Takayama, K., Kano, K., and Miki, K., *Measurements of oxidoreductase-like activity of intact bacterial cells by an amperometric*

*method using a membrane-coated electrode.* Analytical Chemistry, 1996. **68**(1): p. 192-198.

15. Zhou, H.F., Kasai, S., Noda, H., Ohya-Nishiguchi, H., Shiku, H., and Matsue, T., *Characterization of the peroxidase activity of single algae protoplasts by scanning electrochemical microscopy.* Bulletin of the Chemical Society of Japan, 2003. **76**(9): p. 1757-1762.
16. Middlemiss, J.K., Anderson, A.M., Stratilo, C.W., and Weger, H.G., *Oxygen consumption associated with ferric reductase activity and iron uptake by iron-limited cells of Chlorella kessleri (Chlorophyceae).* Journal of Phycology, 2001. **37**(3): p. 393-399.
17. Weger, H.G. and Espie, G.S., *Ferric reduction by iron-limited Chlamydomonas cells interacts with both photosynthesis and respiration.* Planta, 2000. **210**(5): p. 775-781.
18. Weger, H.G., *Ferric and cupric reductase activities in the green alga Chlamydomonas reinhardtii: experiments using iron-limited chemostats.* Planta, 1999. **207**(3): p. 377-384.
19. Sosna, M., Denault, G., Pascal, R., Prien, R., and Mowlem, M., *Development of a reliable microelectrode dissolved oxygen sensor.* Sensors and Actuators B: Chemical, 2007. **123**(1): p. 344-351.

# Chapter 10. Conclusions and Future Work

# Chapter 10 – Conclusions and Future work

## 10.1 Conclusions

Previous chapters demonstrated the possibility to use the algae *Chlorella vulgaris* as the biological material in a p-MFC. A basic p-MFC device was first assembled utilising *C. vulgaris* cells and a potassium ferricyanide (ferricyanide) mediator. The presence of ferricyanide was required to transmit electrons from the cells to the anode. Advantages of this system included the fact it used whole cells, was oxygenic and iron replete; conditions optimum for the longevity of the photosynthetic material and hence the p-MFC device. However, after studying current and power outputs, it was realised a major disadvantage of the p-MFC device was that outputs could not be directly related to cellular activity. To better characterise the complete p-MFC device, the interactions of *C. vulgaris* and the ferricyanide mediator were studied.

*C. vulgaris* is thought to reduce ferricyanide through ferric reductase proteins in its cell membrane. UV-Vis and three electrode chronoamperometry measurements showed the rate of reduction increased with both ferricyanide and algal cell concentration. Under similar conditions (1 mM ferricyanide and $7x10^7$ cells $mL^{-1}$), both measurements gave a reduction rate of around 1 nmol Fe(III) $10^{-6}$ cells $hr^{-1}$ in the dark. Light was shown to slightly increase ferricyanide reduction rates; as shown by chronoamperometry and SECM measurements. However, both chronoamperometry and SECM showed the effect of light was complicated, with transitional patterns upon illumination requiring further study. Rotating disk electrochemistry showed the reduction of ferricyanide was rate limited by mass transport of ferricyanide and ferrocyanide (both to cells, and to electrode), and not kinetics. When total ferrocyanide was calculated (and normalised per $10^{-6}$ cells), the reduction rate increased with ferricyanide concentration but was relatively constant with number of cells. This showed the cells reduced ferricyanide at a certain rate, which was limited by the amount of redox mediator in solution.

Cellular interactions were studied. Ferricyanide was found toxic in the long term at concentrations over 0.001 mM at times over 24 hours. Fluorescence showed ferricyanide, and not ferrocyanide, induced a reversible quenching effect, which increased with concentration. Weger *et al.* suggested that the inhibition of $CO_2$

fixation during extracellular ferricyanide reduction was the major cause of the non-photochemical quenching [1]. This could also explain the toxicity. Oxygen measurements also showed that the presence of ferricyanide decreased the amount of photosynthetic oxygen evolved during illumination. This effect increased with ferricyanide concentration. The reason for the decrease in oxygen evolution was not known, but could be explained by a possible feedback mechanism from the inhibition of $CO_2$ fixation.

The cyanobacterium *Synechocystis* was also found to reduce ferricyanide in a similar way to *C. vulgaris*. Lower rates of reduction were observed per cell with *Synechocystis* than with *C. vulgaris*. With 1mM ferricyanide and $7x10^7$ cells $ml^{-1}$, UV-Vis gave initial dark *Synechocystis* rates of ferricyanide reduction of 0.41 nmol Fe(III) $10^{-6}$ cells hr, ~3.5 lower than that for *C. vulgaris*. Chronoamperometry gave dark *Synechocystis* ferricyanide reduction rates as 0.1 nmol Fe(III) $cm^{-2}$ $10^{-6}$ cells $hr^{-1}$ (with 14 day old cells) compared to 0.5 nmol Fe(III) $cm^{-2}$ $10^{-6}$ cells $hr^{-1}$ with *C. vulgaris*. This was a difference of a factor of five. Using rotating disk in the dark with 22 mM ferricyanide and $9.26x10^7$ cells $mL^{-1}$, total bulk ferrocyanide was ~0.5 nmol $10^{-6}$ $ml^{-1}$ cells with *Synechocystis*, and ~0.75 nmol $10^{-6}ml^{-1}$ cells with *C. vulgaris* (a difference of a factor of 1.5). These differences could be due to a lower reduction ability per *Synechocystis* than *C. vulgaris* cell, due to lower mass. Chlorophyll content of each species was compared and it was discovered that *C. vulgaris* contains a factor of 4.4 more chlorophyll than *Synechocystis* on a cell to cell basis.

As with *C. vulgaris,* rotating disk electrochemistry showed most reduction was limited by mass transport, not kinetics. However, for the lowest cell concentrations tested (with 3 mM ferricyanide), kinetic limitations applied to the rate. Kinetic limited rates of reduction were calculated from the intercepts, and averaged at 1 nmol Fe(III) $cm^{-2}$ $hr^{-1}10^{-6}$ cells (close to the maximum plateaued rate of reduction seen in chronoamperometry with 1mM ferricyanide and increasing cells (14 day old culture)). The similarity makes it likely that the chronoamperometry also measured kinetic limited rates. Calculated heterogeneous rate constants were large, and averaged around 0.08 cm $s^{-1}$. This showed the redox centres responsible for the electron transfer in *Synechocystis* cells were reversible, with correspondingly large reorganisation energies. It is likely that these kinetic limitations were not seen with *C.*

*vulgaris* due to the differences in cell mass – lower cell concentrations of *C. vulgaris* are therefore required to be tested.

Porous titanium dioxide ceramics were prepared to address the lack of a suitable anodic material in p-MFC research. The electrode material developed contained mm sized pores, as well as a nanostructured high internal surface that appeared to aid algal attachment. Despite higher overall algal loading in carbon felt electrodes, ceramic electrodes had good loading as a function of their surface area, and were proved highly biocompatible. Devices constructed using this material with biofilms grown on it had some advantages over previous Indium tin oxide (ITO) and fluorine coated tin oxide (FTO) coated planar glass electrodes. Due to the fact that the basic p-MFC was essentially a thin layer cell, it offered low diffusion distances resulting in relatively large currents for its surface area and fast response times. When the ceramics were assembled in a p-MFC device, the volume (and dimensions) of the anodic chamber was increased to accommodate them. Although this increased diffusion distances, due to the larger volume the algae was grown in (and the fact that the electrolyte in the anodic/cathodic chamber was unlikely to dry out), the p-MFC device offered longer term operation. Biofilms were also more strongly attached to the ceramics than flat ITO/FTO electrodes. Power densities better than many literature reports were shown using the ceramics as the p-MFC anode; an exciting result considering that in this study the cells were not optimised.

Due to the toxicity ferricyanide represented to the cells, finding an alternative was imperative for device optimisation. Cytochrome C (cyt C) and the immobilised redox polymer polyaniline (PANI) were tested for their interaction affinity with *C. vulgaris*. With cyt C, it appeared as if the algae immediately reduced this species upon contact. Additionally, it appeared as if the vast majority of cyt C in solution became complexed with algae, before being released over time in light. The apparent binding of cyt C to algae made it non-ideal for use in a p-MFC. Ceramics were coated with the conductive polymer PANI using a simple method. SEM and culturing studies confirmed that this surface was biocompatible towards the algae *C. vulgaris*, and device studies utilising it as the working electrode showed that the PANI could act as an electron acceptor for the algae. However, the redox state of the PANI was emeraldine salt when in solution with media, decreasing its conductivity. In addition,

the redox activity of the PANI seemed to degrade constantly (as shown by falling device voltage measured in polarisation curves). Consequently the PANI ceramic electrode had no place in the device in the long-term.

Although the project made good headway towards the aims and objectives set out in chapter 1, much more work is needed to make p-MFC devices economically viable.

## 10.2 Future Work

Future work on the p-MFC device should focus on the continuation of the original project aims. More understanding is required on the process of mediator reduction by cells, the source of reductive equivalents in light and dark and the p-MFC device in general. Additionally, full optimisation of all components of the p-MFC device is required to increase power outputs.

Despite the best efforts in this thesis, the precise contributions of light and dark processes towards the reduction of a mediator have still not been satisfactorily resolved. Although most experiments performed showed most reductive equivalents were produced by dark (respiratory processes), with small amounts of extra being produced in light (from photosynthesis), no straight forward relationship was found to exist. Although NADPH is thought the main reductive equivalent that reacts with a mediator, this should be investigated. Future experiments are required whereby photosynthetic inhibitors (such as DCMU) are added to experiments run in parallel to those without. This would allow (with a high degree of certainty) the discrimination between the reductive equivalent contributions of different metabolic cell processes (i.e respiration and photosynthesis). Ideally, an oxygen sensor should also be continuously used in all measurements to enable the photosynthetic activity to be determined, which gives a measure of cell health. Other useful measurements could include SECM and further rotating disk electrochemistry in dark and light, not only to determine the difference illumination makes to electron transfer, but also to determine if mediator reduction follows Michaelis-Mentin kinetics. Methods for this are outlined in papers by Torimura *et al.* [2] and Kasuno *et al.* [3].

Due to the fact that the reduction of ferricyanide by cells has been shown to be limited by mass transport, stationary conditions in a device are not ideal. More generally, measurements at stationary electrodes are not ideal as they are not under steady state conditions, with the concentration of the reduced mediator at the surface of the electrode not remaining constant. This makes it difficult to validate any findings due to the complex thermodynamics and kinetics of the system. In addition to this, a long running self sustaining device is more achievable under systems of flow, whereby biological waste products can be removed. This makes future work in the form of flow cells imperative.

This project also only considered two photosynthetic species; a typical alga and a typical cyanobacterium. A much greater search is needed to identify a better suited species; with many requirements existing. Performance of a p-MFC is known to degrade over time, in part due to cell electron starvation due to the high currents being drawn from it. A species well tolerated to this is required. Other requirements include high biomass production (even in the presence of a mediator), minimized absorption of single cells (if cells in solution are used for example in flow cells), high biomass production and tolerance against shear forces due to continuous flow.

Due to the limitations an artificial redox mediator imposes on a p-MFC system, for example, due to toxicity, either new mediators are required or a species is needed which can form biofilms and transfer electrons directly to the anode. These latter microbial species, classed as anodophiles, have the ability to form a biofilm on the anode itself and utilise a series of conductive components in the extracellular matrix to completely oxidise organic compounds with an electrode as sole electron acceptor. No algal species have been yet been identified which can perform direct electron transfer, although some studies have reported direct electron transfer occurring in various cyanobacteria, including *Synechocystis PCC 6803* [4]. *Synechocystis PCC 6803* was used in this thesis, but no biofilms (required for direct electron transfer) could be created using it. p-MFCs utilising direct electron transfer would be highly advantageous as they are operationally stable, yield a high Coulombic efficiency and eliminate mediator costs [5, 6]. Additionally, this type of species can conserve energy from electron transfer to an electrode[7] making them ideal for use in up-scale MFCs. Disadvantages of this type of p-MFC involve the fact that most redox proteins are

known to undergo slow heterogeneous electron transfer at electrode surfaces, and active sites are typically buried deep within enzymes resulting in poor electrode kinetics [8],

If a mediator is to be used, a natural redox mediator would potentially be most ideal as these are generally much less toxic to cells. Due to the interesting results gained in this thesis with cyt C (chapter 7), other redox mediators found within cells should be tested. Other future mediator candidates could include quinones or humic acids. Rotating disk electrochemistry and UV-Vis are ideal methods to screen for interactions between cells and any added chemicals. For highest p-MFC efficiency, the most ideal redox mediator would have a redox potential only slightly more positive than the reductive equivalents it interacts with. An interesting experiment would be to produce an array of similar mediators spanning a full range of redox potentials; determining which interact with cells would shed some light as to the redox state of the cellular reductive equivalents contributing electrons for p-MFC power output.

Tethered mediators also require further study. There are many benefits to having a layer of mediator tethered to the anode (rather than in solution) with a biofilm grown on its surface; most importantly, the fact that if all anodic reactions are confined to the anode itself a proton exchange membrane (PEM) would not be needed. This would not only reduce the resistance of the p-MFC device, but as ohmic losses would be reduced, the cell voltage ($E_{cell}$) would be increased. Preliminary experiments with biofilms grown on PANI (not shown in this thesis) proved this concept was possible. Other benefits of a tethered mediator would include reduced cost due to lower mediator throughput.

The anode material allows much scope for optimisation. Although in this thesis the production of titanium dioxide ceramics was reported, these were not optimised for biocompatibility and showed lower cell coverage than other material. The surface of the titanium dioxide ceramic could easily be modified to allow cells to more strongly attach by increasing microstructure roughness (according to the attachment point theory, see chapter 8). A micro-structured coating or a technique analogous to light sandblasting is required to roughen the surface. However, FTO coated ceramics as a

whole are non-ideal for use as an anode material due to the need for a two step production (i.e, production of ceramics, followed by FTO coating). Not only is this time consuming, but it is also expensive. If a porous biocompatible material could be made using a conductive substrate, anode processing would become much more economically viable. In practice, a conductive material such as reduced $TiO_2$ or Magnelli phases could be used. These would then require no extra conductive coating.

Overall, the p-MFC device has exciting implications for future energy production. However, as virtually every aspect of the device needs to be further improved to make it viable, it is unlikely that power output from p-MFCs will rival that of MFCs (or other energy devices) any time in the near future. As p-MFCs can potentially offer extremely beneficial carbon neutral/ capture benefits compared to a MFC, perhaps this is not so important. Using a photosynthetic species offers the potential for the production of carbon neutral energy (as carbon is sequestered in photosynthesis, before being released during respiration). An even greater advantage would be to sequester carbon entirely; to this end one idea is to use metal-organic frameworks to permanently sequester the carbon dioxide and this is a major part of the continuation of the project by another student. No one renewable power source is likely to dominate in the future. p-MFCs could be used where a self sustaining power source is needed in remote places. It is also likely that where photosynthetic material is cultured in large batches for biomass for biofuels, a p-MFC device could be installed to additionally produce a power output. Waste remediation could also simultaneously be performed. In this way, the use of algae would become overall much more economically viable.

## 10.3 References

1. Weger, H.G., C.N. Walker, and M.B. Fink, *Ferric and cupric reductase activities by iron-limited cells of the green alga Chlorella kessleri: quantification via oxygen electrode.* Physiologia Plantarum, 2007. **131**(2): p. 322-331.
2. Torimura, M., et al., *Electrochemical investigation of cyanobacteria Synechococcus sp PCC7942-catalyzed photoreduction of exogenous quinones*

*and photoelectrochemical oxidation of water.* Journal of Electroanalytical Chemistry, 2001. **496**(1-2): p. 21-28.

3. Kasuno, M., et al., *Characterization of the photoinduced electron transfer reaction from the photosynthetic system in Rhodobacter sphaeroides to an exogenous electron acceptor.* Journal of Electroanalytical Chemistry, 2009. **636**(1-2): p. 101-106.
4. Pisciotta, J.M., Y. Zou, and I.V. Baskakov, *Light-Dependent Electrogenic Activity of Cyanobacteria.* Plos One, 2010. **5**(5).
5. Ieropoulos, I.A., et al., *Comparative study of three types of microbial fuel cell.* Enzyme and Microbial Technology, 2005. **37**(2): p. 238-245.
6. Chaudhuri, S.K. and D.R. Lovley, *Electricity generation by direct oxidation of glucose in mediatorless microbial fuel cells.* Nature Biotechnology, 2003. **21**(10): p. 1229-1232.
7. Lovley, D.R., *Bug juice: harvesting electricity with microorganisms.* Nature Reviews Microbiology, 2006. **4**(7): p. 497-508.
8. Zhao, F., R.C.T. Slade, and J.R. Varcoe, *Techniques for the study and development of microbial fuel cells: an electrochemical perspective.* Chemical Society Reviews, 2009. **38**(7): p. 1926-1939.

# Chapter X. Appendices

# x.1 Appendix A – Experimental used in all chapters

The appendix outlines experimental techniques crucial to the culturing of the biological material, used throughout all chapters.

## x.11 Photosynthetic material

The algal species *Chlorella vulgaris* and the cyanobacterial species *Synechocystis PCC 6803* were maintained on sterile agar plates (2 % wt / V) under a 24hr light regime (Table 1). Colonies were isolated from bacterial contamination using a standard microbiological streaking technique. Stock cultures were kept as sterile as possible, and all cell work utilised good aseptic technique. This involved working in a flowhood, and sterilising all materials/equipment/work surfaces for cell manipulations by autoclaving or with 70 % ethanol.

After agar plates were left to grow for approximately 2 weeks, samples of the pure colonies were used to inoculate 250 mL flasks containing 100 mL of sterile media (either Bolds Basal Medium with 3 fold Nitrogen and Vitamins (3N-BBM+V) for *C. vulgaris* or BG11 for *Synechocystis*). In this manner, new cultures were made every 2 weeks. Conical flasks were stoppered with a sterile foam bung and covered using sterilised tin foil. Cultures were left on an orbital shaker (rotating at 100 rpm) and a lightbox (from Lightbox UK). After culturing for approximately 21-35 days (after which cells had come out of logarithmic growth phase), cells were deemed ready for use.

Table 1 shows the agar recipe used for all cell work, tables 2 and 3 shows the 3N-BBM+V media recipe and 3N-BBM+V trace element solution for *C. vulgaris* and tables 4 and 5 shows the BG11 media recipe and BG11 trace element solution for *Synechocystis*. All chemicals were from Sigma Aldrich, with purities>98%.

| **Substance** | **Amount** |
|---|---|
| Agar | 20 g |
| 3N-BBM+V or BG11 media | 1 L |

**Table 1 Agar recipe for solid cultures of both *C. vulgaris* and *Synechocystis* cells**

| Substance | Amount |
|---|---|
| $NaNO_3$ | 1.5 g |
| $CaCl_2.2H_2O$ | 0.05 g |
| $MgSO_4.H_2O$ | 0.0844 g |
| $K_2HPO_4$ | 0.1144 g |
| $KH_2PO_4$ | 0.35 g |
| NaCl | 0.05 g |
| Vitamin $B_1$ | 0.0024 g |
| Vitamin $B_{12}$ | 0.00002 g |
| Milli-Q water | 1988 mL |
| Trace Element Solution | 12 mL |

**Table 2.3N-BBM+V media recipe for liquid cultures of *C. vulgaris***

| Substance | Amount (mg $L^{-1}$) |
|---|---|
| $Na_2EDTA$ | 750 |
| $FeCl_3.6H_2O$ | 97 |
| $MnCl_2.4H_2O$ | 41 |
| $ZnCl_2.6H_2O$ | 5 |
| $CoCl_2.6H_2O$ | 2 |
| $Na_2MoO_4.2H_2O$ | 4 |

**Table 3. Trace element solution recipe used in 3N-BBM+V media**

| Substance | Amount |
|---|---|
| $NaNO_3$ | 1.5 g |
| $K_2HPO_4$ | 0.04 g |
| $MgSO_4.H_2O$ | 0.0844 g |
| $CaCl_2.2H_2O$ | 0.036 g |
| Citric acid | 0.006 g |
| Ferric ammonium citrate | 0.006 g |
| EDTA (disodium salt) | 0.001 g |
| $NaCO_3$ | 0.02 g |
| Trace metal mix A5 | 1 mL |
| Distilled water | 999 mL |

**Table 4 BG11 media recipe for liquid cultures of *Synechocystis***

| | |
|---|---|
| $H_3BO_3$ | 2.86 g |
| $MnCl_2.4H_2O$ | 1.81 g |
| $ZnSO_4.7H_2O$ | 0.222 g |
| $NaMoO_4.2H_2O$ | 0.39 g |
| $CuSO_4.5H_2O$ | 0.079 g |
| $Co(NO_3)_2.6H_2O$ | 49.4 mg |
| Distilled water | 1000 mL |

**Table 5. Trace element solution recipe used in BG 11 media**

## x.12 Culturing of Materials

Biofilms were often required to be grown on materials for SEM studies or for use in a p-MFC device. Firstly, the material was sterilised (using 70 % ethanol or by autoclaving). Materials including uncoated ceramics, FTO ceramics, PANI ceramics and carbon materials were added to freshly inoculated liquid culture flasks, and left for the required amount of time on an orbital shaker on a lightbox (lightbox UK). In contrast, flat materials such as FTO glass and ITO plastic were placed within a petri dish, before a concentrated cell solution was pippetted on to their surface. After leaving for approximately 3 hours, after which cells had settled through gravitational forces onto the material surface, the petri dish was topped up with fresh media covered and left for the required amount of time on a lightbox (lightbox UK). Differences in culturing methods related to the differences in stability of the resulting biofilms.

## x.13 Determination of Algal and Chlorophyll Concentration

Experiments required the measurement of the cell concentration (cells $ml^{-1}$) or chlorophyll concentration (g $mL^{-1}$). Chlorophyll concentration was calculated using Ultraviolet-Visible (UV-Vis) spectrophotometry. This protocol involved spinning down 1 ml of culture at 13.2 x $10^3$ rpm in a centrifuge for 10 minutes, before replacing the supernatant with methanol, vortexing for 15 minutes, and repeating the centrifugal process. The methanol caused the cells to denature releasing chlorophyll. The absorbance of the methanol-supernatant at 652 nm was then measured in the UV-Vis spectrophotometer, before total chlorophyll was calculated according to Equation 1 [32]

$$1\ \mu g\ chlorophyll\ ml^{-1} = 28.98\ A_{652}$$

**Equation 1 Absorbance of 1 µg chlorophyll $mL^{-1}$, for the calculation of chlorophyll content**

Alternatively, the cell concentration of *C. vulgaris* was determined using cell counting on a haemocytometer under a light microscope. Cultures were diluted by a known amount (generally 100 times) with fresh media, then a small amount pippetted onto a thoroughly cleaned haemocytometer grid (of known volume – 1 mm x 0.1 mm x 0.1 mm), before counting commenced of the 16 small squares. This was taken to be representative of the parent culture, the concentration (cells $mL^{-1}$) of which could then be calculated by equation 2.

$$Cells ml^{-1} = Total\ cell\ count\ of\ 16\ squares\ x\ dilution\ factor\ x\ 200{,}000$$

**Equation 2 The relationship between haemocytometer and actual cell counts**

Cells could then be diluted or concentrated up to a desired concentration. To concentrate cells, samples in eppendorfs were centrifuged for 2 minutes at 13.2 x $10^3$ rpm, after which the supernatant could be removed to leave a pellet of cells. By adding varying volumes of fresh media, the cell concentration could be adjusted.

## x.14 Light intensity calculations

The incident illumination used in each experiment was calculated using a photodiode, according to equation 3.

$$Wcm^{-2} = Photon\ flux\ (cm^{-2})\ x\ photon\ energy\ (js^{-1})$$
$$= \frac{I(A)}{qQE} \cdot \frac{hc}{\lambda}$$

**Equation 3 Calculation of incident illumination intensity in W $cm^{-2}$, where q = 1.6 x $10^{-19}$, h = 6.626 x $10^{-34}$ and c = 299,792,458 m $s^{-1}$**

## x.2 Appendix B – Published papers